The Mechanism of Lead Poisoning in Catalytic Gas Detectors

by

EHSAN NOORDALLY

A Thesis Submitted for the degree of

Doctor of Philosophy

of

The City University
London

The Department
of
Chemistry

December 1979

C O N T E N T S

ACKNOWLEDGEMENTS

My sincere thanks are due to Dr. R.P. Townsend who organised this project and whose supervision and continued interest in every aspect of the work have been invaluable. I am very much indebted to the English Electric Valve Co. Ltd. for their generous sponsorship of this project, and also to [redacted] of this company whose advice was most helpful. My appreciation is also expressed to the Associated Octel Company Ltd. for supplying gratis the lead alkyls throughout the course of this study. My thanks are also due to many of the staff of The City University for their assistance and advice, and the friendliness and coorperation of the fellow-workers in the heterogeneous catalytic laboratory were most gratifying. Finally, I would like to thank [redacted] for her generous assistance in typing this thesis.

Abstract

Currently, gas detectors are liable to fail unpredictably when working in the field. For the obvious reason of safety the development of reliable detectors of flammable gases at both low and potentially explosive concentrations is essential. The purpose of this investigation has been to study the mechanism by which one poison, tetramethyl lead, deactivates catalytic pellistor type gas detectors. The following objectives have been partially or fully achieved:

(i) An elucidation of the behaviour of catalytic pellistor detectors of more than one type.

(ii) An understanding of the modes by which they are poisoned.

(iii) The prediction of their behaviour in a hostile environment.

(iv) The development of a more reliable gas detector, incorporating zeolites.

The detectors studied were basically two types : the VQ1, which consists of an alumina bead supporting a platinum/palladium catalyst mixture, and the VQ3, which is similar in design but comprises a thoria supported palladium catalyst. The detectors were poisoned in a specially designed rig with which the catalytic activity could be monitored continously. A number of physicochemical techniques were employed to examine the interactions of lead with catalyst on the surface.

Of the principal components of a typical gasoline mixture, tetramethyl lead was shown to be the cause of detector deactivation. Modified detector beads coated with alumina did not show a significantly improved resistance to poisoning. However, zeolite-coated detector beads caused a very marked improvement in poison resistance. Surface studies using techniques such as Scanning Electron Microscopy and Energy

Dispersive Analysis of X-rays revealed that the poison was evenly dispersed over the outer surface, but penetration into the pore structure was small. Furthermore, nitrogen adsorption studies revealed that there is little correlation (undetectable in the present data) between deactivation levels and surface area changes. More work has been recommended in this area.

In the Discussion section, the significance of the experimental results are considered in detail. Lead which is finally present in the oxide form deactivates the catalyst by adsorption on the outer surface without deep penetration into the porous structure, and it appears that the pore mouth poisoning model is an adequate description of the process. Incorporation of synthetic 'large-port' dealuminated mordenite in particular causes the greatest improvement in poison resistance.

CHAPTER 1

INTRODUCTION

CHAPTER 1

1. Industrial Importance of Catalytic Gas Detectors

Catalytic gas sensors have been used for some years in industry for the detection of flammable gases. These were originally developed by the Safety in Mines Research Establishment (SMRE) for the detection of firedamp hazards in coal mines. The accumulation of methane gas in a coal mine constitutes an ever present explosion hazard. Methane is a by-product of the decomposition process which forms the coal, and if the concentration of methane in air exceeds the critical limit of 5% (the so-called lower explosion limit), an explosion can occur. Methane levels are customarily controlled by forced ventilation, but this is not completely successful in preventing localised concentrations exceeding this limit. Hence the availability of a reliable gas detector is an important factor in the quantitative assessment of explosive atmospheres.

Nowadays, catalytic gas detectors are in widespread use in industry, due to the fact that they can be made to respond to a series of flammable fuel vapours other than methane. They have found application in such fields as leak detection associated with storage and transportation of both natural gas and petroleum products. Most modern instruments for assessing explosive atmospheres are based on catalytic oxidation. The general properties of catalytic transducers are discussed in section 1.4, and the pellistor, which is a type of transducer which in recent years has acquired widespread use, is also described in detail. This popularity can be attributed to the fact that they respond to almost all combustible gases to some degree and hence are not specific to methane; also they tend to be more stable than other detection systems when continuously operated in 'poison free' atmospheres.

However, catalytic combustion devices, and in particular

the pellistor, have some distinct disadvantages. They are irreversibly poisoned by traces of silicone oils or lead alkyls and are rendered insensitive by exposure to high concentrations of methane. Unless they are periodically calibrated with appropriate concentrations of methane, the situation can arise in which the user is totally unaware that his unit has been deactivated by poison and is consequently giving low readings. In the mining industry silicone greases and silicone oils are in constant use, and the volatile components evolved from these have the effect of reducing permanently the rate of oxidation of flammable gases on the catalyst and hence the sensitivity of the transducer. Similarly, lead alkyls are notorious poisons for many catalytic systems, and unburnt tetramethyl lead and tetraethyl lead compounds are always present in the atmosphere close to where petroleum is stored, or wherever diesel/petroleum powered traction equipment is being used. These sources prove to be the main cause of damage to catalytic detectors arising from this poison. Even trace quantities of lead alkyls have deleterious effects on the catalyst activity, resulting in irreversible loss of sensitivity. In general gas sensors can be protected from the poison to a certain extent by activated charcoal filters. However, this technique cannot be used for a general flammable gas sensor, since higher hydrocarbons are absorbed by the charcoal along with the poisons and hence remain undetected by the sensor. Thus there is a need for a device resistant to industrial poisons whilst still maintaining a high sensitivity for the higher hydrocarbons.

The main object of this work was to investigate the resistance to poisoning of certain conventional types of catalytic gas detectors to tetramethyl lead vapour, and thence to develop a means of increasing the resistance of these detectors towards this poisoning process.

1.1 Introduction to Heterogeneous Catalysis

By definition, a catalyst is a substance which alters the rate of a reaction without itself being consumed. In terms of transition state theory the process of catalysis involves a lowering of the free energy of activation for the reaction of interest when this reaction is carried out in the presence of the catalytic material. Thus the catalyst effectively provides a more favourable alternate path for accomplishing the reaction; this alternate path is naturally a more rapid one. The basic mechanism of heterogeneous catalysis is such that one or more of the reactants form an intermediate complex with the catalyst surface as a transition state, which then takes part in subsequent reactions to give the final product and the regenerated catalyst.

In heterogeneous catalysis the reaction occurs at a solid/gas or solid/liquid interface and the overall process may be broken down into the following steps:-

(i) transport of reactant to the catalyst surface (this may be only transport to the external surface, but more commonly, transport into the catalyst pores is involved);

(ii) adsorption of reactant onto the catalyst active sites on the external and internal surface;

(iii) conversion of reactants to products;

(iv) desorption of products from the catalyst surface;

(v) transport of the products away from the catalyst.

Steps (ii) to (iv) involve chemical changes and, provided one of these is rate-determining, the reaction will obey the Arrhenius equation, viz

$$k = A \exp(-E/RT)$$

where k is the velocity constant, A is the pre-exponential or frequency factor and E the observed activation energy for the reaction (not necessarily the same as the true activation for the surface reaction if adsorption and desorption processes are rate limiting, when the observed energy of activation can include a heat of sorption term). The subject of mass transfer through the fluid phase to the catalyst surface has been discussed extensively in several texts (1,2,3). Normally, it is highly undesirable for the rate-determining step to be mass transfer of reactant through the gas phase to the catalyst surface; an exception to this, however, is found in the normal design of catalytic detectors, as discussed later (section 1.5.2)

Even when transport to the catalyst external surface is not rate-determining, transport along the pores to the active sites within the solid may substantially alter the effectiveness of the catalyst. Transport of a gas in such a catalyst pore may be by one, or a combination of more than one of three main modes. Two of these involve diffusion, while the third is a forced flow process:-

(i) Bulk diffusion.

(ii) Knudsen diffusion, and

(iii) Poiseuille (forced) flow.

Transport by bulk diffusion occurs when there is no overall pressure gradient along the pore, and when the average pore radius is greater than the mean free path of the gas. Under these circumstances, gas molecules in the pores behave as in the bulk phase. The probability of molecules colliding with each other is far higher than the probability of collisions with the pore walls. Hence under these conditions the rate

of diffusion of a molecule is independent of the pore radius, but is rather a function of the mean free path of the gas and the mean Maxwellian velocity:-

$$D_B \sim \frac{1}{3}\lambda\left[\frac{8kT}{\pi m}\right]^{\frac{1}{2}} \qquad (1)$$

where λ is the mean free path, k is Boltzmann constant, T is temperature and m is the mass of one molecule.

If the gas density is low, or if the pores are quite small so that the mean free path is greater than the mean pore diameter, then the probability of molecules colliding with the pore walls is now greater than that for molecule-molecule collisions. Transport under these conditions is known as Knudsen diffusion and, as might be expected, it is a function of the pore radius:-

$$D_K = \frac{2}{3} r_p \left[\frac{8kT}{\pi m}\right]^{\frac{1}{2}} \qquad (2)$$

where r_p is the mean pore radius in the catalyst.

If the chemical reaction in the pores is such that there is a volume change on passing from reactants to products, a pressure gradient will build up along the pore. Under these conditions, forced, or Poiseuille, flow will be superimposed on top of the diffusive flow. Thus for catalysts with average pore dimensions sufficiently large for bulk diffusion to occur, in the presence of a pressure gradient, bulk flow will be seen, and the bulk flow flux $J_A(x)$ of reactant A in the pore at point x will be defined by a relation such as

$$J_A(x) = -\pi r_p^2 D_B \left[\frac{dC_A}{dx}\right]_x \pm \frac{C_A(x)}{C_T(x)} J_p \qquad (3)$$

where the first term of the right hand side of (3) is just a form of Fick's first law, and the second term involves the concentration of reactant A in the gas $C_A(x)$, the total concentration of gas at this same point $C_T(x)$ and a flux due to Poiseuille flow J_p. The ($\pm$) sign is necessary as the forced flow may be in the same, or in the opposite direction to diffusive flow.

J_p is an inverse function of the viscosity coefficient, and directly proportional to the fourth power of the pore radius r_p. The strong dependency on r_p means that for small pores, such as those in which Knudsen diffusion occurs, Poiseuille transport is inefficient compared to diffusion. Thus, unlike the situation with large pores, it is genarally assumed that Poiseuille flow can be ignored in small pores, and that Knudsen flow is indistinguishable from Knudsen diffusion. The theory and mathematical approach towards diffusion and reaction in porous catalysts is treated in detail in section 1.6.2.

As mentioned earlier, three distinct chemical processes may be involved in an elementary heterogeneous catalytic reaction: the chemisorption of one or more of the reactants, the surface reaction itself, and the desorption of the products. Adsorption of the reactant is universally accepted as the most important step in the overall process of catalysis. That is why studies of adsorption process itself and the chemistry of the adsorbed state assume a dominant role in all investigations seeking a more fundamental understanding of catalytic chemical processes. There are basically two kinds of adsorption:

(i) Chemisorption (4,5), whereby new chemical bonds are formed between

the reactants and the surface atoms of the catalyst, and

(ii) Physisorption (6), which is similar to, and bound up with, the process of condensation, and is in effect a weaker form of adsorption whereby the reactant molecules are held to the surface by Van der Waals forces.

A reaction over a catalyst surface may involve only chemisorption, or a combination of chemisorption and physical adsorption. For a bimolecular reaction, the former case is described as conforming to Langmuir-Hinshelwood kinetics, whereas for the latter case, the term is Rideal-Eley kinetics (7). Whatever the kinetics, the number of active sites and hence the rate of reaction is a function of properties of the catalyst such as the total surface area, the active surface area, and the porosity. The total surface area and the porosity are conveniently evaluated by low temperature nitrogen physical adsorption-desorption isotherm measurements.

The kinetics of these chemical controlled surface processes need to be considered in order to formulate rate and equilibrium equations for these steps. It is necessary to consider the overall kinetics observed when each of these steps is rate-determining. They cannot be isolated from each other because the rate of adsorption depends on the availability of surface sites, which in turn depends on the equilibrium coverage by products. Kinetics of adsorption-desorption of fluid-solid catalytic reactions are treated in detail in several texts (3,8).

In catalysis, chemical composition alone is not enough to determine activity. As pointed out above, physical properties such as surface area, pore size distribution and particle size also play an important part. These properties are governed to a large extent by the preparative procedure. Catalysts are usually made by methods involving precipitation, or gel formation, or a simple mixing of components (9). In cases where the catalyst is a precious metal such as platinum, palladium or gold, where

expense is a major consideration, catalyst carriers (10) are used, which provide a means of obtaining large surface areas. After initial preparation of the carrier, or support, the catalyst is then impregnated onto its surface by dipping the support into a suitable solution containing the catalyst, followed by removal of excess solution and drying. The nature of the support can affect both the catalytic activity and selectivity because the support can influence the surface structure of the atoms of the dispersed catalytic agent through the ease with which sintering can occur, which, of course, affects the active surface area.

Several theories have been put forward to attempt to explain what factors are important in determining catalytic activity and selectivity. Many years ago Sabatier (11) suggested the formation of intermediate chemical compounds and, since then the chemical factor has always been recognised as important. Later Taylor (12), Balandin (13), and Beeck (14) developed theories which place more emphasis on the role of the surface structure. Balandin in particular proposed the famous multiplet hypothesis (15) which interprets relative activities of different catalyst for a particular reaction in terms of geometrical arrangements on the surface. According to this concept, the catalytic activity of solid surface depends on the spacings of atoms; certain surface interatomic distances facilitate adsorption of reactant molecules. Following Pauling, Boudart (16) and Beeck (14) developed the electronic theories of catalysts which attempted to correlate catalytic activity with the electronic theories of the catalyst in particular, d-electron character. The criterion for a solid to be catalytically active was connected with its ability to accept or donate electrons. Extending this concept, in 1948, Dowden and co-workers (17,18) proposed the classification of catalysts on the basis of electron mobility, as conductors, semiconductors, and insulators.

It is generally accepted to-day that in practice for any particular catalytic reaction all the above mentioned factors can be important. Certainly, to attempt to interpret data in terms of any one theory is over-simplistic. The enormous advances in surface spectroscopic techniques of recent years has led to a more cautious attitude towards theories of catalytic behaviour (19,20).

1.2 Heterogeneous Catalytic Oxidation of Methane

Much work has been done on the catalytic oxidation of methane with the end in view of finding a suitable catalyst. The main products of the reaction are carbon dioxide and water; although partial oxidation does occur over some catalysts to give carbon monoxide, hydrogen and formaldehyde (21,22,23). Most of the investigations have been concerned with a comparison of activities of different catalysts and supports to give complete oxidation products.

Platinum (24-31), palladium (25,28,29,32,33), silver (29,34), gold (25), copper (28,29,35) and nickel (36), supported on either asbestos, silica gel or pumice have been investigated. Metallic oxide catalysts such as vanadium pentoxide (28), copper oxide (27,28,37), nickel oxide (27,37), palladium oxide (27,38), cerium oxide (27), zinc oxide (27,28), and oxides of uranium and beryllium (23) supported on asbestos and pumice have also been studied. Anderson et al (39) examined the catalytic activity of the first transition series metals supported on high surface area γ-alumina. The complete oxidation of methane on bulk oxides of the first transition series (40) has been studied by a continuous flow method. It seems that there are distinct differences in both the observed activation energies and the activity series between reactions on the bulk oxides (40) and the corresponding oxides supported on high area γ-alumina (39). A general conclusion is that palladium is the most effective catalyst in the oxidation of methane, and that the reaction rarely involves the formation of intermediate products. The influence of the catalyst support on the oxidation of methane over palladium has also been studied using a microcalorimetric bead reactor (41). The nature of the support was observed to have no detectable influence on the catalytic activity during a given experiment, but was found to affect

the long term stability of the catalyst. Alumina was found to be the most suitable carrier as it is a refractory material, able to stand high temperatures without disintegrating even after prolonged use.

Firth (42) looked at the complete oxidation of methane on a series of palladium/gold alloys on alumina carrier using the microcalorimetric bead technique (43) with the end in view of finding a suitable catalyst for the pellistor type gas detection system. He was able to measure rates, orders and apparent activation energies for the reaction. The results indicated the participation of d-orbitals of the surface metal atoms in the reaction, and evidence was also found for the existence of a relatively stable intermediate. Other studies were those of Mezaki and Watson (44) and Ahuja and Mathur (45) who investigated the kinetics of methane oxidation over palladium catalysts in the temperature range 320 - 380°C. Nevell (46) has made a through study into the mechanism of methane oxidation over supported palladium catalysts. Also examined were the activities of palladium/thoria catalysts of different compositions over a range of temperatures. Firth and Holland (47) studied the complete oxidation of methane over palladium, platinum, rhodium, and iridium using a microcalorimetric technique. Their results indicated that the activation energies are proportional to the Pauling bond energies of the oxygen-metal bond in the region where the order in oxygen is low. Cullis et al (48) examined the partial oxidation of methane from a kinetic and mechanistic viewpoint over palladium/palladium oxide catalysts in a pulse flow microreactor (49). The system used was designed especially for the identification of unstable intermediates, but only traces of formaldehyde, carbon monoxide and water were observed among the principal products of carbon dioxide and water. They proposed a mechanism for the overall reaction in which the rate-determining step is a surface reaction between oxide ions and dissociatively adsorbed linearly-bound methylene

radicals. Firth and co-workers (50) showed that the oxidation reaction over platinum catalyst proceeds by two kinetic routes, involving different oxygen species. One route is inhibited by competition for the weaker oxygen adsorption sites from water or hydroxyl groups. The absence of inhibition observed in the presence of an alumina support was taken to indicate that water is preferentially sorbed on the alumina rather than the platinum surface after it is formed.

Few studies have been carried out using molecular sieves containing transition metal ion as catalysts for methane oxidation and consequently the kinetic data in this area is limited. Firth et al (51,52) looked at the complete oxidation of methane over zeolites containing palladium, platinum, rhodium and iridium using a microcalorimetric technique. They concluded that the isolated ions of these noble metals are able to adsorb methane and oxygen, but only with platinum does the methane and oxygen adsorb competitively. They also found that the activation energies for the reaction show that the rate-determining step is the same on each catalyst. Rudham and Sanders (53) studied the catalytic oxidation of methane by 13x molecular sieves in which 20% of the sodium had been replaced by transition metal ions, using an isothermal flow reactor with reaction temperatures between 253-563°C. The oxidation products were solely carbon dioxide and water. They described the kinetics of the reaction as being first order in methane and zero order in oxygen.

A summary of the results obtained by different workers is shown in Table 1. Although the results obtained by different workers are not always in good agreement, it can be generally stated that the reaction is zero order with respect to oxygen due to the strong adsorption of oxygen on the metal, and that the order with respect to methane is unity. One possible reason for the observed differences in behaviour is the use of

Catalyst/ Support	Temp. Range (°C)	Method	Reaction order in		Reactant mixture composition	Ref.
			CH_4	O_2		
Pd/alumina	350-500	static bead	1.0	0	0.5-1.0% CH_4 in $O_2 + N_2$	(41)
80:20 Pd/ThO on alumina	400-600	static bead	0.8	0	0.5-5.0% CH_4 in O_2	(46)
Pd/alumina	300-340	differential flow	-	-	6-30% CH_4 in O_2	(54)
Pd/silica	200-400	integral flow	-	small -ve	-	(55)
Pd/alumina	320-380	integral flow	1.0	0	-	(44)
Pd/alumina	200-250	integral pulse flow	-	-	CH_4 pulse in O_2	(39)
Pd/13x zeolite	300-400	static bead	1.0	0.3 - 0.4	-	(51,52)
Transition metal/13x	253-563	flow system	1.0	0	3-3.5% CH_4 in air	(53)

TABLE 1 - Summary of Results on Methane Oxidation

different catalyst supports, studies having been made with palladium for example over such different supports as alumina, silica gel, and molecular sieves.

1.3 Gas Detection Systems

Numerous techniques have been used for measuring flammable gases. Some of the desirable characteristics of a satisfactory gas detector are safety, accuracy, reliability, short response time and durability. In this section, the principles behind some of the commonest gas detection devices will be mentioned. A comprehensive review (56) on evaluation of methanometry in coal mines was published in 1972.

(a) Thermal Conductivity

Since the thermal conductivity of a gas mixture is a function of the individual gases present in the mixture, in principle, the overall thermal conductivity can be used as a measure of composition. In practice, the thermal conductivity of the gas mixture to be analysed is usually compared with a reference gas such as hydrogen, nitrogen or air. The thermal conductivity method is usually applied to the determination of the composition of a binary mixture, provided the two gases differ to a sufficient degree in their conductivities. The greater the difference between the two gases, the greater the sensitivity of the method.

(b) Heat of Combustion

The heat of reaction evolved by a gas when it burns above a filament can be used to identify combustible gases in a mixture. As the gas is passed over the heated filament, its combustion raises the temperature and the resistance of the filament as compared to that of a reference filament. If the reference and the active filament are connected together to form two

arms of a Wheatstone bridge circuit, then the degree of unbalance of the bridge provides a measure of the concentration of combustible gas passing over the filament.

(c) Optical Properties

Optical gas detectors work on the principle that the refractive index of the combustible gas may differ from that of air. Thus if light is passed through a reference cell containing only air and also through a cell containing a test gas, the optical fringes obtained will be different if the refractive indices are different. By adjusting a prism to return the fringes to the test gas original position, it is possible to infer how much the refractive index of the test gas differs from air, by the amount of prism deflection required. This may be related to the percentage of the test gas in the mixture. If contaminants are substantial, and have refractive indices very different from the test gas, results can be quite inaccurate.

(d) Infra-red Gas Analysers

Continuous analysis of gas streams for a single component can be carried out effectively by means of an infra-red absorption technique, provided that the desired component shows an absorption band located at least partly in a region where other possible contaminant gases do not absorb.

(e) Flame Lamp

The flame lamp (sometimes called the Davy lamp), which is still used in mines for methane detection, consists essentially of a flame fed by naptha. In air the flame has a characteristic colour, height and intensity. If combustible gases are present in the atmosphere, the character of the flame changes correspondingly. The flame lamp is a very sensitive indication of the presence of combustible gases in the atmosphere. An experienced observer is able to relate a visual observation of the flame to the combustible gas content.

(f) Dielectric Properties

As with many of the detectors already described, a gas detector based upon the dielectric principle would work upon a comparison between a reference condenser in air, while the other condenser is exposed to the test gas. The test condenser will vary in capacitance as the proportion of combustible gas increases, and therefore can be calibrated. Again, in common with many detectors already described, the unit is subject to interference by any other contaminant gas with a dielectric constant that differs from that of the air reference.

(g) Semiconductors

This type of gas sensing element relies on the changes in electrical conductivity that are produced in many semiconductor metal oxides when gases adsorb or react on their surfaces. The selection of suitable semiconductor materials and suitable operating conditions makes it possible, at least in principle, to detect and measure a whole range of gases with this type of element. A typical element consists of a small bead of 'doped' zinc oxide deposited between two parallel platinum wires. These wires have a diameter of 25 μm and are positioned 50 μm apart. The oxide bead is doped with platinum to improve its conductivity and is operated at 600°C. The bead temperature is maintained by passing an electrical current from a constant power supply directly through the bead, using the platinum wires as electrodes. In operation, the change in electrical conductivity of the element, and hence the concentration of the test gas, is recorded in terms of a voltage change across the element. The instrument is designed to measure methane concentration in air over the entire range 0-100%.

(h) Compensating Type Catalytic Combustion Device

Most instruments used for measuring concentrations of combustible gases operate by oxidising the gas, using oxygen from the air, over some form of

catalyst. The signal from most catalytic gas detecting elements consists of an electrical resistance change produced in the element by the temperature rise arising from the oxidation of the combustible gas. To measure this temperature rise the element is used in a Wheatstone bridge circuit. A non-active element forms one arm of the bridge, while the opposite arm is formed from an element carrying the catalyst at a suitable temperature. Both elements are contained in separate suitably shaped containers, which are normally designed so as to ensure that diffusion of gas to the surface is the rate-determining step, and both are exposed to the methane/air mixture. This system, which was originally developed to detect methane, can be applied to the measurement of other combustible gases.

Each detection principle exhibits some advantages and disadvantages as compared to others. Catalytic combustion devices are more popular for methanometry than any other type. Primary reasons for this are that this type of device can be designed to be intrinsically safe and in addition can be made sufficiently rugged to withstand the rigorous physical environment of a mine. Naturally, combustion-type devices are affected by the presence of combustible gases other than methane, but not by non-combustible contaminants (except for catalyst poison). Systems dependent upon other gross properties such as refractive index, transmission or adsorption of energy or dielectric constant are affected by virtually any contaminant and tend to be less selective. The most likely devices to exhibit high reliability are those depending on catalytic combustion, or the flame lamp. This is particularly true if a dust filter is provided in the particular case of catalytic gas detectors. The number of contaminants affecting them are also very few but those that do poison the detectors affect them seriously (see section 1.). However, because of their fast

response time, low power consumption and insignificant zero drift and the advantages outlined above, even where the poisons such as lead alkyls are found, the catalytic gas detector is the preferred device, and research with a view to increasing their poison resistance appears at present to be more profitable than seeking an equally reliable detector working on a different principle.

1.4 Detailed Description of Catalytic Combustion Devices

Most modern instruments for detecting firedamp in ranges up to the lower explosion limit (LEL) of 5% utilize a chemical reaction in which the flammable gas is catalytically oxidised and the heat produced is measured indirectly. Three basic properties are required of a transducer which converts methane concentration into an electrical signal by oxidation of the gas and measurement of the heat produced, viz:-

(i) It must have a suitable surface on which methane will readily oxidize.

(ii) The surface must be heated to a temperature sufficiently high to promote an adequate rate of oxidation.

(iii) A sensitive and accurate means of measuring the heat produced due to oxidation is necessary.

The oldest form of transducer for this purpose was just a coil of platinum wire. The latter acted as a heater and a resistance thermometer, and at the same time provided a catalytic surface (admittedly of relatively low surface area) for the oxidation of the test gas. This type of transducer is still used in portable spot-reading instruments. It is not very suitable for use in continuously operating instruments because platinum is a relatively poor catalyst for oxidation of flammable gases, especially methane, and hence the transducer must be operated at high temperature ($> 800°C$) to

obtain sufficient sensitivity. At this temperature the platinum gradually evaporates, especially in the presence of methane (57), resulting in a continuous reduction in the cross-sectional area of the wire with a concomitant increase in its resistance. Thus a coil of this type is characterised by a continuous zero drift, and a relatively short life due to the coil burning out, which is highly undesirable. Attempts to overcome the deficiencies of the simple platinum coil have led to improved forms of transducer, which are now in wide use. One of the first attempts at improving the platinum coil detector involved prevention of excessive heating occurring at its centre when used for detecting leaded petrol vapours. Decomposition of tetraethyl lead and tetramethyl lead on the platinum coil results in a loss of sensitivity due to the formation of an adsorbed layer of lead oxide, which restricts any further oxidation of the flammable gas. In an attempt to overcome this difficulty the transducer was operated at higher temperatures (900°C); unfortunately the problem associated with evaporation of platinum then becomes very serious. The problem of evaporation was especially acute at the centre of the coil, where the temperature is highest, especially when oxidation of combustible gas was occurring. This difficulty was overcome by coating the centre turns of the platinum coil with glass (58), thus reducing the temperature rise produced by oxidation of the gas and at the same time giving some increased mechanical strength to the coil.

Another type of transducer, which operates at lower temperature by using more active catalysts than platinum wire, and which does not encounter the evaporation problem described above, was originally developed at the Safety in Mines Research Establishment (SMRE) in 1959 (59,60), and is known as the pellistor. It consists essentially of a platinum coil embedded in a refractory material (usually alumina) which acts as a support for the catalyst. In this system the platinum coil acts dually as both a

heater and resistance thermometer, but not as the catalyst (as in earlier models). The supported catalyst promotes the oxidation process at such a temperature that evaporation problems are minimal (~600°C). The most suitable catalyst for oxidising combustible gases are the metals of group VIII of the periodic table. Within this group, palladium and platinum are by far the most widely used. The practical advantage of the pellistor is therefore much greater reliability, since (i) the zero drift is insignificant, (ii) it operates at a lower temperature (thus keeping power consumption to the minimum) and (iii) the alumina bead protects the platinum coil from shock. It is therefore widely used in all types of gas detection instruments. In one respect, however, it is inferior to the platinum coil detector: the supported catalysts are rapidly and irreversibly poisoned in hostile atmospheres by lead alkyl vapours and/or silicone vapours. It was in an attempt to overcome this specific problem that the project described in this thesis was undertaken.

Another successful transducer, using a more active catalyst than platinum wire, is that patented by Seiger (61). A core of woven silica fibre is wound with the platinum resistance thermometer, and then impregnated with supported palladium catalyst. This method of construction makes the transducer resistant to mechanical shock, and enables it to be produced in a range of sizes for different applications. Detectors following this design are widely used in continuously operating gas instruments.

Another more recent invention involves the use of catalyst with a significantly larger surface area (62) than those previously employed. This transducer is similar in design to the pellistor type transducer, but is more complex in construction. It has a layer structure of ceramic and glass with an outer coating of platinum catalyst. It is claimed (62) that this construction produces greater stability, and enables

the detection range for combustible gases to be extended downwards towards lower concentration, even in the 100ppm range.

Many other forms of catalytic transducers have been developed during the past decade, but those described above are the commonest.

1.5 The Pellistor

The pellistor (59) has been used in a number of fundamental investigations under the name "microcalorimetric bead technique" (41,42, 43,47,50-52,63-65). The pellistor (or microcalorimeter as it is occasionally called) consists essentially (Figure 1) of an eleven-turn coil of 50 μm diameter platinum wire with a pitch of 125 μm, embedded in a bead of alumina of approximately 1 mm diameter. The alumina bead (0.3 mg) is formed by a thermal decomposition process, using the coil as a heater, by successively dipping the coil in a saturated solution of aluminium nitrate and then heating it electrically to around 600 °C. This process is repeated until the bead is about 1mm in diameter. The catalyst is deposited on top of the alumina by dipping the bead in an aqueous solution of the metal salts followed by thermal decomposition. Sufficient metal (0.4 mg) is deposited to ensure a homogeneous spread of catalyst over the alumina. The platinum wire leads from the coil are spot-welded to copper wire terminals which are in turn embedded in a polyester resin plug to ensure rigidity. As mentioned before this complete detector then forms one arm of a Wheatstone bridge. The balancing arm (generally called the compensator) is of a similar design, but is chemically inert, that is, the alumina bead supports no catalyst. To ensure that no oxidation of methane takes place over the compensator, the latter is treated with potassium hydroxide and heat treated to 800 °C as a final stage in its

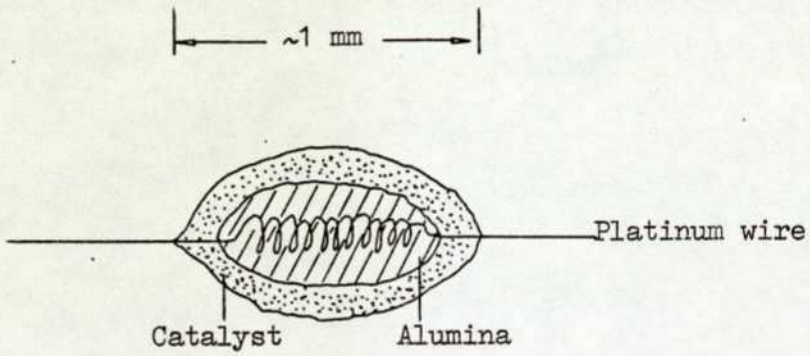

Figure 1. Pellistor bead

preparation.

1.5.1 Bridge Circuitry

Figure 2 shows the calorimeter forming one arm of a Wheatstone bridge with the balancing arm made up of the compensator element. A trimming resistor T is connected across the compensator element in order to reduce any slight difference in thermal properties between the calorimeter and the compensator. The resistors R_1 and R_2 are selected individually for each instrument type so as to bring the range of zero adjustment into the region of fine control; in addition they are chosen to be of sufficiently high resistance to draw little current. The zero-control potentiometer Z is connected as shown and usually has value of 1 kΩ. The applied voltage across the bridge is different for each type of pellistor, depending on the catalyst, and the temperature at which a suitable rate of oxidation of the test gas can be maintained.

In addition to the transducer itself, the other main component of the sensing unit is the design of the system which enables the test gas to reach the calorimeter. The flow system originally developed at SMRE is a simple one, and is shown in Figure 3 (66). The sampling gas is drawn through a tube of activating charcoal to remove as many impurities as possible then through a tube lined with gauze, usually 60 BSS mesh stainless steel. Each of the two pellistors is mounted at the centre of a cavity which opens at one end to the gauze cylinder. The gases diffuse through the gauze and are transported by convection currents within the cavities to the centre where they diffuse through a film of stagnant gas to the surface of the pellistor. Products diffuse out by the reverse process and a new equilibrium is set up within two or three seconds of a change in

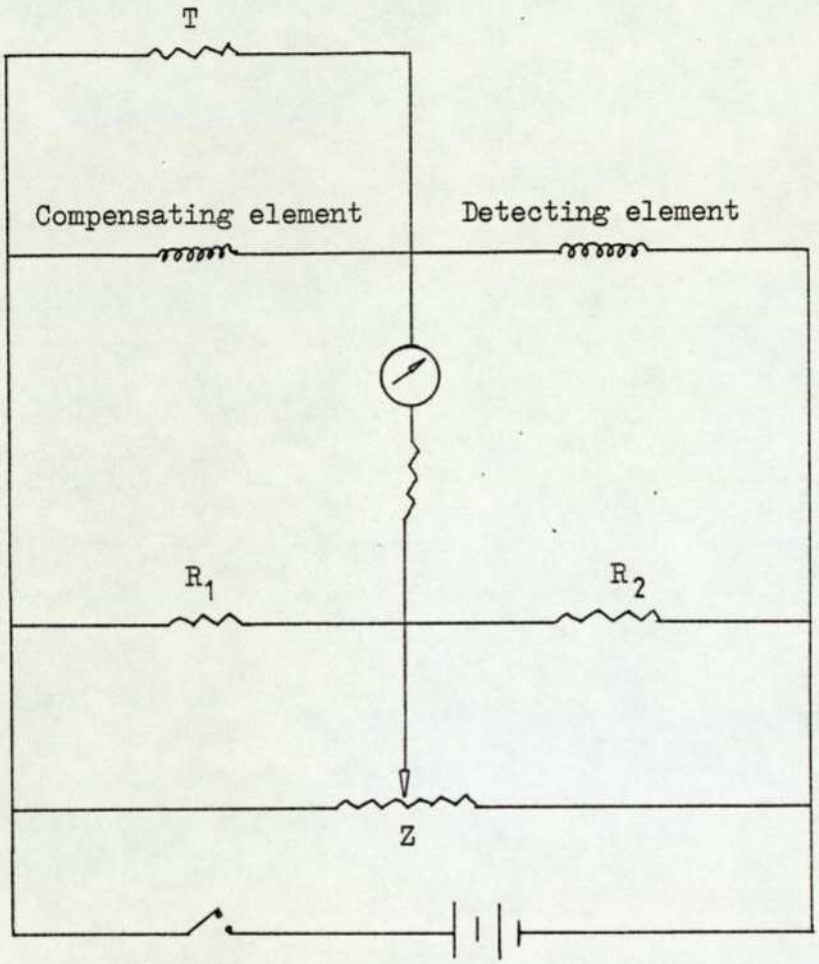

Figure 2. Basic circuit diagram for pellistor type gas detector

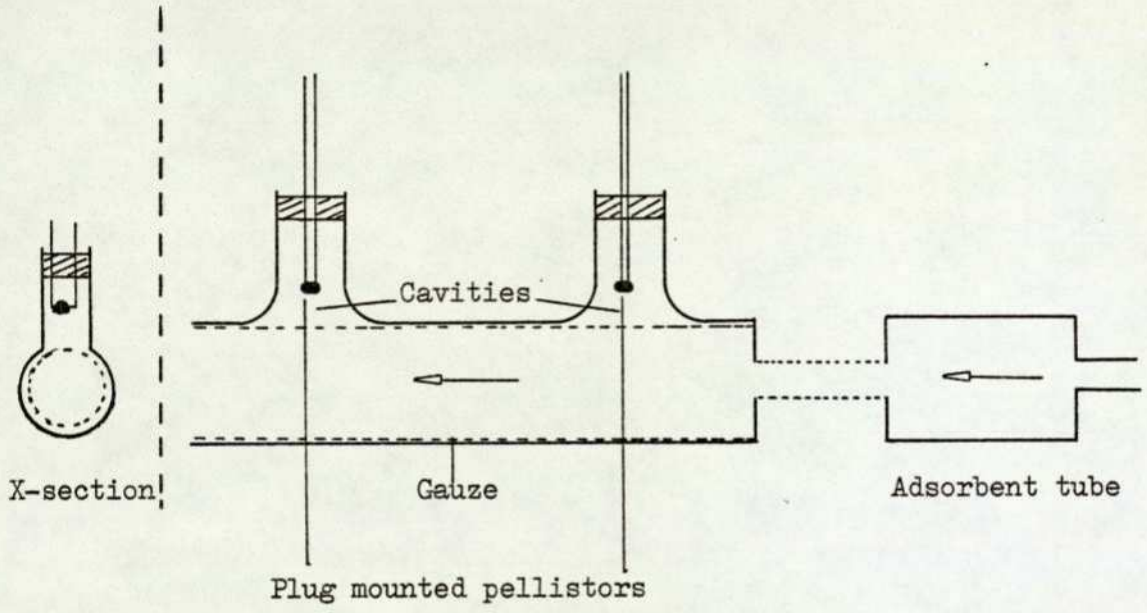

Figure 3. Flow system

concentration of the fuel. Diffusion through the gauze limits the amount of gas entering the cavity, but the rate of oxidation on the pellistor (and hence the output from the bridge) is governed by film diffusion through the boundary layer of gas surrounding the pellistor.

1.5.2 Principle of Operation

The basis of this instrument is a response to the catalytic oxidation of the sampled atmosphere at a suitable temperature; the heat of oxidation causes the temperature and hence the resistance of the catalytic calorimeter to rise. The resulting resistance change ΔR forms the basis of the instrument signal. The potential V generated across the bridge by the resistance change ΔR forms the output of the device (Figure 4).

For a Wheatstone bridge of the type described earlier (42,67), potential V in volts produced across the bridge by a small rise in resistance is given by (Appendix I):-

$$\frac{\Delta R}{\Delta V} = \frac{(R_1 + R_3)}{I_2 R_4} \qquad (4)$$

where R_1 is the resistance of the catalytic calorimeter with the bridge balanced. R_3 is the fixed resistance in the arm in series with the compensating calorimeter. I_2 is the current through R_4 and the compensator. ΔR is a function of the rise in temperature ΔT of the pellistor. A detailed derivation which enables calculation of kinetic data for methane oxidation using the microcalorimeter bead technique is given by Firth (42), and further details regarding the direction of flammable atmospheres by catalytic devices have also been reported (67).

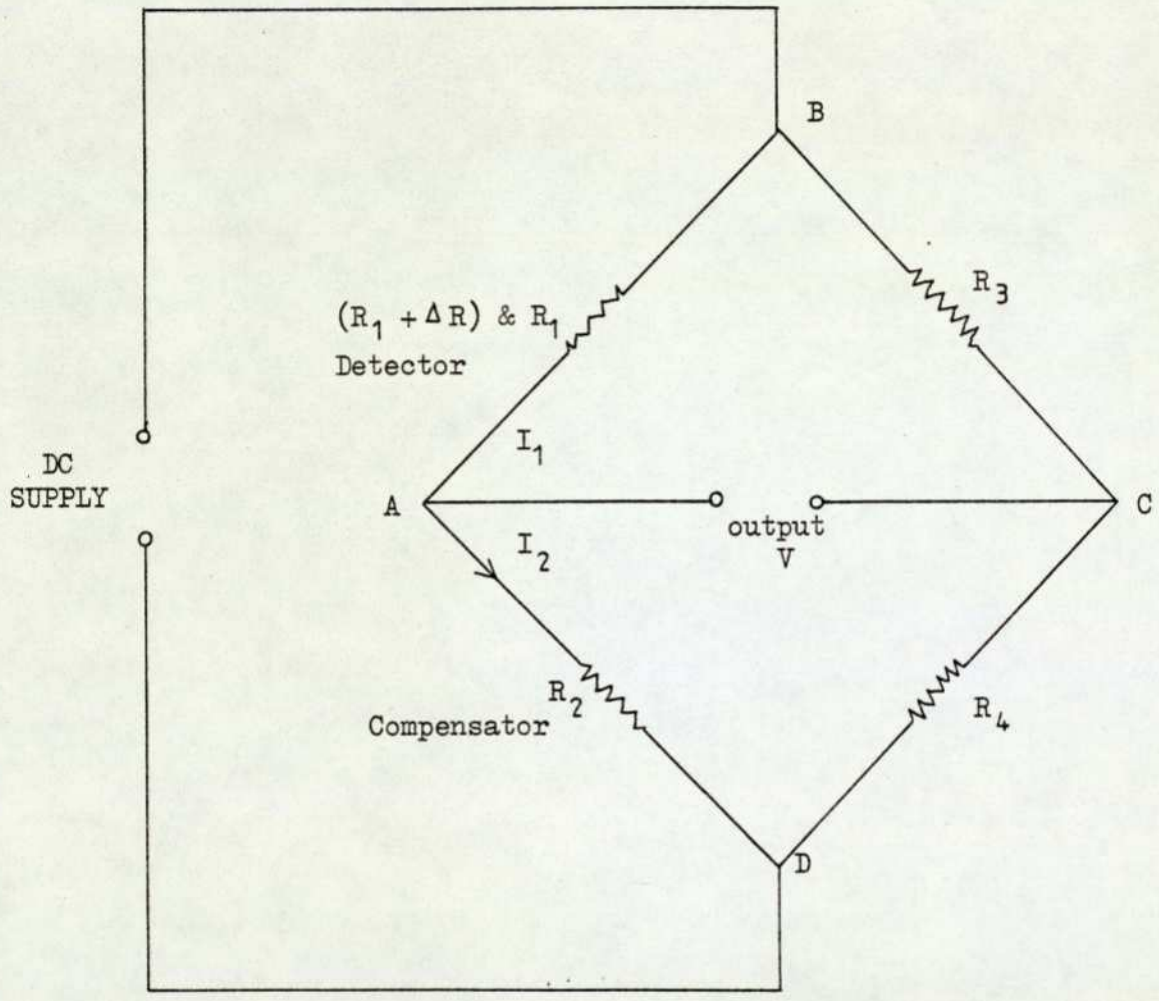

Figure 4. Wheatstone bridge circuit

An important point is mentioned in section 1.5.1. In contrast to many catalytic systems, the calorimeters are operated under conditions where the rate-determining step for oxidation of the fuel is film diffusion controlled (i.e. by the rate of diffusion of the fuel to the catalyst surface through the stagnant boundary layer close to the pellistor). Diffusion controlled is achieved by providing an ample amount of catalyst at a temperature high enough to ensure that the rates of adsorption of reactant, surface reaction and desorption of product are sufficiently high. Firth et al (67) have shown that the out of balance voltage V is proportional to the concentration of the fuel, and for different combustible gases V may be expressed (Appendix I) as

$$V = K \Delta H D_{12} (F) \qquad (5)$$

where ΔH is the enthalpy of combustion of the fuel, D_{12} is an inter-diffusion coefficient for gas 1 into gas 2, and (F) is the thickness of the depletion (or boundary) layer. The above expression has been verified satisfactorily (67) using various concentrations of different gases. In the case of mixtures of flammable gases, the signal obtained is the sum of the signals arising from the individual gases that comprise the mixture. It follows that an instrument which is to be used for measuring gas mixtures should be calibrated with that air mixture.

In summary, therefore, the current situation is that the mechanism by which the pellistor gas detector produces a signal is now well understood, and its operating reliability is excellent in conditions where the explosive hazard is well specified. The most serious limitation of this device is now its susceptibility to certain commonly encountered

catalyst poisons. An empirical approach towards effecting an improvement in pellistor poison resistance is clearly not the best way to solve this problem, and the theory of catalyst poisoning has developed considerably in the last twenty years. An introduction to the different poisoning theories is therefore provided, in the next section.

1.6 Poisoning Theories

The phenomenon of catalyst poisoning has been recognised throughout most of the history of catalysis research, but it is only relatively recently that our understanding of the chemistry and kinetics of poisoning has advanced significantly. In 1951, Maxted (68) presented a review of work on the poisoning of metallic catalysts, and earlier Voorhies (69) reported on catalyst deactivation due to carbon deposited on cracking catalyst (i.e. the phenomenon of "coking", which is usually considered separately to poisoning). Since then there have been many studies of poisoning problems, in particular the mechanism by which poisoning occurs and determinations of poisoning rates. However the bulk of the problem has still to be fully explored and understood.

Deactivation processes can be broadly divided into three classes. These are:

(a) Poisoning: Loss of activity caused by strong adsorption of some impurity (normally a feed contaminant).

(b) Fouling: Loss of activity caused by reactant or product degradation on the catalyst surface. Coke formation is the most important example.

(c) Aging: Loss of activity caused by sintering which results in a decrease of the active surface area.

The first in particular, and the second case, are primarily chemical in

nature, while aging is usually thought of as a physical process. The results reported by Maxted were concerned with metals used as hydrogenation catalysts; nonetheless the results are relevant to this work. According to Maxted (68), the common poisons for group VIII metal catalysts can be classified into three groups:-

(i) Molecules containing elements of groups Vb and VIb (but not nitrogen);

(ii) Compounds of catalytically toxic metals and metal ions;

(iii) Molecules containing multiple bonds such as carbon monoxide.

If the molecule containing the group Vb and VIb element has unshared electron pairs or empty valency orbitals, then chemisorptive bonding to the catalyst is possible and the material is a potential catalyst poison. The toxicity of metals or metallic ions towards the catalytic activity of metals has been further surveyed by Maxted and Marsden (70). They emphasize the existence of some connection between the toxicity of a metallic ion and the d-electron character. The main conclusion that they drew from their work (70) is that those materials which are toxic all have occupied d orbitals; when this does not occur, there is no poisoning effect. These observations also hold for derivatives of the metals. In such cases, the occupied s and p levels might be expected to take part in chemisorptive bonding, yet examples are found where the metal is in a compound with the high s and p levels fully occupied in stable bond formation (and therefore not available to take part in chemisorptive bonding), yet the compound is quite toxic. A good example of this, the compound which was the object of this study, is tetramethyl lead. The electronic configuration (using valence bond notation) is

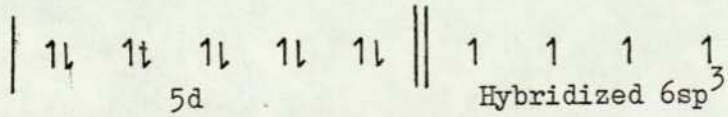

with the hybridized $6sp^3$ levels bonded to the four carbons in the molecule. This molecule is a strong poison, yet there is no opportunity for the s and p orbitals to take part in chemisorptive bonding. The conclusion must therefore be that such metallic compounds poison through the formation of chemisorbed complexes via the d-shell electrons. The nature of this type of bonding is thus fundamentally different from the group Vb and VIb poisons, where bonding is thought to occur via s or p valence electrons. Detailed discussions of surface bonds thought to be involved in adsorption/chemisorption on metals are found in the literature (5,71). A consideration of the kinetics of poisoning processes is particularly apposite to the work reported in this thesis, and is discussed in the next section.

1.6.1 Distribution of Poison

The first studies of poisoning effects on individual catalyst pellets were described by Wheeler (72). He conveniently classified poisoning in terms of two theoretical models: uniform poisoning and pore-mouth poisoning. The poisoning process is described as uniform or homogeneous when the poison is distributed throughout the catalyst pellet pore surfaces uniformly and thereby reduces the absolute activity of the catalyst uniformly. Conversely, pore-mouth poisoning refers to the limiting case of a poison which is confined to a zone from the pore-mouth to some boundary within the pore. Thus in pore-mouth poisoning the pore is divided into active and inactive zones. As the extent of poisoning proceeds, the inner boundary of the active zone moves toward the interior of the catalyst pellet. Wheeler (72) found that pore-mouth poisoning can result in a severe reduction of activity with only small amounts of poison if the catalyst is

operating under conditions in which pore diffusion processes are influencing the rate of reaction. In addition he found that the two limiting types of poisoning mechanism predict very different activity behaviour of the catalyst with progressive poisoning.

In order to be able to express the kinetics of poisoning in a mathematical form, reaction rates on porous catalysts as formulated by Wheeler have to be considered from first principles. The equations for steady state reactions in catalyst pores were solved simultaneously, yet independently, by Thiele (73) and Zeldowitsch (74). Thiele's approach was later developed by Wheeler (72,75), by Weisz et al (76-78) and by Wicke et al (79,80). The porous structure of the catalyst can be visualised as a composite of intersecting capillaries (pores), and as molecules flow into a pore by diffusion, reaction occurs due to collisions with the pore walls and the concentration of reactant along the pore decreases accordingly. The equations may be solved either in terms of an ideal single pore, followed by appropriate adjustments to bring the ideal model into line with the real situation existing in the pellet, or they may be solved for the pellet as a whole, when the parameters are 'practical' i.e. they include within themselves allowance for the non-ideality of the situation automatically. The latter case is discussed in the next section.

1.6.2 Reaction Rate in Spherical Catalyst Pellet

The solution for a spherical pellet, which must be applicable to the pellistor, will be considered here, and the further complicating situation of catalyst poisoning will be taken up in the next section. To simplify the treatment, the following assumptions have to be made:-

(i) The porous pellet is homogeneous in structure throughout;

(ii) The pellet is operating under isothermal conditions;

(iii) Diffusion of reactant into the porous structure can be represented by Fick's first law.

(iv) The reaction is irreversible, and the rate of the reaction can be represented by a power function in the concentration of reactant A, given as

$$\text{Rate} = k\, C_A^n\, dS \qquad (6)$$

where k = intrinsic rate constant (this is not necessarily the observed rate constant, but rather a rate constant defined in terms of unit area of pore surface exposed to reactant at a concentration equal to that outside the pellet);

C_A = concentration of reactant A;

n = order of reaction;

S = area of pore walls available for reaction;

(v) Steady state conditions pertain throughout the pellet.

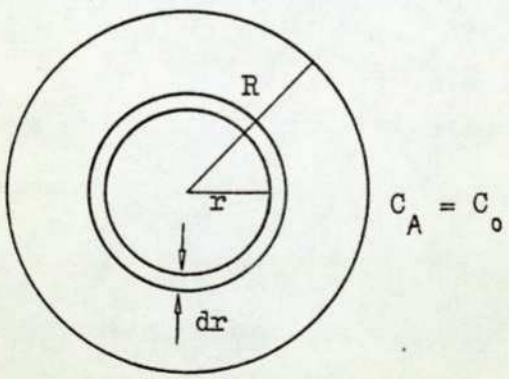

Figure 5. Spherical model for simultaneous diffusion and reaction.

Consider a spherical pellet of radius R (Figure 5) into which molecules are being transported by diffusion only. If the concentration gradient is $\frac{dC_A}{dr}$ at a distance r from the centre, then the inward flow of reactant molecules across the differential annular shell within the pellet

at a distance r from the centre is

$$V_A \text{ (in)} = -4\pi r^2 D_e \frac{dC_A}{dr} \qquad (7)$$

where $4\pi r^2$ is the area of this spherical surface, and D_e is the over-all diffusion coefficient, or effective diffusivity, of reactant in the pore structure. This is not equivalent to either bulk or Knudsen diffusion coefficients, but allows for the porosity and tortuosity of the catalyst structure. Under steady state conditions, the difference in flow of reactant into and out of the differential annular shell must be equal to the rate of reaction in that shell. Thus the fundamental differential equation for reaction within this spherical shell is

$$-dV_A = 4\pi r^2 \, dr \, S \, k \, C_A^n \qquad (8)$$

where S = pore surface area per unit volume of pellet (this is obviously related to the specific surface area as determined by physical adsorption measurements),

$4\pi r^2 dr$ = volume of differential annular shell;

n = order of reaction.

dV_A may also be obtained by differentiating equation (7), and under steady state conditions (7) must be equal to (8). Whence after a few mathematical manipulations (see appendix II), the equation

$$\frac{d^2 C_A}{dr^2} + \frac{2}{r}\frac{dC_A}{dr} = \frac{h^2}{R^2} C_A^n \qquad (9)$$

is obtained, where h, the dimensionless quantity termed the Thiele modulus, is defined as

$$h = R\sqrt{\frac{Sk}{D_e}} \qquad (10)$$

Equation (10) may be solved for different reaction orders n, with the boundary conditions of $C_A = C_0$ at $r = R$ (i.e. concentration of reactant is C_0 at the outside surface of the pellet), and $\frac{dC_A}{dr} = 0$ at $r = 0$ (i.e. no concentration gradient exists at the origin of the sphere). This treatment is carried out in detail in appendix II for the first order case ($n = 1$), as the oxidation of methane can be assumed to be near first order in methane (see table 1.1). For the first order case, the rate of reaction within a spherical porous pellet is found to be

$$R_p = 4\pi R\, D_e\, h\, C_0\left[\frac{1}{\tanh h} - \frac{1}{h}\right] \qquad (11)$$

If the internal surface of the porous pellet were all exposed to reactant at a concentration equal to the external value C_0, the rate would be

$$R_p^{(C_0)} = \frac{4}{3}\pi R^3\, k\, C_0 \qquad (12)$$

An effectiveness factor (f), or fraction of area available as it is sometimes called, may be defined in terms of the ratio of the two rates given in (11) and (12):-

$$f = \frac{3}{h}\left[\frac{1}{\tanh h} - \frac{1}{h}\right] \qquad (13)$$

The hyperbolic tangent of h approaches unity as h increases (greater than about 3), therefore f approaches $\frac{3}{h}$ at large values of h, that is f is inversely proportional to h at large values of $h > 3$. Equation (13) has important practical implications. The significance of h and f are explained below where

$$f = \frac{\text{actual rate for the whole pellet}}{\text{rate evaluated at outer surface conditions}} \qquad (14)$$

The effectiveness approaches unity ($f \rightarrow 1$) as the pellet radius or rate constant is made small, or as the diffusion coefficient (D_e) is made large. In this instance all the surface is fully effective i.e. the rate of reaction at the centre of the pellet is the same as the rate at the outer surface. Conversely, the effectiveness becomes small ($f \ll 1$) for large particles, large rate constant, or small values of diffusion coefficient (D_e). Practically these conditions mean that the reaction occurs before the reactant has diffused far into the pellet. Very active catalysts (large k) tend to have low effectiveness factors while inactive catalysts tend to have high effectiveness factors.

1.6.3 Kinetics of Poisoning

As mentioned earlier the rates of catalytic reactions are reduced by poisons. The next stage is to show how the reduction in rate varies with the fraction of surface available for reaction as the catalyst surface is progressively poisoned.

Wheeler (72,75) originally developed the mathematical treatment for the two limiting cases of poison distribution, (i.e. uniform poisoning and pore mouth poisoning) for an isothermal, irreversible, first-order reaction in an ideal cylindrical half-pore. It is convenient to

discuss this model here as the difference between the two modes of poisoning is seen with particular clarity if a single half-pore is considered.

Uniform Distribution of Poison

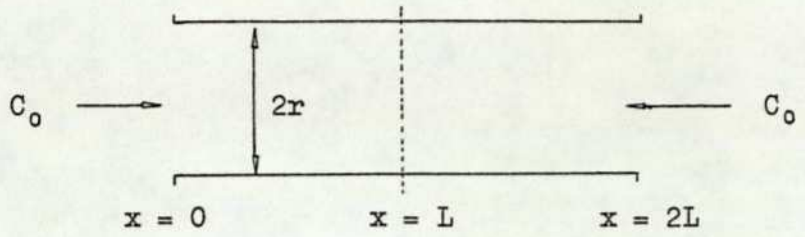

Figure 6. A single pore going through a catalyst

The rate of reaction per half-pore for a cylindrical pore of length 2L and radius r_p (Figure 6) in the case of a first order, isothermal, irreversible reaction is given by

$$R_{\frac{1}{2}} = \pi r_p^2 D \frac{h_1 C_o}{L} \tanh h \qquad (15)$$

As before C_o is the concentration of reactant at the pore mouth, D is either a bulk or Knudsen diffusion coefficient, depending on the radius of the pore and h_1 is the first order Thiele modulus. h_1 is not identical to the Thiele modulus derived from the spherical pellet model:-

$$h_1 = L\sqrt{\frac{2k_r}{r_p D}} \qquad (16)$$

where k is the intrinsic rate constant (see equation (6))

Considering first the case when the poison is evenly distributed along the wall of the cylindrical pore, if α is the fraction of surface poisoned, then the intrinsic activity of the pore after poisoning to this degree must be $k(1 - \alpha)$. It follows that in the case of a poisoned catalyst the Thiele modulus can be written as

$$h_1' = L\sqrt{\frac{2k_r(1 - \alpha)}{r_p D}} = h_1\sqrt{(1 - \alpha)} \qquad (17)$$

where h is the value of h for the unpoisoned pore. Then, from equation (15) the ratio F of activity of poisoned pore to unpoisoned is thus

$$F = \frac{\text{Rate poisoned}}{\text{Rate unpoisoned}} = \frac{h_1\sqrt{(1 - \alpha)}\ \tanh\left(h_1\sqrt{(1 - \alpha)}\right)}{h_1 \tanh h_1} \qquad (18)$$

Using the approximation that when h_1 is small (i.e. $h_1 < 0.2$) $\tanh h_1 \to h_1$ in equation (18)

$$\lim_{h_1 \to 0}\left[\frac{h_1\sqrt{(1 - \alpha)} \cdot h_1\sqrt{(1 - \alpha)}}{h_1 \cdot h_1}\right] = 1 - \alpha \qquad (19)$$

When h_1 is small, the fraction becomes equal to $(1 - \alpha)$. In other words the rate drops linearly with fraction poisoned. At the other extreme when h_1 is large $(h_1 > 5)$ $\tanh h_1 = 1$ and this case

$$\underset{(h_1 > 5)}{F} = \frac{h_1\sqrt{(1 - \alpha)}}{h_1} = \sqrt{(1 - \alpha)} \qquad (20)$$

Equation (20) shows that under these circumstances the activity drops less than linearly with fraction poisoned. Figure 8 shows predicted poisoning curves for the two cases:

(i) h_1 very small (curve A): a linear drop in activity with fraction poisoned. This type of poisoning is termed 'non-selective';

(ii) h_1 very large (curve B): a less than linear drop in activity with fraction poisoned. This type of poisoning is termed 'anti-selective'.

Pore mouth Poisoning

In this type of poisoning, it is assumed that a poison is selectively adsorbed on the outer periphery of the catalyst particle, that is, in the openings of the pore mouths.

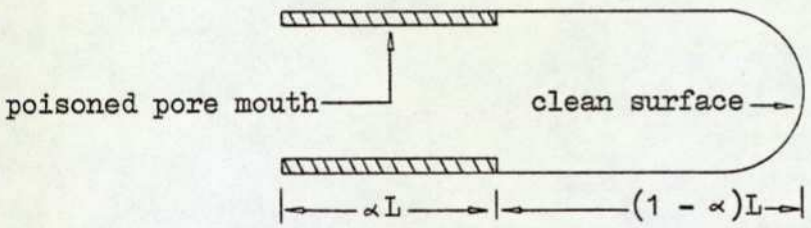

Figure 7. Preferential adsorption of poison near mouth of pore

Considering again the half-pore as shown in Figure 7, it is supposed again that a fraction of the pore is poisoned, this poison being heterogeneously distributed, only being found at the pore mouth. In these circumstances, the rate of reaction in the pore under steady state conditions will be determined by the rate of diffusion through this initial poisoned length of pore. Let the concentration of reactant at the end of this section be C_1. Then for the first order case, the mass balance equation yields

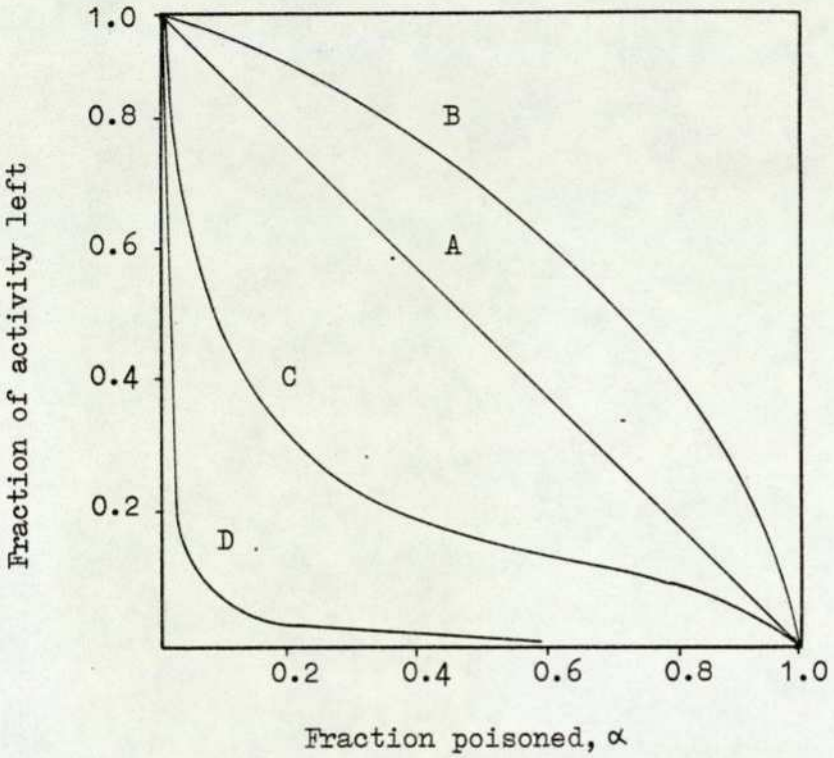

Figure 8. Types of poisoning curves for porous catalysts

Curve A : for a porous catalyst in which h_1 is small and poison is distributed homogeneously

Curve B : homogeneous adsorption of poison with h_1 large

Curve C & D : preferential adsorption of poison near pore mouth. For curve C, $h_1 = 10$ and for curve D, $h_1 = 100$

Quoted from reference (72)

$$\pi r^2 D \frac{C_0 - C_1}{\alpha L} = \pi r^2 D \frac{h_1(1-\alpha)}{L(1-\alpha)} C_1 \tanh\left(h_1\sqrt{(1-\alpha)}\right) \qquad (21)$$

$$h_1' = (1-\alpha) L \sqrt{\frac{2k_r}{r_p D}}$$
$$= (1-\alpha) h_1$$

where h_1' is the Thiele modulus for the poisoned catalyst. Solving equation (21) for C_1 gives

$$C_1 = \frac{C_0}{1 + \alpha h_1 \tanh\left(h_1(1-\alpha)\right)} \qquad (22)$$

Substituting (22) back into the right hand side of the mass balance equation (21), the rate of reaction in the poisoned pore

$$(R_{poison}) = \frac{\pi r^2 D(h_1 C_0/L) \tanh\left(h_1(1-\alpha)\right)}{1 + \alpha h_1 \tanh\left(h_1(1-\alpha)\right)} \qquad (23)$$

As before, the ratio of the rate in the poisoned pore to that in the unpoisoned pore can be derived to give the fraction of activity left in the poisoned catalyst:-

$$F = \frac{1}{1 + \alpha h_1 \tanh\left(h_1(1-\alpha)\right)} \left[\frac{\tanh\left(h_1(1-\alpha)\right)}{\tanh h_1}\right] \qquad (24)$$

Now in an active catalyst, the Thiele modulus, h_1 tends to large value ($h_1 > 5$), and since $\lim_{h \to \infty} (\tanh h_1) = 1$, then for equation (24),

$$F \longrightarrow \frac{1}{1 + \alpha h_1} \qquad (25)$$
$$h_1(1-\alpha) > 2$$

The significance of equation (25) is seen by calculation as follows. Assuming a homogeneous active catalyst, operating under conditions so that $h_1 = 50$ and that

(i) 2% of the surface is poisoned by a pore mouth poisoning mechanism.

Then $\alpha = 0.02$

and $$F = \frac{1}{1 + (0.02)(50)} = 0.5$$

In other words, a 2% drop in surface coverage due to poisoning leads to a 50% drop in catalytic activity.

(ii) 20% of the surface is poisoned by the same mechanism

Then $\alpha = 0.2$

and $$F = \frac{1}{11}$$

Under these conditions only 9% of original activity is predicted to remain. Thus a dramatic drop in activity can be observed when only a minute fraction of the pore surface is poisoned. The cause of this is that poisoning the outer surface of the catalyst has destroyed the original site for reaction, and has forced the reactants to diffuse deeper into the pores before they are able to reach the active parts of the catalyst. In effect, pore mouth poisoning has caused the rate-determining step to shift to a form of film diffusion, but not the normal one, which involves transport through a stagnant boundary layer of gas close to the catalyst surface, but through a film of inactive material surrounding the pellet. Figure 8 shows typical poisoning curves for pore mouth poisoning. Curve C depicts adsorption of poison near the pore mouth for h = 10, and curve D for h = 100.

1.6.4 Lead Alkyl as Poison

The principal commercial application of organolead compounds

is their use as the so-called "antiknock" agents, a discovery due to Midgley and Boyd (81). Antiknock agents are additives in aviation and motor gasolines which are incorporated in order to suppress the reactions that produce the undesirable phenomenon of "knock" in the internal combustion engine (that is, premature combustion of fuel). Knock frequently limits the power output of an engine, and can, if sufficiently severe damage the engine. Although the mechanism of knock is relatively poorly understood, the technology of its control is well developed. Many alkyl lead compounds have been proposed as antiknocks, however those in general use are tetraethyl lead (TEL) and tetramethyl lead (TML). These are always blended in the gasoline with corrective agents or 'scavengers' (mainly ethylene dibromide and ethylene dichloride) which stop the deposition of lead on the engine parts and cause it to be expelled as lead halides. The theory of scavengers has been discussed by Buck and Ryerson (82).

The properties of organolead compounds are in total contrast to those of inorganic lead compounds. Thus among the inorganic compounds, the most stable are those in which lead is in the divalent state. In contrast, with the organolead compounds, the tetravalent derivatives are much more stable than the divalent derivatives. The divalent compounds are, in fact, poorly characterized due to their instability. They do, however, exist as intermediates in the synthesis of tetravalent lead compounds. The bond formation in tetravalent lead occurs through hybridization of the 2s and 2p electrons in the outer shell to give sp^3 hybridization, resulting in a tetrahedral configuration. Thus tetraalkyl compounds are best represented as covalent molecules in which the organic groups are tetrahedrally located around the lead atom. The lead to carbon bond exhibits a high degree of covalent character as a result of the small difference in the electronegativities of the two elements.

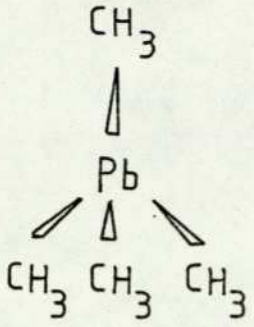

Electron diffraction measurements on tetramethyl lead described in the literature give values of 0.229 nm (83) and 0.220 nm (84) for the lead to carbon bond distance.

Lead forms the least stable and hence the most reactive organometallic derivatives of all the group IVb metals. In general, organolead compounds decompose at fairly low temperatures, are very slowly oxidised in air, and are decomposed by light. Their stability and physical state are strongly dependent on the nature of the organic groups bound to lead. Because of their reactivity to air and their sensitivity to light, organolead compounds are best stored in the dark under an inert atmosphere.

Ever since the toxic action of organolead compounds was recognised there has been renewed interest in their properties, especially bearing in mind their ubiquity in the modern industrial society. The toxic action of many lead compounds has been reported in the literature (85-96), and comparative studies indicate that tetraethyl lead is somewhat more toxic than the tetramethyl analogue (90,91,94,95), although the higher volatility of the latter makes it in principle more dangerous. In general terms, the symptoms of mild cases of exposure to tetramethyl lead or tetraethyl lead are sleeplessness, weakness, irritability, fatigue, headache, and sometimes anorexia, nausea and vomiting. In severe cases convulsions and coma may result, with a mortality rate of $\sim$ 50%. Although the diagnosis is not difficult, the treatment is not specific as there is

no known antidote for these compounds.

A knowledge of the toxicity of these compounds makes it apparent that special precautions must be taken in a laboratory or indeed wherever they are handled. Minimal precautions involve working exclusively in fume-cupboards with good ventilation in the laboratory, thus preventing inhalation. Contact with the skin should be avoided at all costs, hence the use of heavy duty impermeable gloves is recommended. Should there be a spill of organolead compound on the skin, this should be rinsed with kerosene, or light petroleum solvent, and the skin then thoroughly washed with soap and water. In case of accidental spill, the liquid should be quickly absorbed with a rag or absorbent earth, then the spillage area should be swabbed with kerosene, followed by a thorough decontamination of the area. In this context, decontamination implies conversion of the volatile organolead to inorganic lead compounds. Generally saturated potassium permanganate or sulphuryl chloride in kerosene solution is used for the decontamination. Solid or highly concentrated oxidising agents should be avoided, and care must be exercised in the use of all decontaminants; the reagent must be sufficiently diluted to sufficiently retard the rate of decomposition to avoid fire. Glassware should also be decontaminated as outlined above, by first washing with kerosene, then soaking in a solution of sulphuryl chloride in kerosene for one hour, followed by washing with water in the usual way.

Along with the general increase in attention that is being paid to the problem of air pollution, a survey of lead in the atmosphere (97) was carried out some ten years ago. It showed, as might be expected, that the primary source of alkyl lead compounds in the air comes from the vaporisation of these compounds from unburnt gasoline. Thus a number of catalytic converters have been developed to reduce the emissions

of such undesirable products as carbon monoxide and nitric oxide which arise from vehicle exhausts. However, the presence of various lead compounds resulting from the combustion of tetraalkyl lead antiknock has been found to poison the catalyst used in such converters. A wealth of literature therefore arose on this topic, some of which is reviewed below.

In 1971, Yolles and Wise (98) summarised the current theories on the mechanism of lead poisoning. These were physical adsorption on the catalyst with monolayer formation, pore plugging of porous catalysts, and reaction with the catalyst or support to produce an inactive phase or compound. In particular, Roth (99) made a significant contribution towards understanding the mechanism of catalyst poisoning, and Hegedus and Baron (100), using alumina supported platinum catalysts reported that lead(II) sulphate poisons reduce the pore volume of the catalyst in both the micropore and macropore region. Similarly other workers have also shown that there is a correlation between the reduction in catalyst pore volume and surface area on the one hand and the degree of poisoning by lead compounds on the other (101-103). More recently Bucknell (104) carried out investigations into the mechanism of deactivation by lead halides of oxidation catalysts, and found that both surface area and porosity decreases during the deactivation of supported catalysts. The concentration and distribution of poisons on catalyst has been thoroughly investigated (105,106) with a view to providing a better insight into the mechanism of catalyst deactivation.

All the work mentioned above has been concerned with the problem of poisoning of automotive catalysts. No literature could be found that is directly related to poisoning of catalytic gas detectors, though this problem has been recognised ever since the introduction of the pellistor type catalytic gas detector. A few workers have attempted to overcome the

problem by producing a poison resistant detector (64), but no mention has been made anywhere on investigations into the poisoning mechanism. Hence at the beginning of this project very little concrete evidence existed regarding the extent and seriousness of poisoning in catalytic gas detectors. Certainly there are many resemblances between the automotive catalyst and the catalytic gas detector, in the sense that they are both oxidation catalysts, and that both catalysts are deleteriously affected by organolead compounds. However the principles of operation in the catalytic gas detector are somewhat different and hence the starting point in this work had to be a systematic investigation on different types of pellistors currently in use, in order to throw light on whether a pore mouth, homogeneous, or some other type of poisoning process was occurring. This was followed by the development of a catalytic gas detector which is partially or wholly resistant to tetramethyl lead poisoning using zeolite molecular sieves. In the next section, the reasons why zeolites seemed a likely answer to the poisoning problem are explained.

1.7 Improving the Poison Resistance of Catalytic Gas Detectors by Using Zeolites

Attempts at improving the poison resistance of catalytic gas detector have been tried ever since the poisoning problem was recognised. Several means of overcoming this problem was developed. The simplest was a charcoal filter to absorb the inhibitor before it reached the transducer, but this method also removed higher molecular weight hydrocarbons, hence making the transducer more selective towards low molecular weight hydrocarbons, an undesirable property for a detector. Other methods have involved modifying the support surface area, and the pore structure. Based

on the fact that the detector catalyst bead is of necessity small, (having therefore only a small surface area) so that only a small amount of poison can reduce its activity drastically, the reasoning that followed was that if the active sites could be supported on a carrier of much larger surface area, then a larger amount of inhibitor will be required to produce the same harmful effect.

Firth and Holland (64) carried out brief investigations using molecular sieve properties of zeolites to produce poison resistant catalysts. They maintained that by enclosing the catalytic ions or atoms within the micropores of a zeolite, it should be possible to prevent access of large poison molecules to the catalytic ions while smaller reactant molecules still had easy access. On the whole very little has been done in producing a poison resistant catalytic transducer apart from the work reported by Firth and Holland (64,51,52). The ultimate aim of this project has been to produce a catalytic sensor bead resistant to tetraalkyl lead poisoning using zeolites, but following a different principle to that suggested by Firth and Holland (64), by incorporating into the conventional supported catalyst zeolite crystallites as selective sorbents.

The rest of this section is devoted to an introduction to the possible advantages of using zeolites. Basically, zeolites are crystalline aluminosilicates consisting of three dimensional lattices of silica and alumina tetrahedra (SiO_4 and AlO_4). Thus the silicon and aluminium atoms are coordinated tetrahedrally through oxygen atoms. Wherever an aluminium atom is incorporated, in effect replacing a silicon atom isomorphously within this lattice, there results a unit negative charge on the lattice. In addition, the structure is very open, resulting in molecular sized channels and cages. It is the combination of the charged

lattice and the open structure which gives zeolites their useful properties, which may be summarised under three headings, viz:-

(i) catalytic;

(ii) selective adsorptive (molecular sieve), and

(iii) ion exchange.

Now it is frequently the case that the exploitation of one of these properties is of a particular interest in some specified process. However, that property can rarely be considered in isolation to the others. For example, if it is desired to use a zeolite as a catalyst for a particular reaction, the selective adsorptive properties must also be taken into account in order to ensure that the reactant can readily reach the active sites. In addition, the ion exchange behaviour might also need to be considered when examining the feasibility of making a particular metal-zeolite catalyst. Similarly the sieving properties of a zeolite must also be considered even when the primary interest is in the ion exchange characteristics of those zeolites.

In brief, the importance of zeolites can be attributed to the following features:-

(i) a three dimensional lattice containing uniform pores of molecular dimensions;

(ii) a high internal 'surface area' which is only accessible to molecules able to diffuse through the porous network;

(iii) excellent thermal stability at relatively high temperatures.

Much of the early work on naturally occurring zeolites and synthetic zeolite materials (107,108) was done by Barrer and co-workers. Since then numerous investigations on the crystal chemistry, the synthesis, the ion exchange behaviour, and on interactions between zeolites and gases, as well as surveys covering different aspects of the field have been

published. Several good reviews on different aspects of the subject have been published (109,110). In addition, an excellent book by Breck (111) treats the different aspect of zeolites(with the exception of catalysis) on a comprehensive basis. Catalysis has been dealt with separately in a recent monograph (112).

Zeolites can be represented by the general formula

$$M_{2/n}O \cdot Al_2O_3 \cdot xSiO_2 \cdot yH_2O$$

where M is a group I or II cation (often sodium), x is always equal to or greater than 2 since AlO_4 tetrahedra can only be joined to SiO_4 tetrahedra, and n is the cation valence. There are a great many naturally occurring zeolites of this kind, but the faujasite and mordenite classes are of particular interest. The discussion here will be confined to the latter type.

The structure of the sodium form of natural mordenite has been described by Meier (113). Basically, the pore structure consists of parallel adsorption channels having an approximately elliptical opening with major and minor diameters of 0.695 nm and 0.581 nm, respectively. There are smaller side pockets perpendicular to the main channels which can adsorb only molecules smaller than n-butane (114). These side channels have restrictions which essentially prohibit motion of molecules from one main channel to the other. Because of the two dimensional nature of its pore structure, mordenite is susceptible to loss of much of its adsorptive capacity by the presence of small amounts of impurities (115). By varying the synthesis conditions, it is possible to prepare mordenites which have different adsorptive properties due to some change in structure. Mordenites have been classified as 'large port' or 'small port', depending on whether or not they sorb large molecules (116). Further varieties of mordenite

can be produced by removing aluminium from the structure by strong acid treatment with hydrochloric acid (117). Mordenite is a particularly stable zeolite, both from the thermal and chemical viewpoints, being able to resist temperatures in excess of 700°C, and acid solutions of pH's as low as 2. In addition, its crystalline structure survives substantial dealumination (117).

To use zeolites as a means of providing resistance to poisoning, it is now obvious that the primary interest must be in their adsorptive properties. However the approach here can be two-fold:-

(i) A detector could be designed with catalytically active centres within a zeolite lattice, which are available to small gas molecules, but not to tetraalkyl lead compounds. The zeolite therefore may be regarded as 'sieving out' the tetraalkyl lead compounds.

(ii) A conventional catalyst bead could be covered with a zeolite/binder mixture. The zeolite crystals would be catalytically inactive and contrary to the concept of (i), would in fact preferentially sorb the poison molecules. Bearing in mind the size of the poison molecule, this method of improving the resistance of the catalyst to poisoning would only be effective with the zeolites having the larger pore sizes, that is zeolites of the types X, Y, L or 'large port' mordenite mentioned above.

In conclusion, the eventual aim of the present investigation was to incorporate 'large port' hydrogen mordenite or dealuminated mordenites prepared by acid leaching, into the conventional catalytic pellistor type gas detector in order to improve their poison resistance.

1.8 The Present Work

At the beginning of this project very little was known about

the poisoning of the pellistor type catalytic gas detector by lead alkyls. Initial investigations carried out by the English Electric Valve Co. Ltd. and the Associated Octel Co. Ltd. had shown that a series of these detectors containing palladium/platinum and palladium/thoria catalysts were rapidly poisoned by low concentrations of lead alkyls. The ubiquitous nature of lead and its powerful poisoning effects made the development of a detector resistant to lead poisoning an urgent necessity.

In this work, the goal set out has been achieved by primarily carrying out a series of controlled poisoning experiments. Techniques such as scanning electron microscopy for topographical studies of the surface, and a gravimetric sorptive method for surface area determinations, have provided means towards the elucidation of the above problem.

The next stage of the programme consisted of the development of a cheap, reliable detector resistant to lead poisoning. A single possibility, using different materials, was exploited, one which makes the catalyst permeable to methane but not to lead alkyl (through a preferential sorptive rather than a molecular sieve effect) and thus not subject to catastrophic poisoning. Surrounding the conventional catalyst with an inert layer of zeolite which prevents access of the poisoning species to the active sites resulted in a detector with very substantially improved resistance to tetramethyl lead poisoning. 1% methane in air was used as the test gas. Tetramethyl lead (TML) was chosen as the poisoning agent rather than tetraethyl lead (TEL) for the simple reason that although both TML and TEL are blended in gasolines as a mixture, TML is more stable than TEL and hence its handling in the laboratory is easier. It is quite certain that their poisoning actions are only slightly different if not similar. More complex situations involving mixtures of poisons (TML & TEL) should be considered after having laid down the foundation work with a simpler system.

CHAPTER 2

EXPERIMENTAL

CHAPTER 2

2. Materials

Pellistors

The pellistors were supplied by English Electric Valve Co.Ltd. (EEV). These were already made up, tested, and conditioned. They were manufactured according to a particular recipe, hence throughout the course of this project, the beads that were used have a constant catalyst composition. Primarily two types of catalyst detector beads were studied, viz:-

(i) the VQ1, consisting of alumina carrier impregnated with a palladium/platinum catalyst;

(ii) the VQ3, consisting of alumina carrier supporting palladium/thoria catalysts. The thoria also improved the mechanical strength of the bead, and rendered the bead resistant to sintering when used in the presence of high concentrations of flammable gases.

Each of these beads were supplied paired up with a compensator and appropriate trimming resistor, ready to be fitted into the Wheatstone bridge circuit, as described in section 1.5.1. Other prototype beads utilizing the same catalysts as above, but having slight structural differences, will be introduced further on in this work. Later, modifications involving zeolites were used; these were prepared from the commercially available synthetic sodium mordenite (Na-Zeolon), supplied by Norton Chemicals (USA).

Catalyst Poison

Tetramethyl lead (TML) was the primary poisoning agent. As TML is a highly toxic liquid, and will explode violently if ignited, it is stored and supplied in the presence of toluene, the standard concentration being 80% $^{w}/_{w}$ in toluene. n-heptane was used as a substitute for gasoline; the TML/toluene mixture was therefore dissolved in this as the solvent. However, commercial gasoline contains, in addition to lead alkyls,

'scavengers',especially dibromoethane and 1,2-dichloroethane. Therefore, in order to comply with the realistic situation, these scavengers were also added to the poison mixture. Preliminary investigations carried out by Associated Octel Co. Ltd. (AOC) and the English Electric Valve Co. Ltd. (EEV) using similar mixtures, had indicated that lead from TML was probably responsible for the deactivation of the catalysts. These indications were confirmed by carrying out initial poisoning experiments using each of the components of the poisoning mixture separately. In other contexts, it has been shown that dibromoethane is the important poison rather than lead alkyls when noble metals are used as automotive exhaust catalysts (118,119, 120). Because only TML appeared to be responsible for the poisoning action, the poisoning mixture that was used thereafter consisted of n-heptane and TML/toluene. n-heptane, 1,2-dichloroethane and dibromoethane were all obtained from BDH. Tetramethyl lead in toluene (scavenger free), containing 1.58 cm^3 TML per dm^3 n-heptane, was supplied by AOC.

Gases

Compressed air from British Oxygen Co. Ltd. (BOC) was used as the carrier gas for the poison. 1% methane in air was also obtained from BOC, and used as the calibration fuel (i.e. test gas). Nitrogen gas 'white spot grade' was used as the adsorbate for surface area measurement, again supplied by BOC.

2.1 Assay of the Beads

Initial studies of the surface of the compensator beads, VQ1 and VQ3 beads were carried out using a JEM JEOL 100B scanning electron microscope (SEM) with an energy dispersive analysis of X-rays (EDAX) attachment.

2.1.1 Scanning Electron Microscopy

Before examining actual samples, the optimum operating conditions of the microscope (4) were established, as follows:-
The surfaces of a specimen were studied by producing a dark field image, in which a white image was seen against a black background. The accelerating voltage used was 40 kV, with spot-size 3 and condenser aperture 3. Micrographs at magnification x1000 and x3000 were recorded. The filament used did not allow for higher resolution but gave a high beam current and hence a high count rate for the X-ray signal. It was suggested that by reducing the condenser aperture to 4, one could improve the magnification by a factor of between 2 and 3, and still obtain good resolution. This was tried but found to be unsuccessful. Ideally, a different electron gun should be used to improve the magnification by a factor of 10, with still good resolution, and if a still higher resolution is required, one should resort to transmission microscopy and prepare the specimens accordingly. However the above-listed settings together with the filament used, gave an adequate resolution, which allowed the study of most of the surface features of the pellistors. The specimens were mounted on carbon discs to facilitate examination in the microscope, by adhering the bead on to the disc with silver paint. Examination was made with the specimen at fixed angles of either 0° or 30° to the detector to enable comparison of the surfaces of individual beads of the same kind. Photographs of representative areas were taken at magnifications of x1000 and x3000. At magnification x1000, 1 cm was equivalent to 10 μm, so the beam was scanning approximately 1/10 of the bead surface. Charging of the specimen was observed in some cases, but coating was not found to be essential, and was generally avoided. Those specimens that were coated were covered with a thin film of evaporated

carbon and gold, thus not only providing a good conducting surface, but also enchancing the contrast as well. An important disadvantage of coating was that it gave a poor X-ray signal, and elements present in minor quantities could not be detected.

It is known that SEM is a discriminatory technique in the sense that the operator tends to pick up any 'special' or 'odd' features of interest on the surface rather than the common features. Also,the fact that the same bead cannot be used for miscroscopic examination twice, (i.e. before poisoning and after poisoning), makes it difficult to assess if there is any change in the surface structure of any particular bead due to poisoning. The solution to this problem has been to examine numbers of beads and carry out statistical analyses of the surface features. Series of VQ1, VQ3, compensator beads and other prototype beads were therefore examined. In addition, cross-sectional examinations were also undertaken, to discover any revealing internal features. These examinations involved both unpoisoned and poisoned specimens. The micrographs are included in the Results section.

2.1.2 Energy Dispersive Analysis of X-rays

This technique is known as 'electron probe microanalysis', or X-ray microanalysis (122). The principle of the method is as follows: a finely focussed electron beam (electron probe) is directed, or scanned, onto the surface of a sample whose chemical composition is to be examined. The very small volume of material irradiated by the electron beam then emits a complex X-ray spectrum which includes the characteristic wavelengths of the various elements present at the point of impact of the electron beam. Spectrographic analysis of this X-ray spectrum can also permit the respective concentrations of these elements to be determined, but quantitative

work by this technique is time consuming and requires standards of known concentrations and composition prepared in the same way as the sample, and calculations are made complex by the introduction of other correction factors. Also the surface under examination needs to be flat. However rough estimates can be drawn from the intensities of the K, L and M lines, and chemical analyses can then be carried out for accurate determination of trace element concentrations.

Elemental analyses were carried out by this technique in order to determine the distribution of elements under and on the bead surface. Here again the standard operating conditions previously established (section 2.1.1) were maintained in order to obtain comparative data. Since this technique is semi-quantitative and very much dependent on sample geometry, all the spectra were recorded when the electron probe was scanning the front edge of the bead surface with the bead tilted at an angle of 30° to the detector. This arrangement maximised the collection of emitted X-rays, giving a large signal with minimum background interference. The spherical shape and the surface roughness of the bead made it very difficult to carry out even semi-quantitative analyses, but by comparing line intensities of different elements present, a rough estimate of the amount of one element as a comparative percentage of other elements present was obtained. Here again cross-sectional analyses were carried out in order to determine the extent of distribution of elements throughout the bead. Several spot analyses of the surface were also included, which essentially consisted of focussing the scanning beam to a fine spot on the surface and obtaining a spectrum of the elements present in that region only, whilst keeping all other parameters such as angle of tilt, accelerating voltage, spot size, and condenser aperture constant. Comparison of the spectra obtained this way with those obtained when the beam was scanning a large area of surface,

revealed whether the elements on the surface were evenly dispersed or segregated.

Preliminary elemental examinations of the beads prior to poisoning revealed the presence of impurities such as nickel and sulphur. The presence of nickel could be explained as follows from the method of manufacture. The alumina pellet was formed by clipping the prepared platinum coil onto nickel terminals and dipping it in aluminium nitrate solution followed by electrical drying. This process was repeated continually until a pellet of required size was obtained. The nickel contamination therefore arose from gradual dissolution of the termini during the dipping and heating cycles. As the solution of aluminium nitrate aged, the amount of nickel ions in solution increased and these are eventually deposited together with the alumina on the platinum coil; this was evidenced by the fact that cross-sectional analyses of the beads using EDAX showed traces of nickel. Polarographic analyses of beads randomly chosen were also carried out for the presence of nickel; the experimental details and results are given in Appendix V . The presence of sulphur was found to be a storage problem. It was noticed that if compensator beads were kept for prolonged periods, they turned yellow. Elemental analysis by EDAX of these beads showed a substantial amount of sulphur. It is known (68) that sulphur is a potential poison for many catalytic system, but it is unlikely that its contribution towards the deactivation of the present catalysts was at all significant, mainly because the sulphur was a surface deposit from the atmosphere, and readily burnt off when the operating voltage was applied across the Wheatstone bridge circuit. Confirmation that the sulphur was only a surface deposit from the atmosphere was obtained by cross-sectional analyses using EDAX, which showed no trace of sulphur.

In brief, both topographical studies and elemental analyses

using the above-mentioned techniques were carried out for both unpoisoned and poisoned catalyst beads. This procedure provided comparative data for the two cases.

2.2 The Poisoning Rig

A flow diagram of the rig is shown in Figure 9 and a photograph of the actual rig is included as Plate 1. The following items were required for setting up the rig.

Quantity	Items
2	Solenoid valves (Dewrance Controls Ltd.).
1	Regulator reducer valve.
1	Regulator pressure release valve.
4	Needle valves.
4	Rotameters with needle valves (0-1 $dm^3 min^{-1}$).
2	Midget impingers (Quadrant Glass Co. Ltd.).
3	500 cm^3 glass bubblers.
6	PTFE 'O' ring ball joints (Youngs Co. Ltd.).
1	Charcoal column with quickfit screw thread (Fisons).
3	Funnels with B14 glass stoppers and with PTFE taps (Fisons).
3	Glass to metal seals (Jencons).
1	Waterbath.
1	Cylinder of 1% methane/air mixture (British Oxygen Co. Ltd.).
1	Cylinder of compressed air (British Oxygen Co. Ltd.).
3	Pressure gauges, range 0-30 psi.
1	240V timer switch to operate 2 solenoid valves (Electroplan).
1	Honeywell 2-channel recorder, range 0-100 mV.

Key to Figure 9

Y : Glass bubblers containing TML/n-heptane solution

G : Flowmeters

H : PTFE ball joints

K : Funnel with PTFE taps

P : Midget impingers

D : ICl bubbler for exit stream

E : Pellistor blocks

F_1, F_2: Solenoid valves

B : Pressure release valve

A : Pressure reducer valve

R : Drying column (activated charcoal)

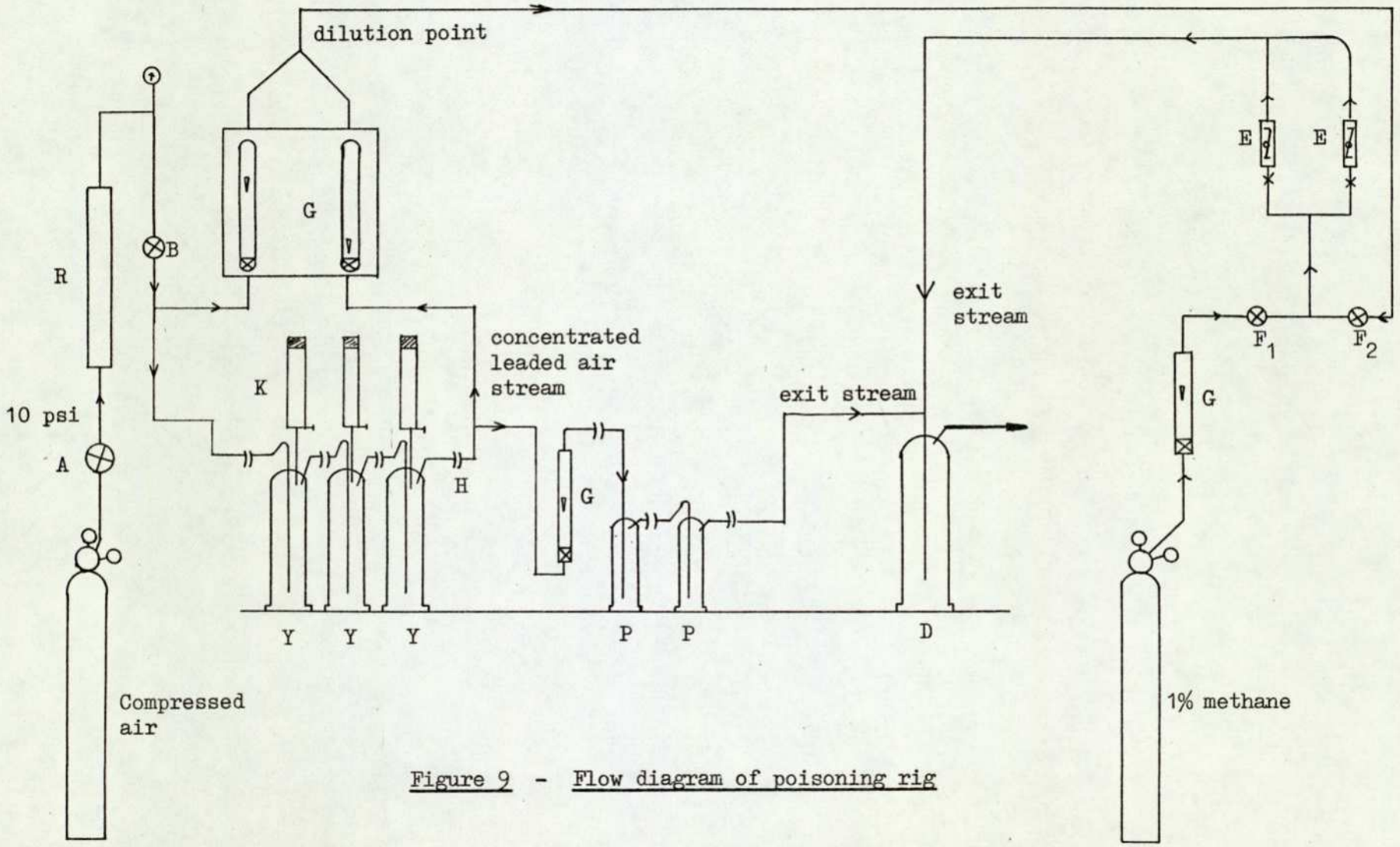

Figure 9 - Flow diagram of poisoning rig

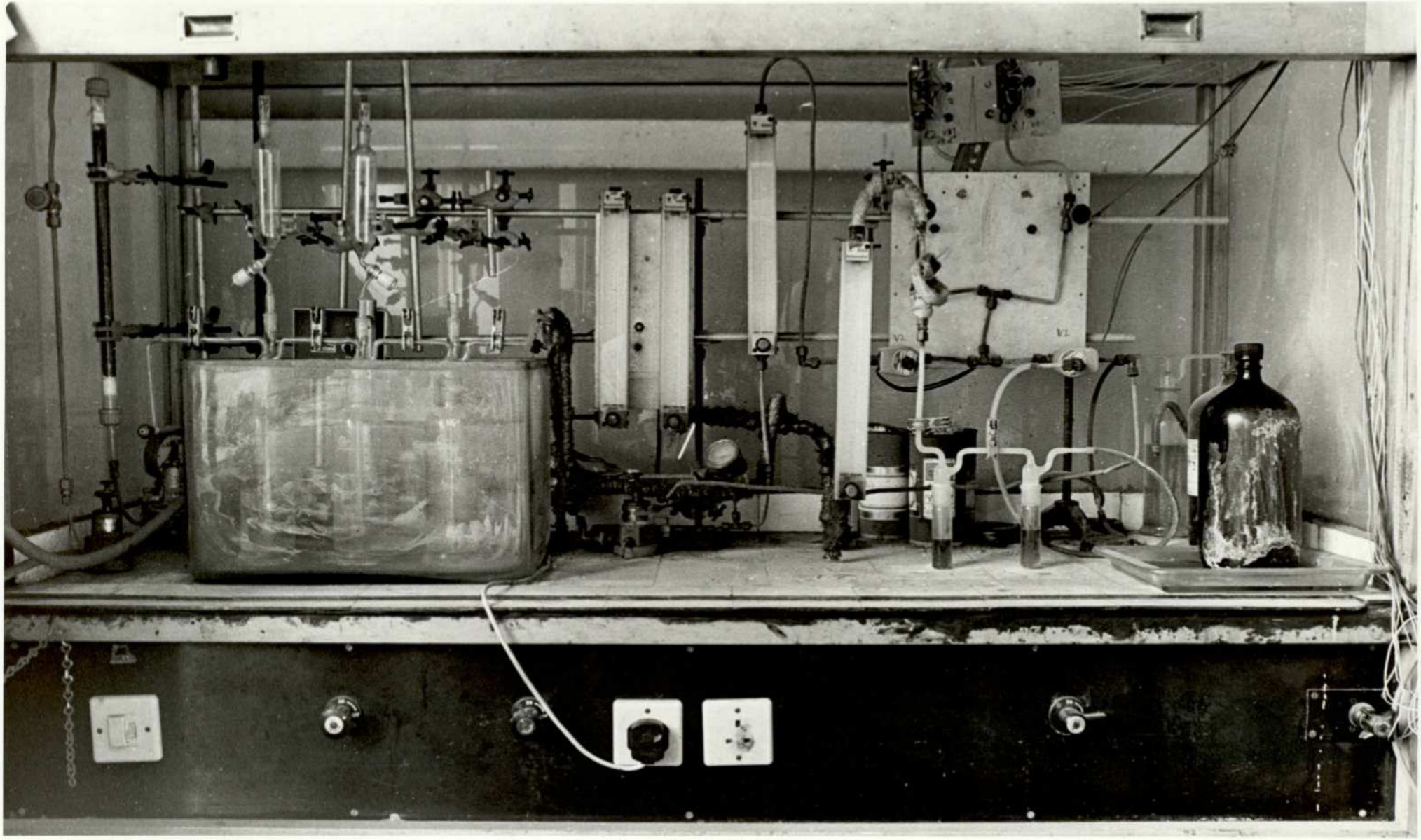

Plate 1 - Poisoning rig

1	Stabilised DC power supply (0-7 V) (Farnell).
1	1 kΩ potentiometer, 10 turn helical type.
6	B14 PTFE seals (Fisons).
3	B19 PTFE seals (Fisons).
2	Pellistor blocks (English Electric Valve Co. Ltd.).
2	Wheatstone bridge circuits (as described in section 1.5.1), mounted on the pellistor blocks (see Figure 10).
	Connecting wires 16/0.2 mm; 4 amp.
	Activated charcoal.
	¼" Simplifix connections.
	¼" Copper pipes, reinforced nylon tubing, and PVC tubing.

PTFE, copper and glass were used for any part of the flow system which would be in contact with the leaded air stream; lead is adsorbed on almost any material except for those mentioned above (123). PVC tubing was used for the exit stream, and was burnt after use. PTFE seals and PTFE 'O' rings were used throughout instead of grease, because the latter poisons the detectors rapidly, especially if the grease is silicone based. The bubblers contained solutions of TML in n-heptane ($0.36\ cm^3\ dm^{-3}$) at room temperature, through which air was bubbled. The stock solution of TML in n-heptane was stored in a brown winchester bottle in the fume cupboard which had been specially modified for use with lead alkyls. The amount of lead in the air stream was determined by trapping the lead in iodine monochloride solutions contained in the midget impingers. Analysis of the iodine monochloride solution gave integral values of lead concentration, expressed as mg per cubic metre of air. The air was supplied from the compressed air cylinder, after being fed through an activated charcoal filter at 70 kPa back pressure. The activated charcoal was packed

in a vertical tube, with glasswool used to retain the charcoal in the tube and so prevent entry into the pipework. The air pressure was reduced to 15 kPa above atmospheric pressure before entering the bubblers.

The variable DC supply was assembled as shown in Figure 10 and the bridge set at 2 V for VQ1 and 2.5 V for VQ3 detector beads. A zeroing potentiometer having a resistance of approximately 1 kΩ was connected as shown, using a 10-turn helical wire. All electrical connections were soldered. The elements were mounted in blocks with the compensator at the gas inlet. With air flowing through the blocks at 0.5 $dm^3 min^{-1}$, and the bridge voltage set at an appropriate value, first the zeroes were recorded, then the sensitivity of the detector bead was checked with a 1% methane in air (flowrate also set at 0.5 $dm^3 min^{-1}$, with a back pressure of 35 kPa). Solutions of TML in n-heptane, as obtained from Associated Octel Co. Ltd. (see section 2) were further diluted with n-heptane to the desired concentration. Early experiments (unpublished communications, AOC) had shown that an air stream containing concentrations of TML in air of between 20 and 25 mg m^{-3} would poison the element in a matter of hours; therefore this concentration seemed an appropriate one to use for this study. Sample calculations on expected lead concentrations in the atmosphere above such a solution are given in detail in Appendix III. Solution containing 0.36 cm^3 of TML per dm^3 n-heptane was used throughout this project. On bubbling air through a series of containers holding this solution, the resulting leaded air stream was diluted with 'clean' air in a volume ratio of 1:4 respectively. A convenient choice of flowrates was 400 cm^3 of 'clean' air to 100 cm^3 of leaded air. The resulting leaded air mixture was next fed into the detector blocks to poison the pellistors. The leaded air stream (before the dilution point) could also be bubbled through 2 midget impingers containing 0.2 mol dm^3 iodine monochloride solution in order to trap the

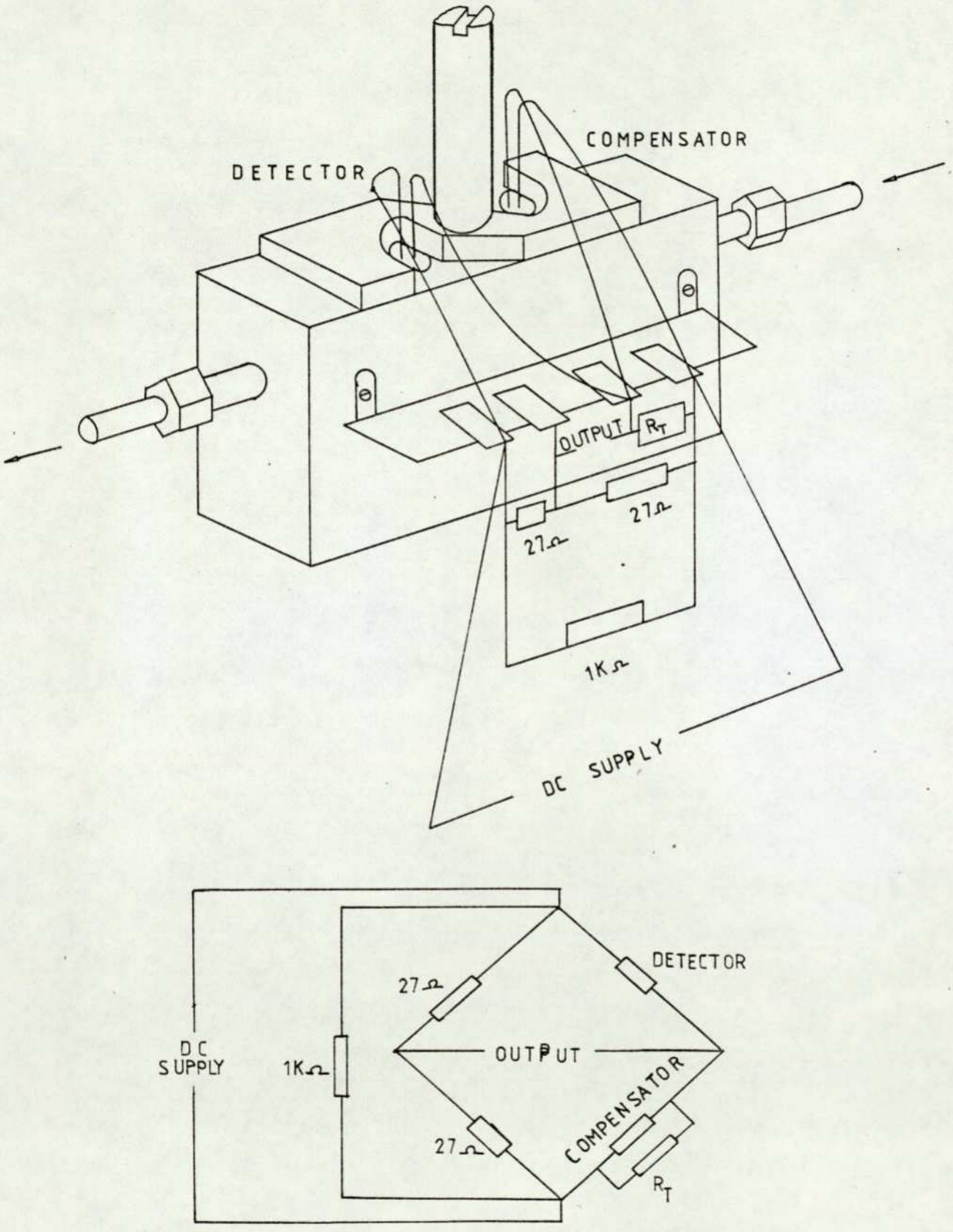

Figure 10 - Pellistor block with bridge circuitry

lead. Analysis of the leaded iodine monochloride solution gave an indication extra to its calculation of the concentration of lead in the stream.

When the rig was first built, air was passed for two days, followed by pure n-heptane for 24 hours to clean the system. A 'dummy' run was next carried out by placing VQ1 pellistors in position and monitoring alternatively zero readings with air only flowing, followed by signals arising from the 1% methane air mixture. These alternate checks on sensitivity and zero drift were carried out until the zero drift ceased, which was indicative of the system being clean and free of inhibitors. The rig was then considered ready for poisoning runs.

2.2.1 Safe Handling of Tetramethyl Lead

The safety code of practice laid down by the manufacturer (AOC), was rigidly adhered to. All handling of TML was carried out in glass trays in the fume cupboard; the working top of the fume cupboard itself was covered with special glass tiles fixed with a non-adsorbent resin cement. High density PVC gloves were worn when pouring solutions. All glasswares were decontaminated after use, this decontamination process itself being carried out in the fume cupboard. A solution of 10% sulphuryl chloride in kerosene was prepared as the decontaminating agent. Being a strong oxidising agent, it converts tetramethyl lead to lead chloride. (Other oxidising agents such as bromine may be used, but the reactions are sometimes too violent. Concentrated nitric acid must never be used, as it reacts explosively). The sulphuryl chloride/kerosene solution was poured into the contaminated container and reaction was allowed to take place ($\sim$30 min); the residue was discarded and the glassware washed thoroughly with 'teepol'. The decontaminating agent was kept in a dark winchester

bottle in the fume cupboard, away from the TML residue bottle. The sulphuryl chloride/kerosene solution underwent slow decomposition, usually lasting for 4 weeks; the bottle must be kept uncorked as hydrogen chloride gas is emitted continuously. Any TML residue or contaminated material was always kept in the fume cupboard and only disposed of by burning in an open air space. As a further precautionary measure, all exit streams from the rig were bubbled through iodine monochloride solution before venting into the atmosphere, in order to trap as much lead as possible.

2.2.2 Iodine Monochloride Solution

When TML vapour is bubbled through iodine monochloride solution (0.2 mol dm^{-3}), the lead alkyl is converted to lead chloride. The concentration of lead in the air can be determined by analysis of the solution. Iodine monochloride solution was prepared according to Andrews' Reaction (124), using analytical grade reagents only, as follows

$$KIO_3 + 2\,KI + 6\,HCl \longrightarrow 3\,ICl + 3\,KCl + 3\,H_2O$$

112 cm^3 of 25% (w/v) potassium iodide solution were mixed with an equal volume of hydrochloric acid (specific gravity 1.18 g cm^{-3}), and the resulting solution was allowed to cool to room temperature. 18.7 grams of potassium iodate were added slowly with constant stirring until an orange clear solution was obtained, which was diluted to 250 cm^3 with distilled water to give a 1 mol dm^{-3} solution. This solution was kept in a dark bottle, and diluted five times to give 0.2 mol dm^{-3} iodine monochloride solution.

2.2.3 Lead Analysis

There are several well established analytical methods for lead, viz:-

(i) titration using ethylene diamine tetra-acetic acid (EDTA)

(ii) polarography

(iii) colorimetry (125)

(iv) gas liquid chromatography (126-129)

(v) atomic absorption spectrophotometry (130)

Sharpiro and Frey (131) have compiled a chapter on methods of lead analysis. The volumetric analysis is best suited for high concentrations of lead and was consequently not used. The polarographic method was unsuitable as the dropping mercury electrode reacted with the iodine monochloride, forming a black coating on the electrode which was suspected to be a chloride of mercury. The colorimetric method, (commonly known as the single extraction mixed colour method (SEMC)) with dithizone was avoided too, because the procedure proved to be too lengthy and very tedious. Atomic absorptiometry was found to be the most rapid, sensitive and specific method. It was adopted throughout this project. The chromatographic method was not tried as it is really a method applied for analyses of mixed lead alkyls on a qualitative, or at best, semiquantitive basis.

2.2.3.1 Analysing for Lead in ICl Solution by Atomic Absorption Spectrophotometry

The lead vapour was bubbled through the 0.2 mol dm^{-3} iodine monochloride solution contained in the midget impingers, where all the lead was trapped. The instrument used was a Perkin Elmer 290B with an air-acetylene flame oxidising (lean, blue), using a slit setting of 0.7 nm. The absorption line for lead occurs at a wavelength of 283.3 nm. The

following solutions were prepared:-

A. A master stock solution

1000 µg cm : 1.59848 g lead nitrate was dissolved in 1 dm^3 deionized distilled water.

B. A blank solution

Diluent : 50 cm^3 of 0.2 mol dm^{-3} iodine monochloride solution were diluted to 500 cm^3 with deionized distilled water.

C. Working standards

10 µg cm : 1 cm^3 of stock solution A was diluted to 100 cm^3 with blank solution B.

20 µg cm : 1 cm^3 of stock solution A was diluted to 50 cm^3 with blank solution B.

30 µg cm : 3 cm^3 of stock solution A were diluted to 100 cm^3 with blank solution B.

D. Sample solutions

The leaded air stream was bubbled through two midget impingers containing 25 cm^3 0.2 mol dm^{-3} iodine monochloride at a flow rate of 200 cm^3 min^{-1} for 1, 2 or 3 hours. The leaded iodine monochloride solutions were diluted to 500 cm^3 with deionized distilled water, to bring the solution to a similar strength to the blank and the standards. The amount of lead per cubic decimetre of air was then calculated from the average weight of lead collected per hour over the three samples. From this value the amount of lead reaching the pellistors after the dilution point was calculated.

2.3 A Concise Description of the Poisoning System

Figure 9 shows a flow diagram of the rig. It consisted essentially of three glass bubblers containing concentrations of TML in n-heptane of 0.36 $cm^3\ dm^{-3}$ (see Appendix III) at room temperature, through which air was bubbled at a constant flow rate. Part of the exit stream of lead vapour was bubbled through 0.2 mol dm^{-3} iodine monochloride solution, analysis of which gave the concentration of lead (described above). The remainder of the exit stream of lead vapour was diluted with air in the ratio of four parts of air to one of lead vapour. The diluted leaded air stream was fed to the pellistor blocks at 500 $cm^3\ min^{-1}$, via a solenoid valve controlled by a timer switch. 1% methane in air was used as a calibration standard to check the sensitivity of the beads. Here again the flow rate was set at 500 $cm^3\ min^{-1}$, the flow also being controlled by a solenoid valve, and the time switch. A two-channel recorder of range 0-100 mV was used to monitor the out of balance voltage across the bridge. The pellistors were powered by a dc constant voltage unit.

The poisoning runs involved exposing the beads to TML/n-heptane/air mixtures for 40 min, after which the sensitivity to 1% methane was monitored for 20 min. The alternate procedure was then continued for as many hours as necessary. Since two pellistor blocks were incorporated in the system. each run provided two sets of readings. All pellistors were poisoned with TML/n-heptane/air mixtures containing 20-25 mg m^{-3} of lead as TML.

VQ1, VQ3 and also a series of other beads which had been modified in various ways to improve poison resistance were tested. The same basic catalyst mixtures found in VQ1 and VQ3 beads were used in the modifications. Initial modifications involved depositing a layer of alumina on top of the conventional VQ1 or VQ3 beads (these were labelled VQ1/VQ7 and

VQ3/VQ9 respectively). These modifications were followed by LD1 and LD1/LD7 beads. The former of these consisted of the carrier deposited on the coil from a mixture of both aluminium nitrate and a weak solution of palladium catalyst, followed by the usual platinum/palladium catalyst, followed by the usual platinum/palladium impregnation of the conventional VQ1 type bead. The latter modification was LD1 detector with a further layer of alumina added. Still further modifications were the LD1/LD$^{3}/_{1}$, which were LD1 beads with a homogeneous mixture of alumina and the VQ1 catalyst composition, and the LD1/LD$^{3}/_{1}$/LD7, which were LD1/LD$^{3}/_{1}$ beads with an external alumina coating. Numbers of each of the above types of detector beads were tested to determine their poison resistance, then further poisoning experiments involving beads containing zeolites were carried out. These latter are described in detail in the next section.

2.4 Zeolite Coated Beads

The reasons for considering zeolites were introduced in section 1.8. The zeolite used was hydrogen mordenite, which was prepared from synthetic sodium mordenite (Norton Na-Zeolon). More than one type of hydrogen mordenite was used, viz:-

(i) hydrogen mordenite prepared from ammonium mordenite, and

(ii) dealuminated hydrogen mordenites which were prepared by acid treatment of sodium mordenite. Acid treatment resulted in samples of different levels of aluminium deficiency with larger pores.

2.4.1 Preparation of Hydrogen Mordenite via Ammonium Mordenite

A 200 g sample of sodium mordenite was exchanged with

separate aliquots of 1 dm^3 of 1 mol dm^{-3} ammonium chloride solution four times. For each exchange the zeolite was equilibrated with the ammonium chloride solution at 60°C overnight. Finally the zeolite samples were washed four times with distilled water, and dried in an oven at 60°C. The ammonium mordenite thus obtained was stored in a desiccator over saturated ammonium chloride solution, so that the zeolite could take up an equilibrium uptake of moisture (this takes between one or two weeks). Thermogravimetric analyses (TGA) of the sample were undertaken in both air and nitrogen, and chemical analyses. In order to prepare the hydrogen form, the sample was heat-treated at 450°C over nitrogen for 24 hours; this procedure drove off the ammonia leaving hydrogen mordenite, yellowish grey in colour.

2.4.2 Thermogravimetric Analyses

A Mettler 'Thermoanalyser 2' thermobalance was used to measure thermal stabilities. This gave a continuous record of temperature, weight of sample, rate of weight change. In addition, a means of accomplishing differential thermal analysis (DTA) was incorporated. A flow of air or nitrogen (60 cm^3 min^{-1}) through the balance housing and past the sample removed the gaseous products as they were formed. The maximum sensitivity of the instrument for TGA was a change in weight of 0.02 mg, full scale deflection being 1 mg. The sample size used was normally 50 mg. From the recorder traces obtained the temperature range over which ammonia was driven off could be found.

2.4.3 Hydrogen Mordenite - dealuminated forms

This form of hydrogen mordenite is in effect aluminium

deficient, and is prepared by acid treatment of sodium mordenite. Two reactions occur on acid treatment (132). The first is an ion exchange reaction, in which sodium ions are replaced by hydronium ions. Concomitant with the ion exchange reaction, the acid treatment leaches out aluminium from the aluminosilicate framework, giving degrees of aluminium deficiency which are a function of the strength of acid used. Two samples of 100 g of sodium mordenite were exchanged with 5 mol dm^{-3} hydrochloric acid five times, followed by washing with distilled water (five times). The slurry was then dried in an oven at 60°C. The dealuminated hydrogen mordenite thus obtained was also stored in a desiccator over ammonium chloride solution.

2.4.4 The Coating Method

A series of prototype beads were produced using the above described two different forms of hydrogen mordenite. These beads were made by coating the conventional VQ1 and VQ3 beads with mixtures of the zeolite and kaolin (purchased from BDH), the latter being added to act as a binder. Ratios of H-MOR to kaolin of 8:2, 6:4 and 4:6 were tested; the optimum ratio was found to be 6:4. For each preparation a slurry containing 10 g of mixture in 66 cm^3 of water was prepared. The beads were then coated by placing a drop of the slurry onto the bead surface using a syringe, followed by slow drying, which was usually achieved by applying a gradually increasing voltage across the bead. This process was repeated until the whole surface was evenly covered. The weight of zeolite coating ranged between 0.5 - 0.7 mg. In order to compare the hydrogen and dealuminated mordenites with sodium mordenite, poisoning runs were also carried out for VQ1 and VQ3 specimens which had been coated with sodium mordenite

and kaolin in the same ratios as described above. In addition, beads coated with 100% kaolin, and with 100% dealuminated form of hydrogen mordenite were examined, in order to assess the relative contributions of the zeolite and clay to the overall poison resistance.

All the zeolite-coated beads were poisoned using similar procedures to their non-zeolite prototypes (section 2.3). Their sensitivity to 1% methane were also checked in a manner earlier described (section 2.3). After several hours of exposure to the poisoning mixture, the beads were examined by SEM and EDAX. The zeolite coatings were difficult to examine by SEM because the zeolite coatings proved so fragile that as soon as the bead was removed from the post for mounting on the carbon disc, the zeolite coating crumbled to a powder. Only a few beads were examined successfully. Similarly, analyses by EDAX were very difficult; to analyse quantitatively for the lead therefore, atomic absorption spectrophotometry on dissolved samples was employed.

2.4.5 Analysis of Lead in the Poisoned Pellistors

Six VQ1 beads coated with ratios of 6:4 hydrogen mordenite (dealuminated) : kaolin were poisoned for 23½ hours each using lead concentrations (as TML) in air of 20-25 mg m^{-3} . The coated beads were then dissolved in a platinum crucible by adding two drops of water, two drops of sulphuric acid and 10 cm^3 of 40% AR hydrochloric acid. The solution was evaporated to dryness in a fume cupboard and the process of dissolution followed by evaporation was repeated until all the beads had dissolved leaving only the platinum coil. The residue was boiled in 1% nitric acid. Finally the lead concentration was determined by atomic absorption spectrophotometry, using a Perkin Elmer 370 instrument, with an air-acetylene flame, oxidising

(lean, blue), and with a slit setting of 0.7 nm. The absorption line for lead occurs at a wavelength of 283.3 nm. The amount of lead in the sample solution was deduced by comparisons with working standards.

2.4.6 Characterisation of Zeolites

The zeolites used were characterised by both chemical analyses and surface area determinations. In this section the methods of analysis are treated in detail.

2.4.6.1 Water

A weighed aliquot of ammonium mordenite in a platinum crucible was heated for thirty minutes at 1000°C. The weight loss gave the weight of water, ammonia (and ammonium as ammonia) in the zeolite.

Let mNH_3 be meq hg^{-1} of ammonia in zeolite. (hg = 100 g)

Let mNH_4^+ be meq hg^{-1} of ammonium in zeolite.

$$\text{The w/w percentage } NH_3/NH_4^+ = \frac{mNH_3,\ mNH_4^+ \times 17{,}18}{1000}$$

NH_4^+ content was expressed as $(NH_4)_2O$, viz:-

$$\text{w/w percentage } (NH_4)_2O = \text{w/w \% } NH_4^+ \times \frac{50}{36}$$

Then percentage H_2O = w/w % weight loss - (w/w % NH_3 + w/w % $(NH_4)_2O$)

and hence

$$m_{H_2O} = \frac{\text{w/w \% } H_2O}{18} \text{ mol } hg^{-1}$$

2.4.6.2 Ammonia

Reagents: standard hydrochloric acid ampoules (0.1 mol dm^{-3}).

20% sodium hydroxide solution,

standard borax solution (0.5 mol dm^{-3} of sodium tetraborate decahydrate),

50 cm^3 of standard hydrochloric acid were pipetted in a volumetric flask. A weighed sample of the ammonium mordenite was placed, with distilled water washings, into the flask of the Kjeldahl apparatus. After addition of small quantity of boiling chips to the flask to assist boiling, the apparatus was connected up, care being taken to eliminate leaks. About 50 cm^3 of the 20% sodium hydroxide were introduced into the Kjeldahl flask, and the suspension was boiled for thirty minutes, all expelled ammonia and condensate being trapped in the volumetric flask containing the standard hydrochloric acid. After the thirty minutes had elapsed, the flask was lowered away from the condenser, and only then was the heat turned off. This was to stop the hydrochloric acid being sucked back into the Kjeldahl apparatus.

Next, the hydrochloric acid was titrated against the borax solution. Analyses were carried out in duplicate. For the titrations, methyl red was a suitable indicator. In addition, 50 cm^3 aliquots of the standard hydrochloric acid were titrated directly against the borax solution.

Let a be the volume (cm^3) of borax required to neutralise the hydrochloric acid in the Kjeldahl analysis.

Let b be the volume (cm^3) of borax required to neutralise 50 cm^3 of 0.1 mol dm^{-3} hydrochloric acid.

Let g be the weight (g) of zeolite taken.

Let m be the concentration of standard hydrochloric acid. Then,

$$m_{NH_3,\ NH_4^+}/\text{mol hg}^{-1}\text{(zeolite)} = \frac{5000m(b-a)}{bg}$$

2.4.6.3 Silicon Analyses

After ignition of the zeolite sample (section 2.4.6.1), the weighed residue was treated with two drops of distilled water, 1 drop of concentrated sulphuric acid and 20 cm^3 of 40% hydrofluoric acid. The solution was evaporated to dryness on a hotplate, then ignited. The process was repeated until the ignition residue gave a constant weight. The difference in weight of the ignited sample before and after hydrofluoric acid treatment was taken to be equal to the weight of silica originally present in the sample, since it can be assumed that the ignition rendered other metals (sodium and / or aluminium) in the oxide form before and after.

2.4.6.4 Aluminium

Aluminium was determined by a rapid and accurate titrimetric method (133). The aluminium was first extracted and dissolved according to the procedure outlined below.

Reagents: 1,2-cyclohexylenedinitrilo tetraacetic acid (CDTA) 0.05 mol dm^{-3},
standard zinc solution 0.05 mol dm^{-3},
xylenol orange (aqueous solution) as indicator,
hexamethylenetetramine (Hexamine) for pH adjustment,

The aluminium was extracted by a fusion method. A sample of the zeolite was weighed (W_1) in a platinum crucible, and five times this weight of a potassium carbonate/sodium carbonate fusion mixture was added and intimately mixed with the zeolite using a glass rod. The crucible was partially covered with a platinum lid, and heated gently at first, and then more strongly to $\sim$ 1000°C for 20 minutes using Meker burners. The crucible was allowed to cool below red heat until the melt had just solidified, then cooled rapidly by immersing the outside wall of the crucible in a shallow bath of distilled water. The crucible was placed on its side, with the lid, in a porcelain dish, which was half-filled with water ($\sim$30 cm^3).

The dish was next covered with a clock glass, and concentrated hydrochloric acid was added ($\sim$30 cm^3). When effervescence had ceased, the acidity was tested and more acid was added if the solution was alkaline. After warming over a steam bath for one hour, the clock glass was removed and washings from the glass was transferred to the dish. 1 cm^3 of concentrated sulphuric acid was added and the suspension allowed to evaporate to complete dryness over a steam bath, the crucible and lid being removed, cleaned and all residues added to the porcelain dish as soon as possible after evaporation had commenced. 30 cm^3 of 1:1 hydrochloric acid were added to the dry residue with a few drops of concentrated sulphuric acid, and the suspension was again evaporated to dryness. Finally 30 cm^3 of 5% hydrochloric acid were added to the residue and the suspension digested on the steam bath for 10 minutes then filtered hot through a No. 42 Whatman filter paper. The precipitate was washed thoroughly with hot 5% hydrochloric acid, followed by distilled water. The filtrate and washings was made up to 250 cm^3 with 5% hydrochloric acid, and retained for titration.

To the acid sample an excess of 0.05 mol dm^{-3} CDTA was added. The pH was adjusted to between 5.5 and 6 with hexamethylenetetramine. (If the sample was too acid and required more than 2 scoops of buffer ($\sim$8 grams), the pH was then adjusted with dilute ammonia. If aluminium was precipitated because of insufficient CDTA during the pH adjustment, 1:1 nitric acid was added to dissolve the precipitate, and more CDTA was added followed by adjustment of the pH). 5-6 drops of xylenol orange was added as indicator, the excess CDTA was titrated with standard 0.05 mol dm^{-3} zinc solution. The colour changed from lemon yellow to intense red at the end-point.

Let V_1 be volume of CDTA solution added of molarity M_1,

Let V_2 be volume of zinc solution used of molarity M_2,

Let V_x be volume of aluminium solution used,

then

$$\frac{(V_1 - V_2)M_1 \times \text{Atomic wt. of Al} \times V_x}{1000\ V_x} = \text{Weight of aluminium } (W_2)$$

$$\% \text{ w/w aluminium} = \frac{W_2}{W_1} \times 100$$

2.5 Surface Area Determinations

Introduction

The determination of the specific surface area and other surface properties is an essential requirement of any study of catalysis, and this is particularly true in the present case, as some postulated mechanisms of catalyst poisoning involve changes in surface properties (98). For this reason a significant proportion of the time spent on experimental work was devoted to the construction and operation of different surface area apparatus which operated on the principle of nitrogen adsorption. The determination of surface properties of catalyst is frequently achieved by the use of nitrogen adsorption method. A very common adsorption method, which is a static one, relies on determining the quantity of vapour adsorbed and desorbed from a catalyst at liquid nitrogen temperature as a function of the relative pressure of nitrogen above the sample. Detection can be by observing either (or both) weight and volume changes. This procedure enables a complete adsorption-desorption isotherm to be obtained. From this information, the surface area may be determined using the method based on the now famous work of Brunauer, Emmett, and Teller (BET), (134)

or the "Point A" or "Point B" method (135). The pore distribution may be determined using a method based on the Kelvin equation (136-138) or using a mercury porosimeter (139).

The fundamental assumption of the BET theory is that the forces active in the condensation of vapours are also responsible for the binding energy in multimolecular adsorption. By equating the rate of condensation of gas molecules on an adsorbed layer to the rate of evaporation from that layer, and summing for an infinite number of layers, the following expression is arrived at:-

$$\frac{p}{V_a(p_o - p)} = \frac{1}{V_m c} + \frac{c - 1}{V_m c} \cdot \frac{p}{p_o}$$

where V_m is the volume of gas (cm^3 at N.T.P) able to cover the whole surface of adsorbent with a unimolecular layer of the gas (monolayer capacity).

V_a is the volume of gas adsorbed at pressure p (cm^3 at N.T.P).

p_o is the saturation pressure of the adsorbate.

p is the equilibrium pressure.

c is a constant given by $c = A \exp \frac{E_1 - E_2}{RT}$

$E_1 - E_2$ being the difference between the heat of adsorption of the first layer and the heat of the second and subsequent layers, and A, the preexponential term, is a function of the adsorption and desorption rate constants.

By plotting the function $\frac{p}{V_a(P_o - P)}$ against p/p_o the so-called BET plot is obtained. From the slope, $\frac{c-1}{V_m c}$, and the intercept, $\frac{1}{V_m c}$, the monolayer capacity can be obtained, since

$$V_m = \frac{1}{\text{slope} + \text{intercept}}$$

The BET equation is not applicable to Type I, IV, V isotherms, and zeolites give Type I, so with these the Point A or Point B methods are applicable.

2.5.1 Methods of Measuring Surface Area

The methods available for surface area determinations can be classified in 2 main catergories, viz:- the dynamic method and the static method. Both have been used most frequently and successfully. The dynamic method, that was initially investigated, utilizes the same principle of operation as the static method, but differs in the manner of obtaining the adsorption isotherm. The dynamic method, more commonly known as the continuous flow gas chromatographic technique, was employed as follows. Nitrogen was passed over the sample, and the relative pressure was varied by dilution with helium. The amount of nitrogen adsorbed or desorbed over a catalyst sample was determined by concentration measurements of the exit gas using a microkatharometer detector. This method was introduced by Nelson and Eggertsen (140) and later improved by other workers (141, 142). It is claimed that with this technique, surface area ranges between 0.1 $m^2 g^{-1}$ to 70 $m^2 g^{-1}$, or larger, can be measured. It was tried for the detector beads but was found to be unsuccessful. A description of the apparatus and method used has been given by Bucknell (104), who improved the technique for low surface area measurements; however the main reason for the failure in this present work was due to the beads being of very much lower surface area than that which had been previously

employed (104), which meant that the amount adsorbed was very small, and hence sample loops of very small volume were required for calibrating the katharometer. These loops were not available, and since the number of sample beads were also only available in a limited quantity the problem could not be overcome by using a very large number of beads. Consequently this method was unsuitable.

Static methods, whether volumetric or gravimetric, operate on the same principle, except that the former measures gas volume changes as a function of pressure, whilst the latter measures weight changes. A volumetric method was used for large surface area measurements, especially the zeolites. The instrument employed was a Carlo Erba 1800 series absorptiometer,which can measure surface areas ranging up from 1 $m^2 g^{-1}$. This method was obviously not sensitive enough to measure the surface area of the detector beads. For these, the only method that gave reasonably accurate results was a gravimetric one, using a Cahn Vacuum Electrobalance, which permitted the measurement of very low surface areas. The quoted sensitivity of the Cahn Balance was a minimum detectable weight change of sorbate gas of $\Delta w = 10^{-7} g$; normally, the weight changes obtained in this work were two orders of magnitude higher, thus yielding satisfactory results.

2.5.2 The Gravimetric Method and Modification

The use of a vacuum microbalance for obtaining adsorption isotherms was first reported by McBain (143) in 1926 and most textbooks on the subject give detailed descriptions of his apparatus, illustrating the principles of the method, which are still basically adhered to to-day. References 144,145 and 146, all on vacuum microbalance techniques, were

found to be particularly helpful.

The original BET work measured the volume of the monolayer V_m ; in the gravimetric method, a slight modification is needed in the mechanics of the calculation. V_a and V_m are replaced by M_a and M_m respectively, so that the mass of the monolayer is determined. The specific surface area (SSA) is then calculated as outlined below.

Calculation of Specific Area (SSA) from the Monolayer Capacity

Let M = molecular weight of adsorbate gas,

N = Avogadro's Number (6.023×10^{23} mol^{-1}),

W = mass of sample,

a = cross-sectional area of an adsorbed molecule,

then using the value of M_m found from the BET plot, the SSA is given by

$$\Sigma \ /m^2 \ g^{-1} = \frac{a \ N \ M_m}{M.W}$$

Values of the cross-sectional area 'a' may be obtained from the relation (147)

$$a = 4 \times 0.866 \left(\frac{M}{4.2 \ N.d} \right)$$

$$a = 1.5296 \left(\frac{M}{d} \right)$$

where M = molecular weight, N = Avogadro's Number, d = density of adsorbate. This equation yields values of 1.62×10^{-19} m^2 if the liquid density value of nitrogen is employed, or 13.8×10^{-19} m^2 if the calculations are based on the solid density. The value of 15.4×10^{-19} m^2 gave best correlations, and Harkins and Jura (148,149) have shown that this latter figure is most probable. Livingston (150) has provided further evidence for the acceptance of 15.4×10^{-19} m^2 . The overall impression of the

writer, gained from a close examination of the volume of literature available, is that there is a good case for accepting the value of 15.4×10^{-19} m^2, but continuous use of $a = 1.62 \times 10^{-19}$ m^2 by most workers has gradually led to its general acceptance, in the interest of more reliable comparison. The error of about 5% represents the maximum limit of experimental error in a properly conducted BET determination.

2.5.2.1 The Apparatus

Figure 11 shows a schematic diagram of the gravimetric apparatus, and a picture of the actual set-up is also included (Plate 2). The assembly was constructed of Pyrex glass except for the sample tube, which was of silica glass, and ground glass cones and sockets were used wherever possible. The whole system can be divided into 3 stages.

(a) The Electrobalance

The particular balance employed was a Cahn Instrument Electrobalance RG model, which has a maximum adsorbate capacity of 1 g and an ultimate sensitivity of the order of 0.1 μg on its most sensitive range. The electrobalance is based on the null-balance principle, which is generally accepted as being the most accurate and reliable method of measurement. When the sample weight changes, the beam tends to deflect momentarily. The flag moves with it, causing a change in quantity of light reaching the phototube, and hence the phototube current. (In actual use the bottom of the flag is above the bottom of the phototube compartment opening, and not as shown in the simplified illustration - Figure 12). The phototube current is amplified in a 2 - stage servo amplifier, and the enlarged signal is applied to a coil attached to the beam, which is in a magnetic field. The current in the coils then acts like a dc motor, exerting a force on the beam which tends to restore it to the original balance position. Thus the change in electromagnetic force necessary to maintain

Key to Figure 11

A,B,C	:	Weight loops
A_1,C_1	:	Hangdown tubes
T_1	:	Gas storage reservoir & cooling trap
T_2	:	Cooling trap
T_3	:	Cooling trap
F_1	:	Furnace
G_2	:	Mercury manometer
P_1,P_2	:	Pirani heads
P_3	:	Penning head
D.P	:	Diffusion pump
Z	:	Rotary pump
B1,B2	:	Gas storage bulbs
Q	:	Flowmeter
R	:	Needlevalve
D,E,E_1,G H,K,L,M, N,S,J,P,T	:	High vacuum taps
V	:	Baffle valve
U	:	Roughing valve
W	:	Backing valve
Y	:	Air admittance valve

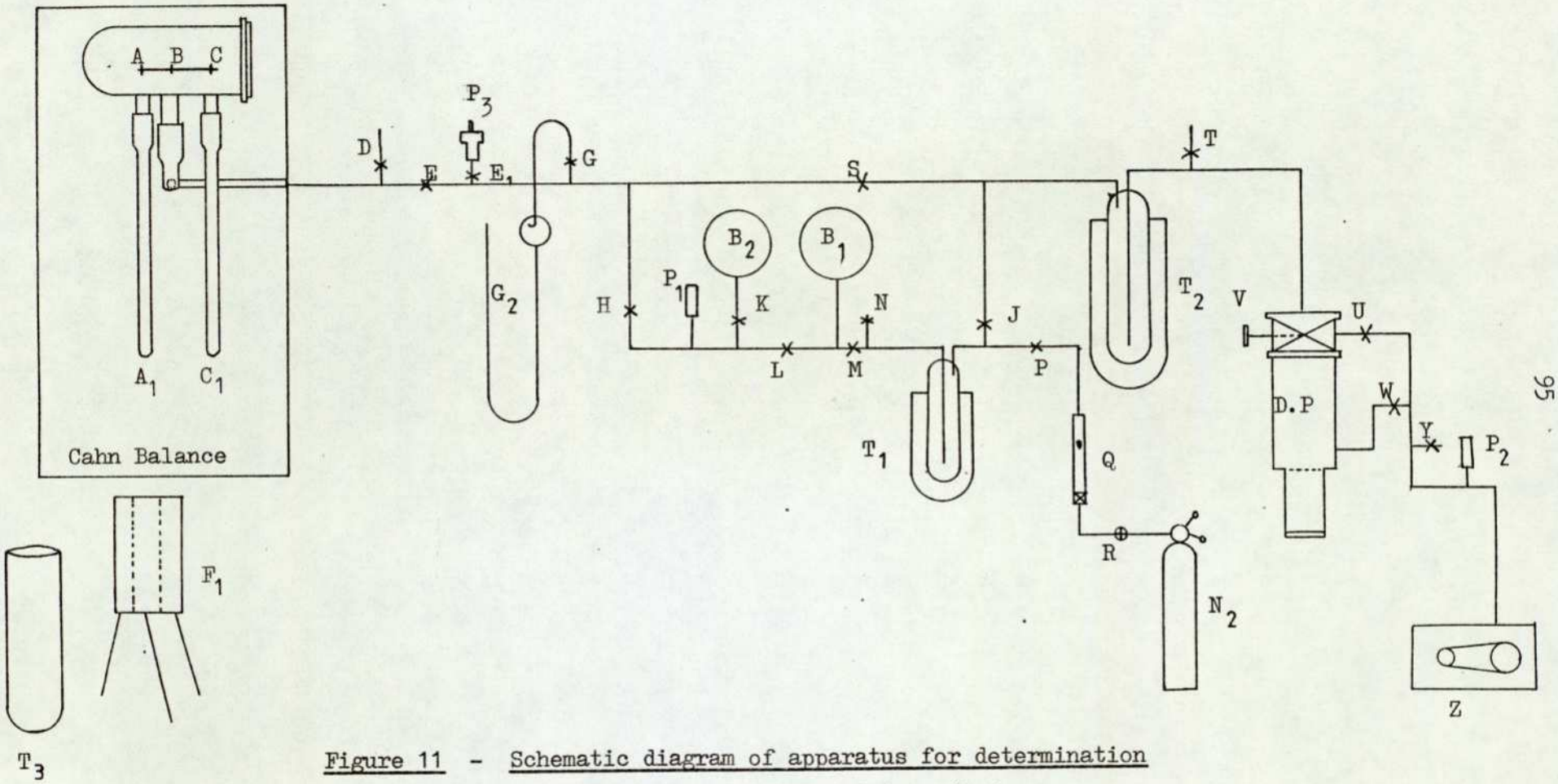

Figure 11 - Schematic diagram of apparatus for determination of surface area by gravimetric method

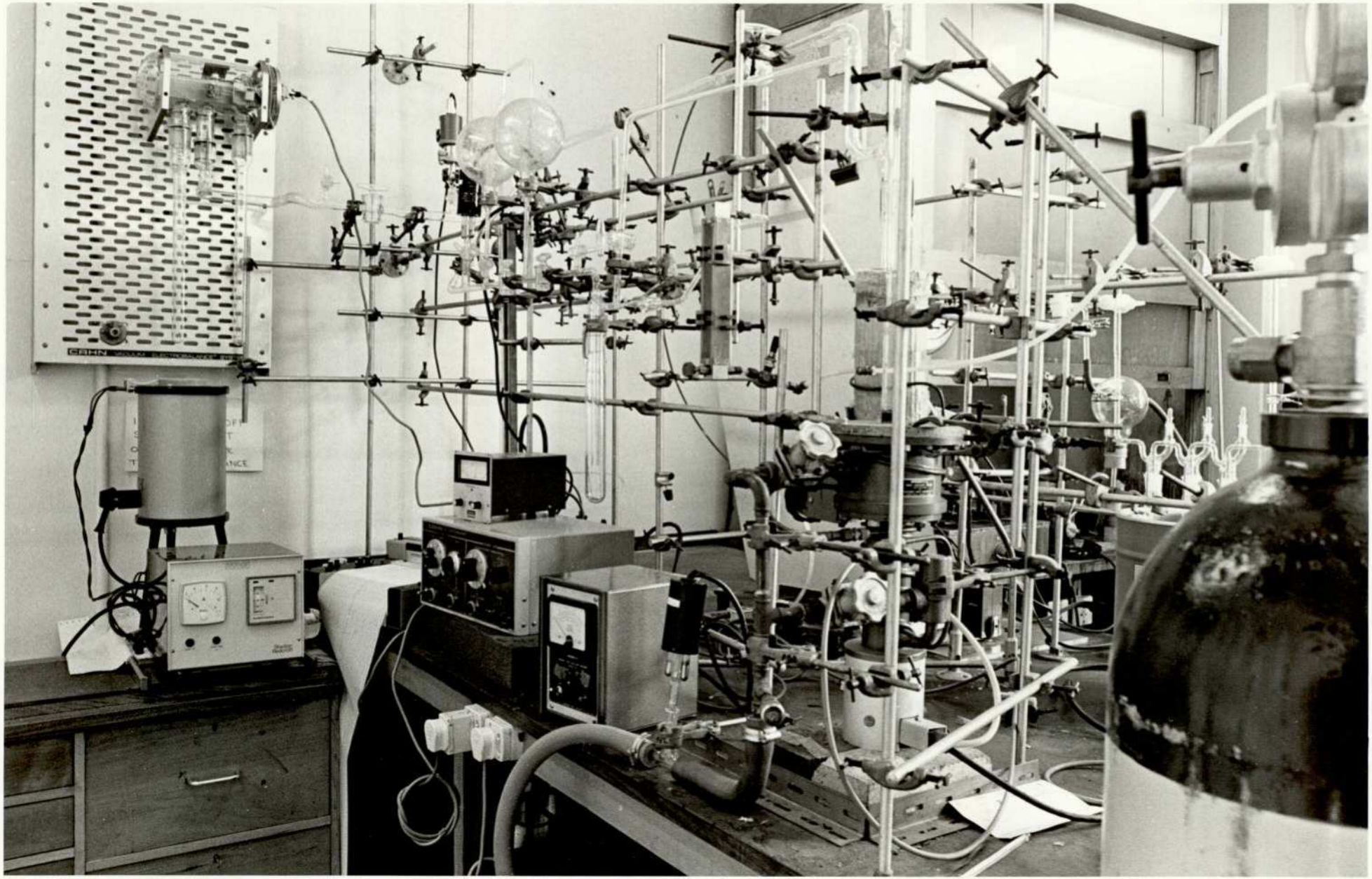

Plate 2 - Gravimetric surface area apparatus

Figure 12 - Schematic diagram of electrobalance

the balance in the null position can be equated to the change in the sample weight. The beam is always in dynamic equilibrium, with the sum of the moments on it equal to zero. The Cahn Balance design is such that the restoring force is so fast that the beam appears visually to be locked in place. The signal from the electrobalance is fed to the main instrumentation, which houses a series of range selector switches, calibration controls, and finally outputs to a variable span recorder with the 1 mV range most frequently used.

(b) The Vacuum System

An Edwards-ED50 rotary oil-sealed vacuum pump, fitted with a magnetic non-return valve, was used to back an Edwards F203-A watercooled oil diffusion pump, fitted with a thermal cut-out switch. This combination achieved a vacuum of 1.33×10^{-3} N m^{-2} (10^{-5} torr) in the outgassed system. Pressure measurements were made using Pirani heads P_1, P_2, and Penning head P_3, situated as shown in Figure 11. The Pirani heads were switched into a central gauge with scales reading from 0 - 6.65×10^{-1} N m^{-2} (0 - 5×10^{-3} torr) and 0 - 1.33×10^{2} N m^{-2} (0 - 1 torr), and the Penning head was connected to a gauge with scale reading from 1.33×10^{-1} - 1.33×10^{-5} N m^{-2} (10^{-3} - 10^{-7} torr). Above 1.33×10^{2} N m^{-2} (1 torr), pressure were read on the mercury manometer. During initial pumping out, the diffusion pump must be by-passed until the critical backing pressure was reached. By judicious use of valves and switches, any part of the system can be isolated and evacuated without affecting the rest.

(c) The Gas Supply System

Nitrogen gas (white spot) for adsorption, was introduced from a high pressure gas cylinder through a reducing valve, a needle valve, and flowmeter, and was ultimately stored at 77°K in trap T_1. As required, portions were distilled over into the main (high pressure) storage bulb B1,

from which the low pressure bulb B2 was fed (Figure 11). A small quantity of gas was introduced into the sample tube, and the equilibrium pressure was read off the manometer, and the equilibrium weight change recorded. A complete isotherm could thus be obtained over many pressure decades.

2.5.2.2 Modes of Operation

(i) Initially the balance was calibrated with the empty adsorption pan suspended from the loop selected - loop A in this instance Figure 11. As the sample was not expected to change by a large fraction of its total weight, a substitution weight representing the sample weight was added to the pan. This load was counterbalanced as closely as possible on loop C. Accurate calibration of all dials was ensured by adding and removing calibration weights, and adjusting potentiometers in the circuit. In effect, during this calibration procedure, which was carried out before each run, the balance was being adjusted so that the recorder agreed with the calibration weights and read directly in milligrams. The substitution weight and calibration weights were then replaced by the sample. The system was then ready for outgassing. It was noted that the vacuum zero point differed from that in air by as much as 50 μg or more depending on the sample and counterweight, due to the absence of air buoyancy and aerodynamic currents.

(ii) Having completed the calibration procedure satisfactorily, the sample was placed on the pan and the silica glass sample tube carefully moved into position. Using the mass dial control (potentiometer), the recorder pen was brought onto the chart paper, the adjustments proceeding from the coarsest to the finest recorder ranges available. The total sample weight could then be found from the recorder reading in milligrams, the mass dial reading on the potentiometer and the substitution weight. At this stage

the balance measured the sample weight in air.

(iii) All the ground glass seals were greased with Apiezon L grease. The whole system was flushed with nitrogen gas from cylinder for 5 - 10 minutes. All the taps and valves to atmosphere were closed, and the system evacuated for 16 hours. This evacuation, or outgassing, was accomplished overnight, and was assisted by surrounding the sample tube with a temperature controlled furnace set at 500°C. When the chamber had reached a pressure of $< 1.33 \times 10^{-2}$ N m^{-2} ($< 10^{-4}$ torr on the Penning gauge), the sample was considered to be outgassed. During evacuation, the trap T_2 was surrounded by a Dewar flask filled with liquid nitrogen, to trap any mercury vapour from the manometer and also to prevent any oil vapour from the diffusion pump getting into the system. When the sample had been satisfactorily evacuated, the furnace was removed and the sample tube allowed to cool to room temperature. It was then surrounded by a Dewar flask, filled with liquid nitrogen, the level of which was maintained throughout the run. The system was left pumping for 1 hour or so until thermal equilibrium was established.

(iv) Whilst confirming the sample chamber was leak free, the gas storage reservoir T_1 was surrounded by a Dewar flask filled with liquid nitrogen; and the system was left pumping for $\sim$ 15 minutes. Taps H, J were closed, Pirani head P_1 switched off, and nitrogen was supplied from the cylinder to the reservoir via tap P, flowmeter Q and needlevalve R (Figure 11). Thirty seconds was sufficient to allow enough gas into the reservoir for 4 adsorptions; more gas was condensed in the reservoir afterwards. Some of the nitrogen from the reservoir was transferred to the storage bulb B1, and finally a small portion of the gas was transferred to the low pressure bulb B2.

(v) Taps S was then closed, and since the pumping system was not needed

at this stage, it was switched off, which helped to keep vibration to a minimun. The manometer was read, which gave the value of atmospheric pressure, and this was numerically equated with the saturation vapour pressure (SVP) of pure nitrogen at the temperature of the bath (i.e. 1 atmosphere, p_o). The mass dial (potentiometer) was adjusted until the recorder pen was at the lower end of the chart on the most sensitive scale for the selected weight range. This then yielded the weight of the sample in vacuum at liquid nitrogen temperature, to this all subsequent mass changes were referred. The weight was made up as follows: (selected mass dial range x mass dial reading) + (% recorder reading x recorder range) + substitution weight.

(vi) All the gauges were switched off, and then dry nitrogen in the line between H and K was admitted to the sample tube in the first instance, to increase the absorption pressure by 1.33×10^2 N m^{-2} (1 torr). After allowing 15-30 minuted for adsorption to reach equilibrium, the apparent mass increase was read. It was usually necessary to adjust the mass dial to bring the recorder pen back on the chart paper; and the new corresponding pressure reading was noted (up to 1.33×10^2 N m^{-2} from the mercury manometer). During the first few introductions, only small amounts of nitrogen were admitted such that the increase in pressure was between 0 - 3.99×10^2 N m^{-2} (0 - 3 torr) then on the subsequent introductions, larger amounts of nitrogen were transferred from bulb B2 to the sample chamber whereby producing pressure increases of 3.99×10^3 - 5.32×10^3 N m^{-2} (30 - 40 torr) per introduction. In all 12 introductions were usually carried out for a complete adsorption cycle, although about six are enough for a good spread over the range of applicability of the BET equation. In some cases, with the zeolites (which have microporous structures), the adsorption was Langmuir type (4, 5) and the BET is not applicable. In such cases,

although V_m or M_m had no relation to surface area, it provided information on pore volumes.

(vii) After recording the last adsorption data, tap H (Figure 11) was closed, and any nitrogen that had condensed in trap T_1 was vented into the atmosphere by opening tap N and removing the liquid nitrogen trap. The rotary pump was then switched on, once more by-passing the diffusion pump via the valve U. The Pirani head P_2 was switched on, tap N was closed and tap J was opened. The gas admission section between H and the rotary pump, and the bulbs B1, B2 were next evacuated, Pirani head P_1 was switched on, and when the pressure had reached around 6.65 N m^{-2} (5×10^{-2} torr), tap L was closed and tap H slowly opened. A portion of the gas was thus bled from the sample chamber to bulb B2. Tap H was closed and tap L opened, which allowed for the section to be evacuated again. Meanwhile a new pressure reading from the manometer corresponding to a now decreased weight were both recorded; this gave the first point on the adsorption curve. The procedure was repeated 10-12 times until a complete desorption isotherm was obtained.

(viii) Finally, the isotherms were obtained by plotting weight adsorbed against pressure.

Adsorption-desorption isotherms of the following samples were recorded:-

(i) Hydrogen mordenite - dealuminated form.

(ii) Unpoisoned conventional VQ1 detector beads.

(iii) Poisoned conventional VQ1 detector beads.

(iv) Unpoisoned conventional VQ3 detector beads.

(v) Poisoned conventional VQ3 detector beads.

(vi) Unpoisoned VQ1 detector beads which had been coated with

dealuminated hydrogen mordenite.

(vii) Poisoned VQ1 detector beads which had been coated with dealuminated hydrogen mordenite.

(viii) Unpoisoned VQ3 detector beads which had been coated with dealuminated hydrogen mordenite.

(ix) Poisoned VQ3 detector beads which had been coated with dealuminated hydrogen mordenite.

2.5.2.3 Fine Points of Operation of the Cahn Electrobalance

(i) The balance and the bottle containing it had to be set as near level as possible to prevent the pan touching the walls of the sample tube.

(ii) Silica glass sample tubes were used instead of Pyrex because the samples were degassed at 500°C, which is the softening temperature for Pyrex.

(iii) The adsorption pan made of aluminium foil and nichrome wire was handled with care, otherwise it did not hang straight from the suspension arm. The hangdown wire was 0.05 mm diameter nichrome. It was handled as little as possible to prevent grease contamination from fingers. The following procedure was adopted whenever a desired length was required. A piece of the wire slightly longer than than the desired length was cut from the spool. It was laid down on a large sheet of clean white paper on the bench top. A sharp hook was made at one end using fine-nosed pliers, and the wire was suspended so that it hanged freely. The wire was straightened by attaching a paper clip to its lower end and the wire was heated to redness along its entire length, using a bunsen flame. The straightened wire was now cut as nearly as possible to the desired length and new hooks were made at each end.

(iv) The sample was heated relatively slowly under vacuum, to prevent degradation, or explosion due to entrapped gases and vapours.

(v) The oil diffusion pump was only switched on after a backing pressure of 6.65×10 N m^{-2} (0.5 torr) was attained. The Pirani head P_2 was incorporated in order to detect any leak in the lower end of the rig (i.e. between the diffusion pump and the rotary pump).

(vi) Mode of operation of the oil diffusion pump: the rotary pump was switched on with backing valve W and roughing valve U opened (Figure 11). When the pressure of the system had reached 6.65×10 N m^{-2} (0.5 torr), the water cooling system and the oil diffusion pump heater were turned on simultaneously. After 15- 20 minutes, valve U was closed and the baffle valve V was opened. The ultimate pressure reached with this combination was 1.33×10^{-3} N m^{-2} (10^{-5} torr).

(vii) On the first introduction of nitrogen to the sample and the first removal of nitrogen from the sample, tap H was opened very slowly, because a sudden pressure increase or decrease could cause explosion of the particles or 'cycloning', i.e. the particles being blown off the pan.

(viii) Although the various components of the balance were carefully set up, in some instances they were not perfectly aligned. Then, the sample pan was not hanging like a plumb knob, but was rather touching the sides of the sample tube. There were several reasons for this. One of them was simply due to the presence of a static electricity charge; in such cases the outside of the tube was sprayed with an anti-static spray. In other cases to correct for misalignment, small adjustment was carried out by gently tilting the balance within the bottle either forward or backward.

(ix) The balance was mounted on a rigid brick wall to reduce vibrational noise. Electrical noise accompanying the output signal from the balance was considerably reduced by filtering.

(x) All samples were degassed at the same temperature and for the same number of hours, thereby providing comparative results.

(xi) Spurious mass change was observed at times, but no explanation to this effect was formulated. Disturbances in microbalance experiments have been discussed by Poulis and Thomas (151), and others (144). These disturbances are attributed to buoyancy, aerodynamic currents, thermomolecular flow and thermal transpirations. In the present work, improvement was observed when the counterweight tube was made to the same length as the sample tube, and when the counterweight hangdown wires were made as near identical as possible to the sample hangdown wires.

2.6 List of Experiments

As a conclusion section to this chapter, the series of experiments performed throughout this project are listed below. Results are presented in the same order in the next chapter.

(i) Topographical and elemental studies of poisoned VQ1, VQ3 beads using SEM and EDAX.

(ii) Determination of nickel as an impurity using the polarographic technique.

(iii) Lead analyses of 0.2 mol dm^{-3} iodine monochloride solution using atomic absorption spectrophotometry.

(iv) Poisoning experiments performed on VQ1, VQ3, VQ1/VQ7, VQ3/VQ9, LD1, LD1/LD7, LD1/LD$^{3}/_{1}$, LD1/LD$^{3}/_{1}$/LD7 beads.

(v) Topographical and element analysis of poisoned VQ1, VQ3 beads using SEM and EDAX.

(vi) Chemical analyses of the following:-

(a) Hydrogen mordenite (prepared from ammonium mordenite) and thermogravimetry of ammonium mordenite.

(b) Hydrogen mordenite (dealuminated form) prepared by acid treatment.

(vii) Poisoning experiments performed on VQ1 and VQ3 beads coated with different ratios of zeolite/kaolin mixture.

(viii) Analysis for lead using atomic absorption spectrophotometry for poisoned VQ1 beads coated with dealuminated hydrogen mordenite.

(ix) Adsorption-desorption experiments of dealuminated hydrogen mordenite by the volumetric method using the Carlo Erba 1800 apparatus.

(x) Adsorption-desorption experiments of the following samples, carried out by a gravimetric method using the Cahn RG Electrobalance:-

(a) Dealuminated hydrogen mordenite.

(b) Unpoisoned VQ1, VQ3 beads.

(c) Poisoned VQ1, VQ3 beads.

(d) VQ1, VQ3 beads coated with dealuminated hydrogen mordenite, - both unpoisoned and poisoned examples.

CHAPTER 3

RESULTS

CHAPTER 3

3.1 Topographical Study of Unpoisoned Beads Using Scanning Electron Microscopy (SEM)

VQ3 Beads

Several VQ3 beads were examined under identical conditions. The micrographs obtained were not representative of the same location on each bead, but rather of different positions on the bead surfaces. A couple of the beads showed charging effects. Generally, the surface appeared fairly rough with large void spaces more appropriately described as cracks, non-uniform in size, shape and length, and not following any regular pattern. There were some intraparticle voids as well but these were not very deep. The complex and random geometry showed that it would not be very realistic to describe these cracks or void spaces in terms of a cylindrical pore model. The lumps of catalyst on the surface were fairly smooth, and large compared to the cracks. These surface features are probably inherent in the drying process used in the manufacture of the beads. Examples of the micrographs are displayed on Plates 3 and 4.

VQ1 Beads

Ten VQ1 beads were examined. Micrographs were obtained that were representative of different positions on the bead surfaces. Few exhibited charging effects whilst under examination, and coating was avoided. The surface was characterised by the following features. On some of the beads, unidentified particulate matter was dispersed over the surface, which could be appropriately described as "snow-flake-like", in appearance. Here again there were void spaces or cracks, but these were comparatively small compared to those found in the VQ3 beads. The surface also had more intraparticle voids, which were also deeper than those found on the surfaces of the VQ3 beads. These were comparatively more pronounced in three dimensional

Magnification x1000, angle of tilt 30°

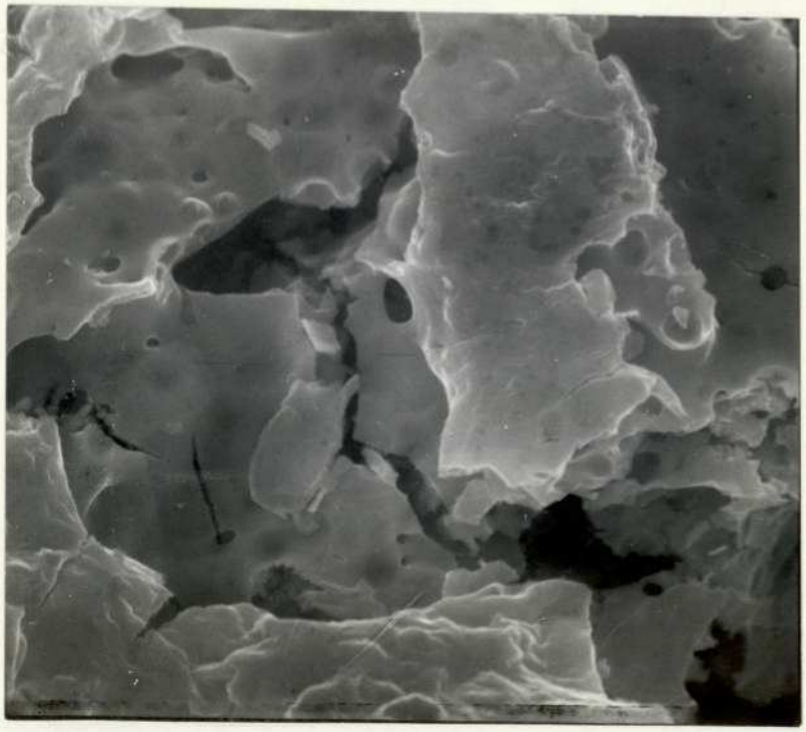

Magnification x3000, angle of tilt 0°

Plate 3 - Unpoisoned VQ3

Magnification x1000, angle of tilt 0°

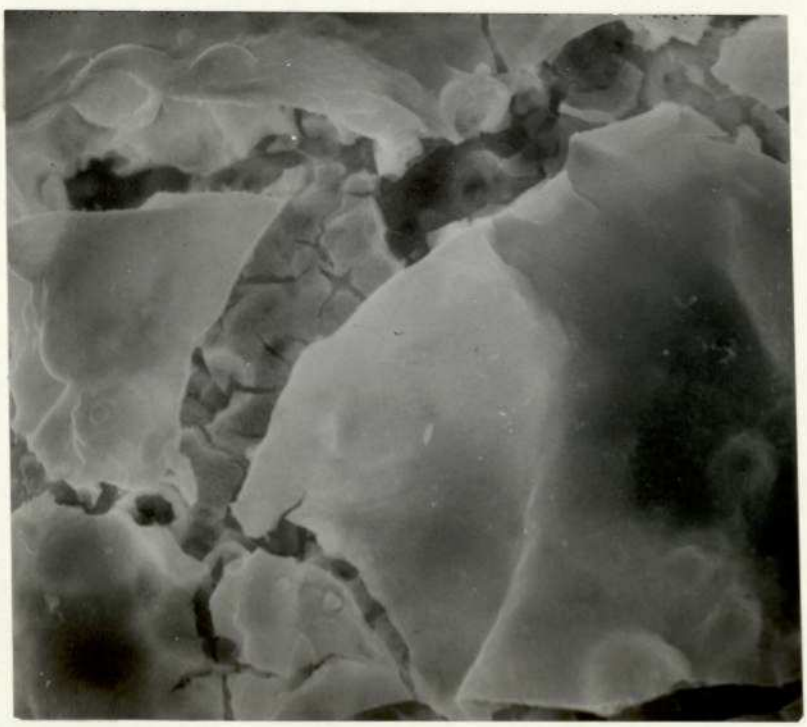

Magnification x3000, angle of tilt 0°

Plate 4 - Unpoisoned VQ3

features, with lumps of catalyst that were smaller in size. These lumps of catalyst looked more like 'globules' of the catalyst solution which had dried, leaving a spherical shell, and in most cases this spherical shell had burst open during the drying process, resulting in the greater overall roughness of the VQ1 beads. A few examples of micrographs of VQ1 beads are depicted on Plates 5 and 6.

Compensator Beads

In general, the surfaces were rough with many intraparticle voids, and had more three dimensional features than the VQ1 or VQ3 beads. There were cracks of irregular dimensions. The topography of the compensator beads was noticeably different from that of VQ1 or VQ3 beads, which may indicate that the topography of the catalyst coating was probably not as strongly influenced by the profile of the underlying alumina carrier as might be expected, i.e. a heavy coating of catalyst existed on the surfaces of both the VQ1 and VQ3. Examples of micrographs of compensator beads are shown on Plates 7and 8.

3.1.1 Statistical Analysis of Surface Features of Pellistor Beads at x1000 Magnification

Whilst the electron microscopy work reported above revealed some general similarities between VQ1, VQ3 and the reference beads, the detailed structures and topographies of the three types of beads did show marked differences, and these differences have been quantified statistically. Due to the fairly rough surface of the beads, with large void spaces more appropriately described as cracks which are non-uniform in size, shape, length, and occurring in an irregular pattern, and also due-to the complex and random geometry of these cracks, it was almost impossible to obtain

Magnification x1000, angle of tilt 30°

Magnification x3000, angle of tilt 30°

Plate 5 - Unpoisoned VQ1

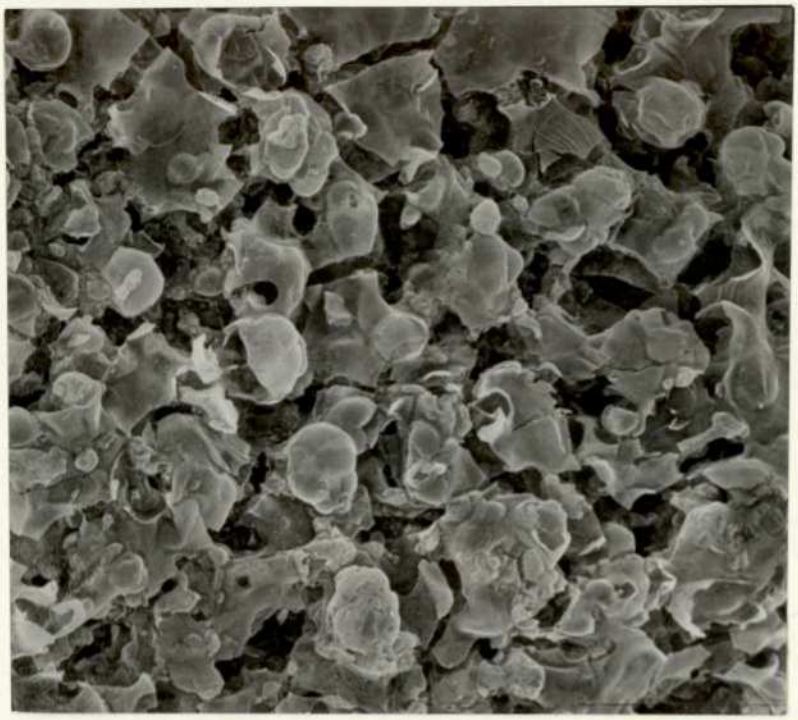

Magnification x3000, angle of tilt 30°

Magnification x1000, angle of tilt 0°

Plate 6 - Unpoisoned VQ1

Low magnification (End view - showing whole bead with platinum coil), angle of tilt 0°

Magnification x1000, angle of tilt 30°

Plate 7 - Unpoisoned compensator

Magnification x1000, angle of tilt 0°

Magnification x1000, angle of tilt 30°

Plate 8 - Unpoisoned compensator

a mean pore (or crack) diameter from the micrographs by direct measurement. However the following method was used to estimate some of the surface features of the beads. A total of seventy cracks from 10 micrographs at x1000 magnification (1mm ≡ 1 μm) were examined; diameter measurements ranged from 0 - 20 μm for VQ1, and 0 - 12 μm for the VQ3 and compensator beads. These data were then assembled in tabular form. Using conventional statistical analysis, standard deviations were calculated and percentage cumulative frequency plots were constructed (see Tables 2 - 4 and Figures 13 - 15). From the plots it is evident that most of the cracks lie in the range of 0 - 8 μm, although in the case of compensator beads, ~85% of the cracks lie in the range of 0 - 6 μm. In the case of the VQ1 and VQ3 beads, around 60% of the cracks are slightly larger in size than in the compensator beads, and that they are fewer. Using the general classification of pore sizes of Dubinin (152), it is apparent that we are examining the macroporous structure of the beads and compensators, and the statistical analysis confirms the general conclusions drawn in section 3.1, viz: that the catalyst coating, whether it be VQ1 or VQ3 composition, changes the nature of the macroporous structure of the beads (cf. Figures 13 and 14 with 15).

3.2 Elemental Analysis of the Unpoisoned Beads Using Energy Dispersive Analysis of X-rays (EDAX)

Several beads of each kind were examined under the same standard conditions as those used for scanning electron microscopy (i.e. an accelerating voltage of 40 kV, condenser aperture 3, and spotsize 3). To facilitate comparison of the spectra, the following previously established standard conditions were maintained for all analyses. The spectrum was recorded when

TABLE 2 - VQ1 DATA

(10 mm ≡ μm)

Class μm	Frequency (f)	Cumulative frequency	%	d	fd	fd^2
0 - 2	4	4	5.71	-2	- 8	16
2 - 4	17	21	30.00	-1	-17	17
4 - 6	16	37	52.86	0	0	0
6 - 8	11	48	68.57	1	11	11
8 - 10	8	56	80.00	2	16	32
10 - 12	6	62	88.57	3	18	54
12 - 14	1	63	90.00	4	4	16
14 - 16	3	66	94.29	5	15	75
16 - 18	1	67	95.71	6	6	36
18 - 20	3	70	100.00	7	21	147
	Σf:70				Σfd:66	Σfd^2:404

summation : Σ

standard deviation : σ

class interval : 2

$$\sigma = \sqrt{\frac{\Sigma fd}{\Sigma f} - \frac{\Sigma fd^2}{\Sigma f}} \times \text{class interval}$$

$$\sigma = 4.20$$

TABLE 3 - VQ3 DATA

(10 mm ≡ 10 μm)

Class μm	Frequency (f)	Cumulative frequency	%	d	fd	fd^2
0 - 2	5	5	7.14	-2	-10	20
2 - 4	18	23	32.86	-1	-18	18
4 - 6	18	41	58.57	0	0	0
6 - 8	13	54	77.14	1	13	13
8 - 10	12	66	94.29	2	24	48
10 - 12	4	70	100.00	3	12	36
	Σf:70				Σfd:21	Σfd^2:135

summation : Σ

standard deviation : σ

class interval : 2

$$\sigma = \sqrt{\frac{\Sigma fd}{\Sigma f} - \frac{\Sigma fd^2}{\Sigma f}} \times \text{class interval}$$

$$\sigma = 2.71$$

TABLE 4 - COMPENSATOR DATA

(10 mm ≡ 10 μm)

class μm	Frequency (f)	Cumulative frequency	%	d	fd	fd^2
0 - 2	17	17	24.29	-1	-17	17
2 - 4	24	41	58.57	0	0	0
4 - 6	19	60	85.71	1	19	19
6 - 8	3	63	90.00	2	6	12
8 - 10	4	67	95.71	3	12	36
10 - 12	3	70	100.00	4	12	48
	Σf:70				Σfd:32	Σfd^2:132

summation : Σ

standard deviation : σ

class interval : 2

$$\sigma = \sqrt{\frac{\Sigma fd}{\Sigma f} - \frac{\Sigma fd^2}{\Sigma f}} \times \text{class interval}$$

$$\sigma = 2.59$$

Figure 13

Cumulative frequency plot - VQ1 beads

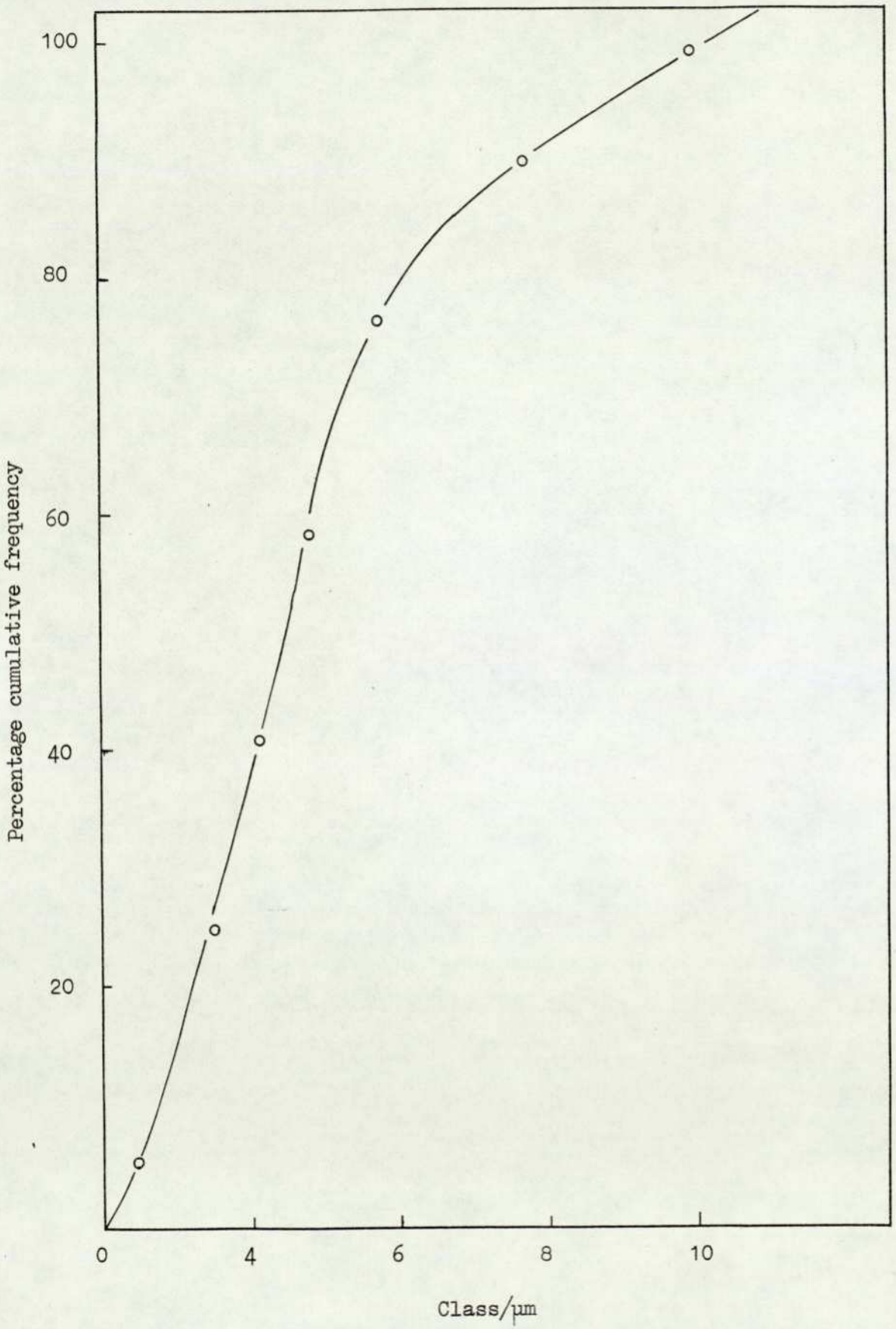

Figure 14

Cumulative frequency plot - VQ3 beads

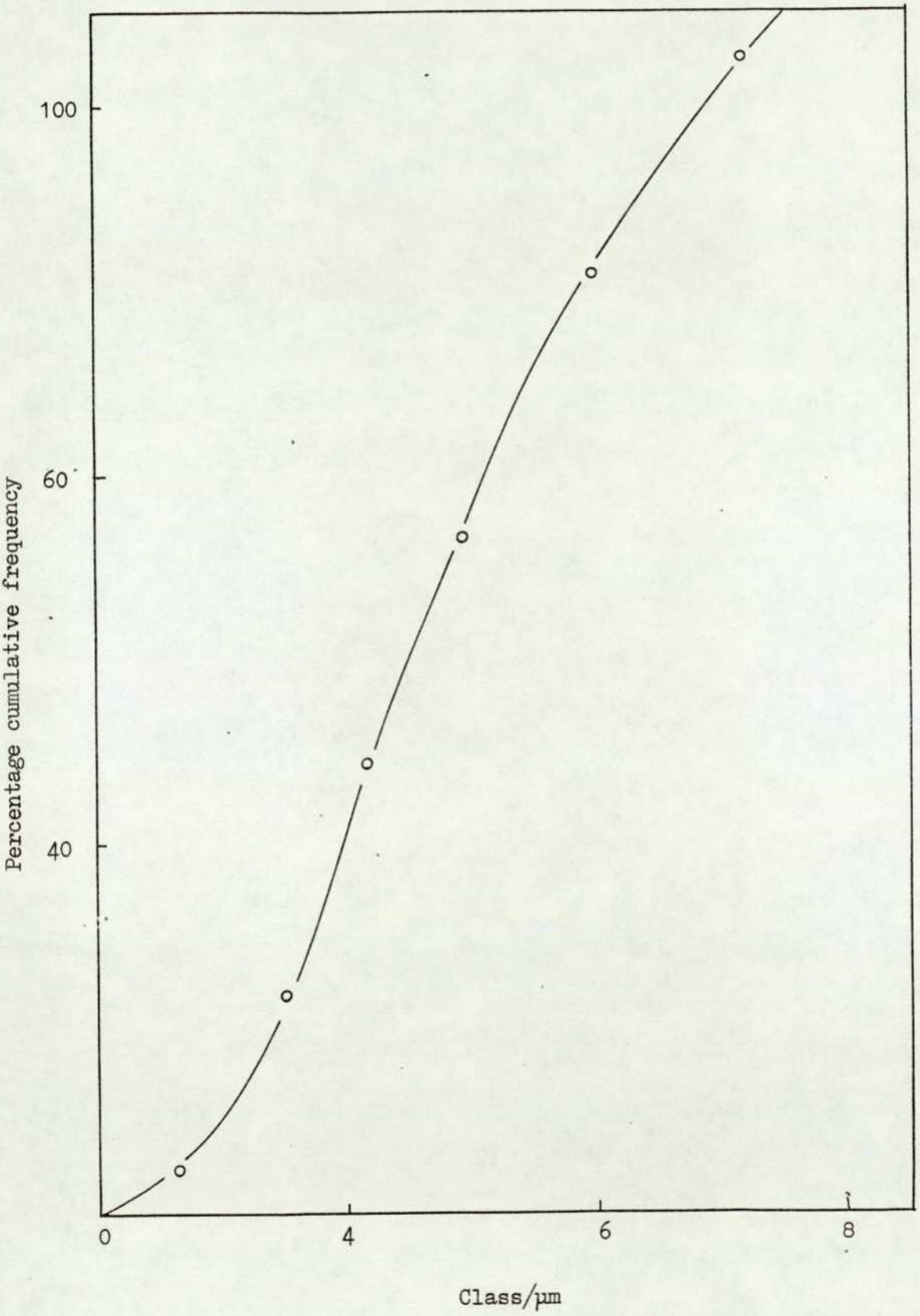

Figure 15

Cumulative frequency plot - compensator beads

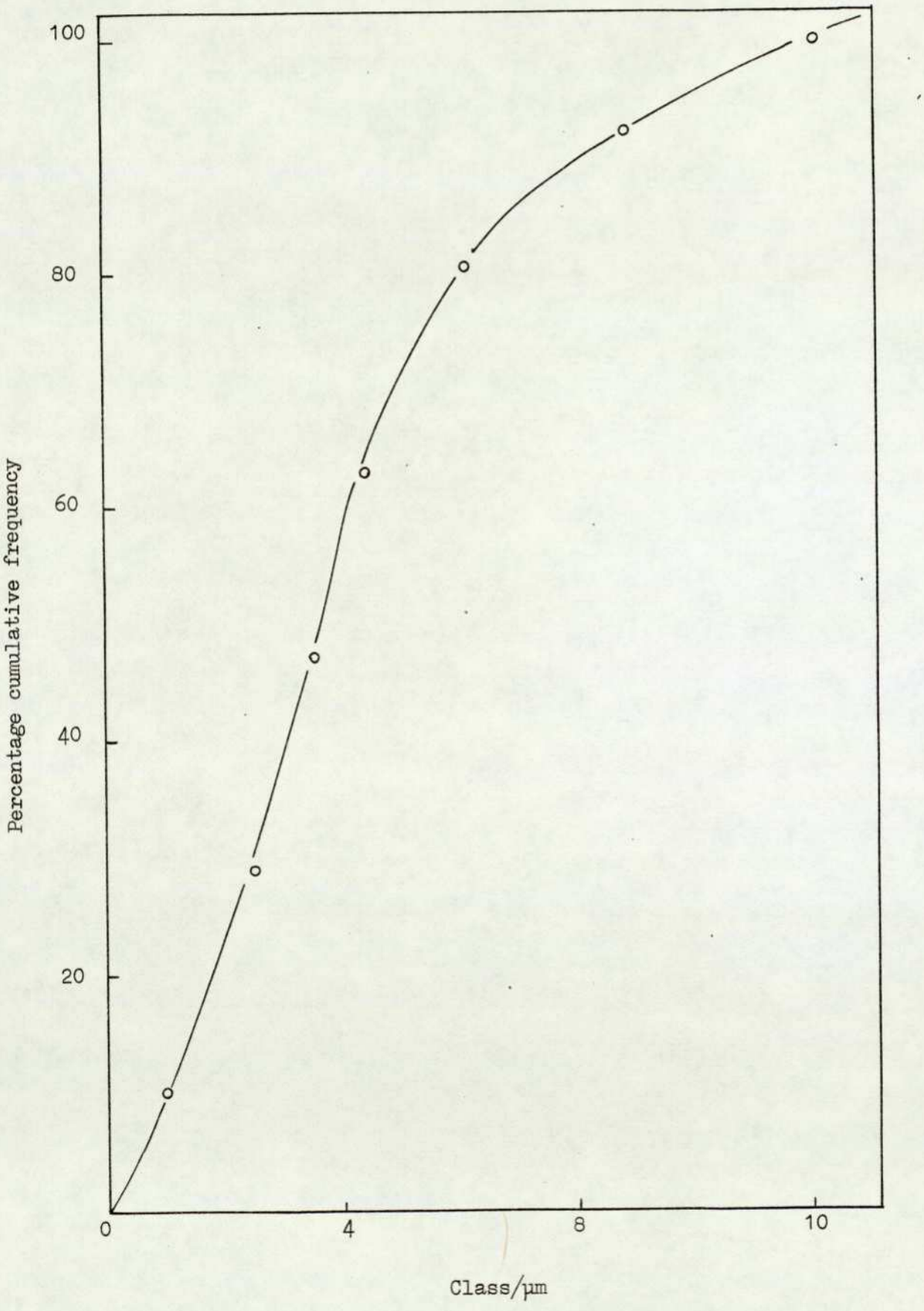

the scanning beam gave a micrograph of x1000 magnification. The spectra were displayed in a histogram form with 80 channels along the abscissa, calibrated in energy (keV) and a vertical scale of 2500 counts, with a maximum line intensity of 1000 counts. The system was arranged so that the beam was scanning the front edge of the bead surface (i.e. facing the detector); this allowed a maximal collection of the emitted X-rays and hence a high count rate. For comparison, some spectra were also recorded when the electron probe was scanning the rear edge of the specimen surface; as might be expected, these were complex, with severe background interference.

VQ3 Beads

The spectrum of a typical VQ3 bead is shown on Plate 9 together with the corresponding "stick diagram". The peaks are identified in Table 5. The spectrum showed as expected the presence of aluminium, palladium, and thorium, but also an unexpected component, nickel. The palladium L lines coincide with the thorium M line at 3000 eV, (see the EDAX chart in Appendix IV). All beads examined showed the presence of nickel. Most of the specimens were studied with the beam incident on the front edge of the specimen surface, angle of tilt of specimen to the detector being 30°. These gave spectra with lines of almost identical intensities, and with the number of counts for the whole spectrum lying within a common range. The intensity of the K line for aluminium was relatively weak compared to the palladium and thorium lines, which again indicated a substantial amount of the catalyst on the surface. (see conclusions drawn in section 3.1).

VQ1 Beads

The spectrum of a typical VQ1 bead with its corresponding "stick diagram" are displayed on Plate 10, with peaks identified in Table 6. The trace showed the presence of aluminium, platinum, and palladium and again nickel, the latter being present (as in the case of the VQ3 beads) in all

TABLE 5

VQ3 Bead

Element	Peak No.	Position eV	Lines
Aluminium	1	1450	$K\alpha$ Al
	1A	1550	$K\beta$ Al
Palladium/Thorium	2	2800	$L\alpha, \beta_1, \beta_2$, Pd, & $M\alpha$ Th
Thorium	3	12850	$L\alpha$ Th
	3A	15500	$L\beta_1$ Th
	3B	16050	$L\beta_2$ Th
	3C	18950	$L\gamma$ Th

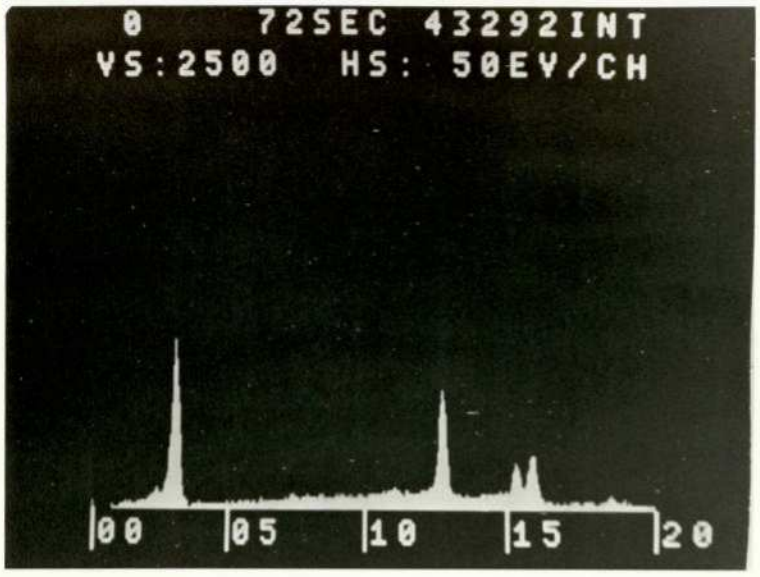

Range : 0 - 20 keV
Sample : Unpoisoned VQ3 bead

Plate 9

TABLE 6

VQ1 Bead

Element	Peak No	Position eV	Lines
Aluminium	1	1450	$K\alpha$ AL
	1A	1550	$K\beta$ Al
Platinum	2	2100	$M\alpha$ Pt
Palladium	3	2800	$L\alpha$ Pd
	3A	2950	$L\beta_1$ Pd
	3B	3150	$L\beta_2$ Pd
Nickel	4	7450	$K\alpha$ Ni
	4A	8250	$K\beta$ Ni
Platinum	5	9400	$L\alpha$ Pt
	5A	11050	$L\beta_1$ Pt
	5B	11250	$L\beta_2$ Pt
	5C	12950	$L\gamma$ Pt

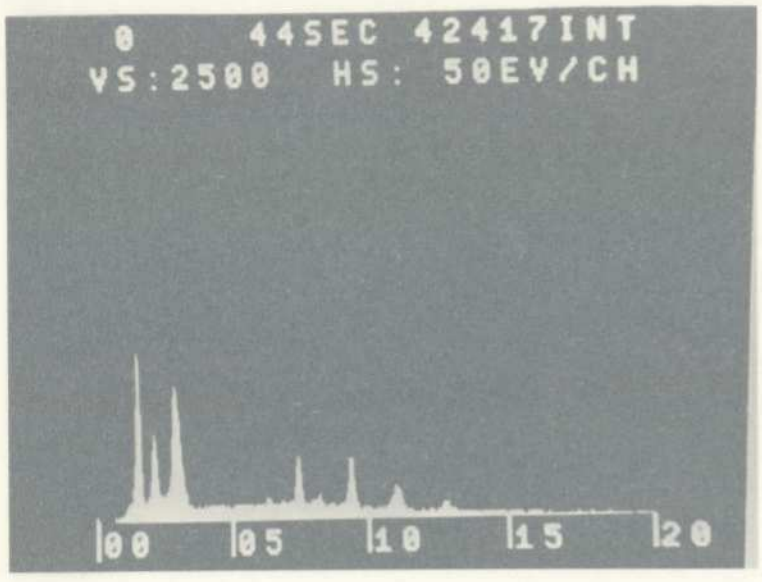

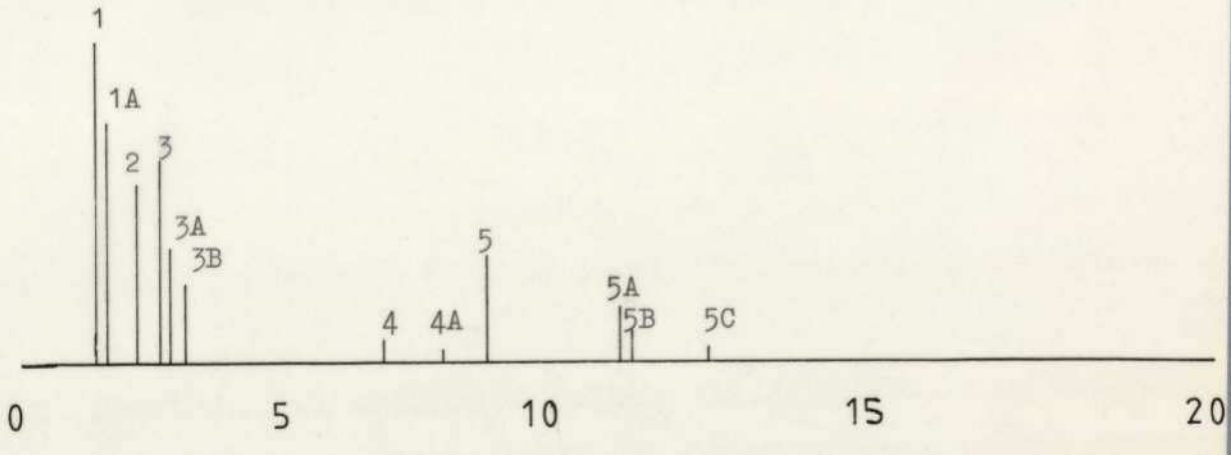

Range : 0 - 20 keV
Sample : Unpoisoned VQ1 bead

Plate 10

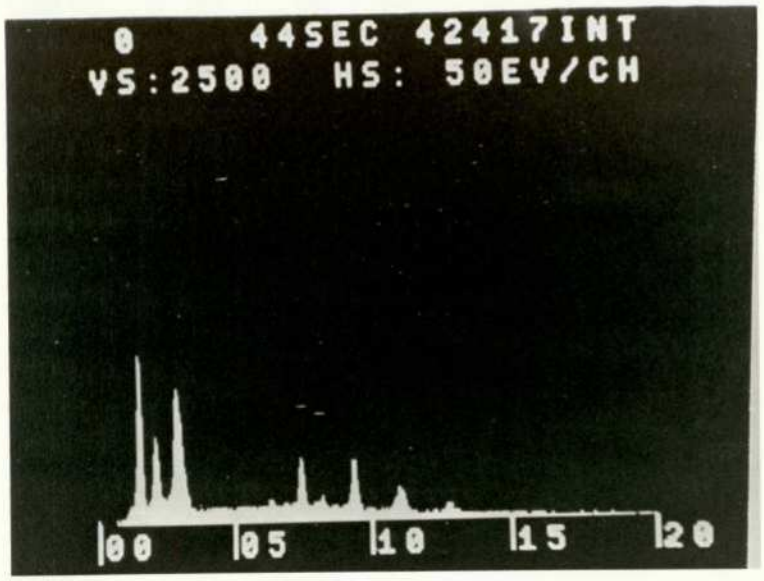

Range : 0 - 20 keV
Sample : Unpoisoned VQ1 bead

Plate 10

the beads examined as an impurity. The spectrum also showed an intense K aluminium line, and fairly strong platinum and palladium lines, indicating a less heavy coating of catalyst on the surface than was observed with the VQ3 beads. A couple of VQ1 beads showed very weak platinum and palladium lines, which suggested a poor coating of catalyst on the bead surface.

Compensator Beads

A typical spectrum with "stick diagram" is illustrated on Plate 11, and the peaks are identified in Table 7. The beads were examined with the probe scanning the front edge of the bead surface and the bead tilted through an angle of 30° to the detector as before. All spectra of different compensator beads were very similar, with an intense K aluminium line, and some slight variation in the K potassium line intensity. (Potassium is deliberately added to the compensator beads when they are manufactured, to 'poison' the surface, thus eliminating as far as possible any catalytic activity on the compensator bead surface). Apart from aluminium and potassium, all spectra showed the presence of nickel and sulphur impurities.

Cross-Sectional Examinations

In order to allow cross-sectional examinations of the beads, setting the bead in an 'Araldite' medium was tried initially, followed by polishing, using the same technique that is employed when preparing metallurgical samples for electron microscopic examination. This technique failed because the 'Araldite' did not penetrate into the porous structure of the bead. Thus during the polishing, the internal part of the bead remained soft and was destroyed by the grinding process. In effect the bead could not be properly embedded. A different approach was therefore adopted as follows. The bead was sliced into two segments with a sharp scalpel, and although some powdering occurred in all cases, in about one in every four attempts the bead was successfully fractured into two parts, which could

TABLE 7

Compensator Bead

Element	Peak No	Position eV	Lines
Aluminium	1	1450	K_{α} Al
	1A	1550	K_{β} Al
Sulphur	2	2300	K_{α} S
	2A	2450	K_{β} S
Potassium	3	3300	K_{α} K
	3A	3600	K_{β} K
Nickel	4	7450	K_{α} Ni
	4A	8250	K_{β} Ni

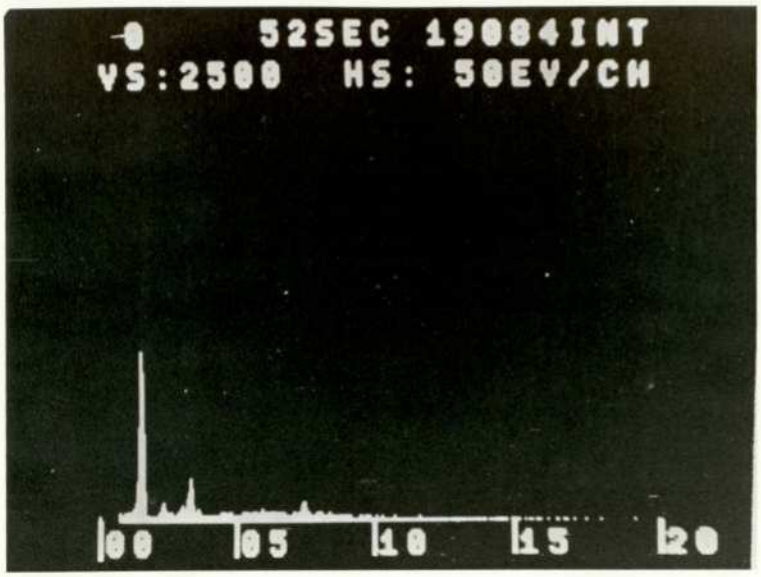

Range : 0 - 20 keV
Sample : Unpoisoned compensator bead

Plate 11

then be examined by EDAX.

The cross-section of VQ1 beads were examined with the beam initially scanning the centre of the bead. The count rate here was very low, and the spectrum showed lines corresponding to aluminium, platinum, palladium, and nickel. When the electron beam was shifted towards the edge of the bead, the count rate increased substantially, especially in the case of lines belonging to platinum and palladium. These observations indicated that the catalyst was situated primarily near the surface of the bead, an effect which was indeed noticeable to the naked eye in terms of difference in colour intensity from the centre to the edge of the cross-section.

3.2.1 Conclusions from Elemental Identification by EDAX

Under the established operating conditions, qualitative elemental identification was carried out successfully, and reliable semi-quantitative estimates based on the relative intensities of the K, L and M lines of the different elements present gave an indication of the distribution of catalyst on both the surface and within the beads. The sets of beads examined showed significant variation in the quantity of catalyst deposited on the alumina support. Sulphur was present as an impurity in the compensator beads examined, and nickel was present in both compensators and catalyst beads. A polarographic analysis (see Appendix V) gave a weight percentage of nickel in the beads of 1.7%. This figure was of the order of magnitude one would estimate from the intensity of the nickel lines in the spectrum. Copper K lines appeared on a few spectra, but this was later proved to be a background interference arising from the copper tray which contained the carbon disc on which the beads were mounted.

3.3 Lead Analysis Using ICl Solutions and Atomic Absorption Spectrophotometry

Atomic adsorption spectrophotometry analysis of lead trapped in 0.2 mol dm^{-3} iodine monochloride solution was carried out using a Perkin Elmer 290B spectrophotometer. The preparation of standard and sample solutions has already been described in section 2.2.3.1. Typical results are shown in Tables 8, 9 and Figure 16. These results gave a measure of the amount of lead in the gas stream. The flow rate of the leaded air stream was set at 100 cm^3 min^{-1} , which was diluted with clean air in a ratio of clean air to leaded air of 4:1 before passing over the detector beads. This gave a resultant total flow rate of 0.5 dm^3 min^{-1} . Therefore the amount of lead getting to the detectors was 24.2 mg m^{-3} , since the analysis showed a concentration in the undiluted stream of 121 mg m^{-3} (see Table 9). This figure deviates slightly from the expected value of 20 mg m^{-3} obtained by theoretical calculation (Appendix III) for the following reasons:-

(1) The correction factor for the atmospheric pressure of the day was not taken into account.

(2) The assumption made in the theoretical calculation that the activity coefficients of n-heptane and TML are unity was obviously an over-simplification.

Bearing these points in mind, agreement between observed and predicted concentrations is good. Lead analyses were carried out for each freshly prepared n-heptane/TML mixture. The results were found to always fall in the range of 20→25 mg lead m^{-3} of leaded air stream.

TABLE 8

Standard solution concentrated/$\mu g\ cm^{-3}$ (ppm)	Percentage response
0 (Blank)	0
10	25
20	50
30	70

TABLE 9

Sample solution: leaded air bubbled (@ 200 $cm^3\ min^{-1}$) through ICl solution for	Percentage response	Amount of lead collected/mg
1 hr	7	1.4
2 hrs	15	3.0
3 hrs	22	4.4

Average amount of lead collected per hour = 1.46 mg. And the amount of lead per m^3 of leaded air stream = 121 mg.

Figure 16

Calibration curve for analysis of lead using atomic absorption spectrophotometer

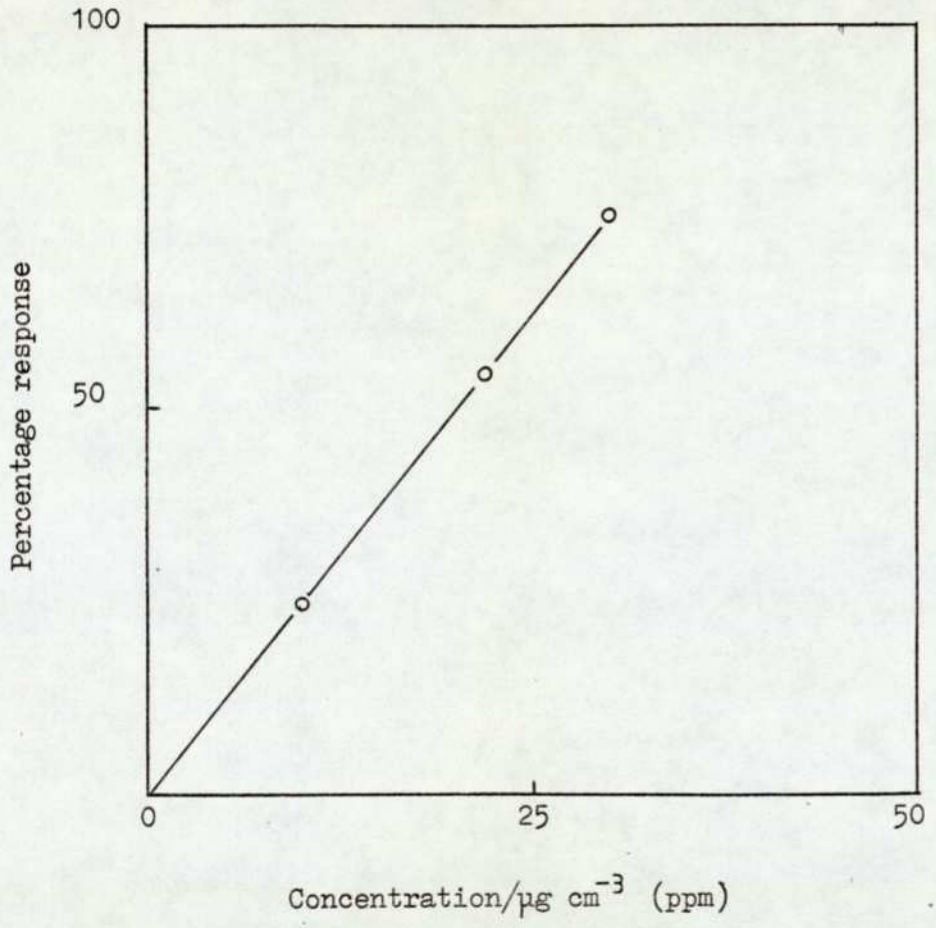

3.4 Poisoning Experiments

Initially the pellistors were poisoned with a mixture consisting of n-heptane, scavengers (dibromoethane and dichloroethane), and TML/toluene. The composition of this mixture was similar to that of commercial gasoline. The sensitivity of the pellistors dropped to half the initial value in 3-4 hours. In order to establish whether the poisoning action was solely due to TML, each constituent of the mixture was separately tested as follows:-

(1) 2 sets of VQ1 pellistors were operated in an atmosphere of n-heptane only for over 45 hours. The results are shown in Figures 17 and 18.

(2) 2 sets of VQ1 pellistors were exposed to an atmosphere of n-heptane/scavenger (dibromoethane and dichloroethane) for 16 hours. These results are shown in Figures 19 and 20.

(3) A set of VQ1 pellistors were poisoned with an n-heptane/TML/air mixture containing 20-25 mg lead m^{-3} of leaded air, (Figure 21).

From this preliminary investigation it was concluded that only TML is responsible for the poisoning action (compare Figures 17-21 and note especially the dramatic drop in sensitivity in the case of n-heptane/TML/air mixture as the poison in Figure 21). Consequently the poisoning mixture used throughout the rest of this work consisted of n-heptane and TML. After having established the optimum operating conditions of the poisoning rig, a series of pellistors were then tested systematically. The poisoning run consisted of exposing the beads to n-heptane/TML/air mixtures for 40 minutes and then monitoring the sensitivity to 1% methane for 20 minutes every hour. Since 2 pellistor blocks were incorporated in the system, each run provided 2 sets of readings. Each series of pellistors were poisoned with n-heptane/TML/air mixtures containing 20-25

Key to poisoning diagrams

o : Response to n-heptane air mixture - Figures 17-18

o : Response to n-heptane/scavengers air mixture - Figures 19-20

o : Response to n-heptane/TML air mixture - Figures 21-50

x : Response to 1% methane

◊ : Air drift, zero set with air flowing

Figure 17. Results of poisoning experiment. Specimen: 453/VQ1, - operated in an atmosphere of n-heptane

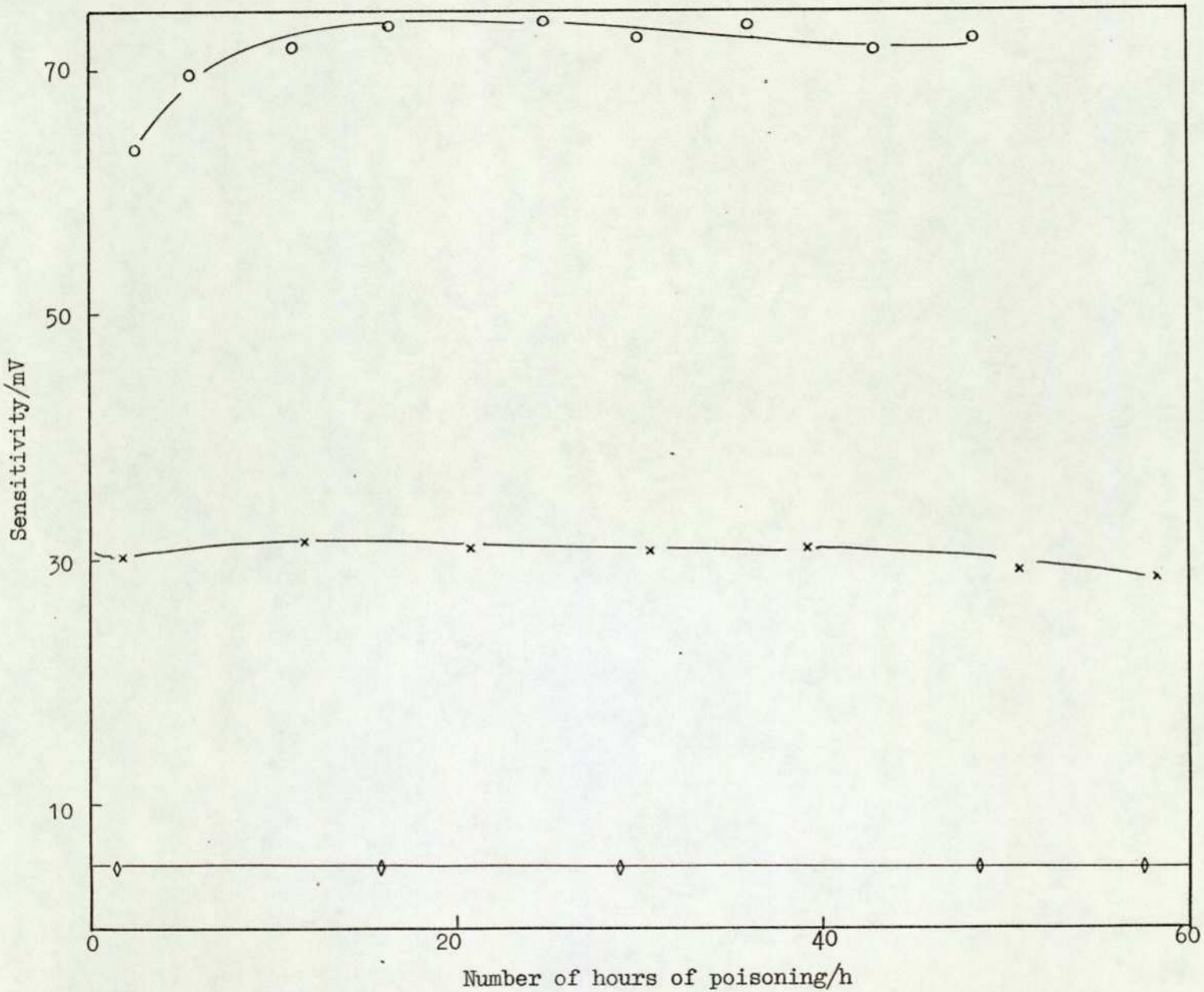

Figure 18

Results of poisoning experiment

Specimen: 461/VQ1, - operated in presence of

n-heptane air mixture as the poison

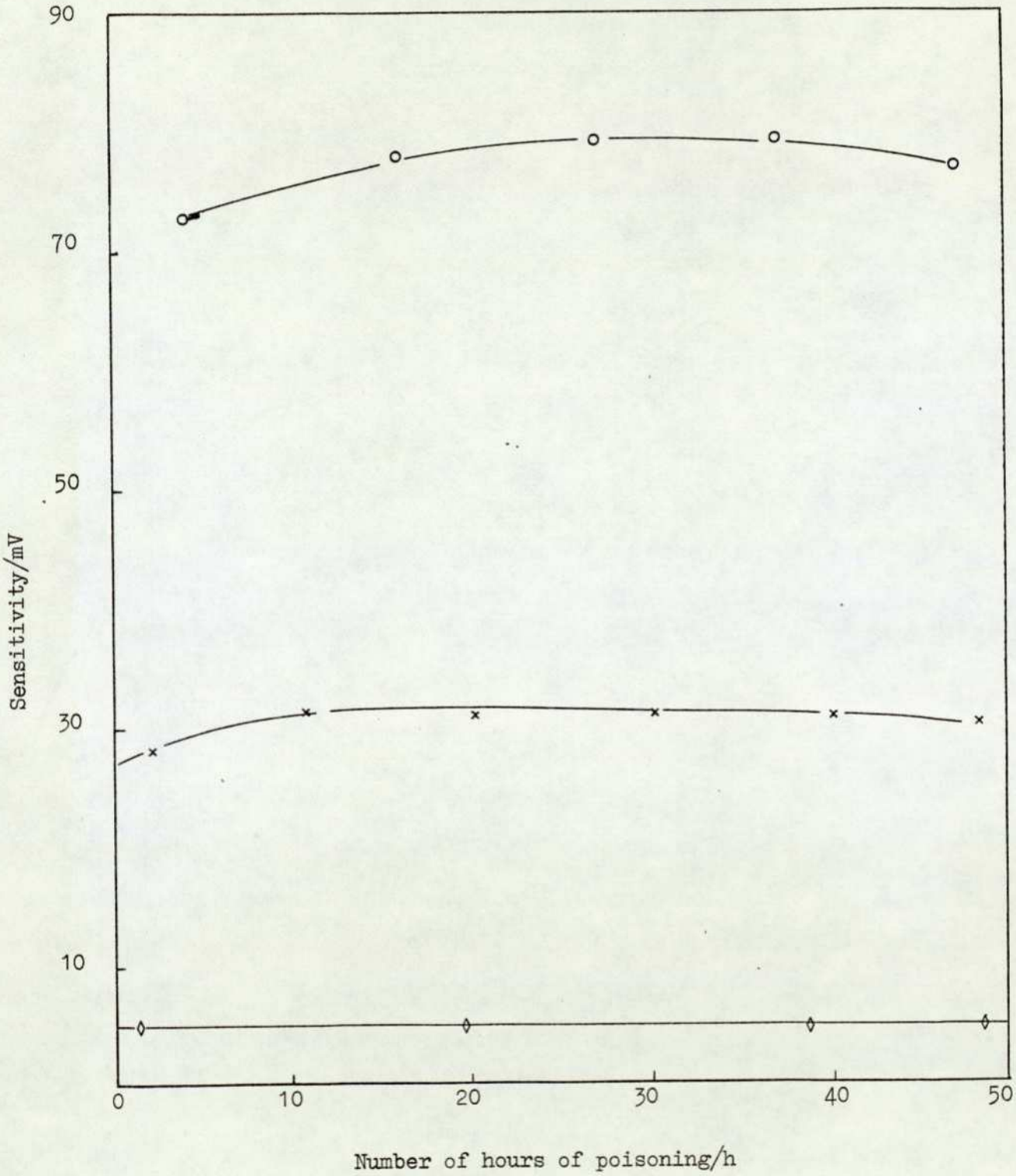

Figure 19

Results of poisoning experiment

Specimen: 304/VQ1, - operated in the presence of n-heptane/scavengers air mixture as the poison

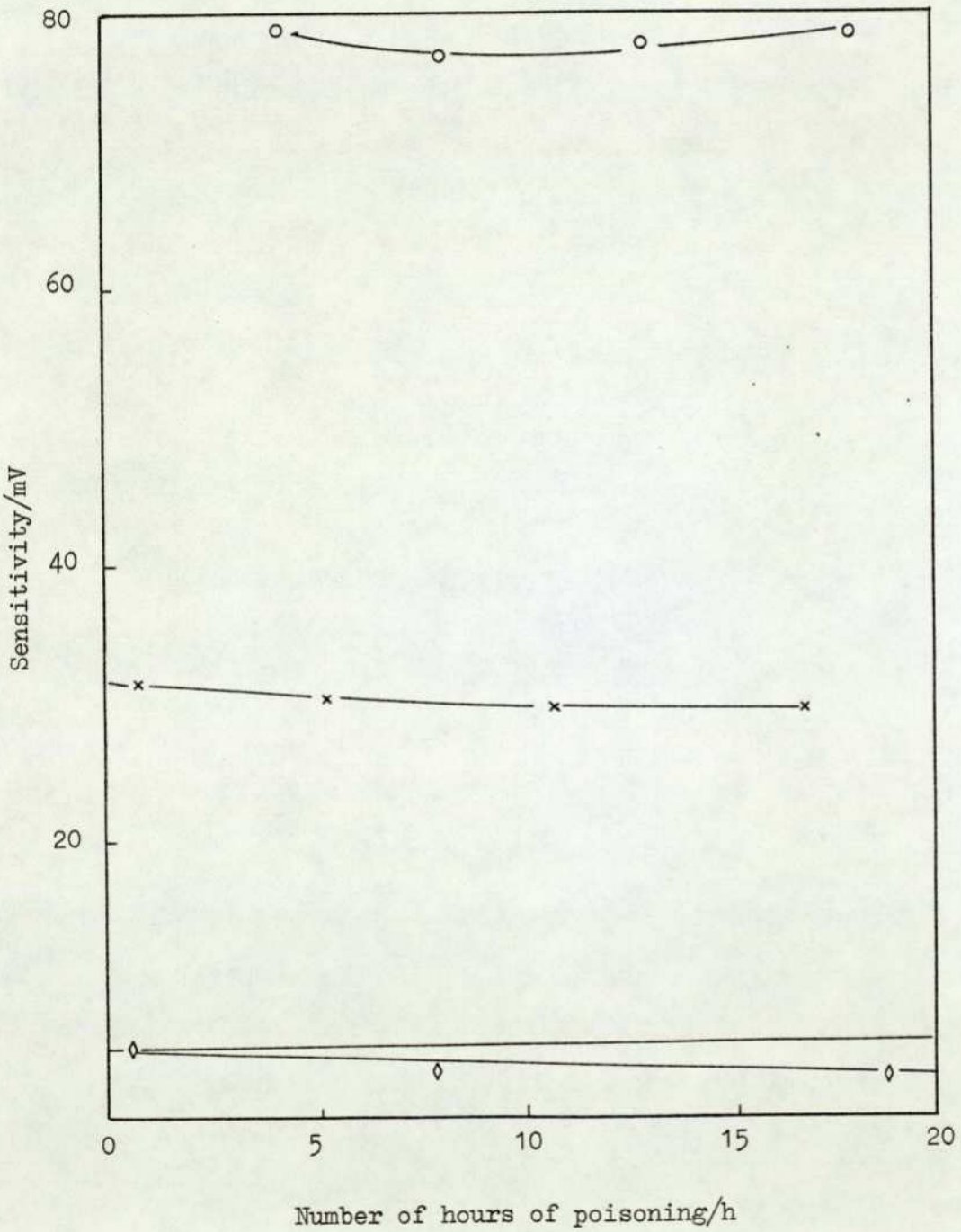

Figure 20

Results of poisoning experiment

Specimen: 306/VQ1, - operated in the presence of

n-heptane/scavengers air mixture as the poison

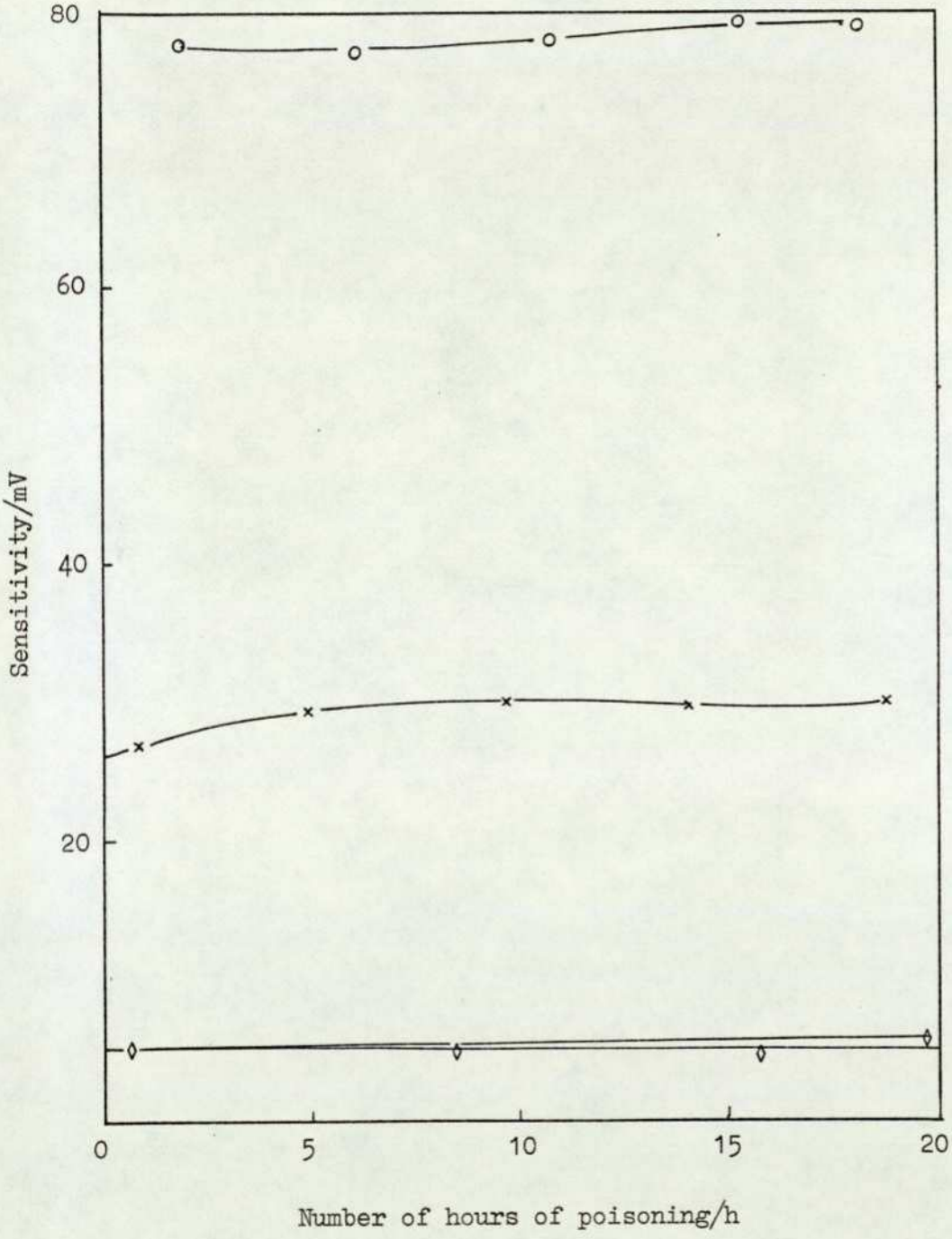

Figure 21 - Results of poisoning experiment

Specimen: 316/VQ1

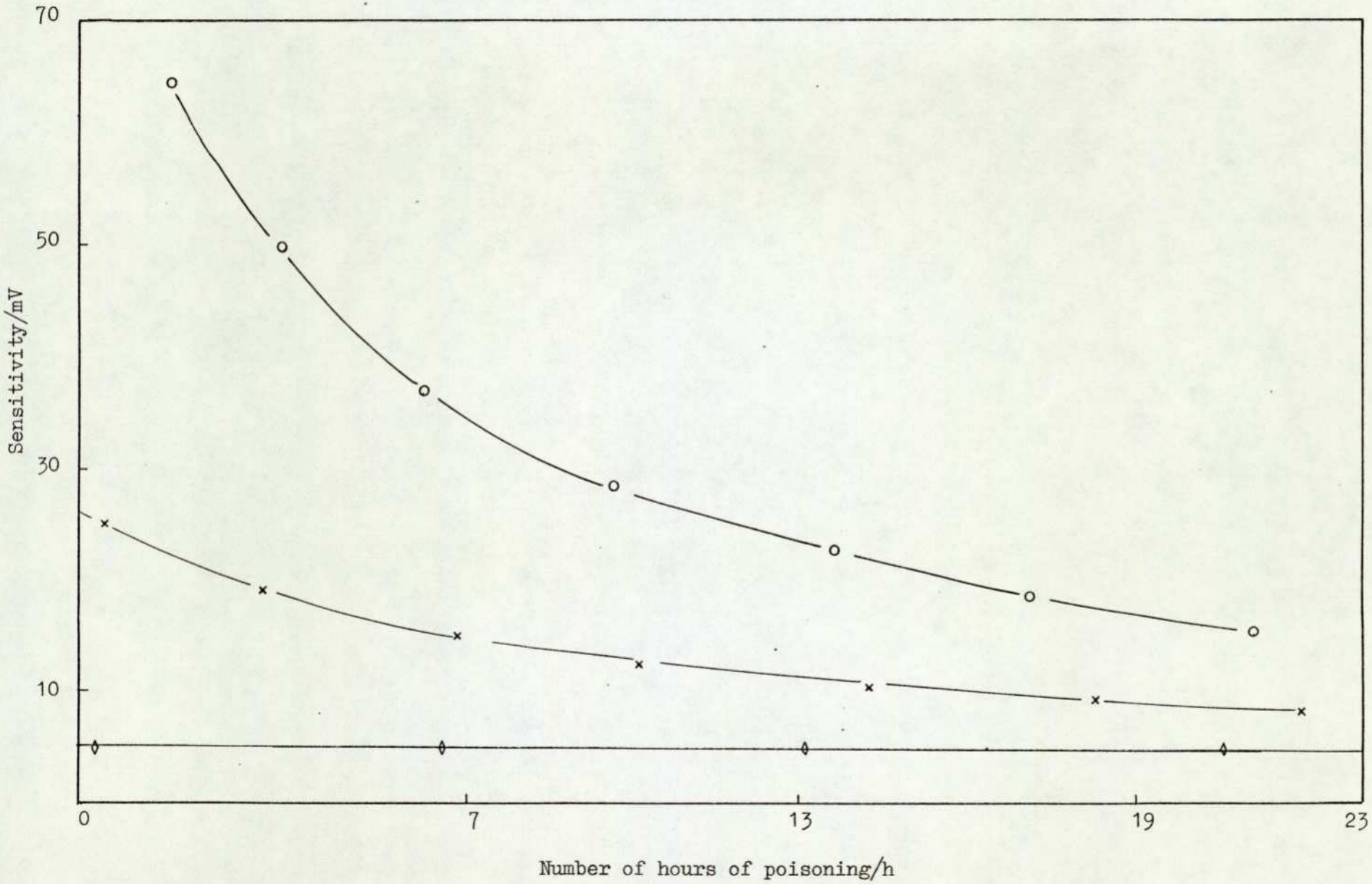

mg m^{-3} of lead as the tetramethyl compound. The results that are quoted below are based on poisoning runs carried out involving at least six, in many cases eight sets of beads of a particular design or type. It is impossible to include the results of every pellistors poisoned, so in the following sections, typical graphs for each case are included.

VQ1 and VQ3 Beads

The initial response to 1% methane always lay within the range of 20-25 mV. After 13 hours of poisoning under the conditions described above, the sensitivity dropped to a value between 20% and 40% of the initial response, the sensitivity being halved after only 3-4 hours. Figures 22 and 23 show typical losses of sensitivity. In addition poisoning results for a series of VQ1 and VQ3 pellistors are summarised in Tables 10 and 11.

VQ1/VQ7 and VQ3/VQ9 Beads

The initial response of these modified beads to 1% methane was approximately half that of a typical VQ1 pellistor (i.e. 10-12 mV). The sensitivity after 13 hours of poisoning, dropped to between 45% and 55% of initial value, but in a non-linear fashion. The initial response was halved after 4-5 hours of poisoning. Figures 24 and 25 show typical curves for sensitivity loss as a function of time. In addition, poisoning results of a series of VQ1/VQ7 and VQ3/VQ9 beads are summarised in Tables 12 and 13. Comparisons of data in Tables 10 and 12 show a substantial improvement in poison resistance (average % residual sensitivity after 3 hours poisoning improves from 60.1% to 79.7%). Similarly, the VQ3/VQ9 beads are more resistant than the VQ1/VQ7, although the scatter of data is more marked than in the VQ1 case.

LD1 Beads

The initial response to 1% methane of LD1 beads were similar to

Figure 22

Results of poisoning experiment

Specimen: 254/VQ1

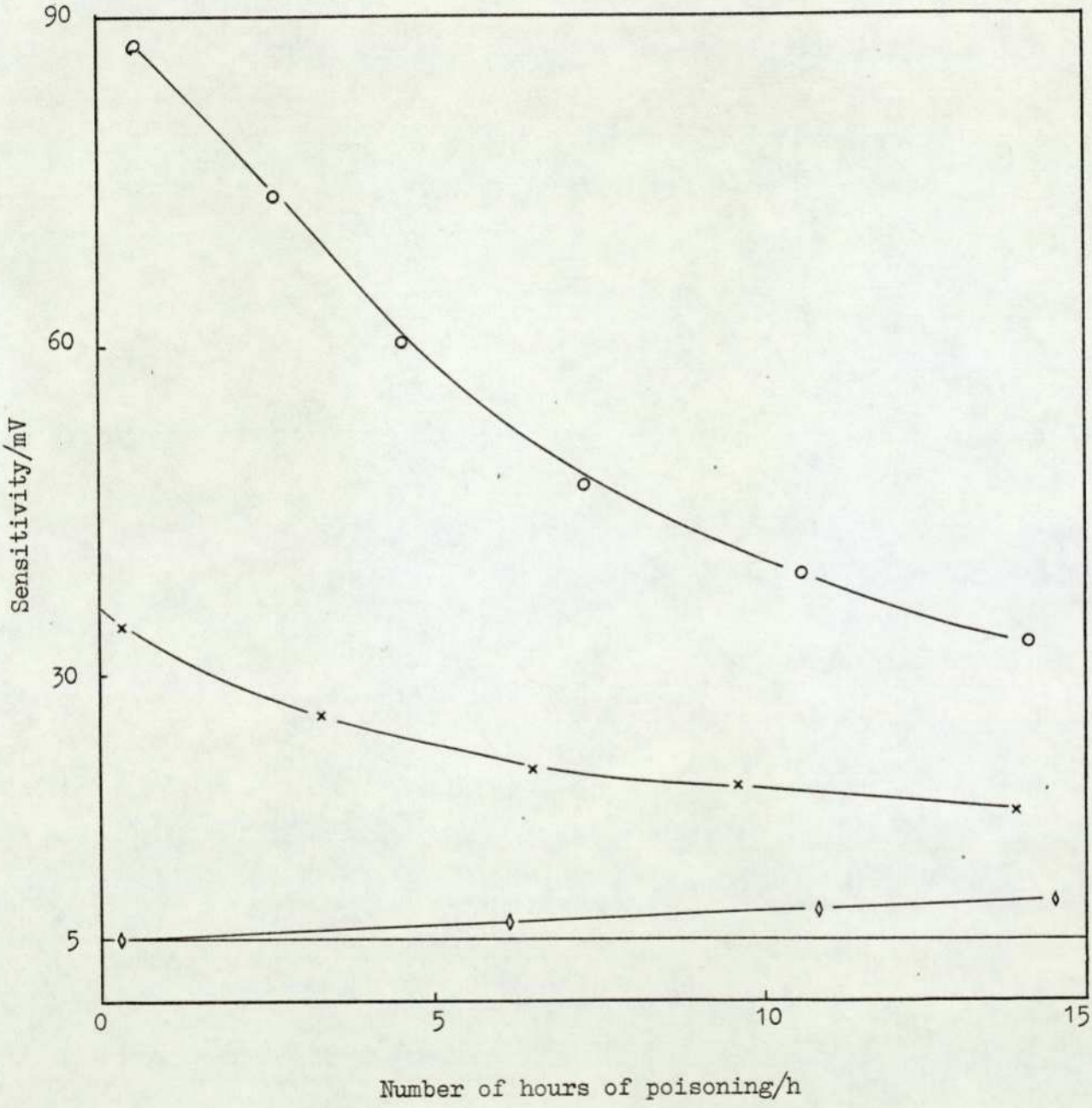

Figure 23

Results of poisoning experiment

Specimen: 910/VQ3

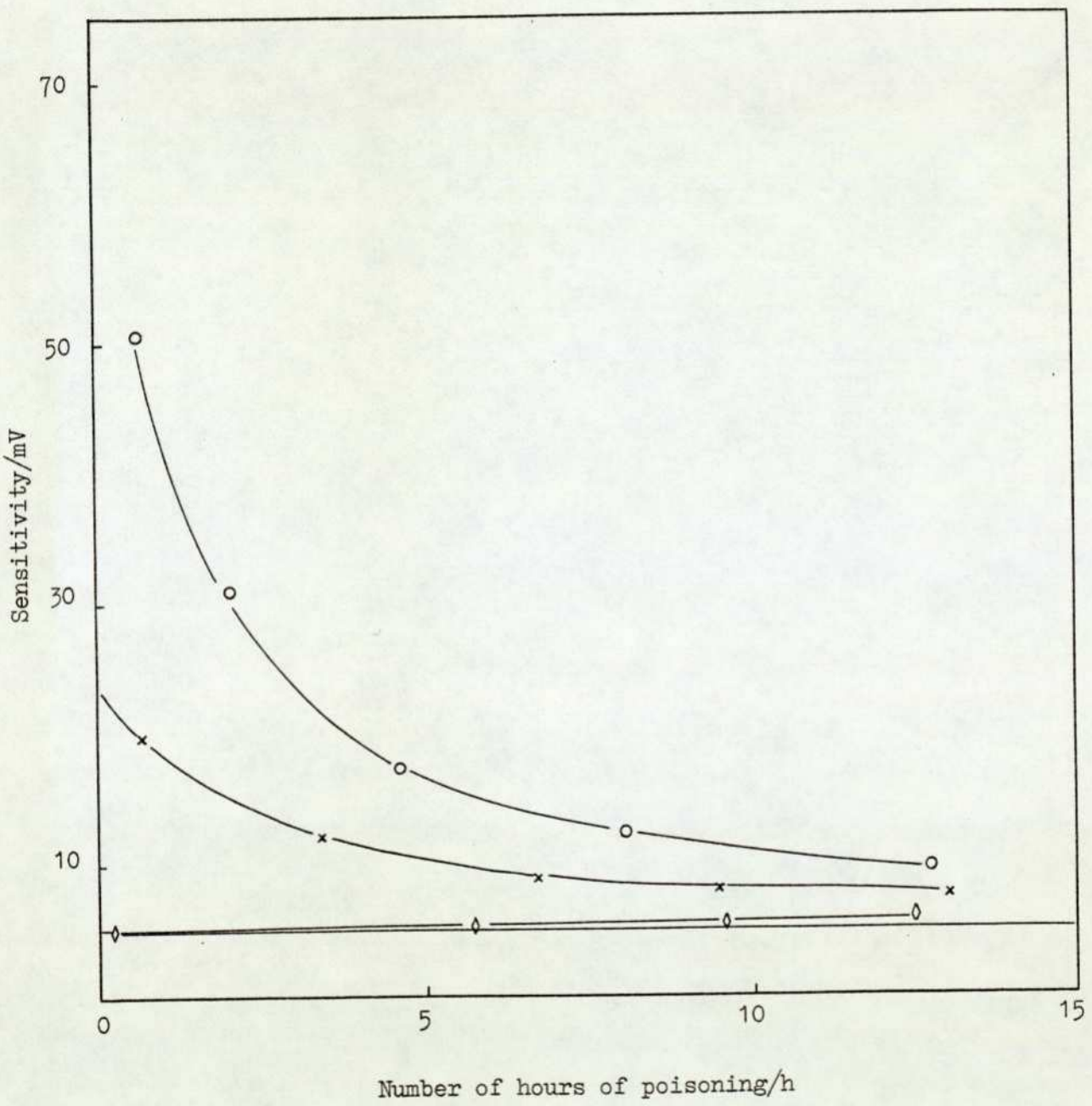

Serial No.	Initial response to 1% CH_4/mV	Final response to 1% CH_4/mV	Percentage sensitivity remaining	Total hours of poisoning/h	Response to 1% CH_4 after 3 hours poisoning/mV	Percentage sensitivity left after 3 hours poisoning	Air drift /mV
254/12/VQ1/R(RT68)	23.5	7.0	29.7	14	16	68.0	+2.5
315/12/VQ1/B(RT100)	24.	4.5	18.7	14	15	62.5	+3.5
317/11/VQ1/B(RT68)	24.5	7.5	30.6	14	15	61.2	-0.5
316/11/VQ1/R(RT56)	20.0	2.5	12.5	14	11.5	57.5	+0.5
291/10/VQ1/B(RT56)	29.0	12.0	41.3	8	17.0	58.6	-
292/10/VQ1/R(RT82)	29.0	9.0	31.0	8	14.0	48.2	-
303/8/VQ1/B(RT56)	20.0	15.0	75.0	3.3	15.0	75.0	+2
294/18/VQ1/R(RT82)	16.0	7.5	46.8	3.3	8.0	50.0	+0.5

TABLE 10 - VQ1

Serial No.	Initial response to 1% CH_4/mV	Final response to 1% CH_4/mV	Percentage sensitivity remaining	Total hours of poisoning/h	Response to 1% CH_4 after 3 hours poisoning/mV	Percentage sensitivity left after 3 hours poisoning	Air drift /mV
910/20/VQ3/R(RT56)	20	2.0	10.0	12	7.5	37.5	+0.5
907/19/VQ3/R(RT47)	23.5	3.5	14.8	14	10.0	42.5	+4.5
903/19/VQ3/B(RT68)	28.0	10.0	35.7	14	18.5	66.0	+2.0
906/18/VQ3/B(RT56)	24.5	10.0	40.8	2.6	-	-	+1.7
905/18/VQ3/R(RT82)	26	10.0	38.4	2.6	-	-	+1.0
903/17/VQ3/B(RT56)	26.5	5.0	18.8	12.6	11.0	41.5	+0.75
904/17/VQ3/R(RT47)	23.0	5.0	21.7	12.6	8.5	36.9	-5.0

TABLE 11 - VQ3

Figure 24

Results of poisoning experiment

Specimen: 678/(VQ1/VQ7)

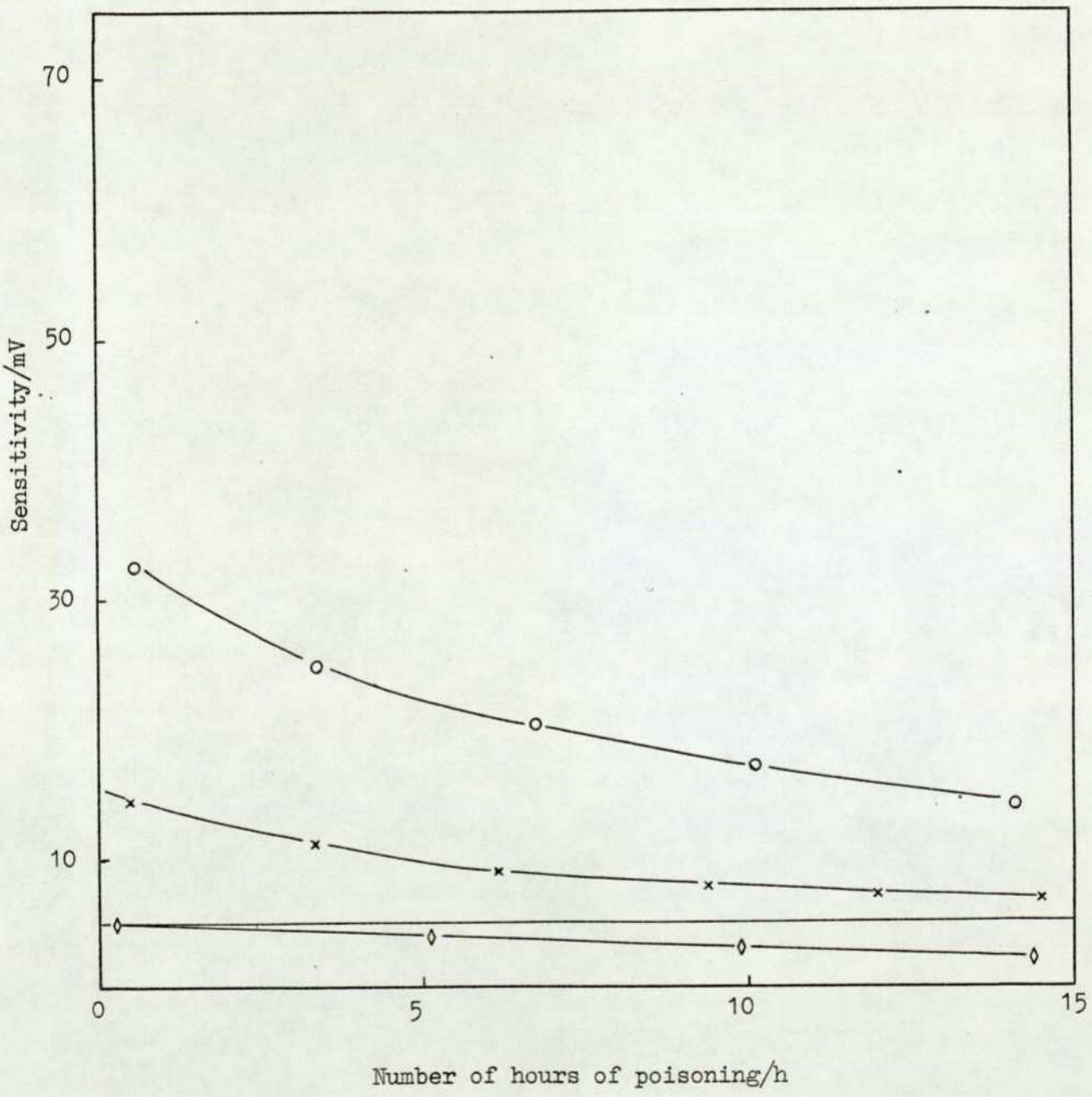

Figure 25

Results of poisoning experiment

Specimen: 981/(VQ3/VQ9)

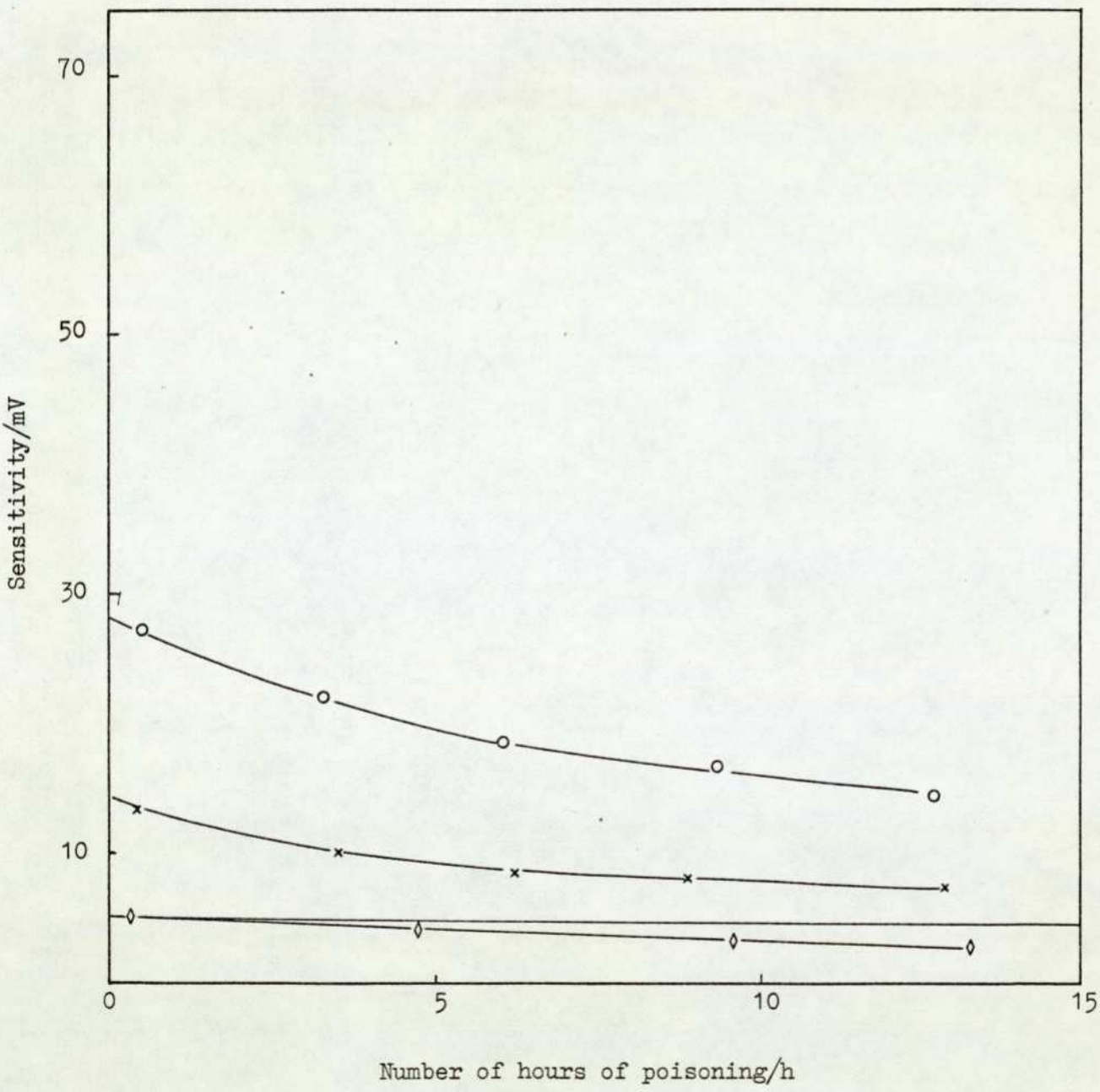

Serial No.	Initial response to 1% CH_4/mV	Final response to 1% CH_4/mV	Percentage sensitivity remaining	Total hours of poisoning/h	Response to 1% CH_4 after 3 hours poisoning/ mV	Percentage sensitivity left after 3 hours poisoning	Air drift /mV
678/15/(VQ1/VQ7)/B(RT-)	9	4.5	50.0	14	7	77.7	-2.5
677/15/(VQ1/VQ7)/R(RT120)	11.5	5.2	45.2	14	9	78.2	-1.0
675/14(VQ1/VQ7)/B/(RT-)	11.0	5.6	50.9	13.3	8.0	72.7	-0.5
676/14/(VQ1/VQ7)/R(RT-)	11.5	5.0	43.4	13.3	8.5	73.9	-1.0
673/13/(VQ1/VQ7)/R(RT-)	12.5	5.2	41.6	14	11.5	92.0	+2.5
674/13/(VQ1/VQ7)/B(RT-)	12.5	5.0	40.0	14	10.5	84.0	+1.5
672/9/(VQ1/VQ7)/B(RT-)	12.0	7.0	58.3	15.3	9.5	79.1	-1.25
671/9/(VQ1/VQ7)/R(RT-)	12.5	4.5	36.0	15.3	10.0	80.0	+1.25

TABLE 12 - VQ1/VQ7

Serial No.	Initial response to 1% CH_4/mV	Final response to 1% CH_4/mV	Percentage sensitivity remaining	Total hours of poisoning/h	Response to 1% CH_4 after 3 hours poisoning/mV	Percentage sensitivity left after 3 hours poisoning	Air drift/mV
987/24/(VQ3/VQ9)/R(RT100)	7.0	4.0	57.1	12.6	5.5	78.5	-5.5
988/24/(VQ3/VQ9)/B(RT120)	7.5	4.25	56.6	12.6	5.5	73.3	-5.0
985/23/(VQ3/VQ9)/R(RT47)	7.0	2.5	35.7	11.3	3.0	42.8	-5.0
981/21/(VQ3/VQ9)/R(RT120)	9.0	5.0	55.5	12.6	5.5	61.1	-2.5
982/21/(VQ3/VQ9)/B(RT120)	8.0	4.0	50.0	12.6	4.5	56.2	-2.5
983/22/(VQ3/VQ9)/R(RT120)	8.5	3.75	44.1	13.3	5.5	64.7	-5.0
984/22/(VQ3/VQ9)/B(RT120)	10.5	7.0	66.6	13.3	9.5	90.4	-2.5

TABLE 13 - VQ3/VQ9

those found with VQ1 pellistors (i.e. 20-25 mV). The sensitivity after 13 hours of poisoning dropped to 20-30% and the initial sensitivity was halved after 3 hours of poisoning. Thus the LD1 beads behaved in a manner very similar to the VQ1 and VQ3 beads. The loss of sensitivity as a function of hours of exposure to leaded atmosphere as shown in Figure 26, and the results obtained from poisoning experiments on a series of LD1 pellistors are summarised in Table 14.

LD1/LD7 Beads

The initial response to 1% methane of this series of pellistors was $\sim$50% that of the VQ1 beads (i.e. 10-15 mV), but the sensitivity after 13 hours of poisoning only dropped to 60-65% of the original, which was a significant improvement over even the VQ1/VQ7 series. The half lives of the LD1/LD7 pellistors were substantially greater than 14 hours in all cases. Typical results, for one particular pellistor of the LD1/LD7 type, is shown in Figure 27, and the results of a series of LD1/LD7 pellistors are summarised in Table 15.

LD1/LD $^{3}/_{1}$ Beads

The initial response to 1% methane was within the range 25-30 mV. After 14 hours of poisoning, the sensitivity dropped to between 10% and 25% of the original, and the half life was only about 3 hours. Thus the behaviour observed was similar to that of the original VQ1 and VQ3 pellistors. Figure 28 shows the results for one particular LD1/LD $^{3}/_{1}$ pellistor, and Table 16 summarises the results of a series of LD1/LD $^{3}/_{1}$ pellistors.

LD1/LD $^{3}/_{1}$/LD7 Beads

The initial response to 1% methane before poisoning lay in the range 6-11 mV. After 13 hours of poisoning the sensitivity dropped to between 40% and 55% of the initial value. Again the latter value was halved in about 3-5 hours (consider Figure 29, allowing also for the zero

Figure 26

Results of poisoning experiment

Specimen: 144/LD1

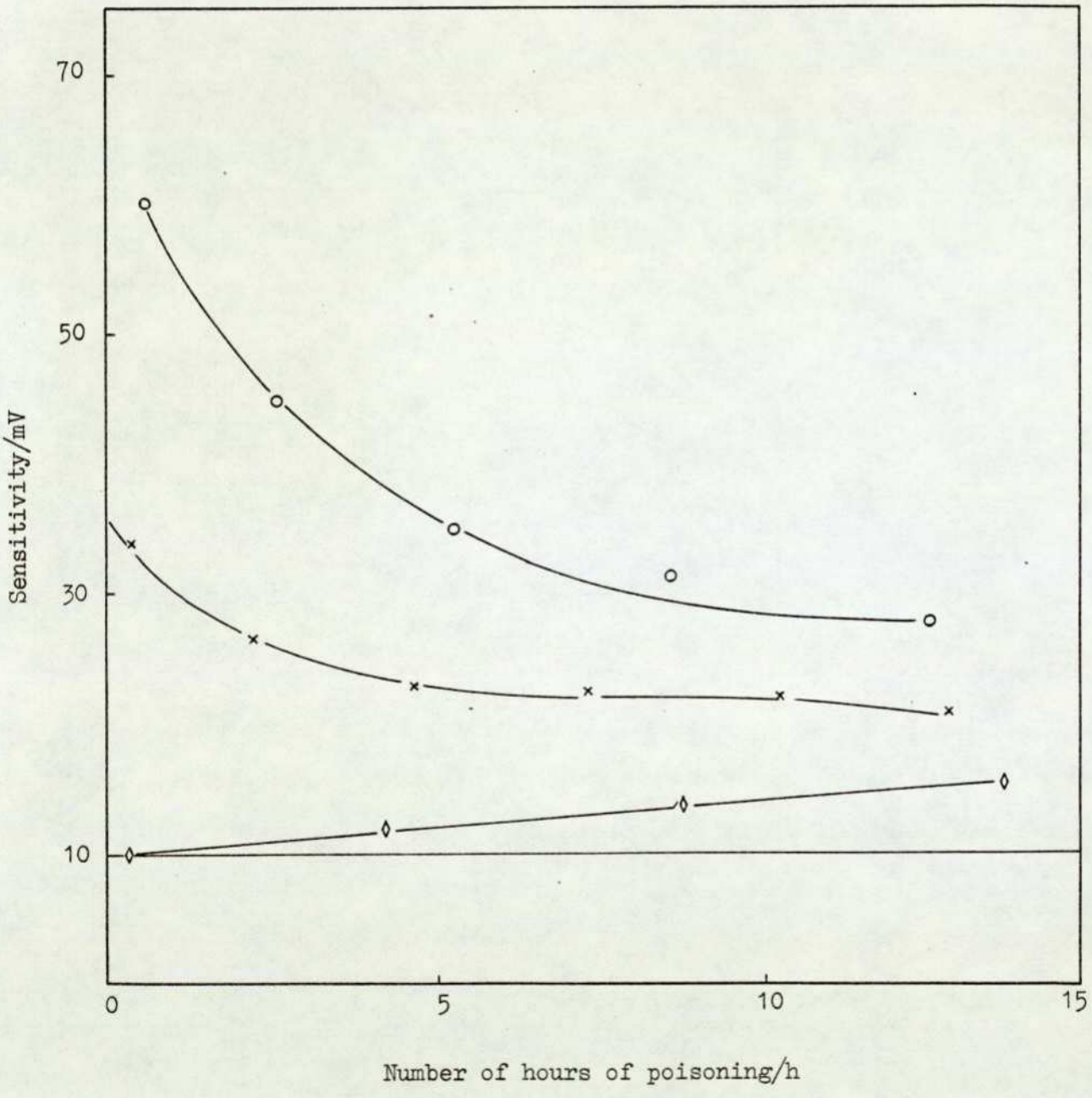

Serial No.	Initial response to 1% CH_4/mV	Final response to 1% CH_4/mV	Percentage sensitivity remaining	Total hours of poisoning/h	Response to 1% CH_4 after 3 hours poisoning/mV	Percentage sensitivity left after 3 hours poisoning	Air drift /mV
146/25/LD1/R(RT56)	24	5.25	21.8	13.3	13.2	55.0	+0.5
144/25/LD1/B(RT56)	26	5.5	21.1	13.3	13.5	51.9	+5.5
148/26/LD1/B(RT56)	20.25	2.0	9.8	14.0	6.5	32.0	+1.0
150/26/LD1/R(RT56)	24.0	3.0	12.5	14.0	9.5	39.5	+1.0
148/27/LD1/B(RT100)	23.0	7.0	30.4	13.3	12.5	54.3	-3.5
145/27/LD1/R(RT56)	27.5	5.0	18.18	13.3	11.5	41.8	+0.5
149/28/LD1/B(RT56)	27.0	5.0	18.5	14.6	13.5	50.0	+2.5
142/28/LD1/R(RT82)	30.0	9.5	31.6	14.6	19.0	63.3	+0.5

TABLE 14 - LD1

Figure 27

Results of poisoning experiment

Specimen: 131/(LD1/LD7)

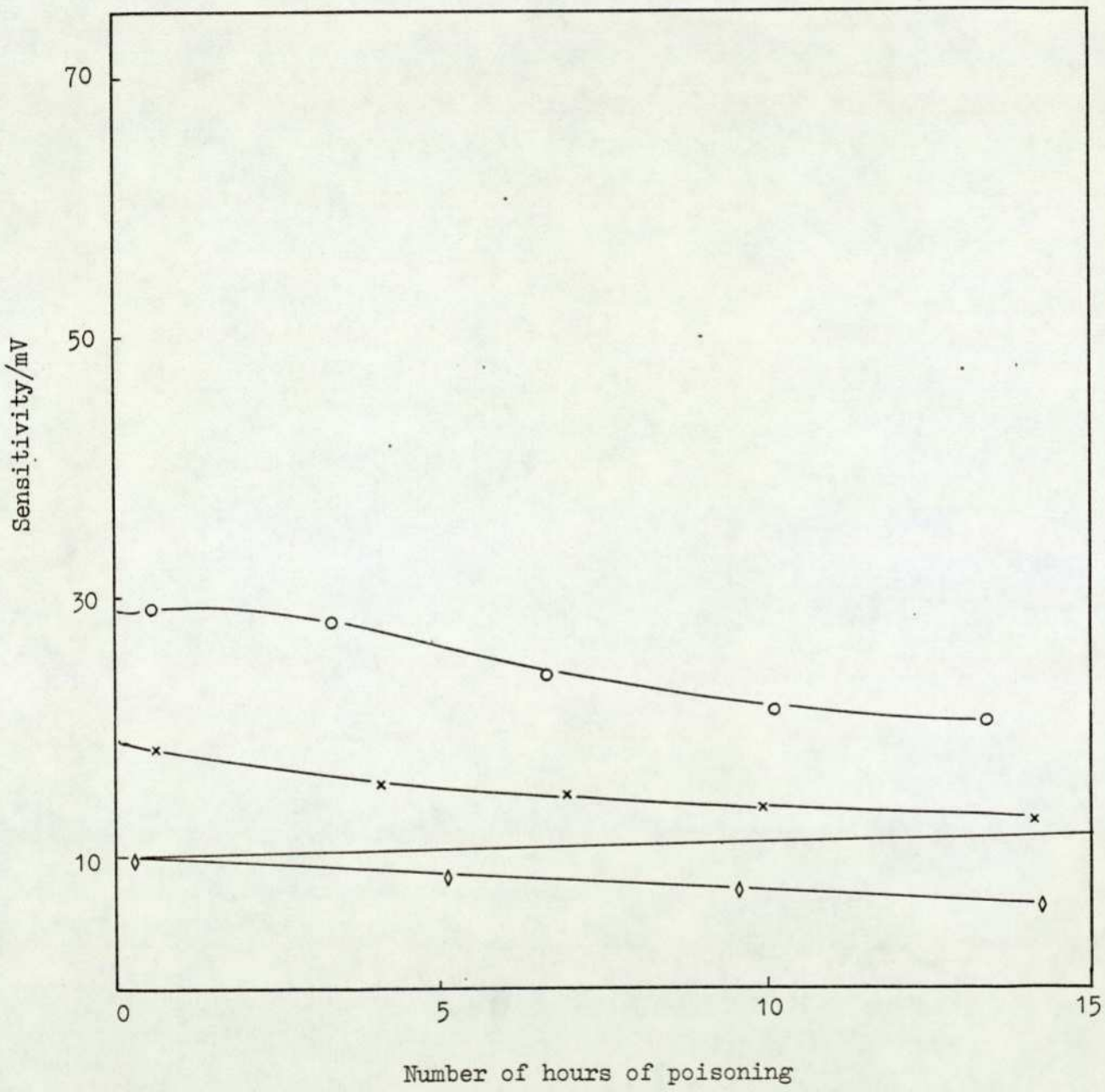

Serial No.	Initial response to 1% CH_4/mV	Final response to 1% CH_4/mV	Percentage sensitivity remaining	Total hours of poisoning/h	Response to 1% CH_4 after 3 hours poisoning/mV	Percentage sensitivity left after 3 hours poisoning	Air drift /mV
132/29/(LD1/LD7)/R(RT-)	10.5	6.5	61.9	14.0	8.75	83.3	+0.25
131/29/(LD1/LD7)/B(RT-)	10.0	6.5	65.0	14.0	7.0	70.0	-3.5
134/30/(LD1/LD7)/R(RT-)	7.0	9.5	-	3.3	7.5	-	+2.5
133/30/(LD1/LD7)/B(RT-)	14.5	13.0	89.1	3.3	13.0	89.6	-0.25
136/31/(LD1/LD7)/R(RT-)	23.5	10.75	45.7	16.0	18.5	78.7	+4.0
135/31/(LD1/LD7)/B(RT-)	10.5	6.5	61.9	16.0	9.0	85.7	-1.5
138/32/(LD1/LD7)/R(RT-)	14.25	9.5	66.6	12.0	12.5	87.7	+3.0

TABLE 15 - LD1/LD7

Figure 28

Results of poisoning experiment

Specimen: 231/(LD1/LD3/1)

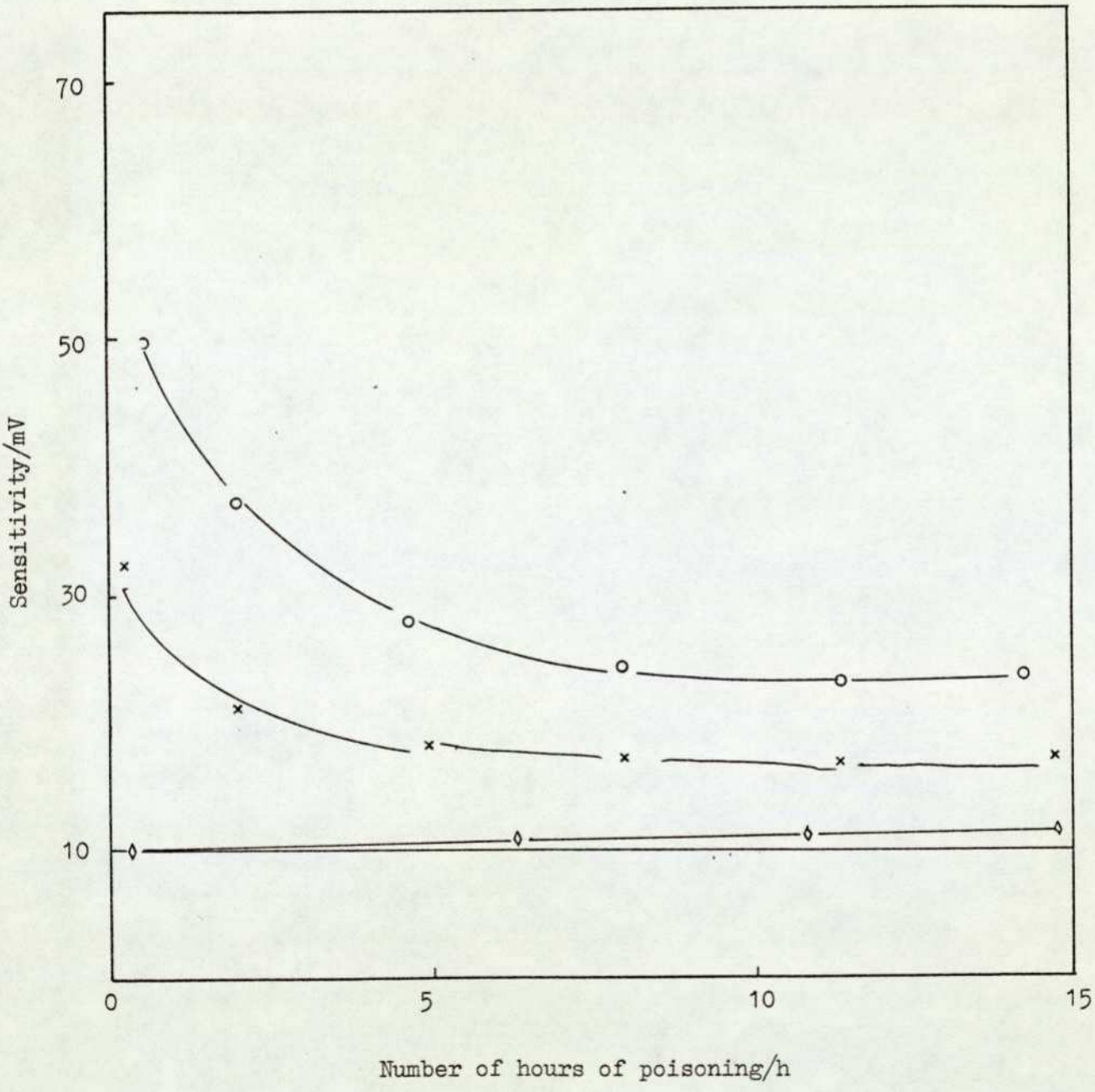

Serial No.	Initial response to 1% CH_4/mV	Final response to 1% CH_4/mV	Percentage sensitivity remaining	Total hours of poisoning/h	Response to 1% CH_4 after 3 hours poisoning/ mV	Percentage sensitivity left after 3 hours poisoning	Air drift /mV
238/36/(LD1/LD3/1)/R(RT56)	26.5	3.0	11.3	16.5	8.5	32.0	+1.0
237/36/(LD1/LD3/1)/B(RT68)	30.0	7.0	23.3	16.5	17.5	58.0	-0.5
235/35/(LD1/LD3/1)/B(RT82)	32.5	8.0	24.6	15.5	17.5	53.8	-4.5
236/35/(LD1/LD3/1)/R(RT82)	32.5	13.0	40.0	15.5	23.5	72.3	+0.75
233/34/(LD1/LD3/1)/B(RT56)	26.5	4.0	15.0	15.5	10.25	38.6	-2.0
234/34/(LD1/LD3/1)/R(RT56)	24.0	6.0	25.0	15.5	10.0	43.7	-4.5
231/33/(LD1/LD3/1)/B(RT56)	27.0	5.0	18.5	14.5	9.0	33.3	+1.0
232/33/(LD1/LD3/1)/R(RT56)	29.5	3.75	12.7	14.5	9.75	32.7	+3.5

TABLE 16 - LD1/LD3/1

drift). The results are shown in Figure 29 and Table 17.

From the above series of poisoning experiments, the general conclusion is that LD1/LD7 pellistors showed greatest resistance to poisoning, with the next best being the VQ1/VQ7 and VQ3/VQ9 series. All three types of beads has an initial response to 1% methane (10-15 mV) which was markedly less than their corresponding unmodified analogues (i.e. the VQ1, VQ3 and LD1). An undesirable quality of all the pellistors tested to this point was the large zero drifts observed during poisoning runs, ranging from -5.0 to +4.0 mV.

3.5 Topographical Study of Poisoned VQ1 and VQ3 Beads Using SEM

The surfaces of both pellistor types appeared rough, with large void spaces which were non-uniform in size, shape and length, and not following any pattern. Comparing with unpoisoned VQ1 and VQ3 beads, it was apparent that no special features such as growths, or deposits of any kind were observed that could be solely attributed to the presence of lead on the surface. Although more globular features could be detected on the surface of some poisoned beads, these were also observed in some unpoisoned beads, so no special significance could be placed on their presence. A series of micrographs of poisoned VQ1 and VQ3 are assembled on Plates 12-19.

The fact that the same detector bead cannot be used for microscopic examination twice (i.e. before and after poisoning) makes it difficult to assess if there has been any change in the surface structure of any particular bead on treatment with the poison. However, by comparing several micrographs of quantities of both poisoned and unpoisoned beads,

Figure 29

Results of poisoning experiment

Specimen: 683/(LD1/LD3/1/LD7)

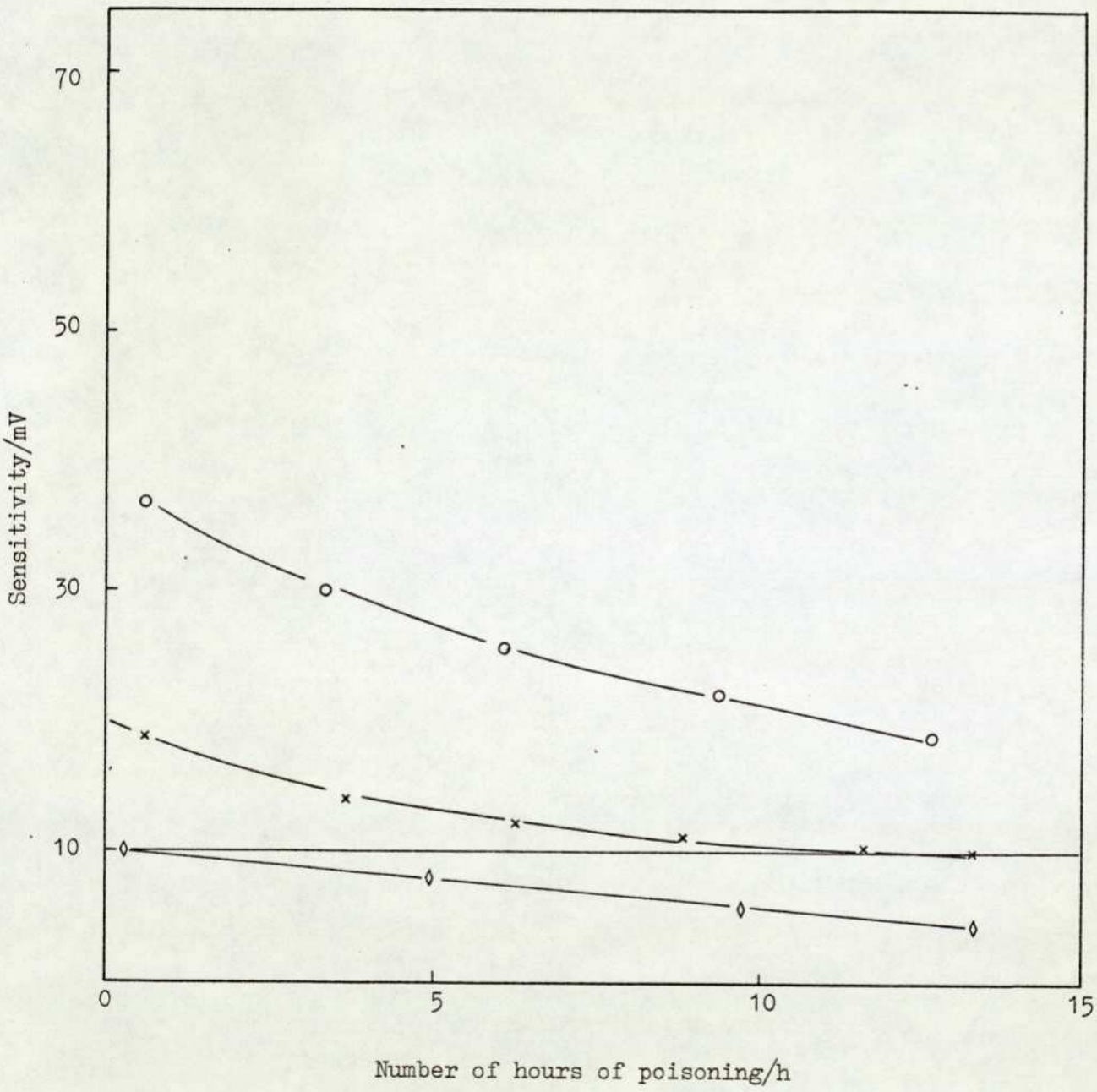

Serial No.	Initial response to 1% CH_4/mV	Final response to 1% CH_4/mV	Percentage sensitivity remaining	Total hours of poisoning/h	Response to 1% CH_4 after 3 hours poisoning/mV	Percentage sensitivity left after 3 hours poisoning	Air drift /mV
683/37/(LD1/LD3/1/LD7)/R(RT-)	10	5.25	52.5	12	6.5	65.0	-5.5
684/37/(LD1/LD3/1/LD7)/B(RT-)	9	5.0	55.5	12	5.0	55.5	-9.0
685/38/(LD1/LD3/1/LD7)/R(RT-)	6.5	3.5	53.8	12	3.5	53.8	-7.0
686/38/(LD1/LD3/1/LD7)/B(RT-)	10.25	5.0	48.7	12	8.0	78.0	-5.0
688/39/(LD1/LD3/1/LD7)/R(RT-)	8.5	4.5	52.9	14	5.0	58.8	-4.5
687/39/(LD1/LD3/1/LD7)/B(RT-)	9.0	4.25	47.2	14	6.25	68.0	-3.5
682/40/(LD1/LD3/1/LD7)/R(RT390)	9.5	4.25	44.7	14	5.5	52.6	-6.75
681/40/(LD1/LD3/1/LD7)/B(RT-)	10.5	4.5	42.8	14	7.0	66.6	-5.75

TABLE 17 - LD1/LD3/1/LD7

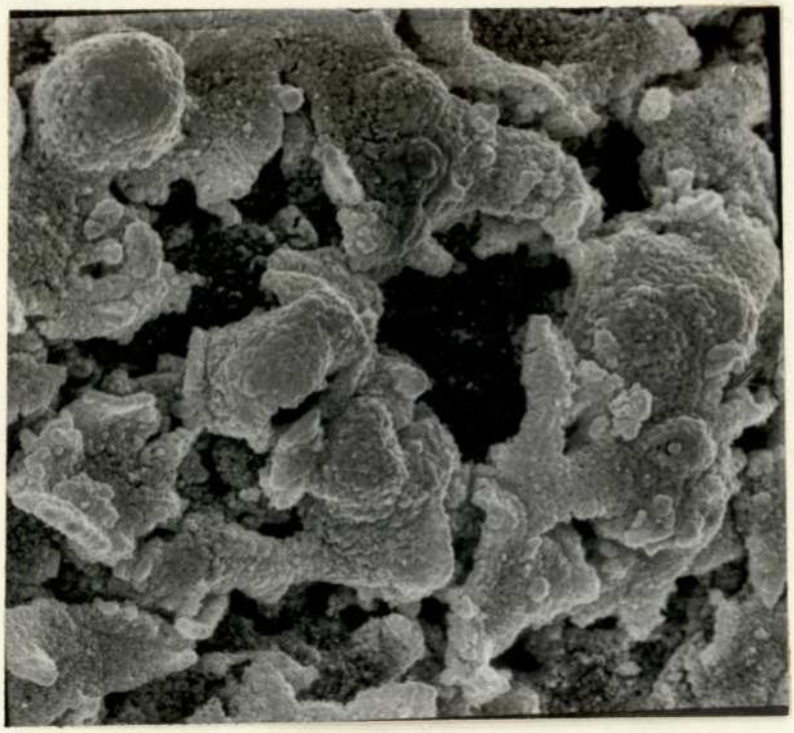

Magnification x1000, angle of tilt 30°

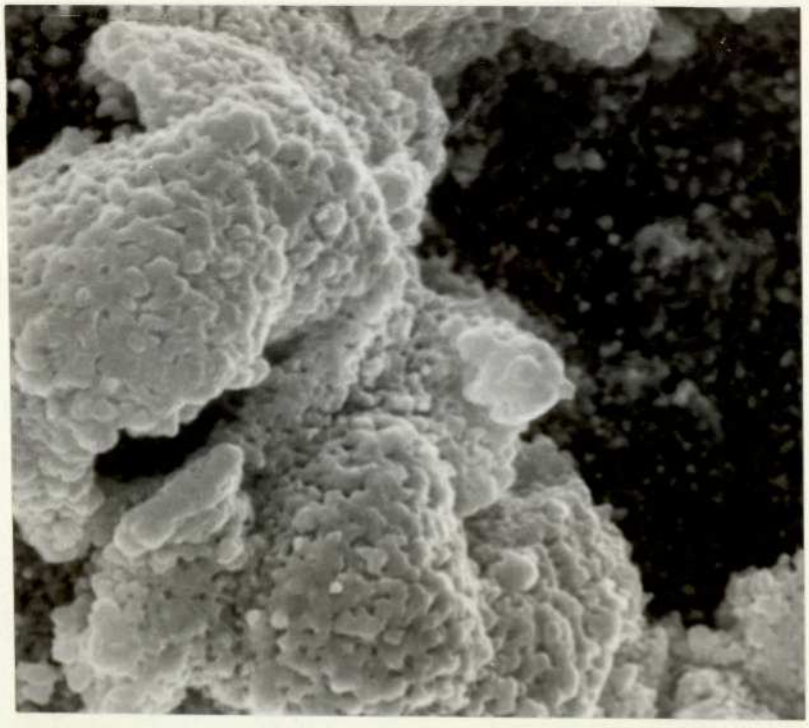

Magnification x3000, angle of tilt 30°

Plate 12 - Poisoned VQ1 (441)

Magnification x1000, angle of tilt 30°

Magnification x300, angle of tilt 30°

Plate 13 - Poisoned VQ1 (537)

Magnification x300, angle of tilt 0°

Magnification x1000, angle of tilt 0°

Plate 14 - Poisoned VQ1 (316)

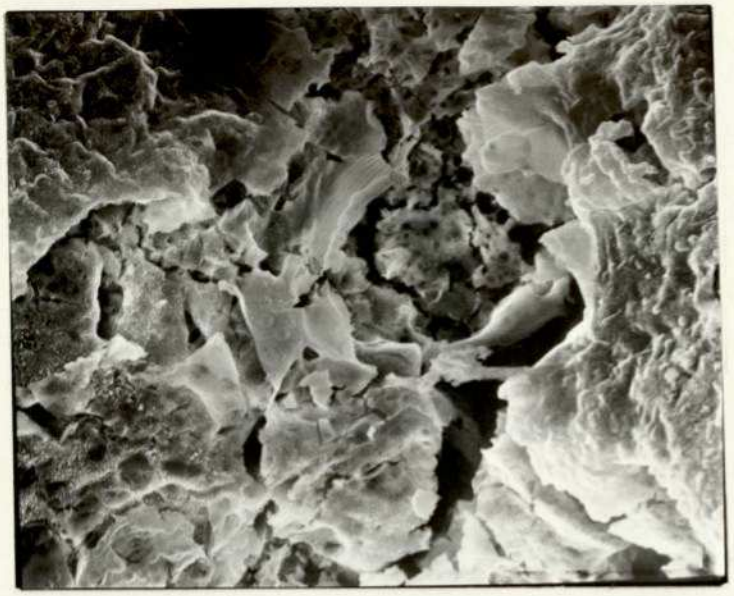

Magnification x1000,
angle of tilt 30°

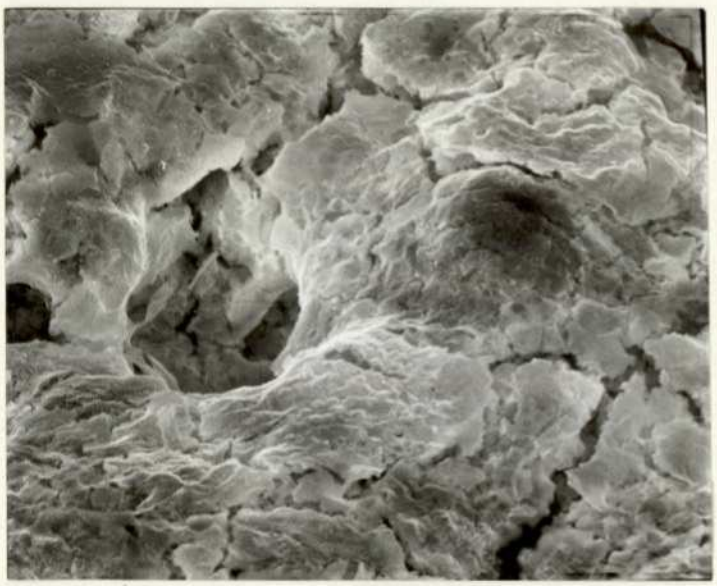

Magnification x1000,
angle of tilt 30°

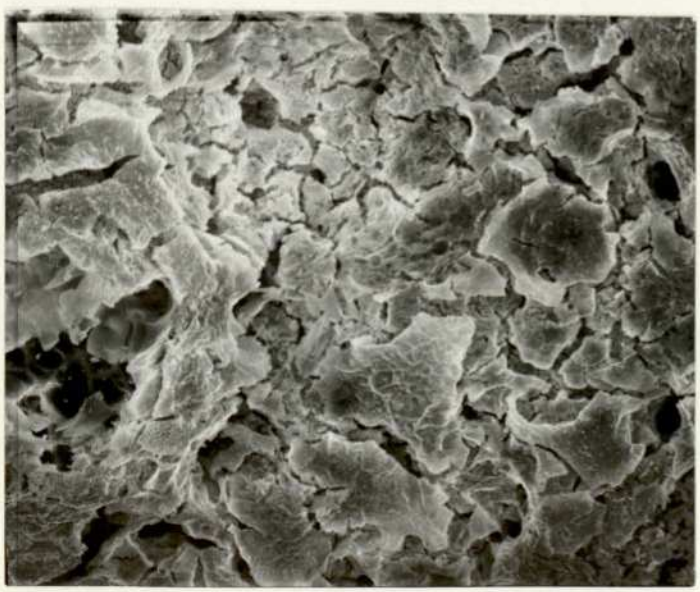

Magnification x1000,
angle of tilt 30°

Plate 15

Poisoned VQ3 (907)

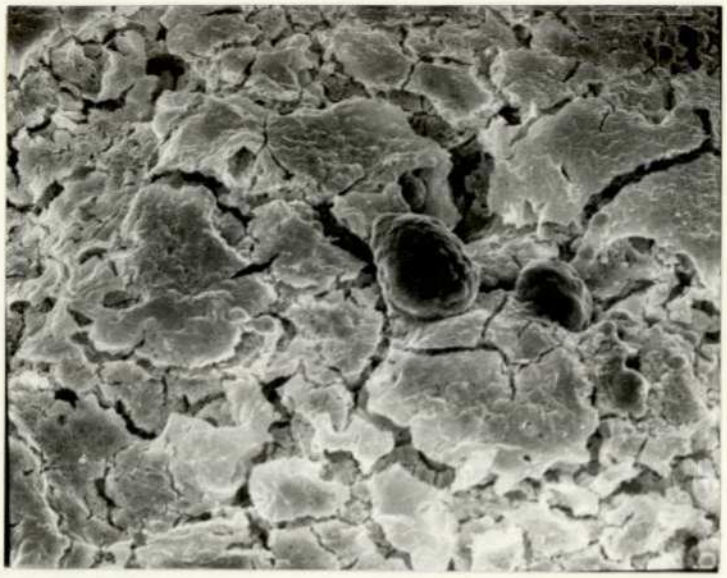

Magnification x1000, angle of tilt 0°

Magnification x1000, angle of tilt 30°

Plate 16 - Poisoned VQ3 (905)

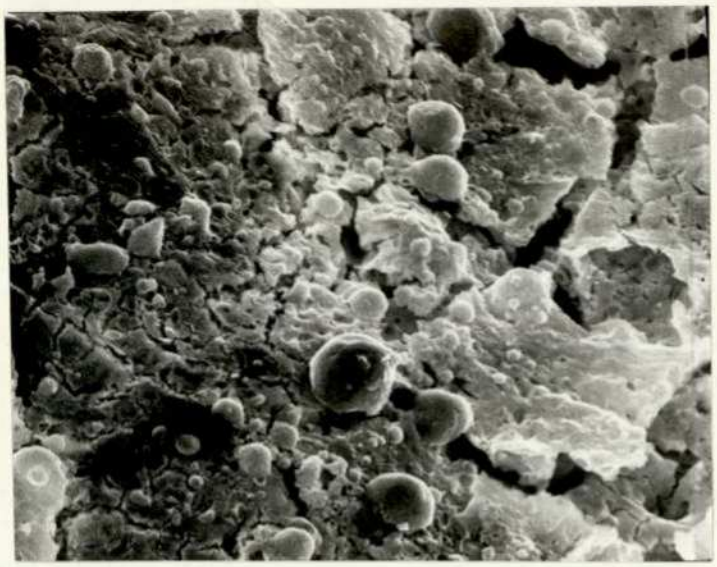

Magnification x1000, angle of tilt 30°

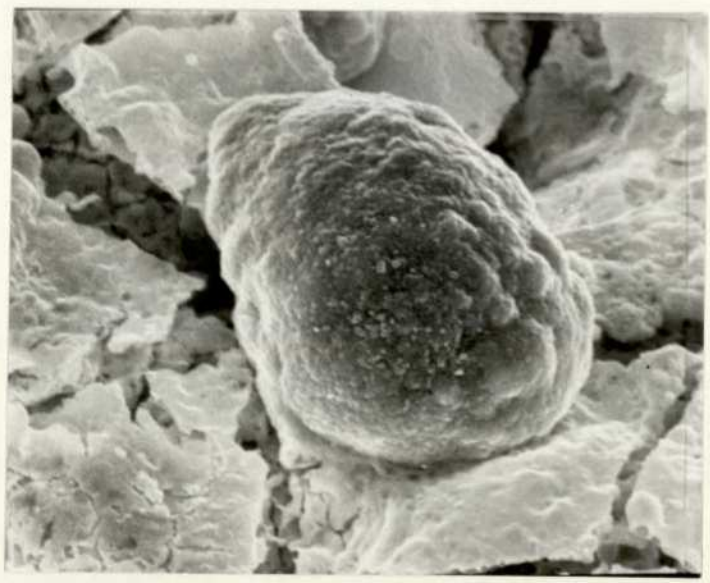

Magnification x3000, angle of tilt 0°

Plate 17 - Poisoned VQ3 (905)

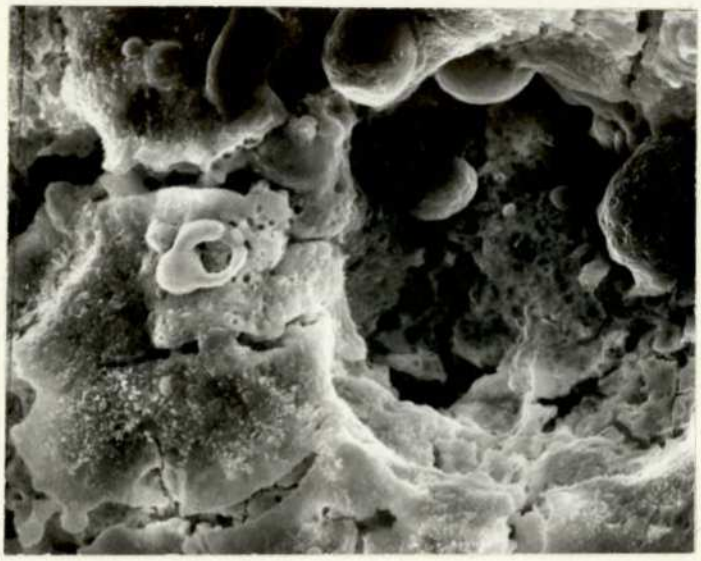

Magnification x1000, angle of tilt 30°

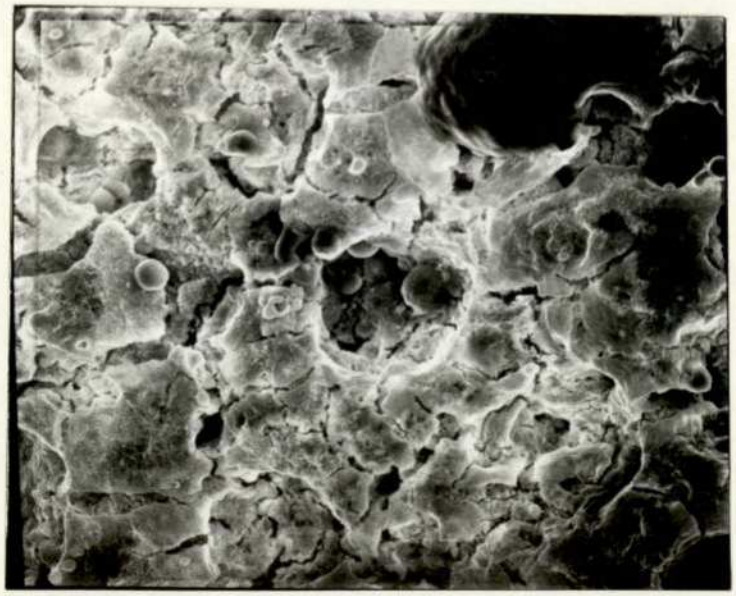

Magnification x300, angle of tilt 30°

Plate 18 - Poisoned VQ3 (903)

Low magnification,
angle of tilt 0°

Magnification x300,
angle of tilt 30°

Magnification x1000,
angle of tilt 30°

Plate 19

Poisoned VQ3 (907)

one can draw a general conclusion that the presence of lead on the surface does not influence the structure and topography of the catalyst surface in any significant way.

3.6 Elemental Analysis of Poisoned Beads Using Energy Dispersive Analysis of X-rays (EDAX)

The spherical shape and surface roughness of the bead made it difficult to carry out quantitative analysis, but by comparing line intensities of different elements present, an estimate of the amount of lead as a comparative percentage of other element present on the surface was obtained.

VQ1 Beads

Several poisoned beads were examined; a typical spectrum of a specimen which had been poisoned for 14 hours with a leaded air stream containing 20-25 mg m^{-3} lead as TML, is shown in Plate 20, together with the corresponding "stick diagram". The lines are identified in Table 18. By comparison, the ratio of the intensities of Lα Pb and Lα Pt for a flat specimen of standard composition (i.e. containing equal amounts of lead and platinum) at 40 kV accelerating voltage and 30° angle of tilt was (0.50/0.56). The ratio of Lα Pb/Lα Pt observed by EDAX in the specimen was (781/568), hence the ratio of lead to platinum was 1.22:1. In effect, there was roughly 1.22 parts of lead to every part of platinum on the surface of the poisoned VQ1 (316) specimen (Plate 20).

VQ3 Beads

A typical spectrum of a poisoned VQ3 bead is shown on Plate 21, together with the corresponding stick diagram. The lines are identified in Table 19. This bead had also been poisoned for 14 hours with the usual

TABLE 18

Poisoned VQ1 (316) Bead

Element	Peak No.	Position eV	Lines	Integral
Aluminium	1	1450	$K\alpha$Al	673
	1A	1550	$K\beta$Al	806
Platinum	2	2100	$M\alpha$Pt	509
Lead	3	2350	$M\alpha$Pb	686
Palladium	4	2800	$L\alpha$Pd	373
	4A	2950	$L\beta_1$Pd	401
	4B	3150	$L\beta_2$Pd	179
Nickel	5	7450	$K\alpha$Ni	378
	5A	8250	$K\beta$Ni	188
Platinum	6	9400	$L\alpha$Pt	568
	6A	11050	$L\beta_1$Pt	278
	6B	11250	$L\beta_2$Pt	249
	6C	12950	$L\gamma$Pt	169
Lead	7	10550	$L\alpha$Pb	781
	7A & 7B	12600	$L\beta_1$ & $L\beta_2$Pb	488
	7C	14750	$L\gamma$Pb	131

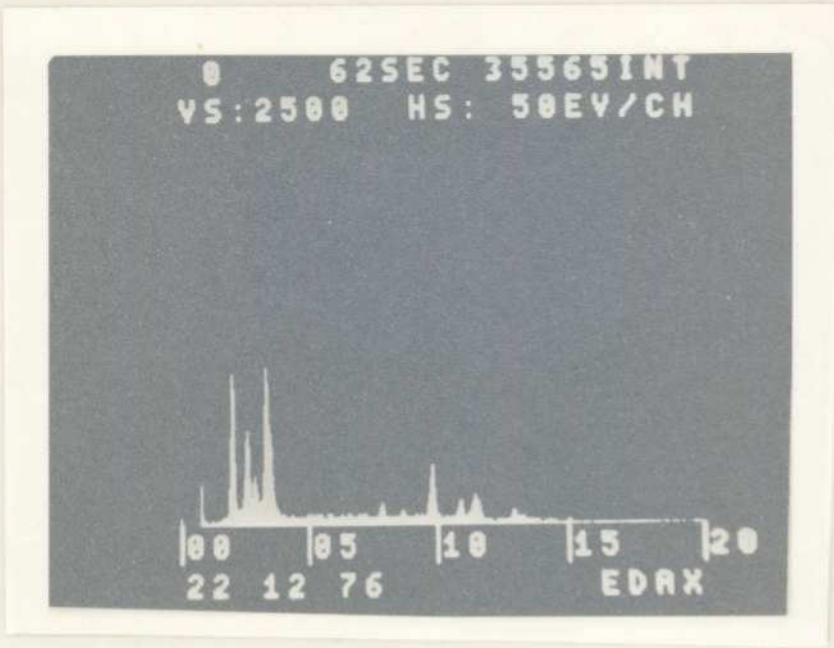

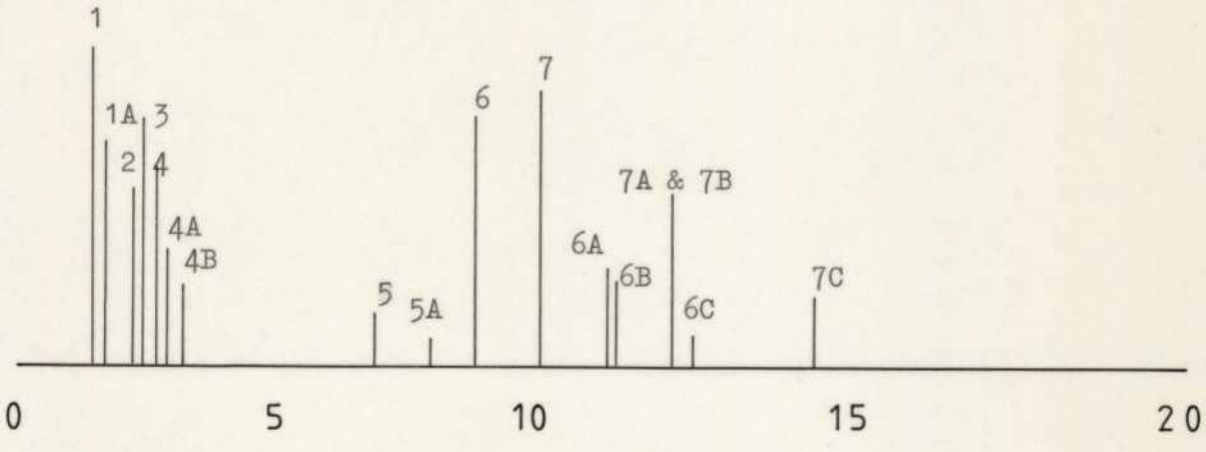

Range : 0 - 20 keV
Sample : Poisoned VQ1 (316) bead

Plate 20

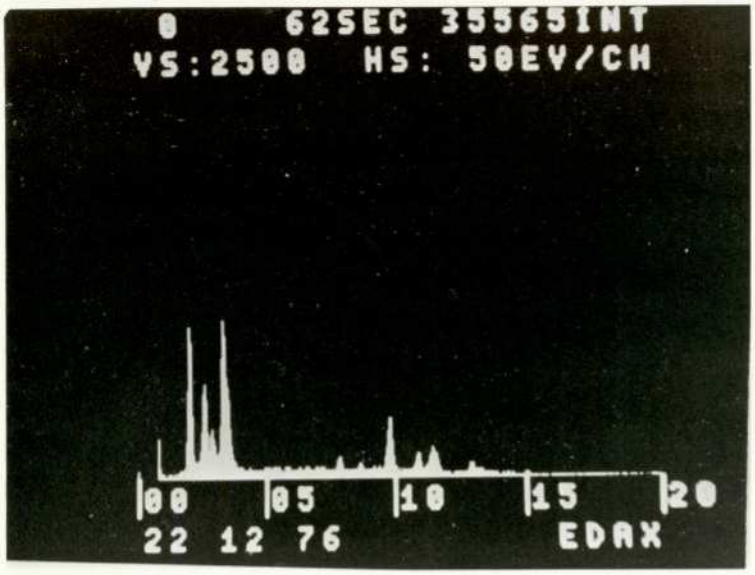

Range : 0 - 20 keV
Sample : Poisoned VQ1 (316) bead

Plate 20

TABLE 19

Poisoned VQ3 (907) Bead

Element	Peak No.	Position/eV	Lines	Integral	
Aluminium	1	1450	K_{α}Al	0	Intensity same a background
	1A	1500	K_{β}Al	0	interference
Lead	2	2350	M_{α}Pb	1596	
Palladium/ Thorium	3	2800	$L_{\alpha,\beta_1,\beta_2}$ Pb, M_{α}Th	2059	
Lead	4	10450	L_{α}Pb	2357	
	4A & 4B	12500	L_{β_1} & L_{β_2} Pb	2439	
	4C	14650	L_{γ}Pb	177	
Thorium	5	12850	L_{α}Th	4181	
	5A	15500	L_{β_1}Th	1518	
	5B	16050	L_{β_2}Th	1703	
	5C	18950	L_{γ}Th	399	
Palladium	6	21000	K_{α}Pd	113	
	6A	23750	K_{β}Pd	46	

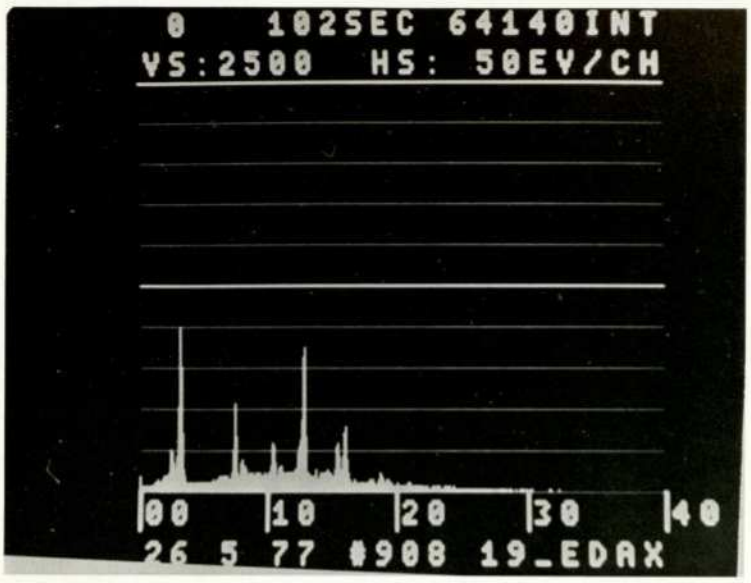

Range : 0 - 40 keV
Sample : Poisoned VQ3 (907) bead

Plate 21

leaded air stream composition. The ratio of intensities of Lα Pb and Lα Th for a flat specimen of standard composition (i.e. equal amounts of lead and thorium) at an accelerating voltage of 40kV and angle of tilt of 30° to the detector was (3/2). The spectrum shown was observed to have a Lα Pb:Lα Th ratio of (2357/4181). Therefore the ratio of amount of lead to thorium on the poisoned beads surface was 0.84:1. In effect there were 0.84 parts of lead to every part of thorium on the surface.

Although both the VQ1 and VQ3 beads under discussion were exposed to lead for 14 hours, the amount of lead on the surface cannot easily be compared either directly or indirectly. This would have been possible if the amount of lead on the surface had been obtained relative to another element appearing in both spectra. In the above cases, the lead and palladium lines which appear in both the VQ1 and VQ3 spectra would have been ideal except that in the case of VQ3, the Lα Pd line coincides with the Mα Th line at 3000 eV, giving an intense peak which affects the result considerably. A very general conclusion that can be drawn from these measurements is that the lead is present on the surface in sufficient quantities to deactivate the bead by at least 80% in each case.

Spot Analyses

In order to find out whether the lead was evenly dispersed or segregated on the surface, several spot analyses of the surface were carried out. These consisted essentially of focussing the scanning beam to a fine spot on the surface and obtaining a spectrum of the elements present at that spot on the surface only, whilst keeping all other parameters constant, (i.e. the angle of tilt of the specimen to the detector, the accelerating voltage and spotsize). This technique gave spectra which were similar to

those obtained when the beam was scanning a large area of the surface, which implied that the lead was very evenly dispersed over the surface.

Cross-sectional Analyses of Poisoned VQ1 and VQ3 Beads

These spectra showed comparatively small traces of lead inside the bead, which implied that very little lead was diffusing into the bead and most of it is being deposited on the surface, at the openings of the pore mouths (or cracks). It is conceivable therefore that the decrease in activity may be partly due to the onset of diffusion limitation of reactant to the remaining active sites through pore mouth poisoning (72), rather than just by a destruction of available catalytically active sites through adsorption of lead.

3.7 Chemical Analyses of Zeolites

Analyses were carried out in duplicate as outlined in section 2.4.6. In the case of ammonium mordenite, a thermogravimetric analysis of the sample was undertaken in the presence of nitrogen in order to determine the temperature at which ammonia was removed to yield hydrogen mordenite. Results of the chemical analyses are shown in Tables 20 and 21 and the thermogravimetric data are depicted in Table 22 and Figure 30. The chemical analyses show that the acid treatment (section 2.4.3) had produced a mordenite sample that was $\sim$30% deficient in aluminium as compared to the original sodium mordenite.

3.8 Poisoning of Zeolite Coated Pellistors

VQ1 and VQ3 beads were coated with different ratios of zeolite : kaolin mixture (as described in section 2.4.4) and then poisoned

TABLE 20

Ammonium Mordenite

	I		II	
Component	% w/w	mol hg^{-1}	% w/w	mol hg^{-1}
$(NH_4)_2O$	5.12	.0985	5.29	.1017
H_2O	10.48	.582	9.47	.526
SiO_2	73.81	1.230	74.58	1.243
Al_2O_3	10.34	.1014	10.33	.1012
	99.75		99.67	

Average $SiO_2:Al_2O_3$ ratio = 12:21 : 1

Average % exchange for NH_4^+ = 98.9%

TABLE 21

Hydrogen Mordenite (Dealuminated Form)

	I		II	
Component	% w/w	mol hg^{-1}	% w/w	mol hg^{-1}
H_2O	16.83	.935	15.91	.884
SiO_2	71.83	1.197	72.29	1.205
Al_2O_3	7.24	.071	7.38	.072
	95.90		95.58	

Average $SiO_2:Al_2O_3$ ratio = 16.80 : 1

Since the sample was prepared from sodium mordenite, there is also 0.07 mol hg^{-1} of Na_2O, which is 4.34 % - this is a maximum value.

	Initial Weight loss reaction	Main weight loss reaction	Weight loss reaction due to NH_3
Weight fraction volatilised (% of dry weight)	1.04	8.10	1.16
Temperature range/°C	25-32	32-240	240-354
Maximum rate of volatilisation/% min^{-1}	-	4.23	6.53
Temperature of maximum rate/ °C	-	101	313
Total moisture/ % of dry weight	-	9.14	-

TABLE 22 - Thermogravimetric Analysis of Ammonium Mordenite in Presence of Nitrogen

Figure 30

Thermogram of ammonium mordenite in presence of nitrogen

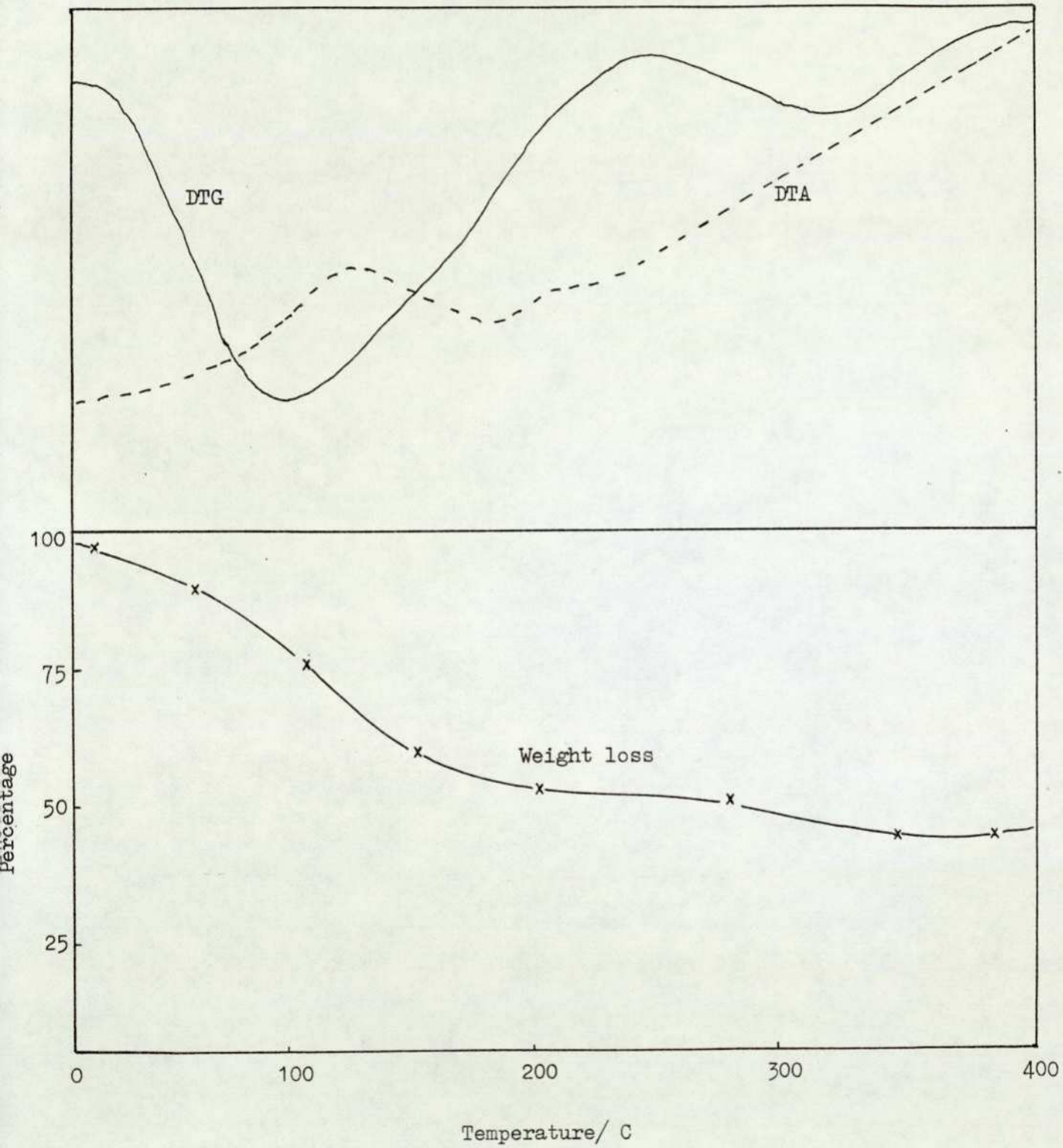

------ : Differential Thermal Analysis (DTA)

——— : Derivative Thermogravimetry (DTG)

x——x : Weight loss

with n-heptane/TML/air mixtures containing 20-25 mg m^{-3} of lead as TML. Photographs of some zeolite coated beads are shown on Plate 22. The results of the poisoning experiments are shown in Figures 31-42 and summarised in Tables 23-26.

The zeolite-coated beads showed substantial improvements over the other types of coated beads (i.e. the VQ1/VQ7, VQ3/VQ9, and LD1 series coated with a layer of alumina) for the following reasons:

(1) Their initial response to 1% methane lay in the same range as the uncoated beads, (20-30mV).

(2) A percentage drop in sensitivity of only 20% was observed in most cases after 12-15 hours of poisoning.

By comparing the results obtained using different ratios of zeolite:kaolin mixture, it seems that the 60:40 ratio tends to exhibit the greatest resistance to poisoning. This is not a suprising conclusion, as the requirement for effective poison resistance must be that the maximal amount of zeolite be incorporated in the bead which is consistent with sufficient kaolin being present to maintain good binding properties in the pellistor.

Further experiments were undertaken to examine relative effectiveness of binder and different forms of mordenite as resistors to lead poisoning. First, beads coated with 100% kaolin were poisoned, in order to see if the clay exhibited any resistance; the results in Figures 43 and 44 show only a slight increase in resistance against poisoning as compared to the original VQ1 beads,which indicates that kaolin was acting merely as a binder. Then secondly, series of VQ1 and VQ3 beads coated with different ratios of sodium mordenite to kaolin were poisoned, with results depicted in Figures 45-50 and Tables 27 and 28. With sodium mordenite, a greater degree of inconsistency was observed with large zero

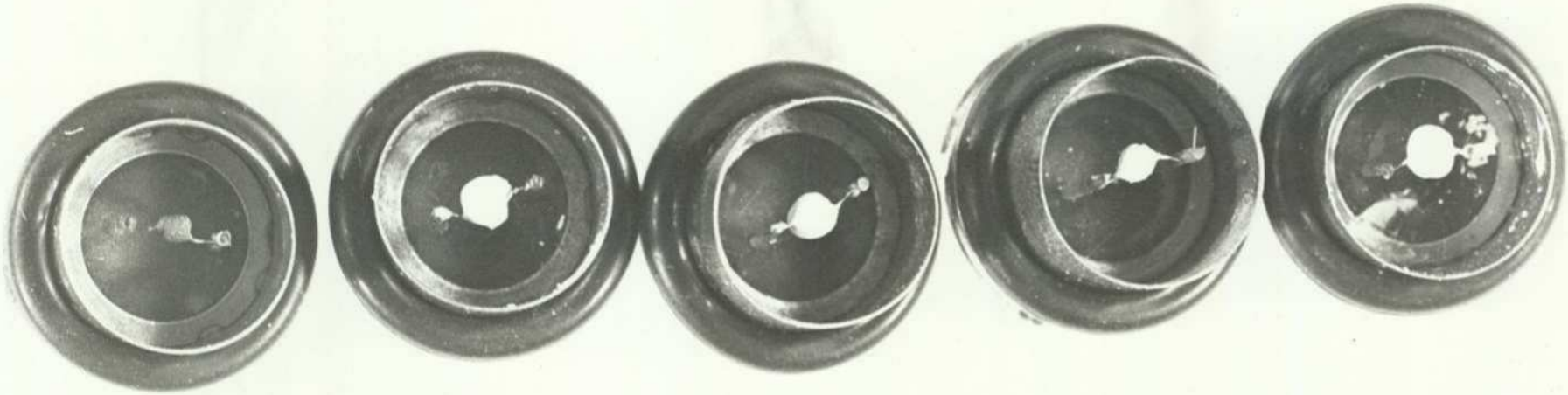

Conventional VQ1 bead

VQ1 coated with 60:40 H-Mor (NH_4^+): kaolin

VQ1 coated with 60:40 H-Mor (DHM): kaolin

VQ3 coated with 40:60 H-Mor (NH_4^+): kaolin

VQ1 coated with 40:60 H-Mor (DHM): kaolin

H-Mor : Hydrogen mordenite
DHM : Dealuminated hydrogen mordenite

Plate 22

Figure 31

Results of poisoning experiment

Specimen: 967/VQ1 coated with 4:6 dealuminated hydrogen mordenite : kaolin

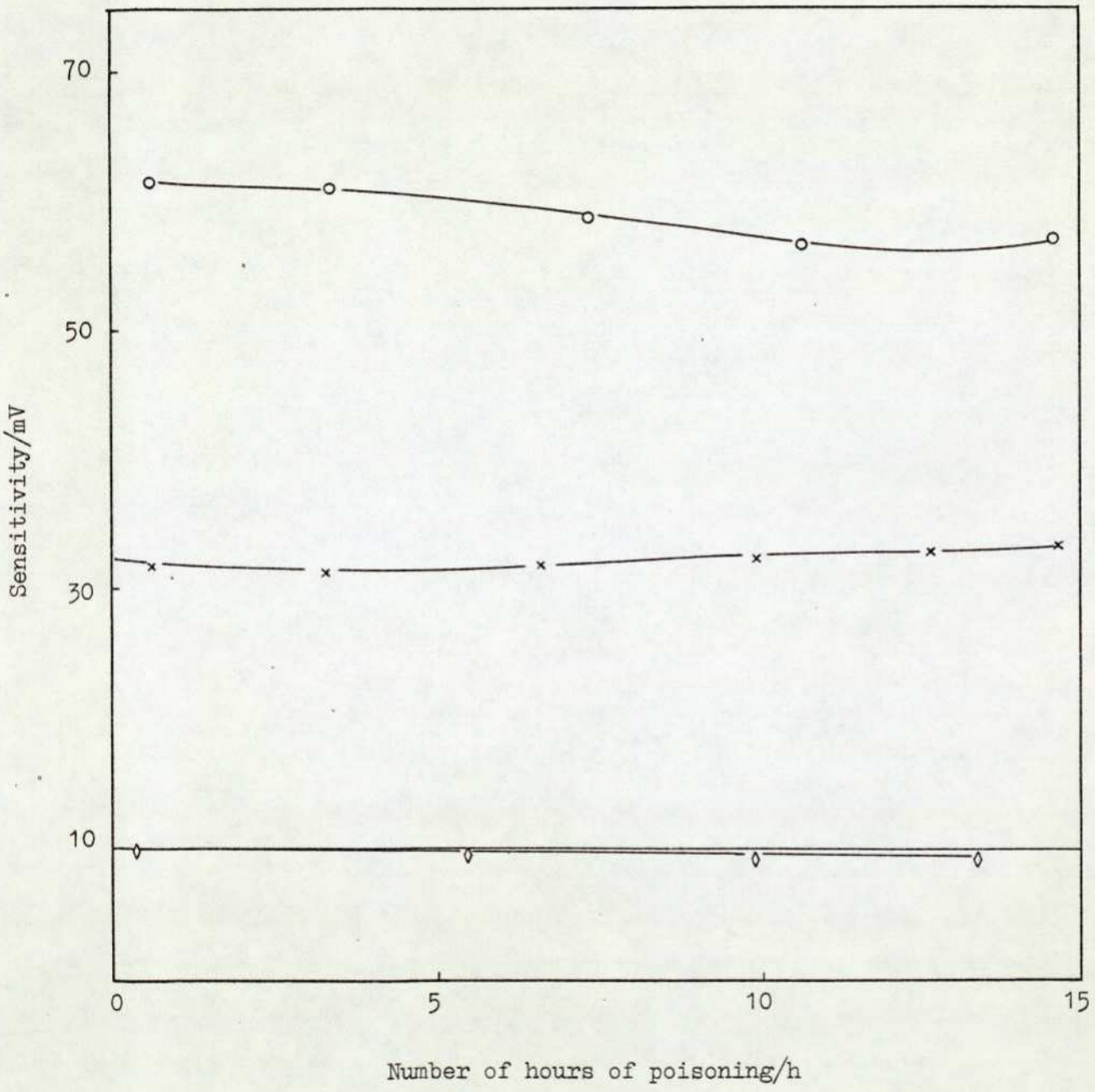

Figure 32

Results of poisoning experiment

Specimen: 965/VQ1 coated with 6:4 dealuminated hydrogen mordenite : kaolin

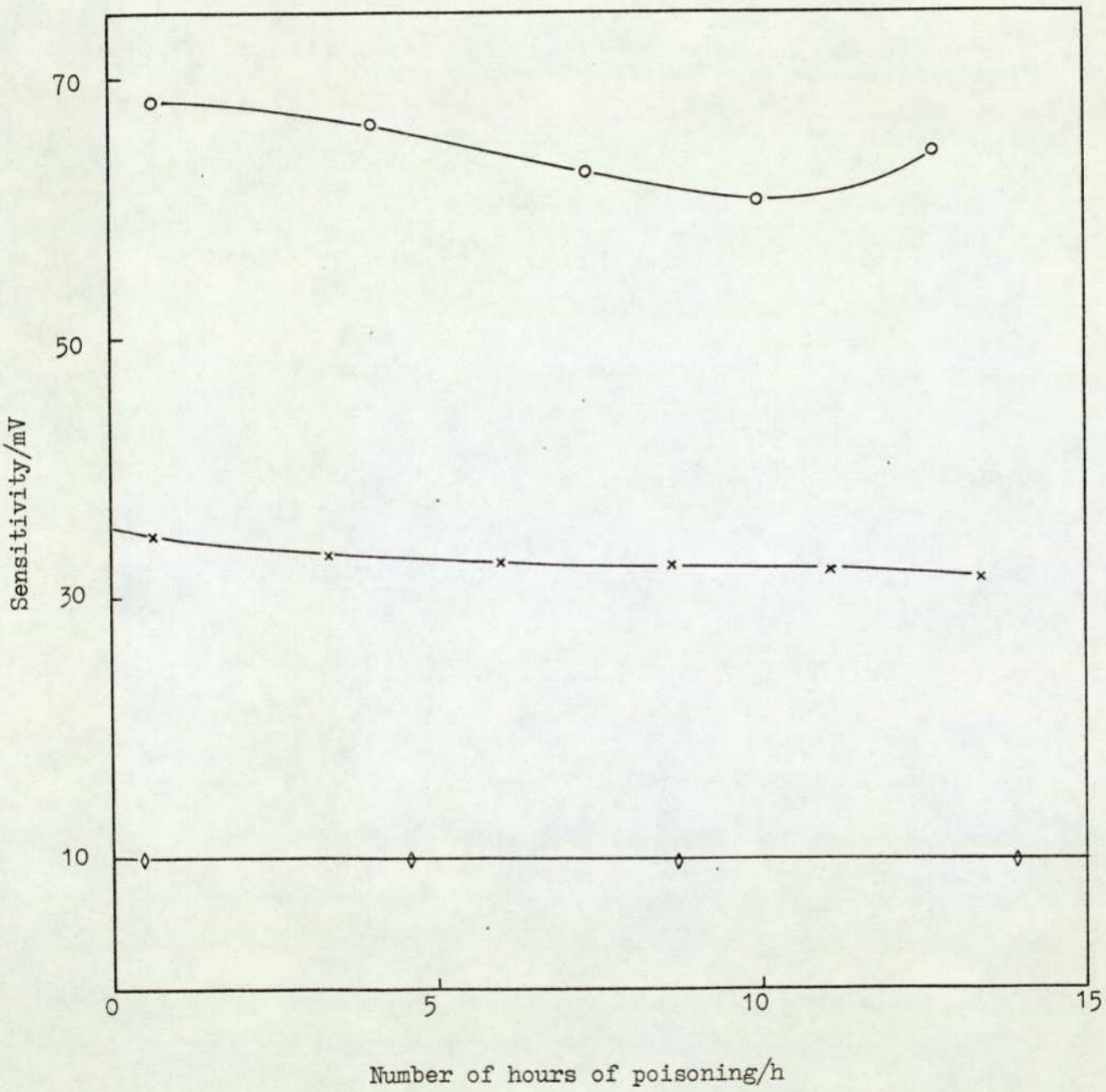

Figure 33

Results of poisoning experiment

Specimen: 962/VQ1 coated with 8:2 dealuminated hydrogen mordenite : kaolin

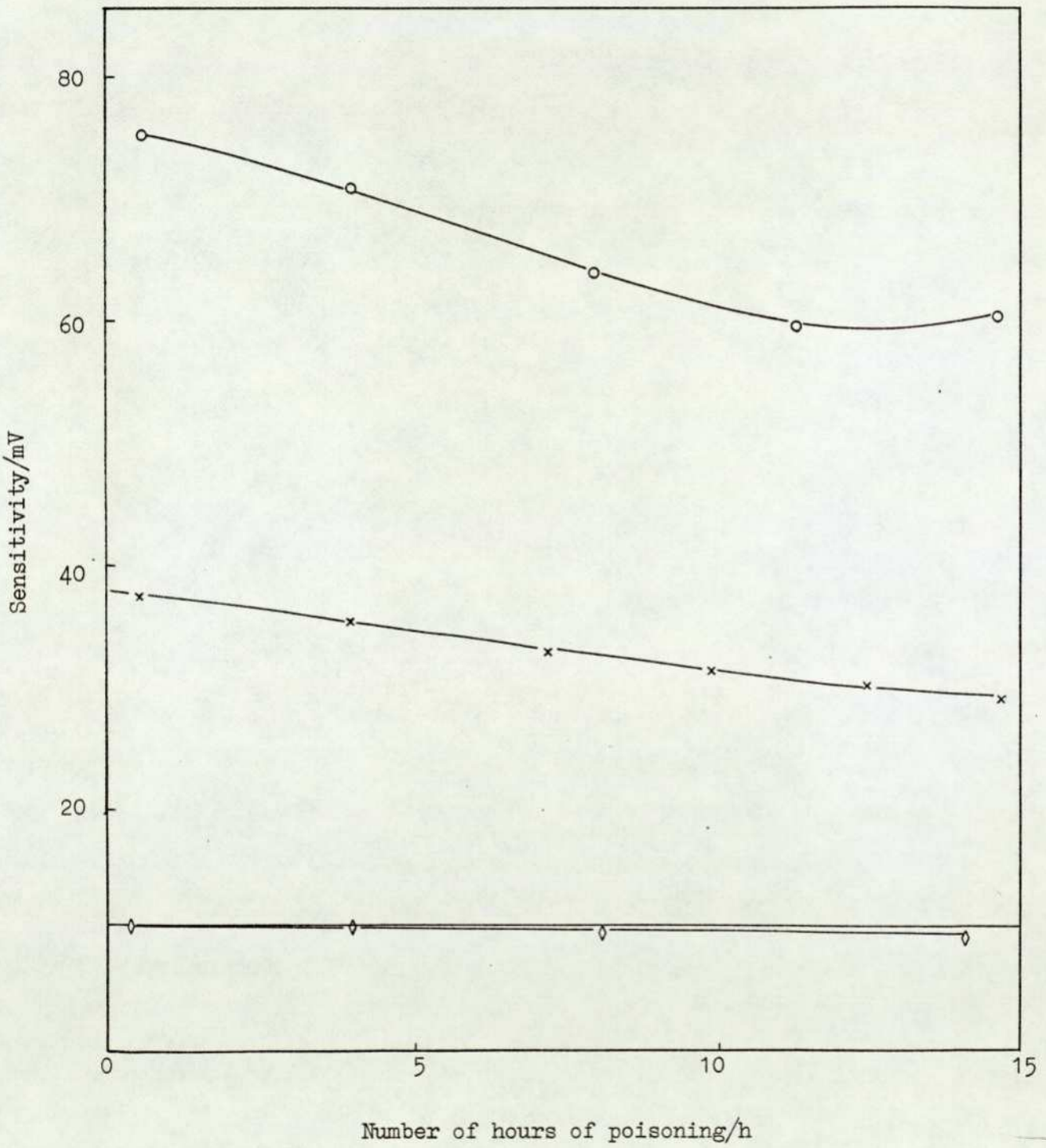

Figure 34

Results of poisoning experiment

Specimen: 695/VQ1 coated with 4:6 hydrogen mordenite (from NH_4^+ form) : kaolin

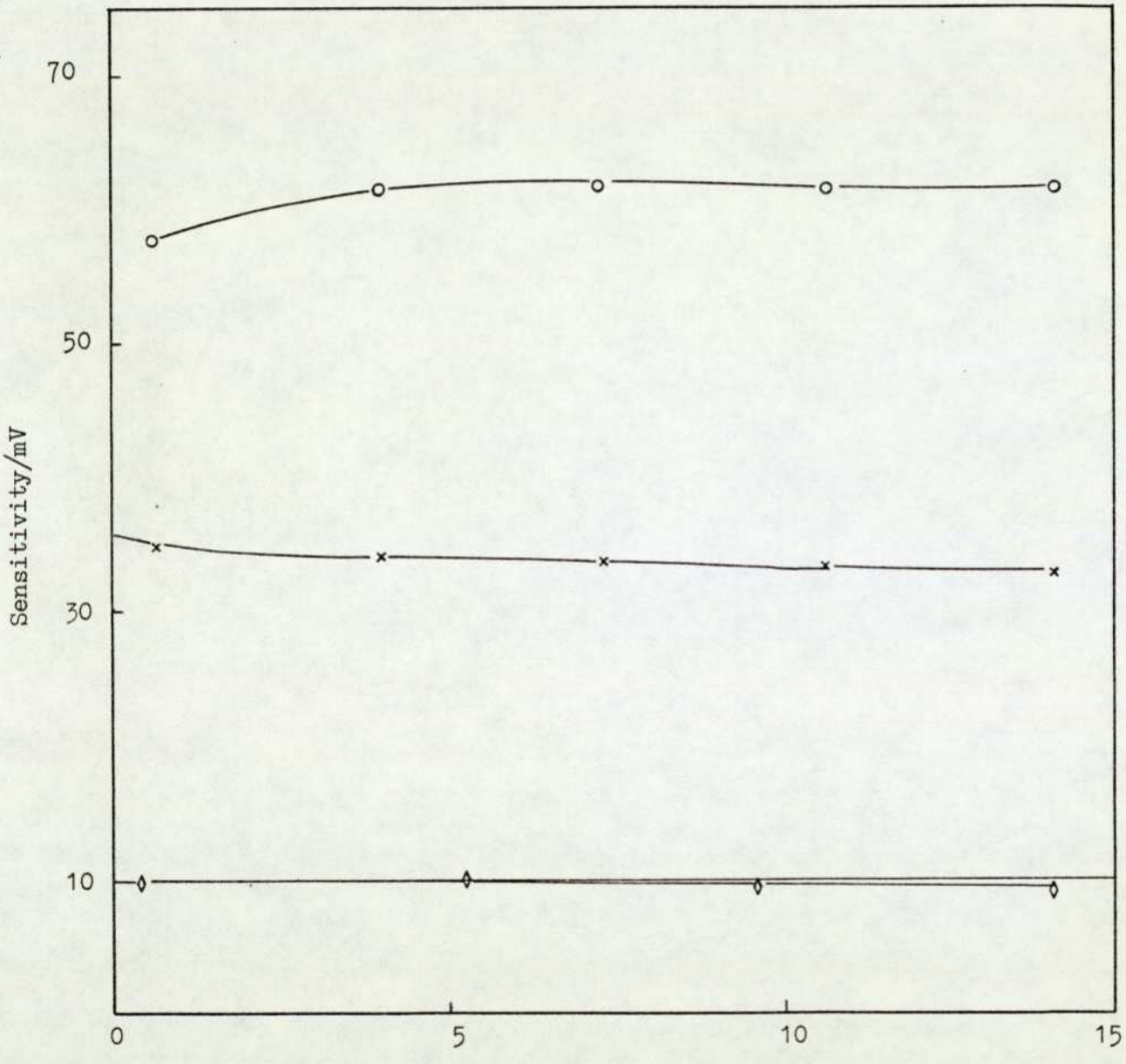

Figure 35

Results of poisoning experiment

Specimen: 740/VQ1 coated with 6:4 hydrogen mordenite

(from NH_4^+ form) : kaolin

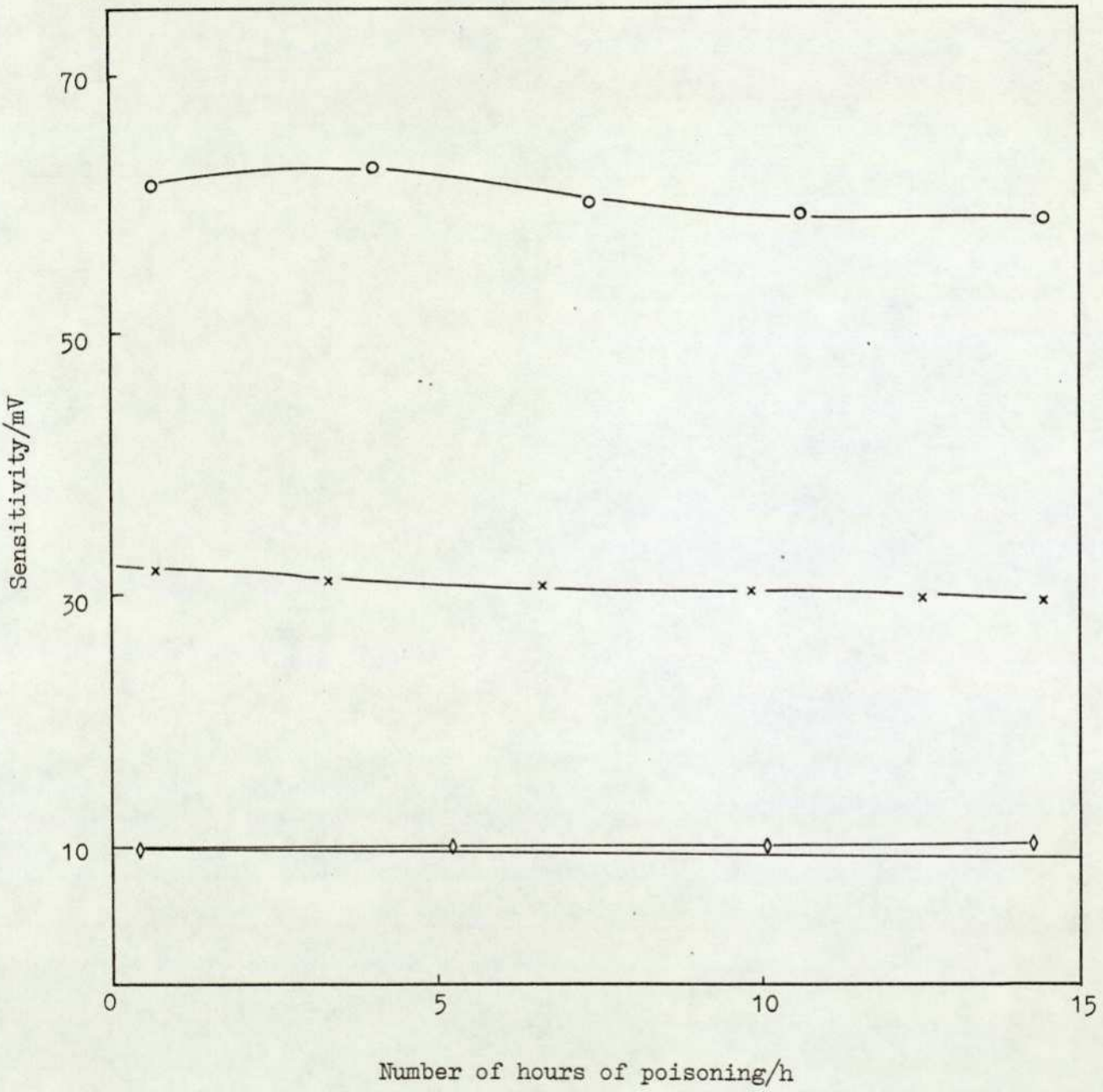

Figure 36

Results of poisoning experiment

Specimen: 735/VQ1 coated with 8:2 hydrogen mordenite (from NH_4^+ form) : kaolin

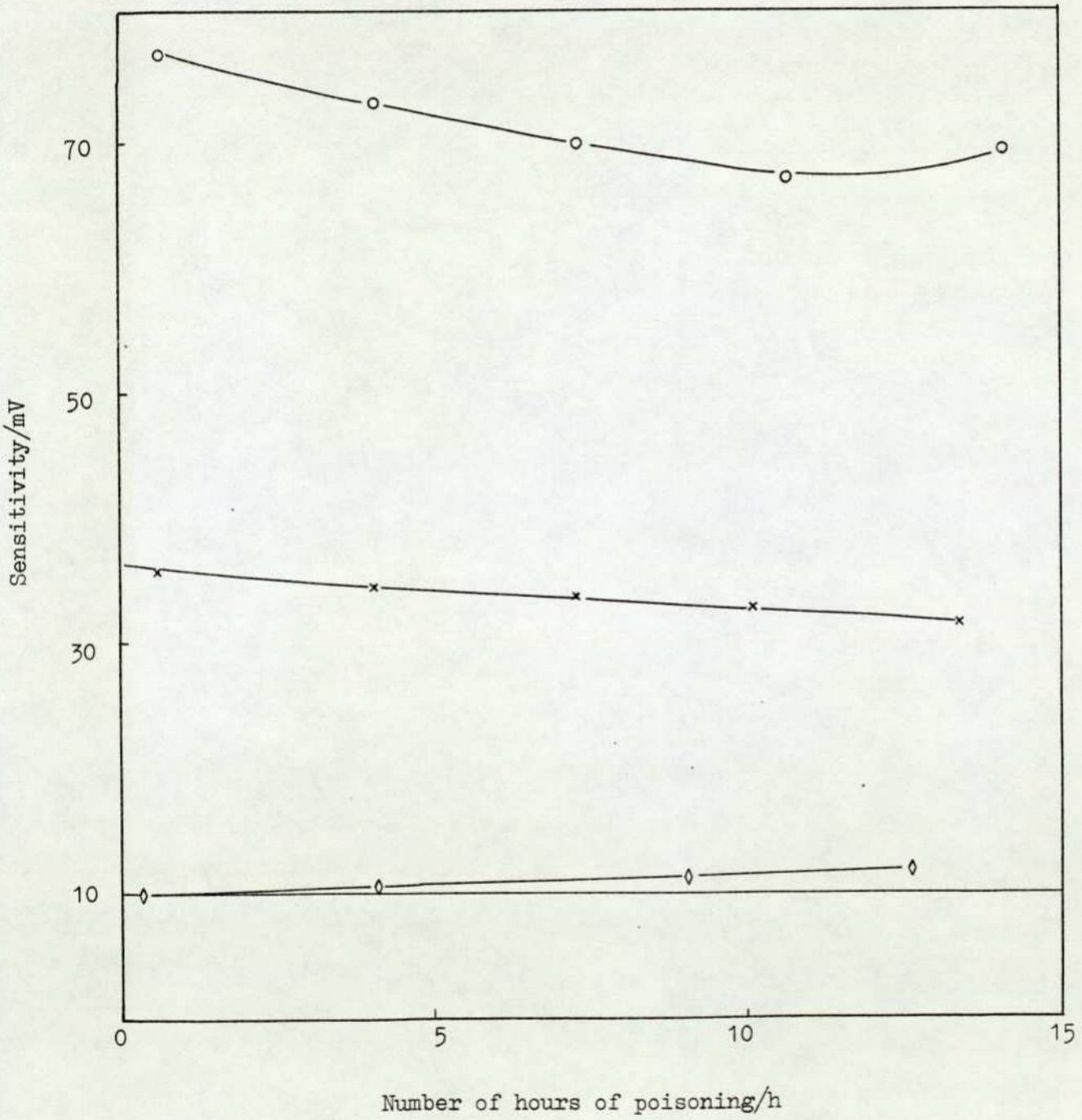

Figure 37

Results of poisoning experiment

Specimen: 615/VQ3 coated with 4:6 dealuminated hydrogen mordenite : kaolin

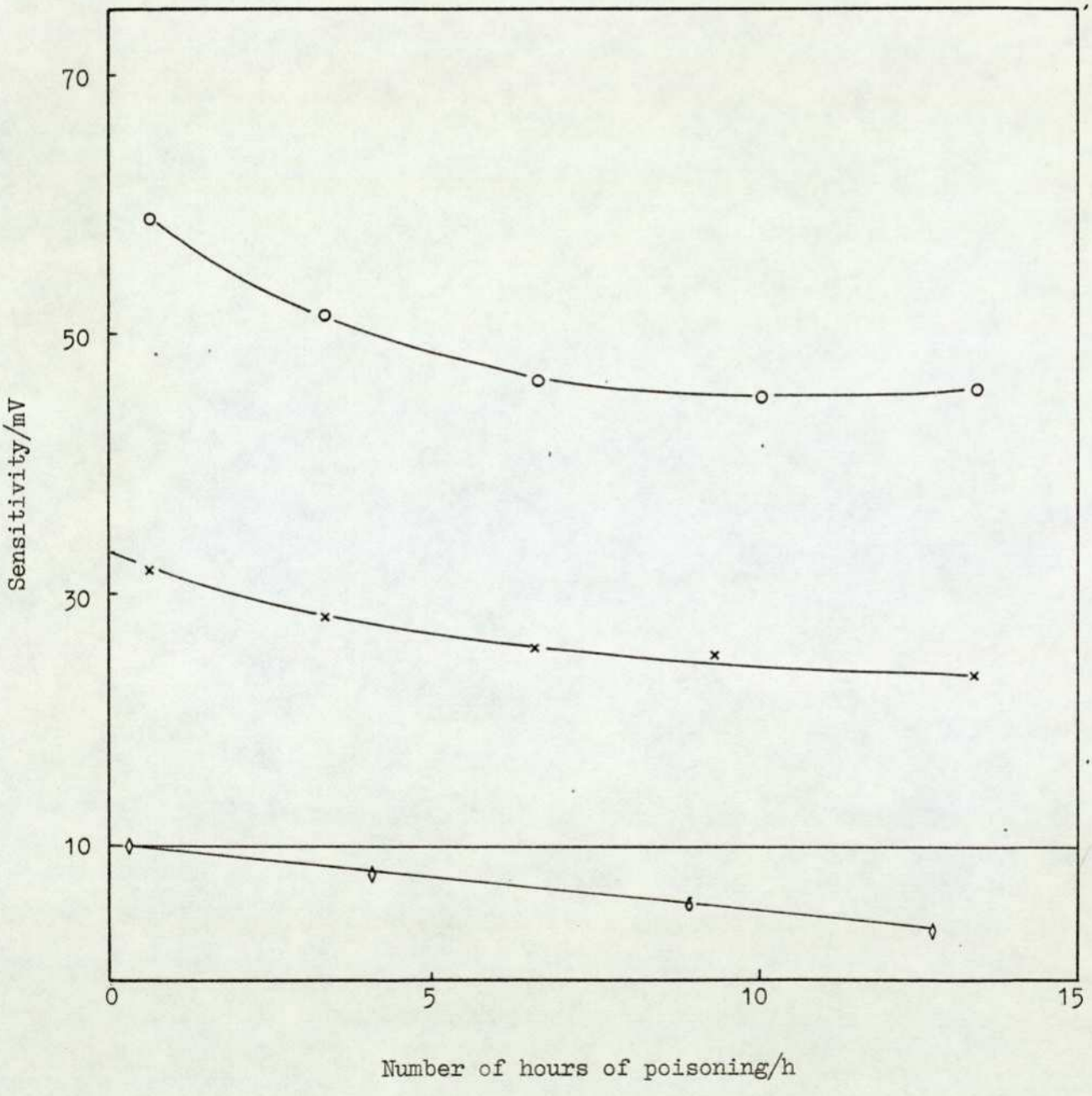

Figure 38

Results of poisoning experiment

Specimen: 667/VQ3 coated with 6:4 dealuminated hydrogen mordenite : kaolin

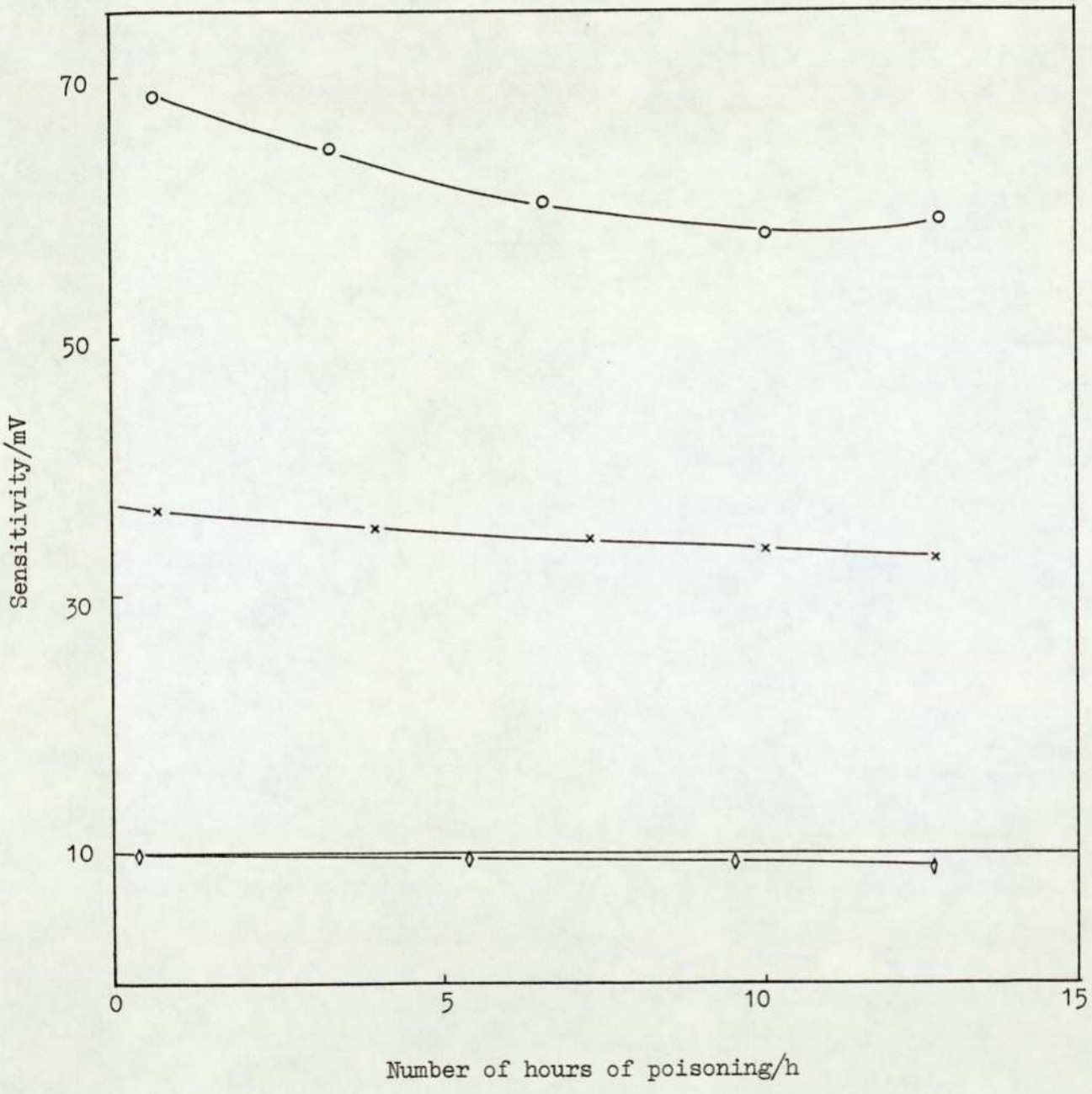

Figure 39

Results of poisoning experiment

Specimen: 811/VQ3 coated with 8:2 dealuminated hydrogen mordenite : kaolin

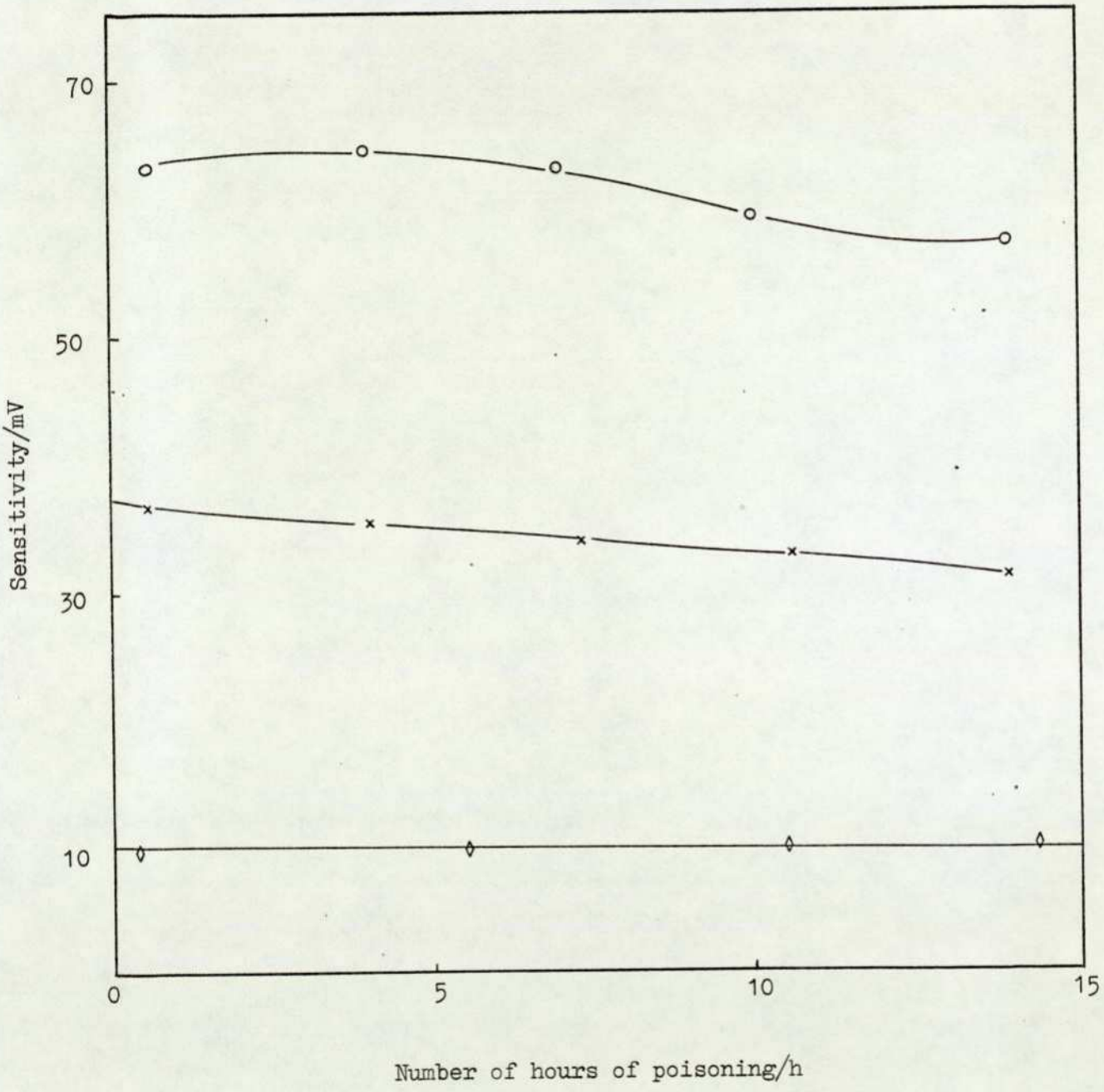

Figure 40

Results of poisoning experiment

Specimen: 446/VQ3 coated with 4:6 hydrogen mordenite (from NH_4^+ Form) : kaolin

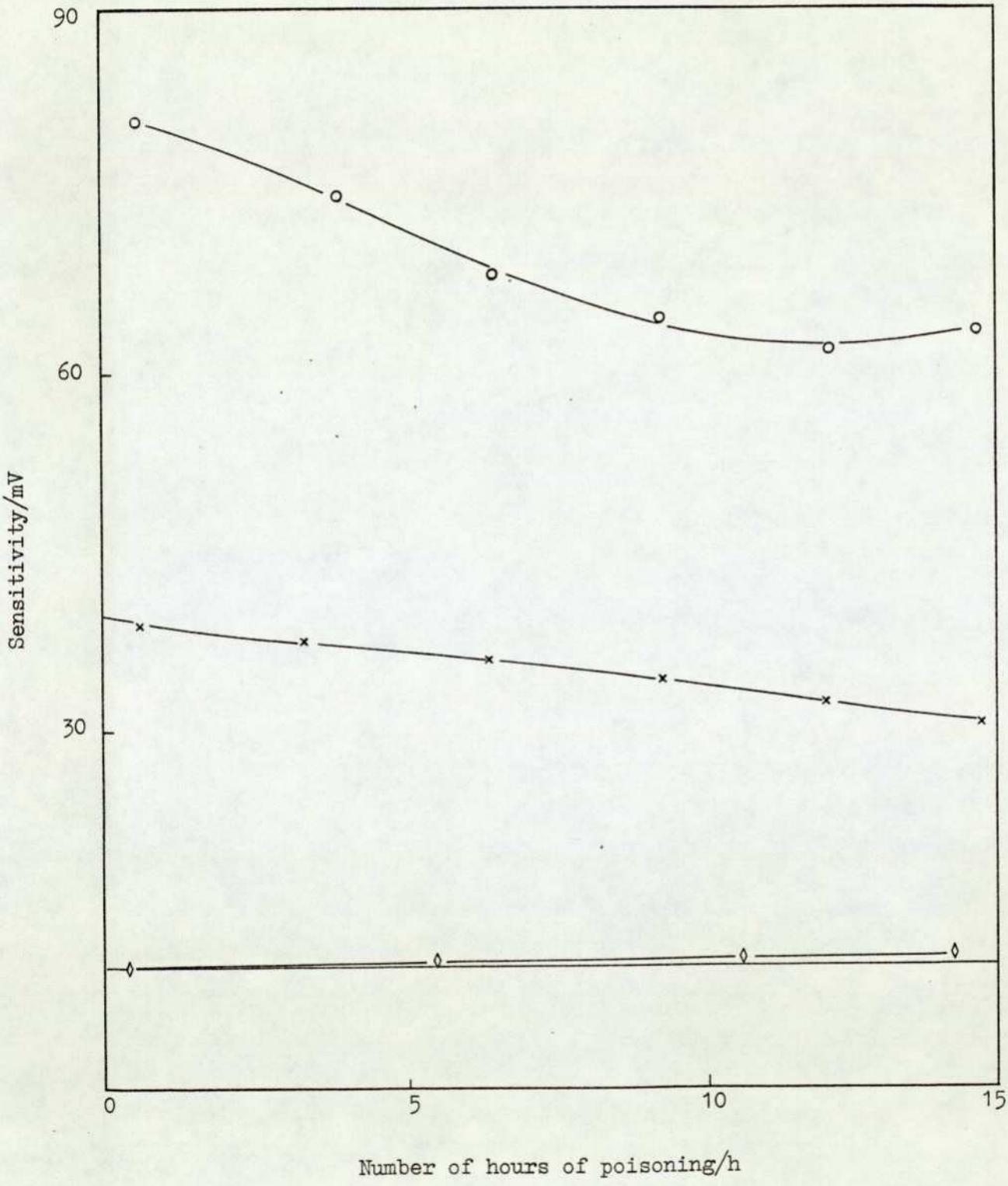

Figure 41

Results of poisoning experiment

Specimen: 444/VQ3 coated with 6:4 hydrogen mordenite (from NH_4^+ form) : kaolin

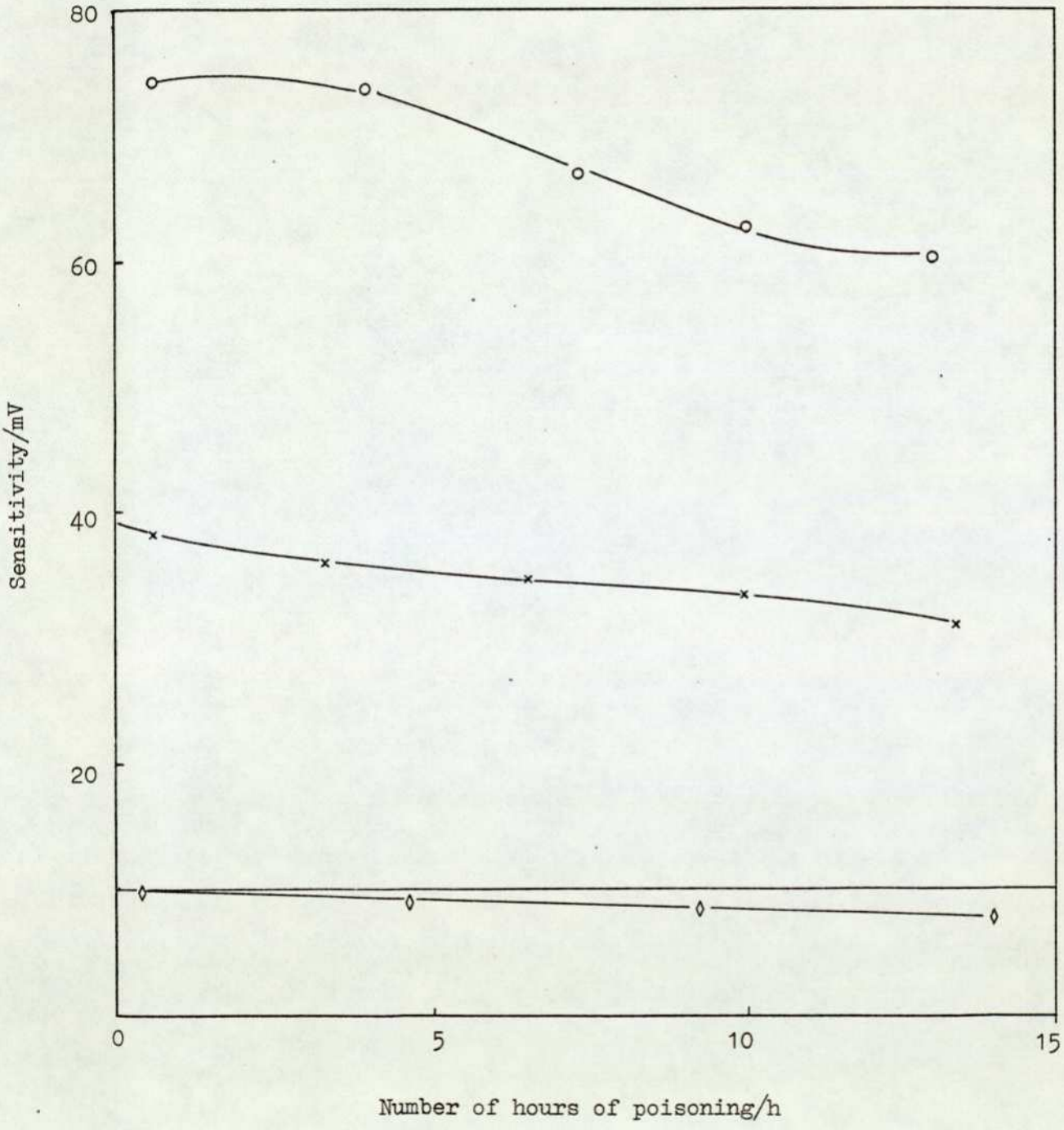

Figure 42

Results of poisoning experiment

Specimen: 443/VQ3 coated with 8:2 hydrogen mordenite (from NH_4^+ form) : kaolin

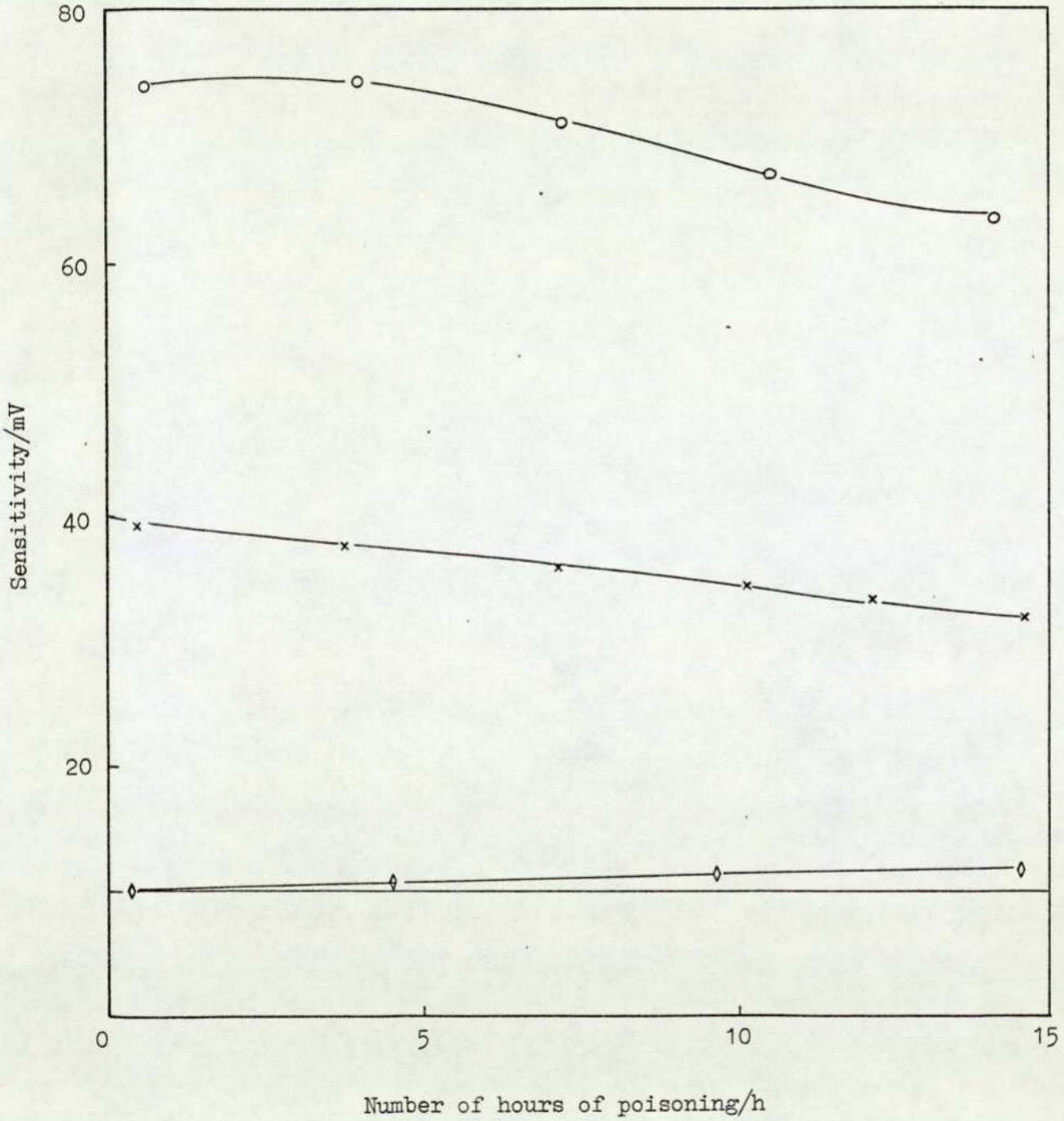

Serial No.	zeolite: kaolin ratio	Initial response to 1% CH_4/mV	Final response/mV to 1% CH_4	Percentage sensitivity remaining	Total hours of poisoning/h	Response to 1% CH_4 after 10 hours poisoning/ mV	Percentage sensitivity left after 10 hours poisoning	Air drift/ mV
966	40:60	22.5	22.0	97.8	16	22	97.8	-5.0
967	40:60	23.5	22.5	95.7	16	21.5	91.5	+0.5
968	40:60	22.5	19.0	84.4	13	20.5	91.1	-0.5
963	60:40	27.5	23.5	85.5	14	24.0	87.3	+1.0
964	60:40	27.5	25.0	90.9	13	24.0	87.3	-1.5
965	60:40	24.0	21.5	89.6	13	22.5	93.8	0.0
960	80:20	22.0	12.5	56.8	28	12.5	56.8	-6.5
961	80:20	18.0	12.5	69.4	28	14.0	77.8	0
962	80:20	27.5	19.5	70.9	15	21.5	78.2	+0.5

TABLE 23 - VQ1 Coated with Dealuminated Hydrogen Mordenite

Serial No.	zeolite: kaolin ratio	Initial response to 1% CH_4/mV	Final response/mV to 1% CH_4	Percentage sensitivity remaining	Total hours of poisoning/h	Response to 1% CH_4 after 10 hours poisoning/ mV	Percentage sensitivity left after 10 hours poisoning	Air drift /mV
700	40:60	23.0	18.0	78.3	14	20.0	87	-1.0
695	40:60	24.0	22.0	91.7	16	23.5	97.9	-0.5
737	60:40	22.0	14.0	63.6	15	18.0	81.8	+4.0
740	60:40	20.0	17.5	87.5	17	19.5	97.5	+1.5
739	60:40	22.0	18.0	81.8	17	16.0	72.7	-0.5
732	80:20	24.5	14.5	59.2	13	15.5	63.3	0
734	80:20	24.0	17.0	70.8	13	19.0	79.2	-2.0
735	80:20	26.0	19.5	75.0	13	21.5	82.7	+2.0
179	100% kaolin	23.5	12.0	51.1	15	12.5	53.2	-7.0

TABLE 24 - VQ1 Coated with Hydrogen Mordenite (from NH_4^+ form)

Serial No.	zeolite: kaolin ratio	Initial response to 1% CH_4/mV	Final response to 1% CH_4/mV	Percentage sensitivity remaining	Total hours of poisoning/h	Response to 1% CH_4 after 10 hours poisoning/ mV	Percentage sensitivity left after 10 hours poisoning	Air drift /mV
615	40:60	22.5	20.0	88.9	13	19.0	84.4	-1.0
675	40:60	23.5	19.5	83.0	13	19.0	80.9	-1.5
614	40:60	22.0	13.5	61.4	12	13.0	59.1	-1.5
667	60:40	26.5	24.0	90.6	12	26.0	98.1	-1.0
662	60:40	27.5	22.5	81.8	16	24.0	87.3	+1.0
666	60:40	27.0	22.0	81.5	16	22.0	81.5	-1.0
811	80:20	27.0	20.5	76.0	16	23.0	85.2	0
812	80:20	28.5	13.0	45.6	16	15.0	52.6	-4.0

TABLE 25 - VQ3 Coated with Dealuminated Hydrogen Mordenite

Serial No.	zeolite: kaolin ratio	Initial response to 1% CH_4/mV	Final response to 1% CH_4/mV	Percentage sensitivity remaining	Total hours of poisoning/h	Response to 1% CH_4 after 10 hours poisoning/ mV	Percentage sensitivity left after 10 hours poisoning	Air drift/ mV
445	40:60	28.5	26.0	91.2	14	26.5	93.0	+3.5
447	40:60	28.0	16.0	57.1	15	17.5	62.5	-4.5
446	40:60	30.5	18.5	60.7	15	22.5	73.8	+1.5
450	60:40	27.5	19.0	69.1	15	21.0	76.4	-1.5
444	60:40	30.5	23.0	75.4	15	24.5	80.3	+2.0
426	60:40	29.0	23.5	81.0	14	24.5	84.5	-2.5
443	80:20	31.5	20.0	63.5	14	22.5	71.1	+1.5
442	80:20	29.5	16.5	56.0	14	19.5	66.1	-2.0
523	100% kaolin	24.0	12.0	50.0	15	11.5	47.9	-7.0

TABLE 26 - VQ3 Coated with Hydrogen Mordenite (from NH_4^+ form)

Figure 43

Results of poisoning experiment

Specimen: 179/VQ1 coated with 100% kaolin

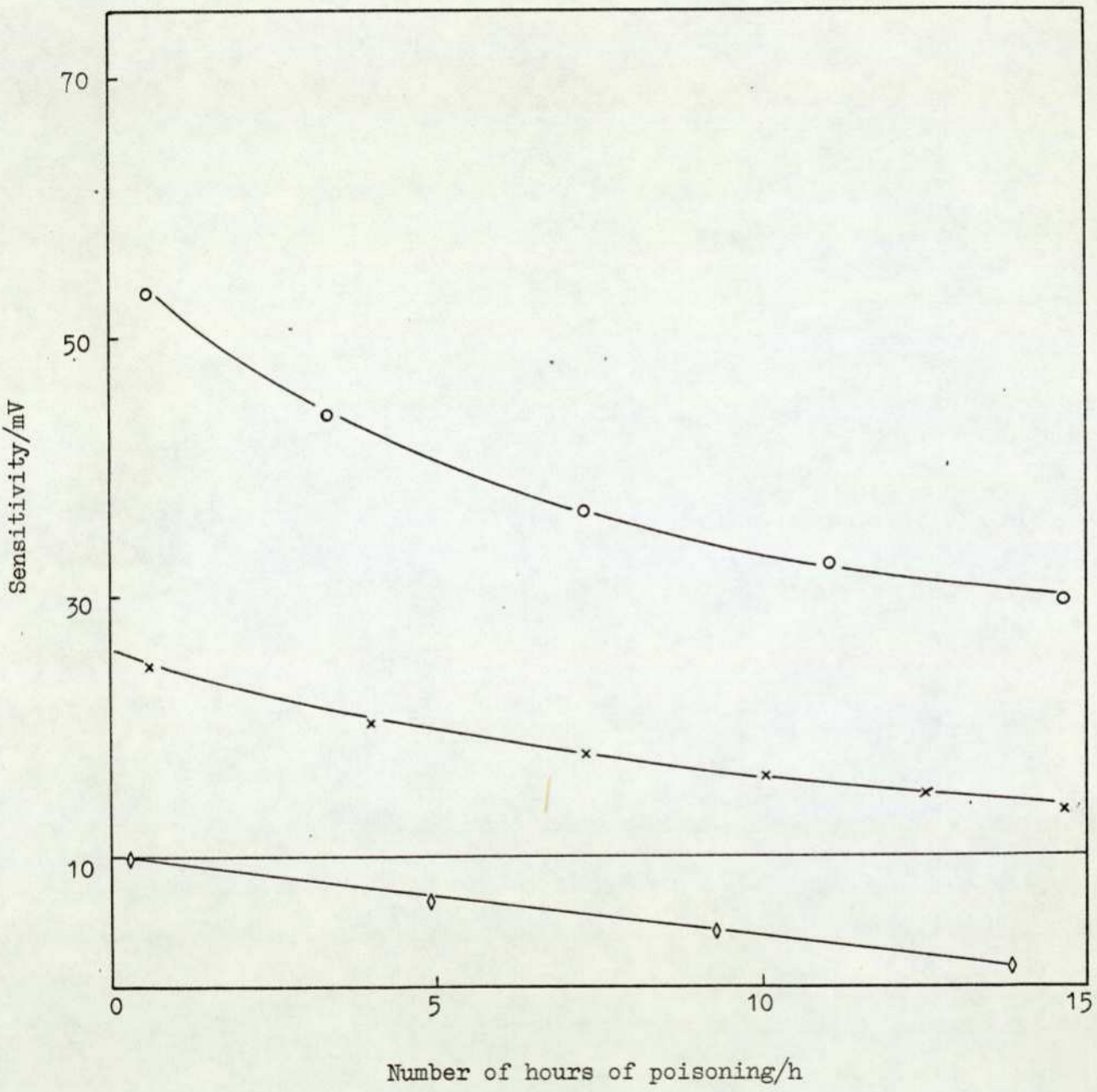

Figure 44

Results of poisoning experiment

Specimen: 523/VQ3 coated with 100% kaolin

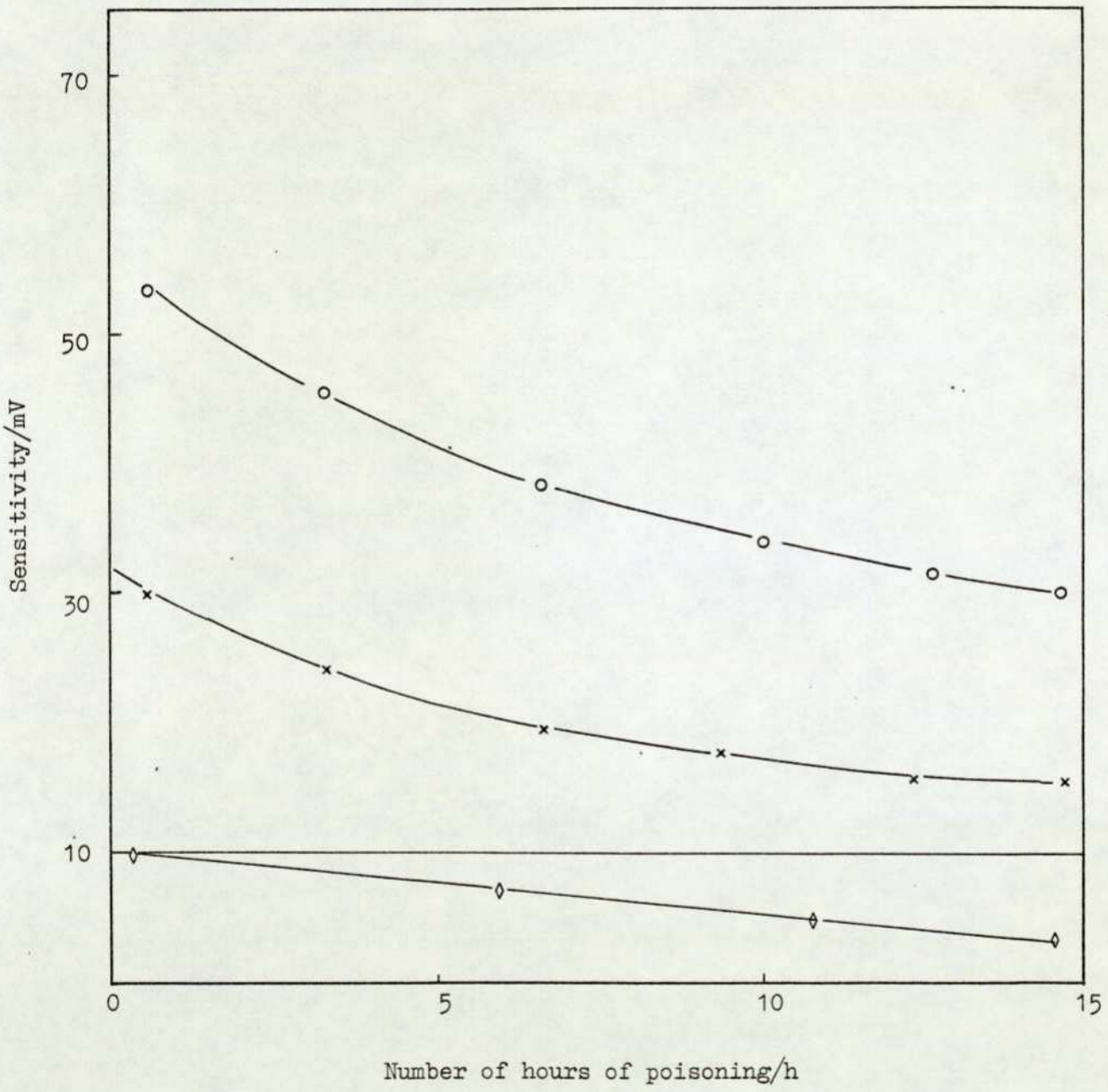

Figure 45

Results of poisoning experiment

Specimen: 170/VQ1 coated with 4:6 sodium mordenite : kaolin

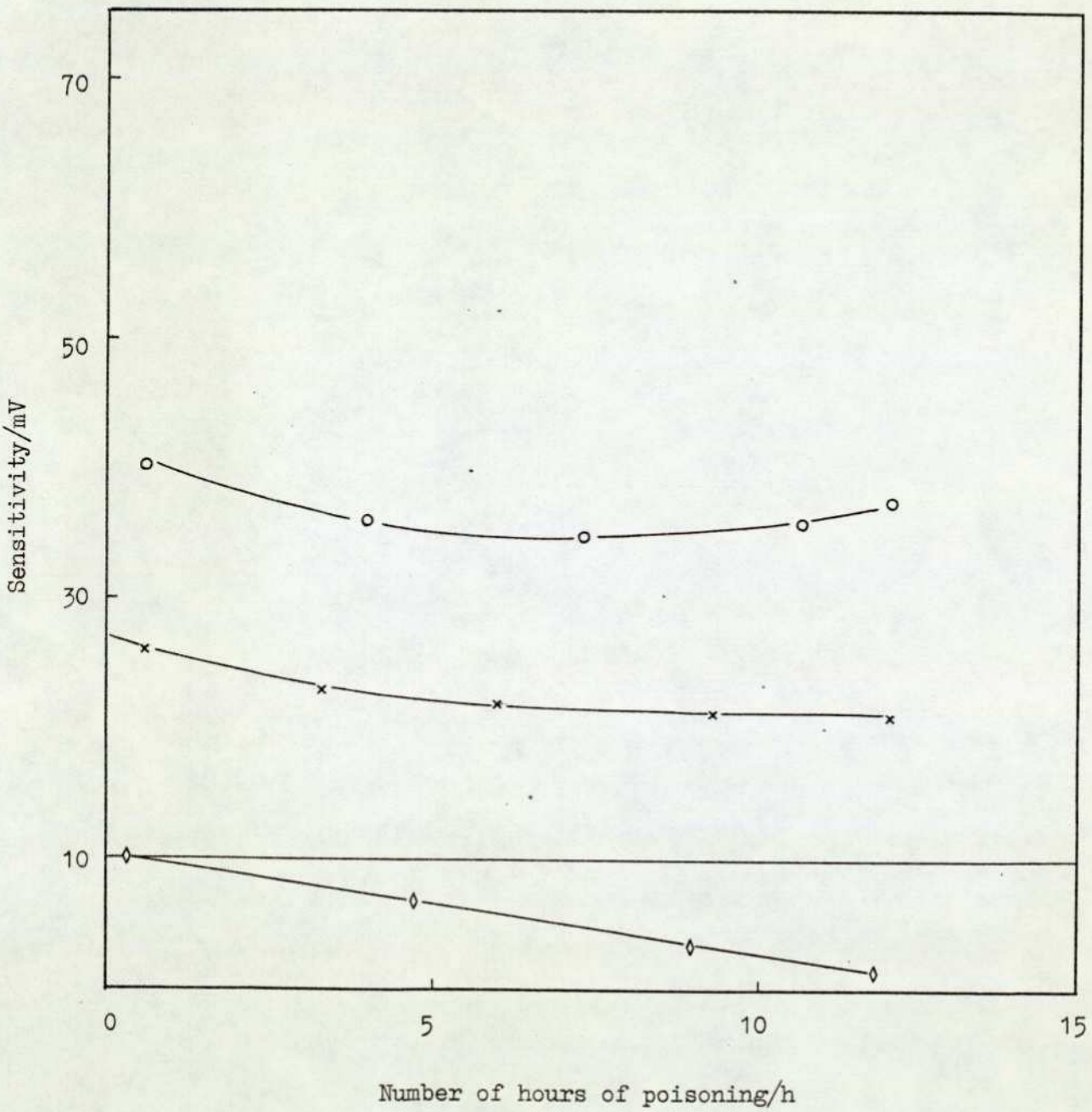

Figure 46

Results of poisoning experiment

Specimen: 136/VQ1 coated with 6:4 sodium mordenite : kaolin

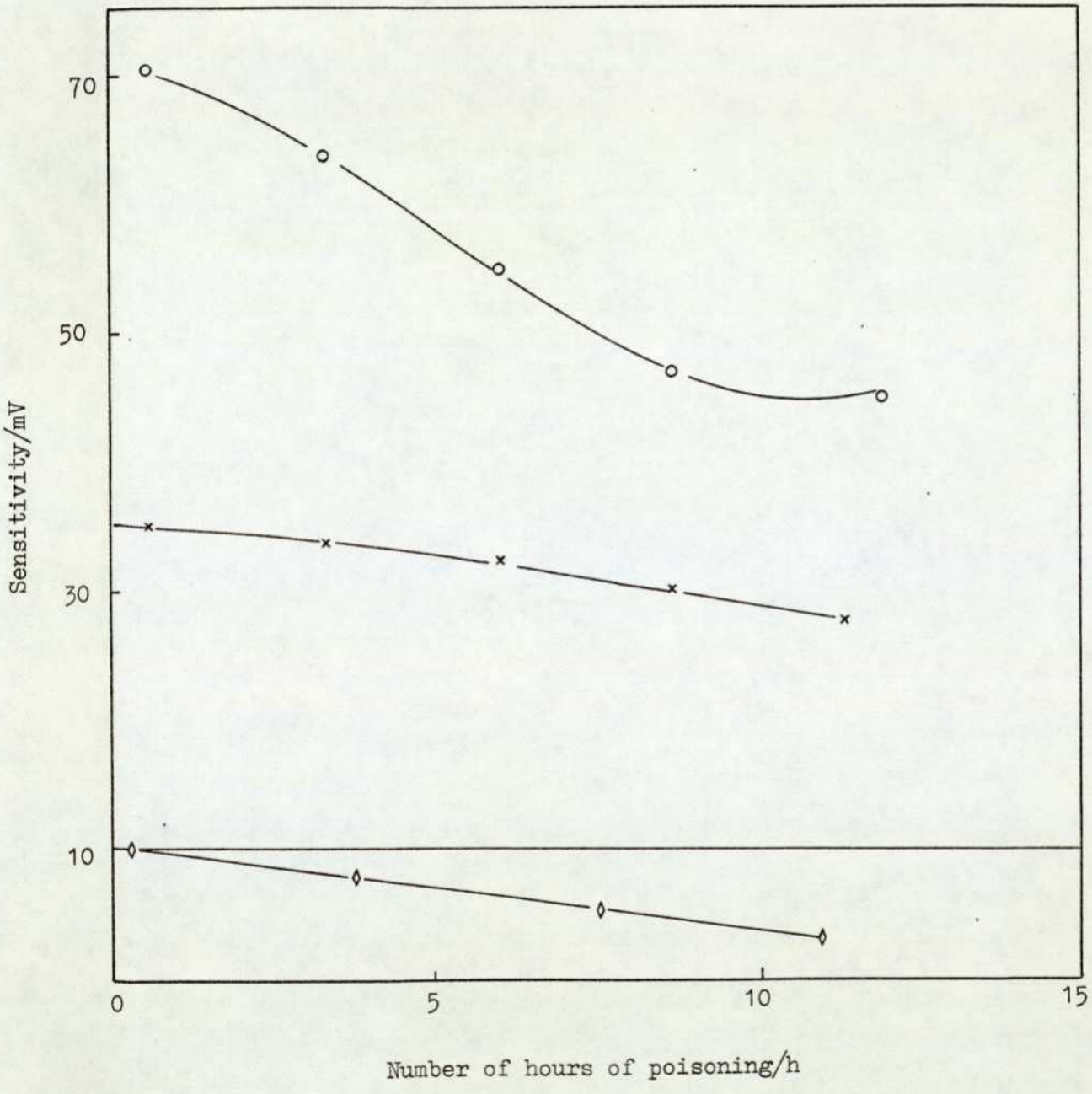

Figure 47

Results of poisoning experiment

Specimen: 538/VQ1 coated with 8:2 sodium mordenite : kaolin

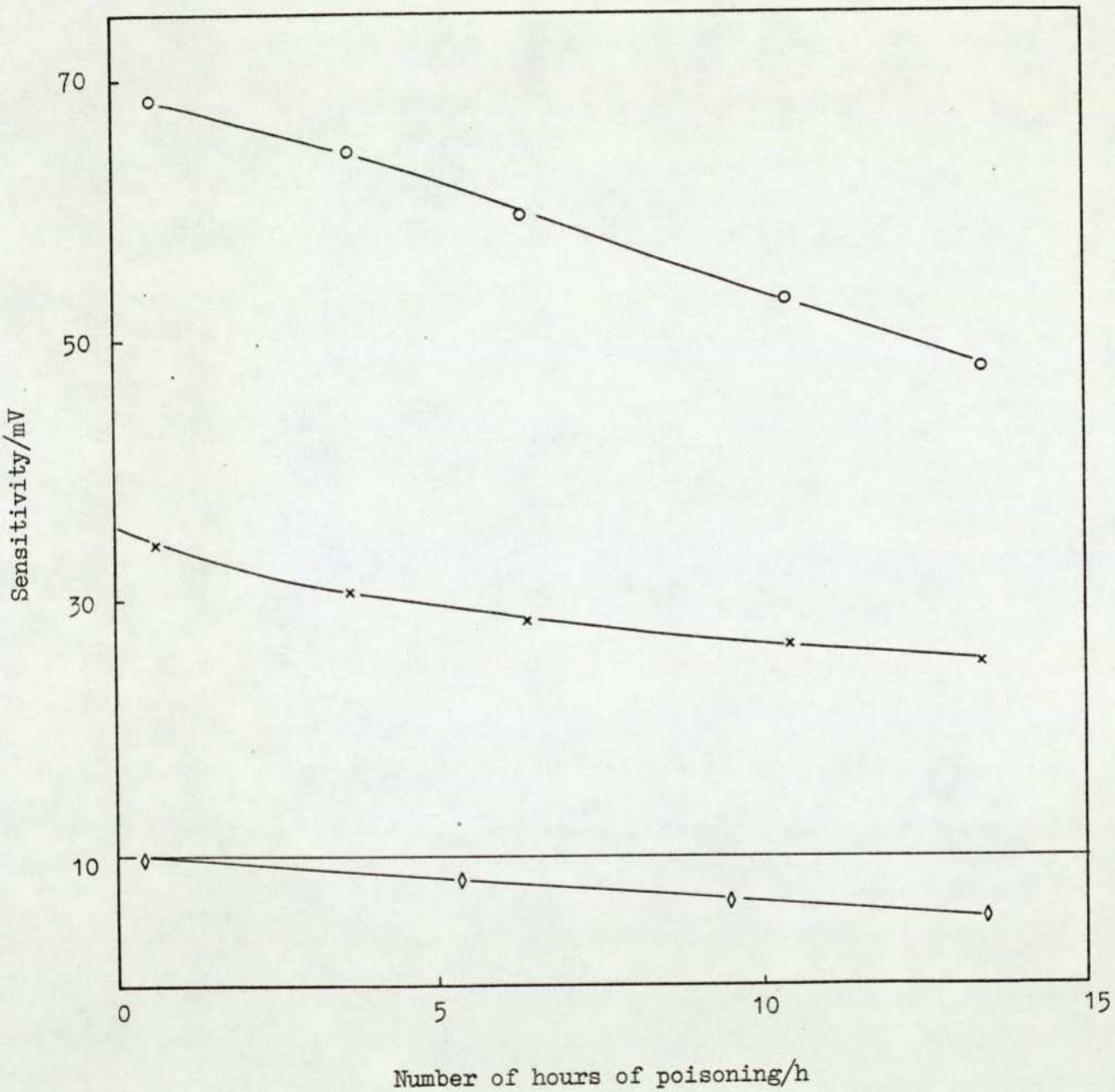

Figure 48

Results of poisoning experiment

Specimen: 170/V03 coated with 4:6 sodium mordenite : kaolin

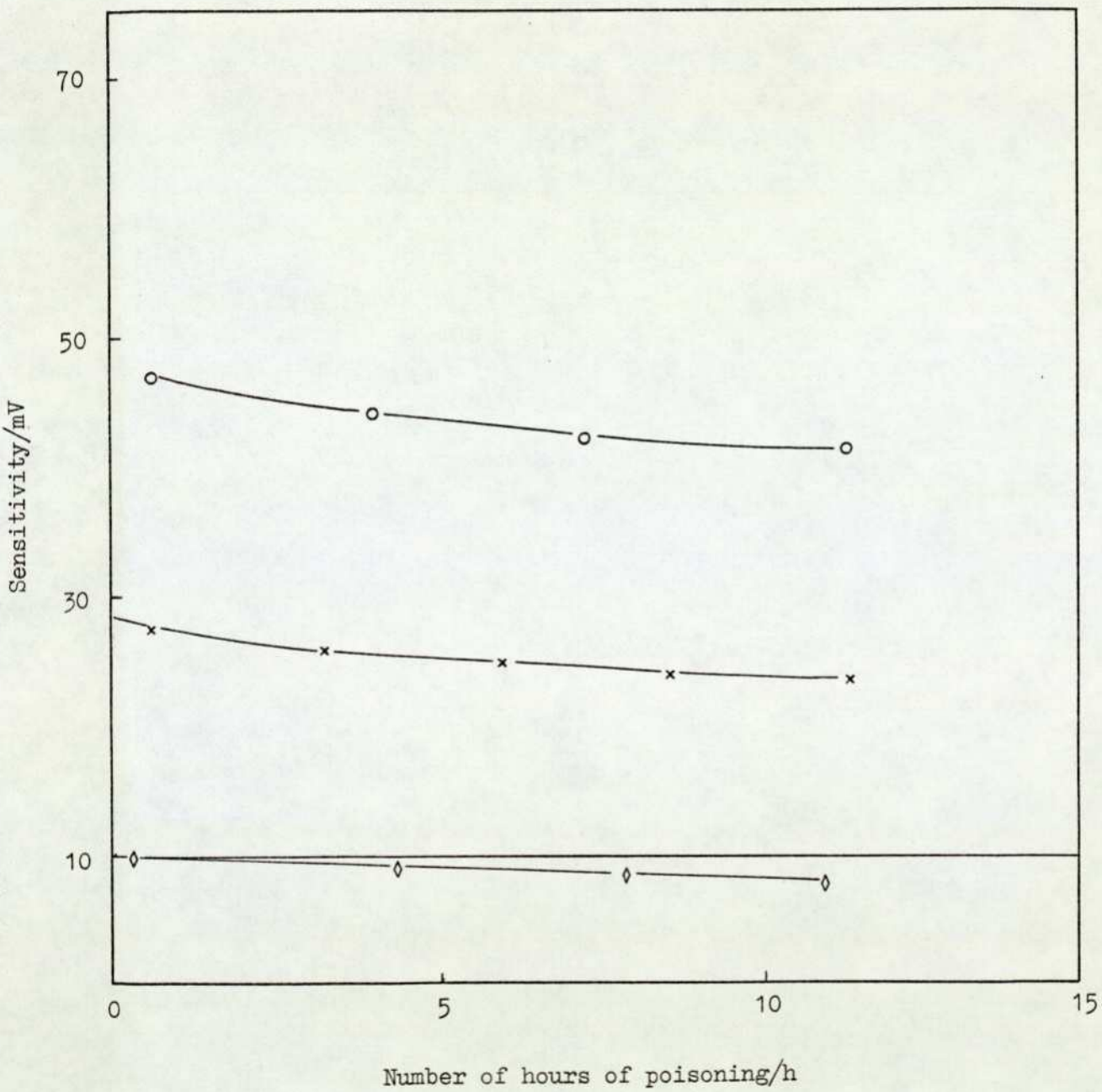

Figure 49

Results of poisoning experiment

Specimen: 165/VQ3 coated with 6:4 sodium mordenite : kaolin

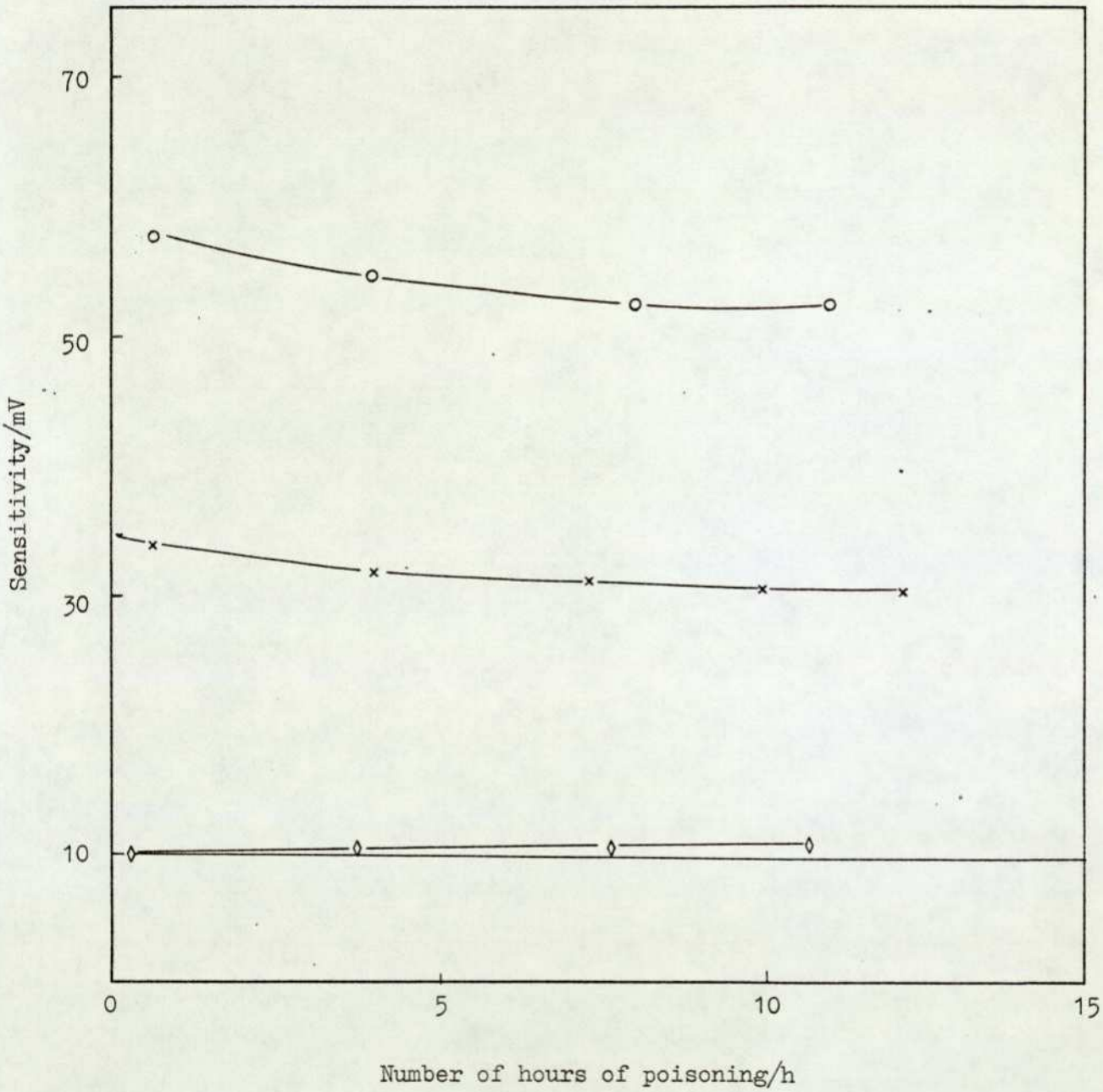

Figure 50

Results of poisoning experiment

Specimen: 157/VQ3 coated with 8:2 sodium mordenite : kaolin

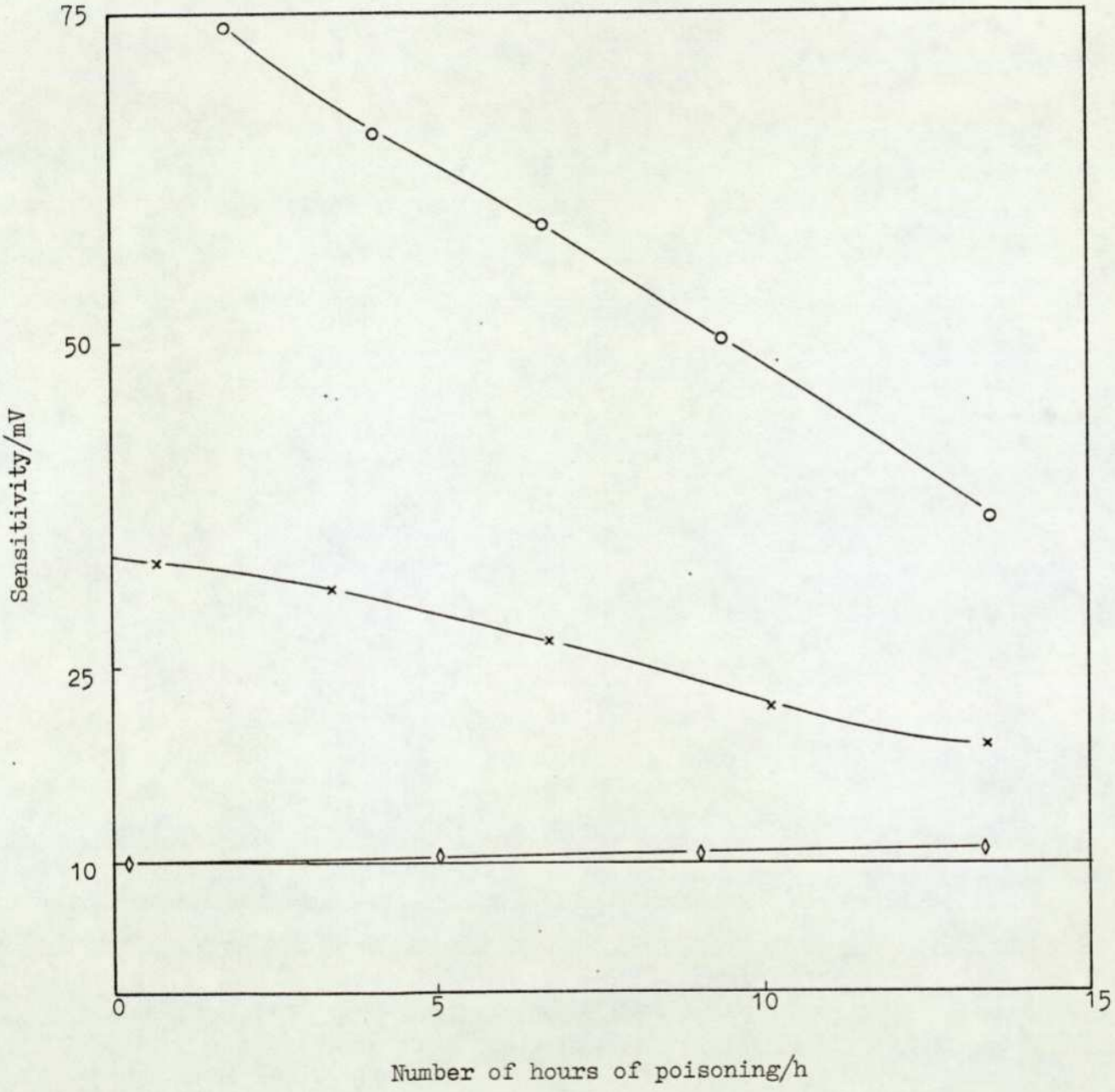

Serial No.	zeolite: kaolin ratio	Initial response to 1% CH_4/mV	Final response to 1% CH_4/mV	Percentage sensitivity remaining	Total hours of poisoning/h	Response to 1% CH_4 after 10 hours poisoning/ mV	Percentage sensitivity left after 10 hours poisoning	Air drift/ mV
170	40:60	17.5	19.5	111.4	12	18.0	102.9	-8.5
176	40:60	17.5	18.5	105.7	12	18.5	105.7	-5.5
173	40:60	15.5	16.5	106.5	10	16.5	106.5	-8.0
160	60:40	18.5	19.0	102.7	10	19.0	102.7	-7.5
136	60:40	24.5	24.5	100.0	11	25.5	104.1	-7.0
135	80:20	19.5	4.5	23.1	11	5.0	25.6	+5.5
538	80:20	24.5	20.0	81.6	13	20.0	81.6	-5.0

TABLE 27 - VQ1 Coated with Sodium Mordenite

Serial No.	zeolite: kaolin ratio	Initial response to 1% CH_4/mV	Final response to 1% CH_4/mV	Percentage sensitivity remaining	Total hours of poisoning/h	Response to 1% CH_4 after 10 hours poisoning/ mV	Percentage sensitivity left after 10 hours poisoning	Air drift /mV
170	40:60	18.0	16.0	88.0	11	16.0	88.9	-2.0
252	40:60	19.5	16.5	84.6	11	16.5	84.6	-2.0
169	40:60	19.0	12.5	65.8	11	12.0	63.2	-2.0
165	60:40	25.0	19.0	76.0	11	19.0	76.0	+1.0
162	60:40	21.0	13.5	64.3	13	14.5	69.1	-7.0
157	80:20	25.0	8.5	30.0	13	11.0	44.0	+1.0
159	80:20	26.0	8.0	30.7	13	11.0	42.3	-1.0

TABLE 28 - VQ3 Coated with Sodium Mordenite

drifts.

In conclusion, beads coated with dealuminated forms of hydrogen mordenite in the ratio of zeolite : kaolin of 60:40 showed the greatest resistance to poisoning, and also the least zero drift. Hence for the remaining studies, most of the effort was concentrated on using and investigating dealuminated hydrogen mordenite.

3.9 Further Lead Analyses

Six VQ1 beads coated with 60:40 ratio of dealuminated form of hydrogen mordenite to kaolin were poisoned in pairs for 23½ hours with n-heptane/TML/air mixtures containing 20-25 mg lead per cubic metre of air. The beads were then dissolved in a platinum crucible for analysis. Two drops of concentrated sulphuric acid were added followed by 10 cm^3 of hydrofluoric acid, and the mixture was slowly evaporated to complete dryness on a hot plate. 10 cm^3 of 0.1 mol dm^{-3} hydrochloric acid were next added, and the mixture was again slowly evaporated down to ~ 3 cm^3. Finally, the solution was diluted to 100 cm^3 with 0.1 mol dm^{-3} hydrochloric acid. The amount of lead in this solution was determined by atomic absorption spectrophotometry using a Perkin Elmer - model 370 spectrophotometer. The absorption line for lead occurs at a wavelength of 283.3 nm. A concentration of lead of 6.3 $\mu g\ cm^{-3}$ (6.3 ppm) was obtained, which corresponds to an average uptake of lead per bead of 105 µg (0.1 mg). This figure may be compared with the total amount of lead that had passed over the beads in the poisoning process (38.07 mg).

3.10 Adsorption and Desorption Experiments

Even using the highly sensitive Cahn sorptiometric balance,

the determination of the surface area of an individual pellistor is is a very difficult task, as the maximum weight change occurring due to the sorption of a vapour may only be of the order of micrograms. This weight change should be compared with the stated maximum sensitivity of the microbalance (0.1 μg). Because of their high internal pore volume, the attainment of reproducible Type I isotherms was a much easier task in the case of pellistors containing zeolites (e.g. Figures 56 and 57).

All the work discussed in this section should be assessed in the light of these foregoing comments. The adsorption and desorption were performed in order to find out whether the deactivation of the catalyst, brought about by the lead alkyl, was in any way affecting the adsorption characteristics of the sample. All adsorption and desorption isotherms of a series of unpoisoned and poisoned VQ1 and VQ3 beads were carried out by the gravimetric method using the Cahn Vacuum Electrobalance (section 2.5.2.1). The sample was degassed at 500°C for 16 hours to a final vacuum of 1.33×10^{-2} N m^{-2} (10^{-4} torr). Figures 51 and 52 show the isotherms of unpoisoned VQ1 and Figure 53 shows that of poisoned VQ1. They all have a similar profile, corresponding to a Type II isotherm (5). Hence applying the BET equation the surface area can be calculated. The isotherms of unpoisoned and poisoned VQ3 beads are shown in Figures 54 and 55 respectively. Here again the isotherms are of Type II. From these results a preliminary, and rather surprising, deduction is that the poisoned samples tend to have a greater surface area than the unpoisoned ones.

Figure 56 shows a typical adsorption isotherm obtained from a large sample of dealuminated hydrogen mordenite. This isotherm was determined by the volumetric method using the Carlo-Erba 1800 instrument. Figure 57 shows the adsorption and desorption branches obtained from a

Figure 51

Adsorption - desorption isotherm

Sample: 10 VQ1 beads - unpoisoned

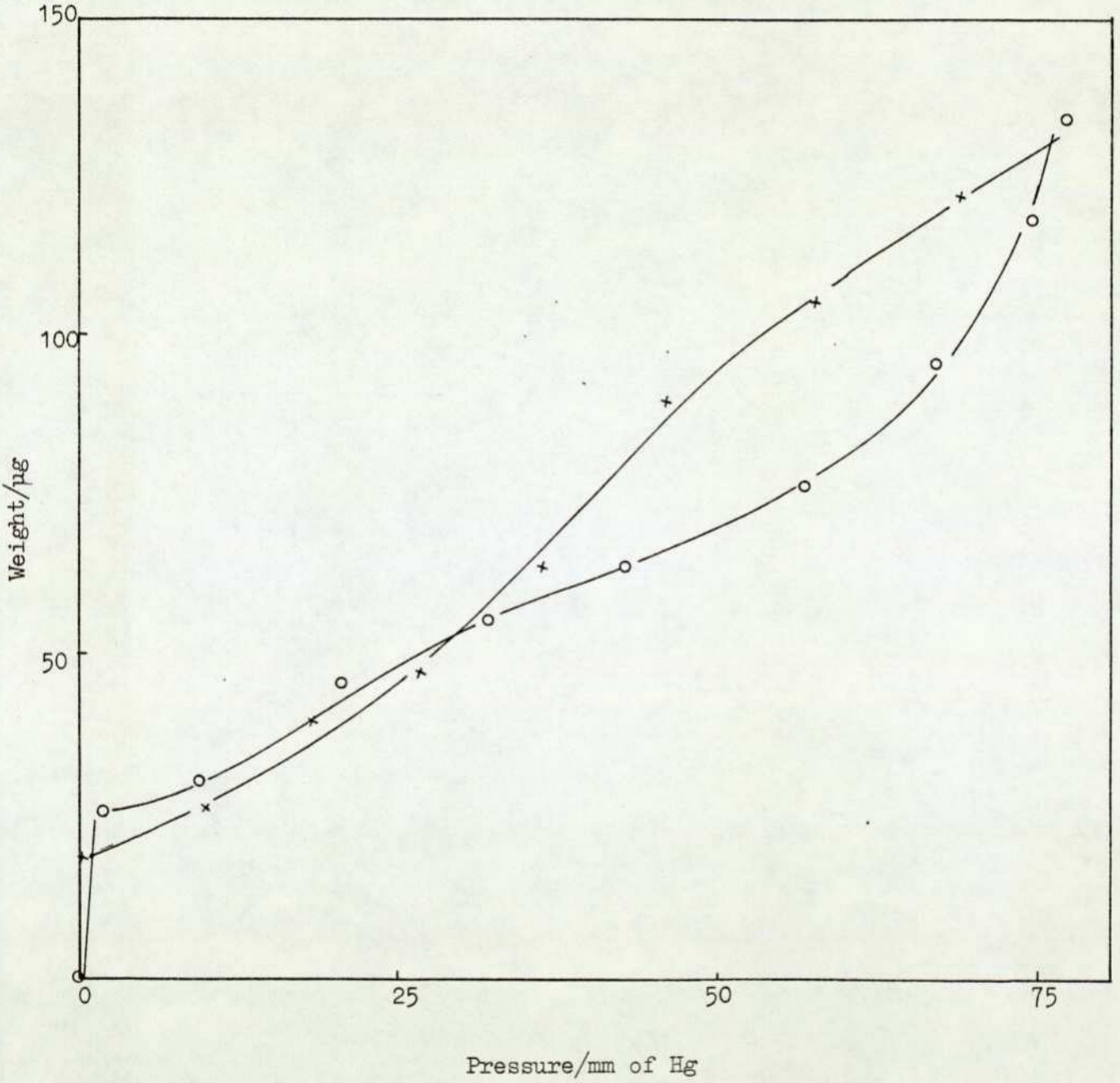

o : adsorption; x : desorption
Sample weight = 16.954
Surface area = 6.16 $m^2 g^{-1}$

Figure 52

Adsorption - desorption isotherm

Sample : 12 VQ1 beads - unpoisoned

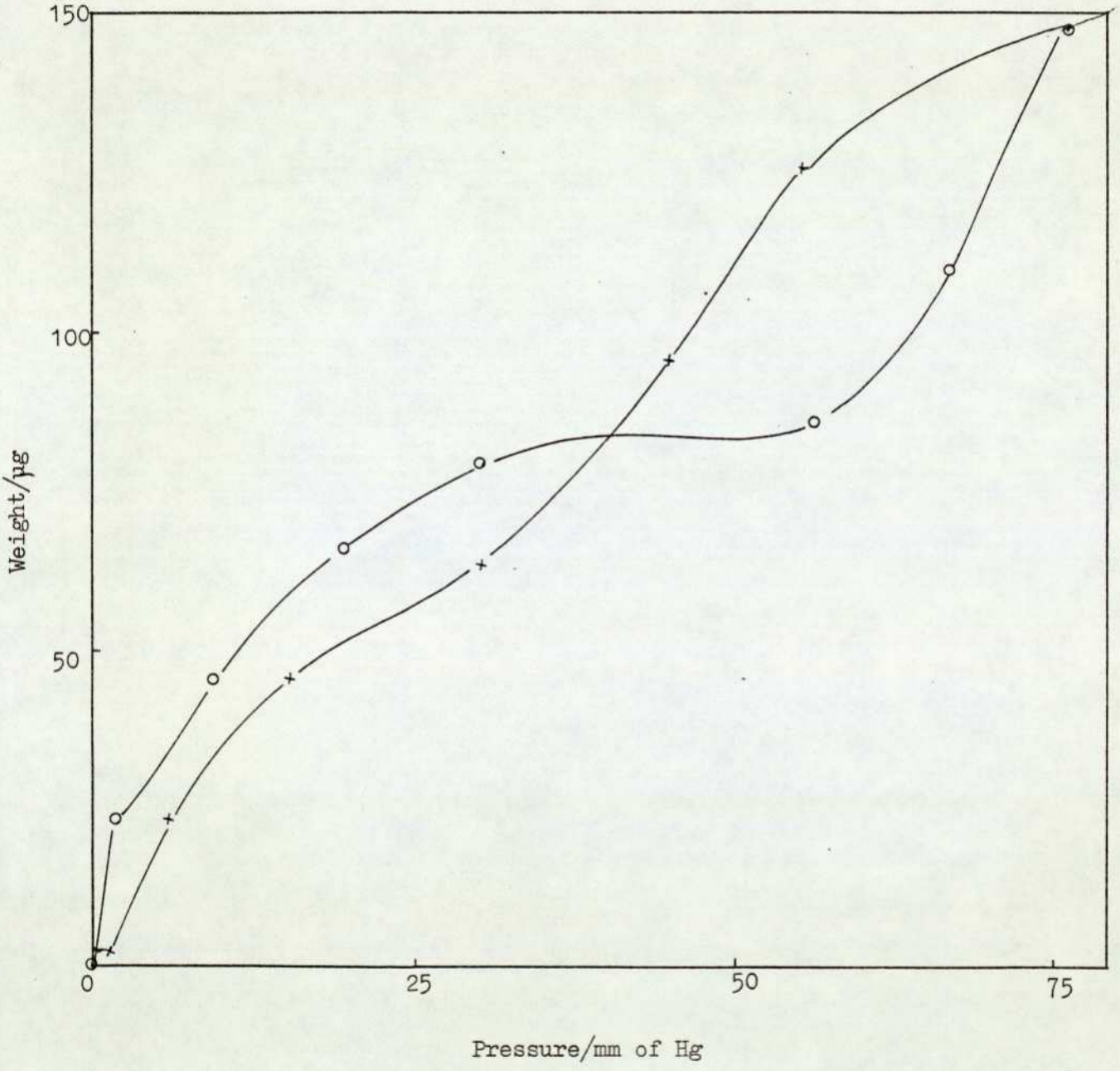

o : adsorption; x : desorption
Sample weight = 16.140 mg
Surface area = 6.47 $m^2 g^{-1}$

Figure 53

Adsorption - desorption isotherm

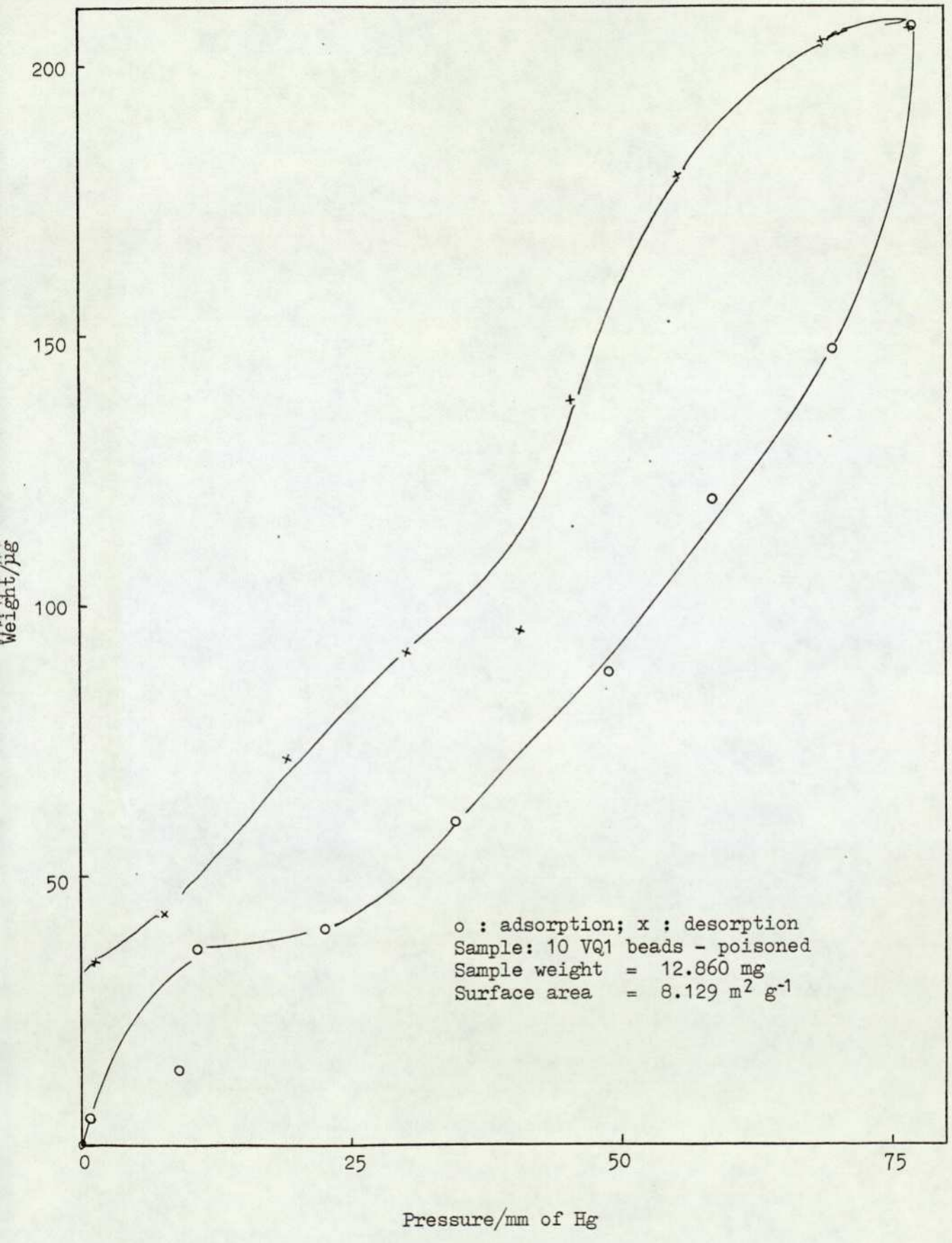

Figure 54

Adsorption - desorption isotherm

Sample: 11 VQ3 beads - unpoisoned

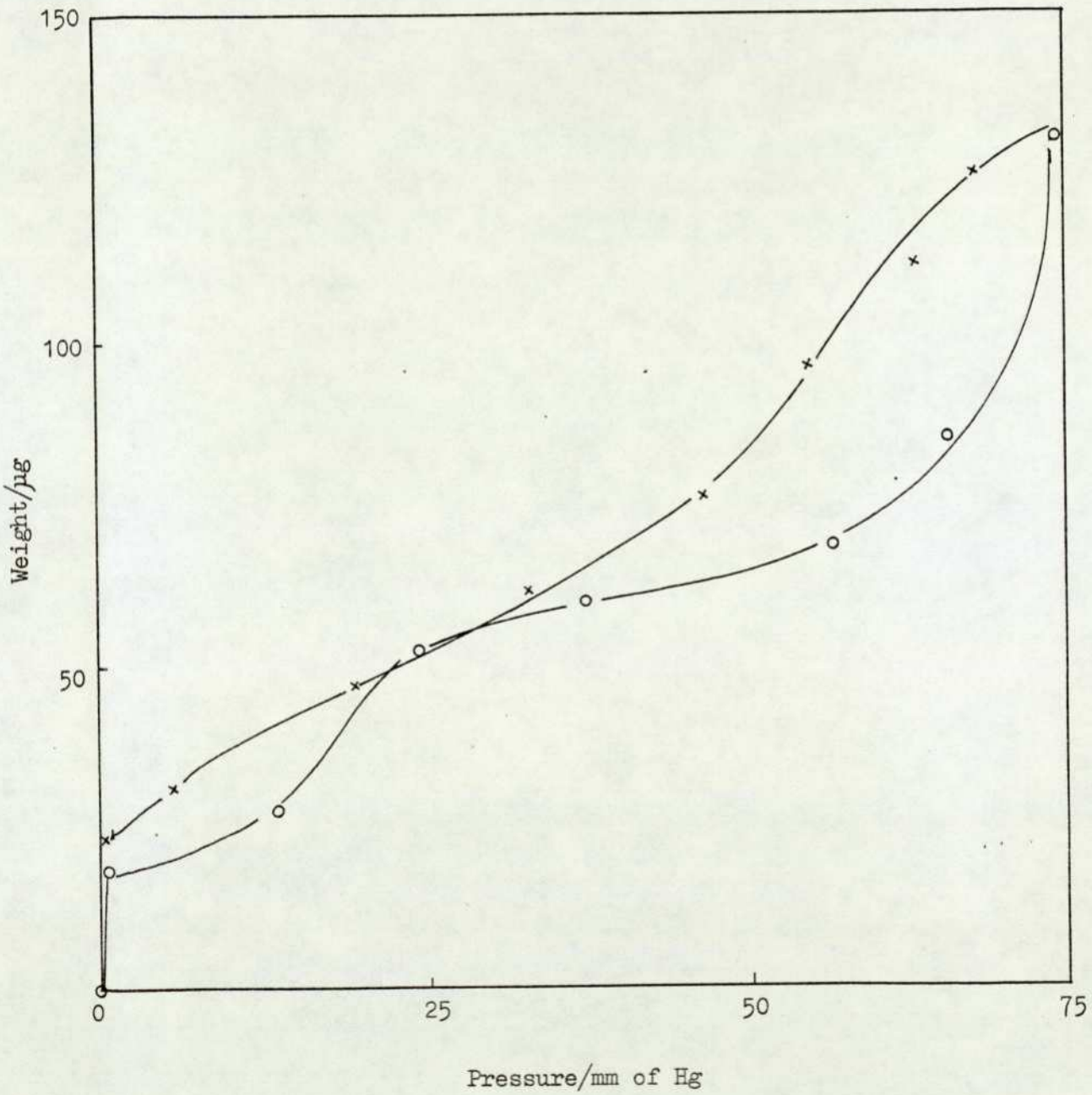

o : adsorption; x : desorption
Sample weight = 20.228 mg
Surface area = 6.374 $m^2 g^{-1}$

Figure 55

Adsorption - desorption isotherm

Sample: 7 VQ3 beads - poisoned

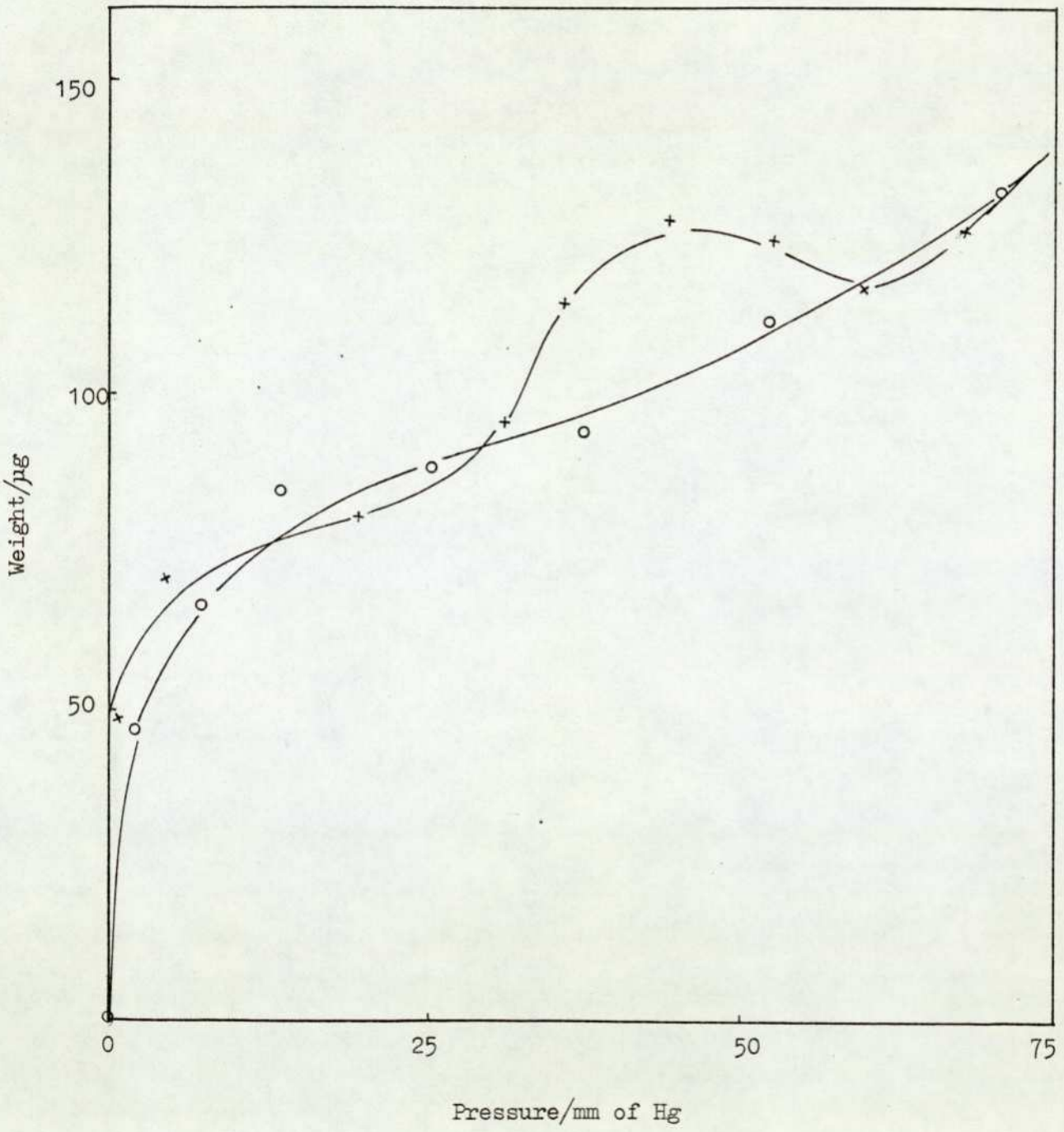

o : adsorption; x : desorption
Sample weight = 10.886 mg
Surface area = 21.12 $m^2 g^{-1}$

Figure 56

Adsorption isotherm - volumetric method

Sample: dealuminated hydrogen mordenite - unpoisoned

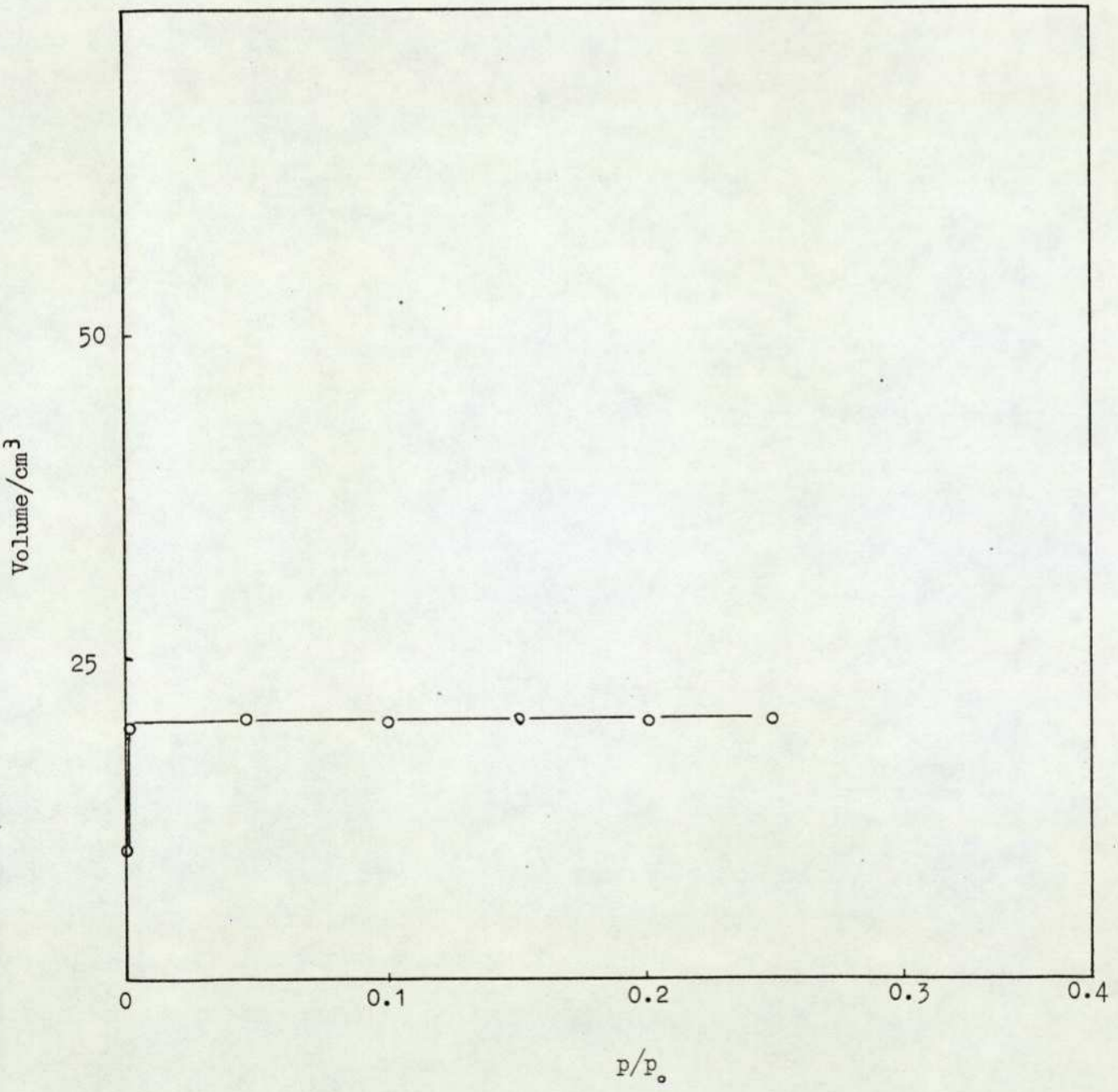

o : adsorption
Sample weight = 0.1772 g
Surface area = 497.78 $m^2 g^{-1}$

Figure 57

Adsorption - desorption isotherm

Sample: dealuminated hydrogen mordenite - unpoisoned

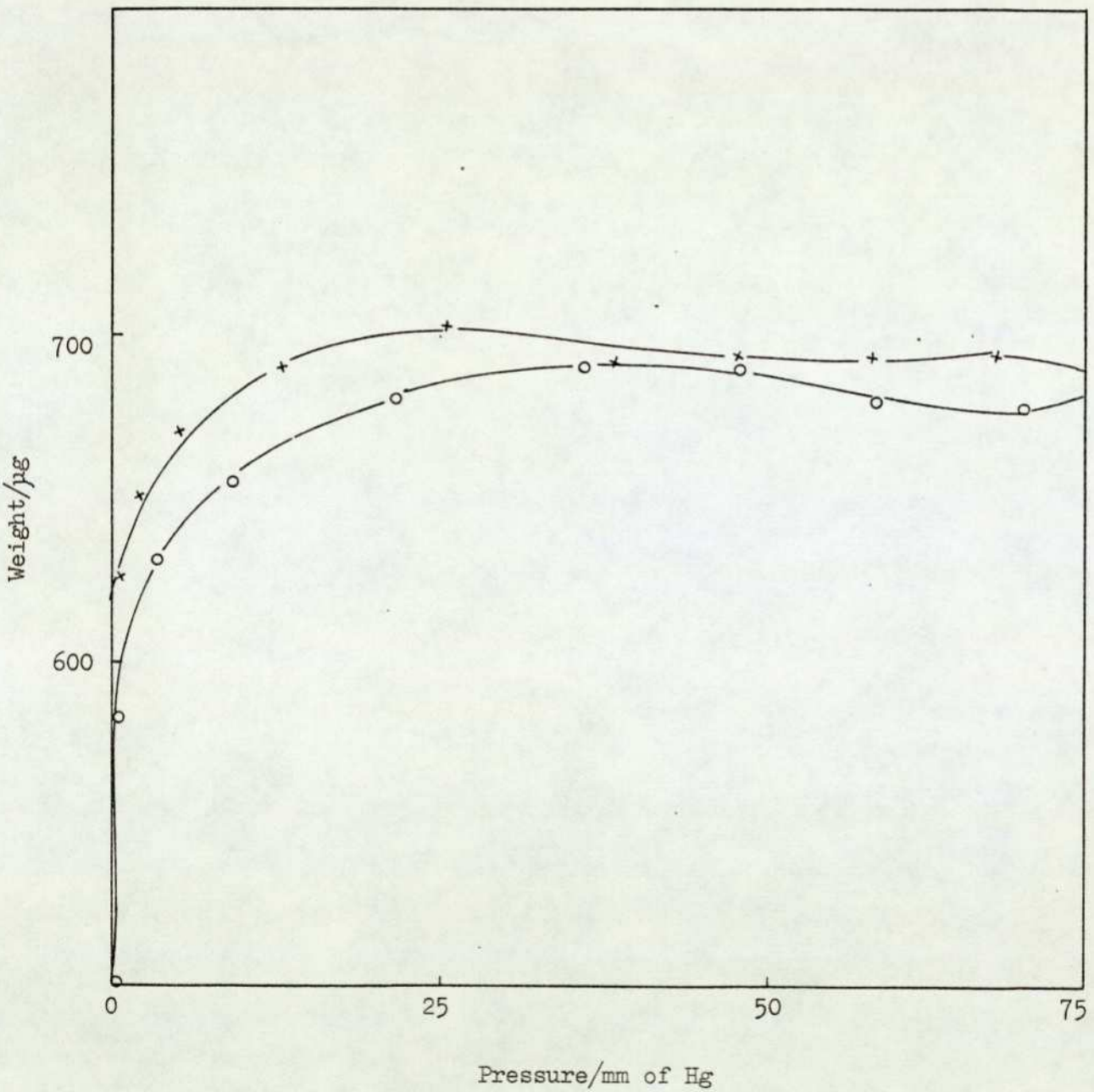

o : adsorption; x : desorption
Sample weight = 4.806 mg
Surface area = 500.31 $m^2 g^{-1}$

sample of only $\sim$ 4 mg of dealuminated hydrogen mordenite (determined, of course, by the gravimetric method). These isotherms are both Type I, which is characteristic of a microporous adsorbent. The values obtained for the "monomolecular equivalent surface area" in both cases are in good agreement ($\sim 500\ m^2 g^{-1}$). Isotherms were also obtained from samples of dealuminated hydrogen mordenite that has been exposed to leaded atmospheres for 4 hours and 6 hours. These are shown in Figures 58 and 59. The profiles of the isotherms are markedly different from the unpoisoned samples. Finally adsorption/desorption experiments were carried out on samples of VQ1, VQ3, beads coated with dealuminated hydrogen mordenite before and after poisoning had occurred. Figure 60 shows the isotherms of a single unpoisoned VQ1 bead coated with a ratio of 6:4 of dealuminated hydrogen mordenite:kaolin. The adsorption isotherm resembles a Type I. In Figures 61 and 62 are shown isotherms for single poisoned VQ1 beads (i.e. a total sample weight of < 1 mg) coated with the same ratio of dealuminated hydrogen mordenite to kaolin. These beads were deactivated to $\sim$ 85% of the original activity and the isotherms show a marked difference from the corresponding unpoisoned one. The isotherm show a large uptake of adsorbate at the low pressure range, and the curve then flattens out to Type I isotherm. Similarly, Figures 63 and 64 show isotherms obtained for unpoisoned single VQ3 beads coated with a 6:4 dealuminated hydrogen mordenite, and as expected, the isotherms are Type I, typical of zeolites. On poisoning, the profile changes, Figure 65 shows the results obtained for one such single poisoned VQ3 bead, again coated with 6:4 dealuminated hydrogen mordenite:kaolin. Once more, the profile of the adsorption isotherm does not strictly fit any of the five types mentioned in the classification (5).

Figure 58

Adsorption - desorption isotherm

Sample: dealuminated hydrogen mordenite - poisoned for 4 hours

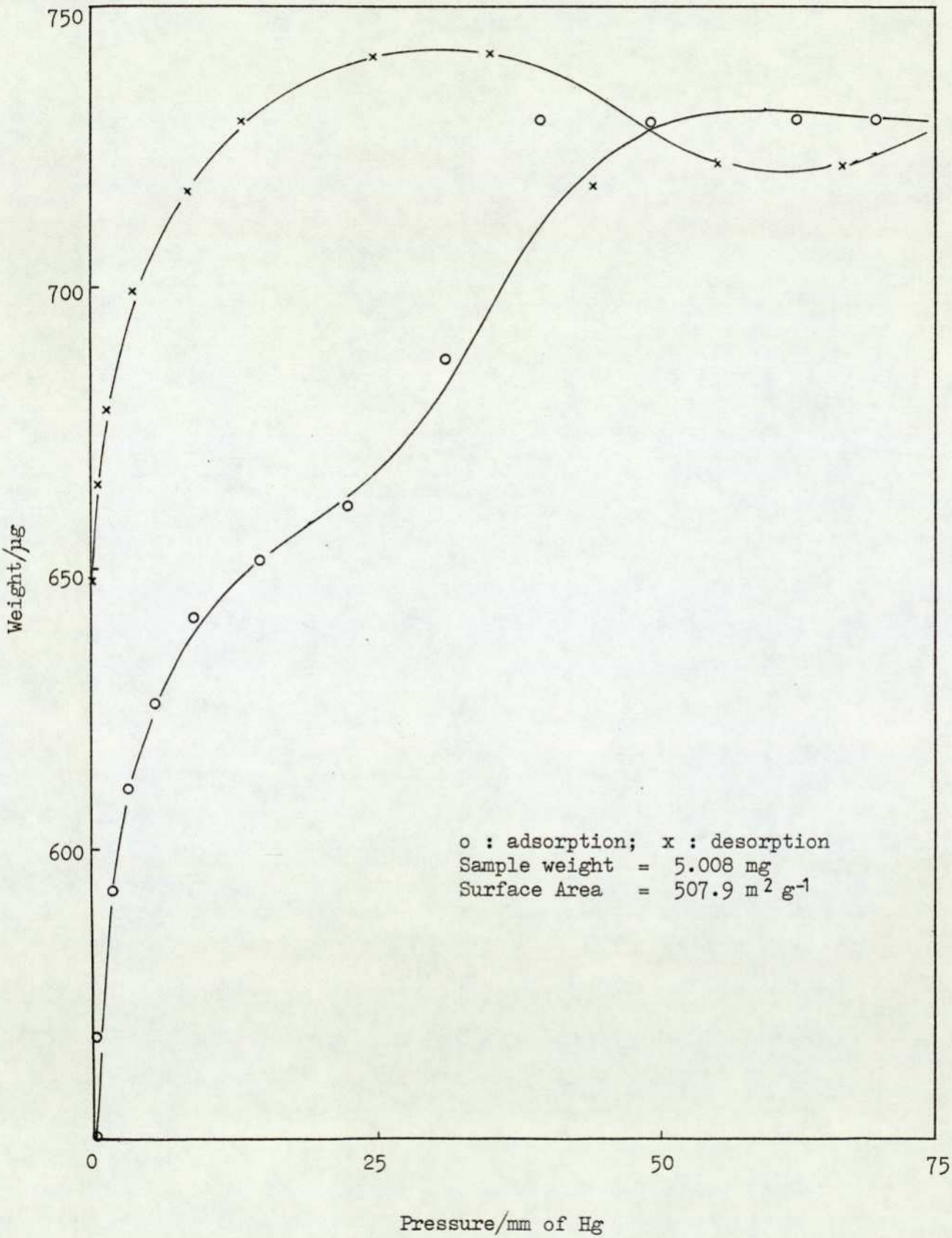

Figure 59

Adsorption - desorption isotherm

Sample: dealuminated hydrogen mordenite - poisoned for 6 hours

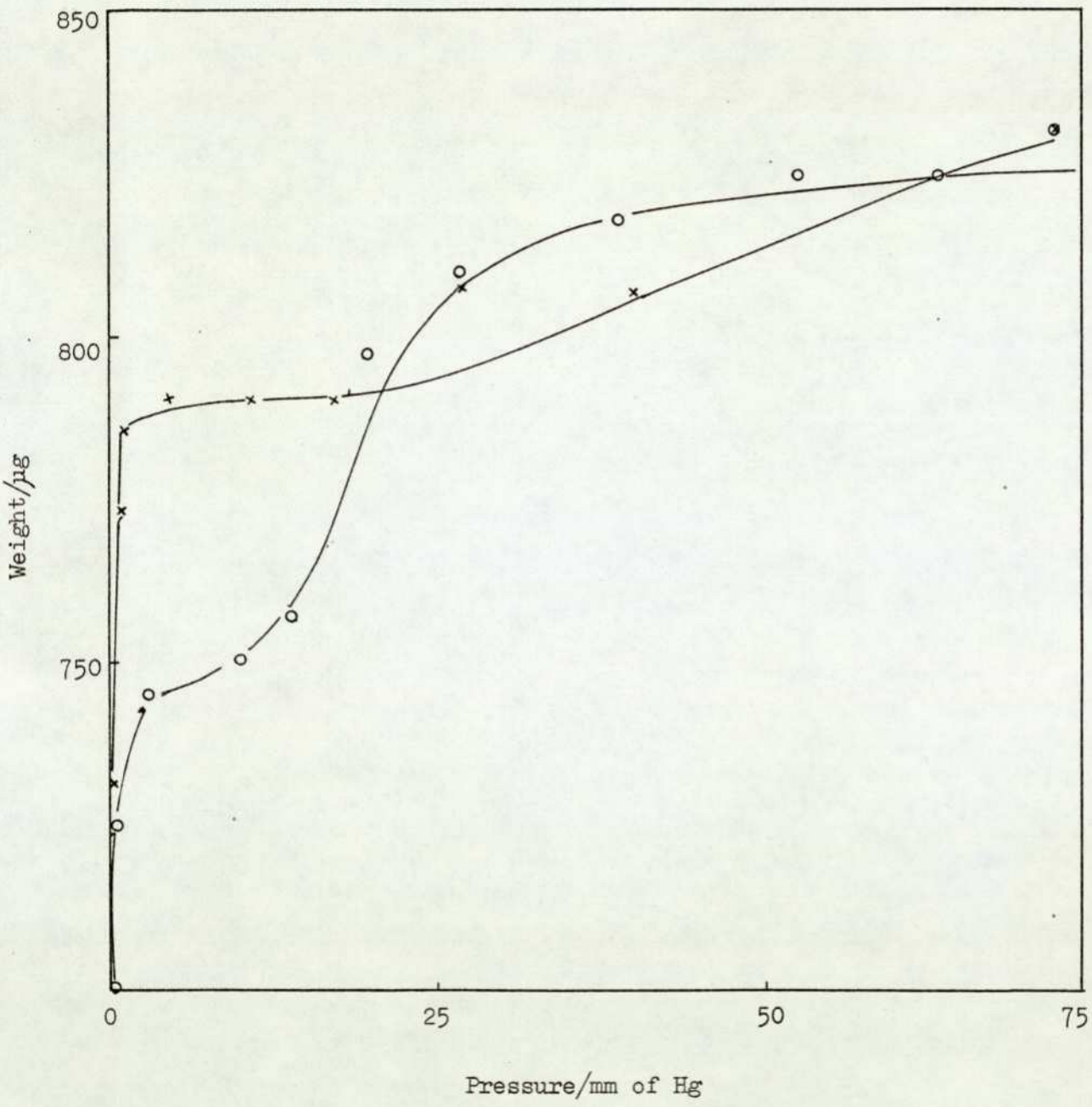

o : adsorption; x : desorption
Sample weight = 5.850 mg
Surface area = 491.14 $m^2 g^{-1}$

Figure 60

Adsorption - desorption isotherm

Sample: single VQ1 bead, coated with 6:4 dealuminated hydrogen mordenite : kaolin, - unpoisoned (426)

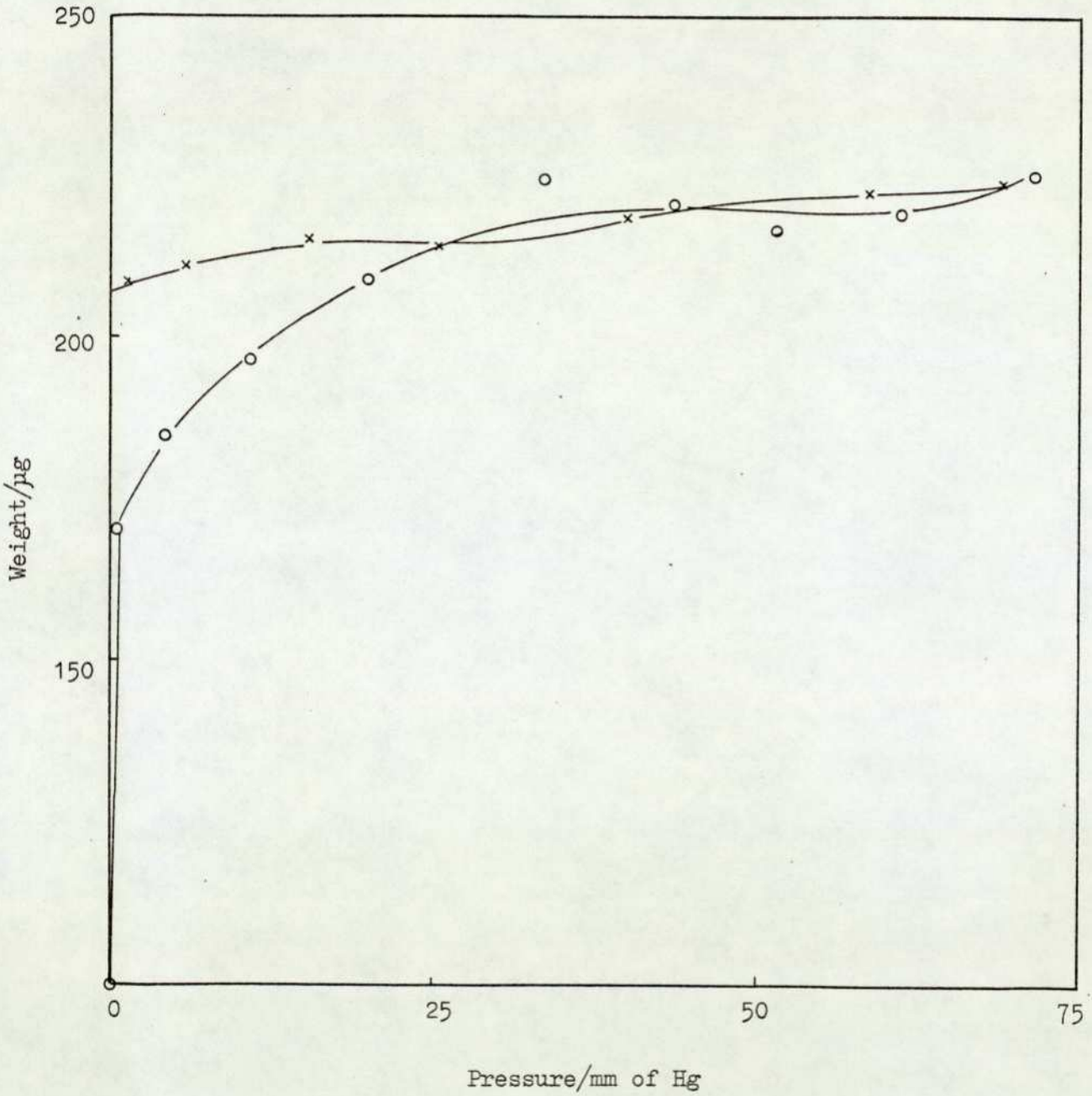

o : adsorption; x : desorption
Sample weight = 3.684 mg

Figure 61

Adsorption - desorption isotherm

Sample: single VQ1 bead, coated with 6:4 dealuminated hydrogen mordenite : kaolin, - poisoned (965)

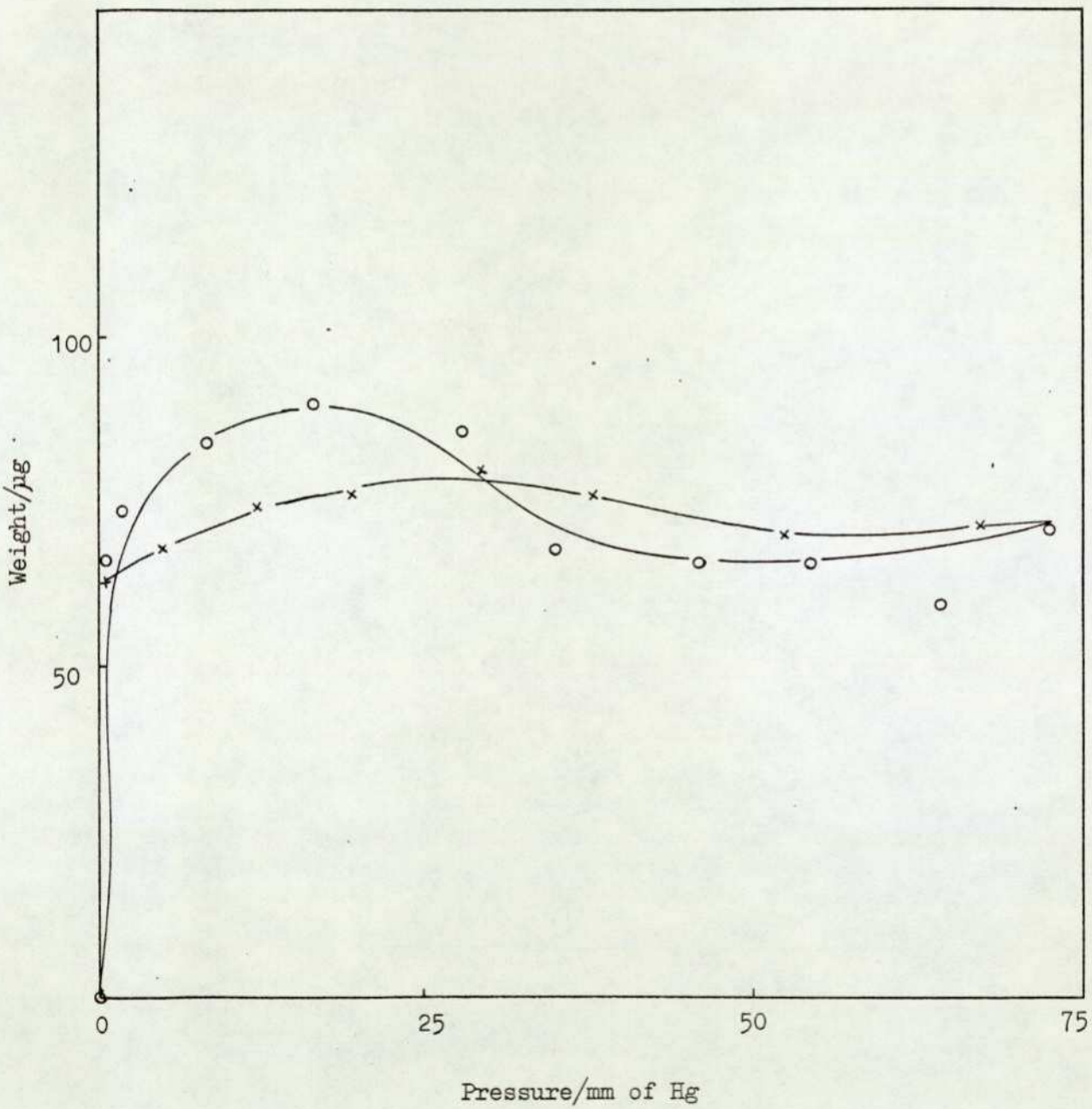

o : adsorption; x : desorption
Sample weight = 2.830 mg

Figure 62

Adsorption - desorption isotherm

Sample: single VQ1 bead, coated with 6:4 dealuminated hydrogen mordenite : kaolin, - poisoned (963)

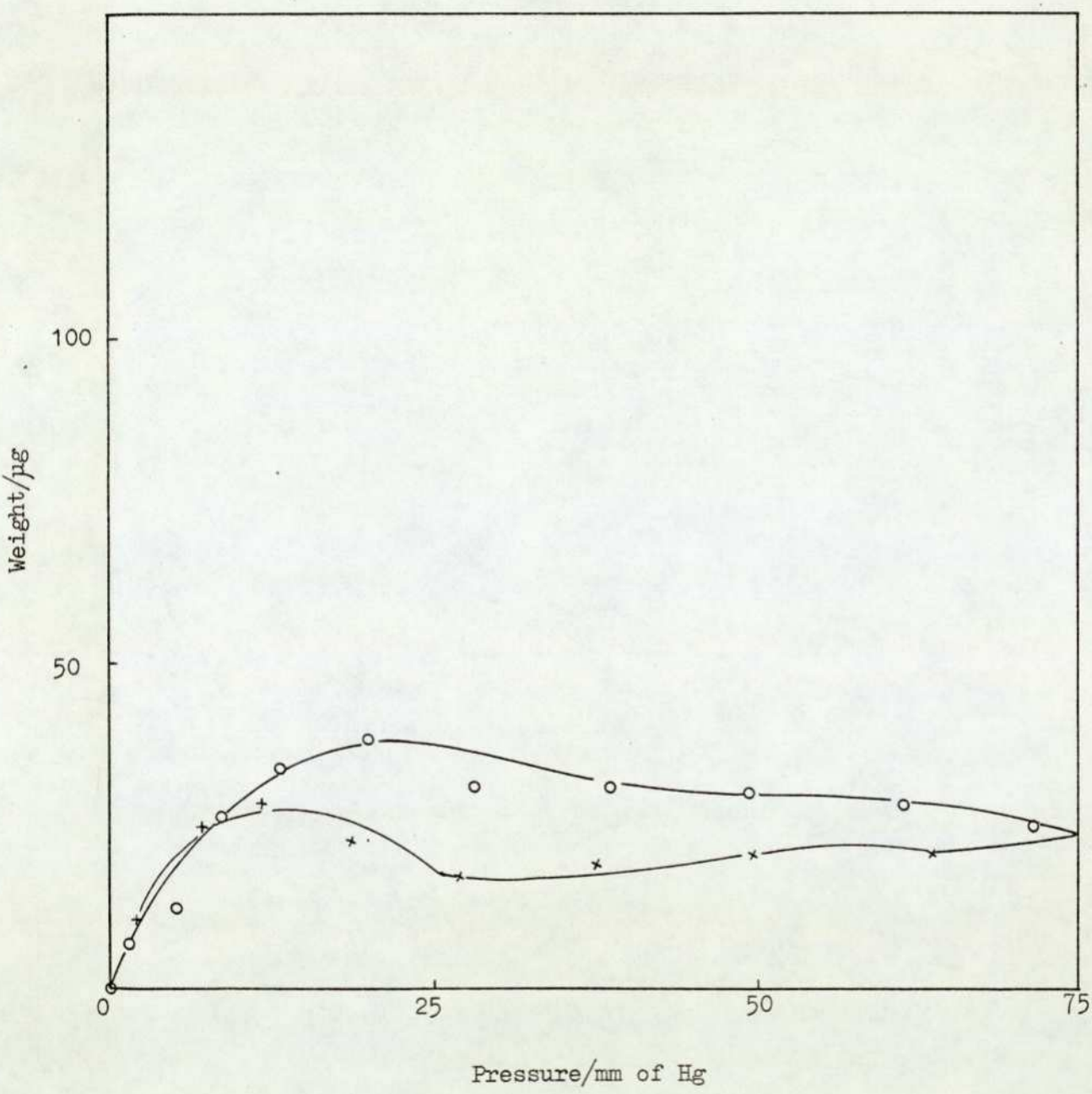

o : adsorption; x : desorption
Sample weight = 1.974 mg

Figure 63

Adsorption - desorption isotherm

Sample: single VQ3 bead, coated with 6:4 dealuminated hydrogen mordenite : kaolin, - unpoisoned (372)

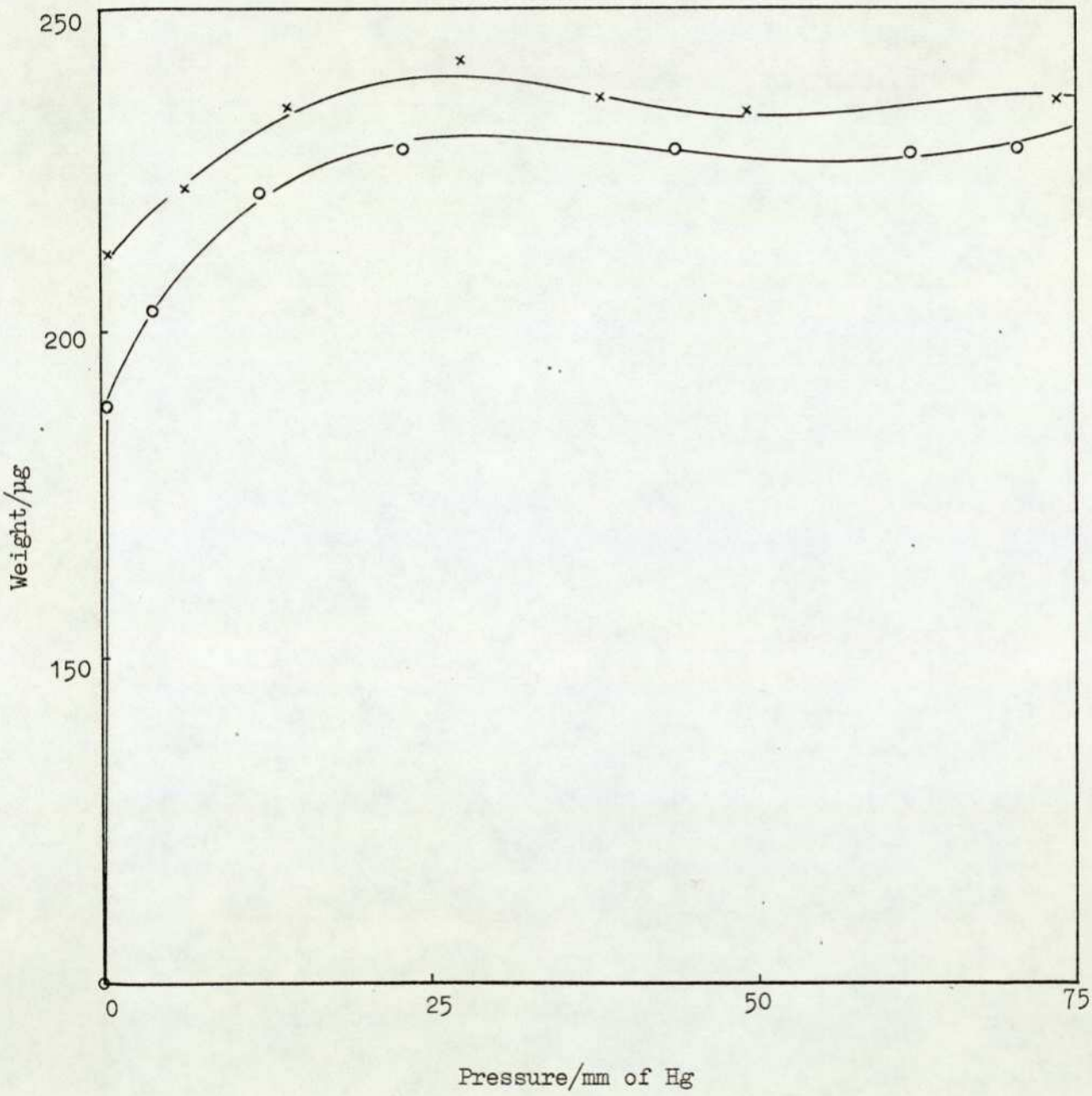

o : adsorption; x : desorption
Sample weight = 4.3280 mg

Figure 64

Adsorption - desorption isotherm

Sample: single VQ3 bead, coated with 6:4 dealuminated hydrogen mordenite : kaolin, - unpoisoned (371)

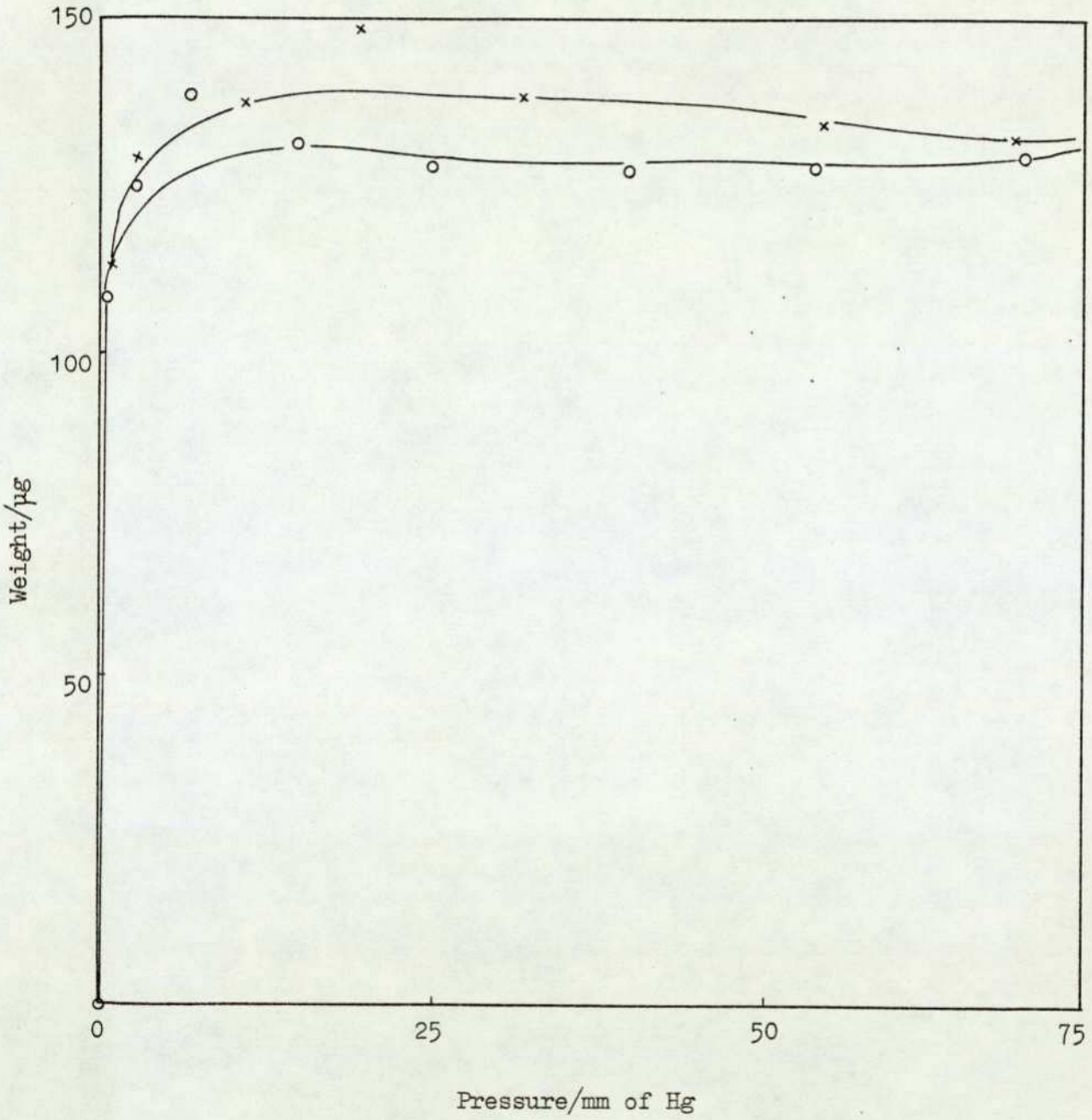

o : adsorption; x : desorption
Sample weight = 3.4435 mg

Figure 65

Adsorption - desorption isotherm

Sample: single VQ3 bead, coated with 6:4 dealuminated hydrogen mordenite : kaolin, - poisoned (666)

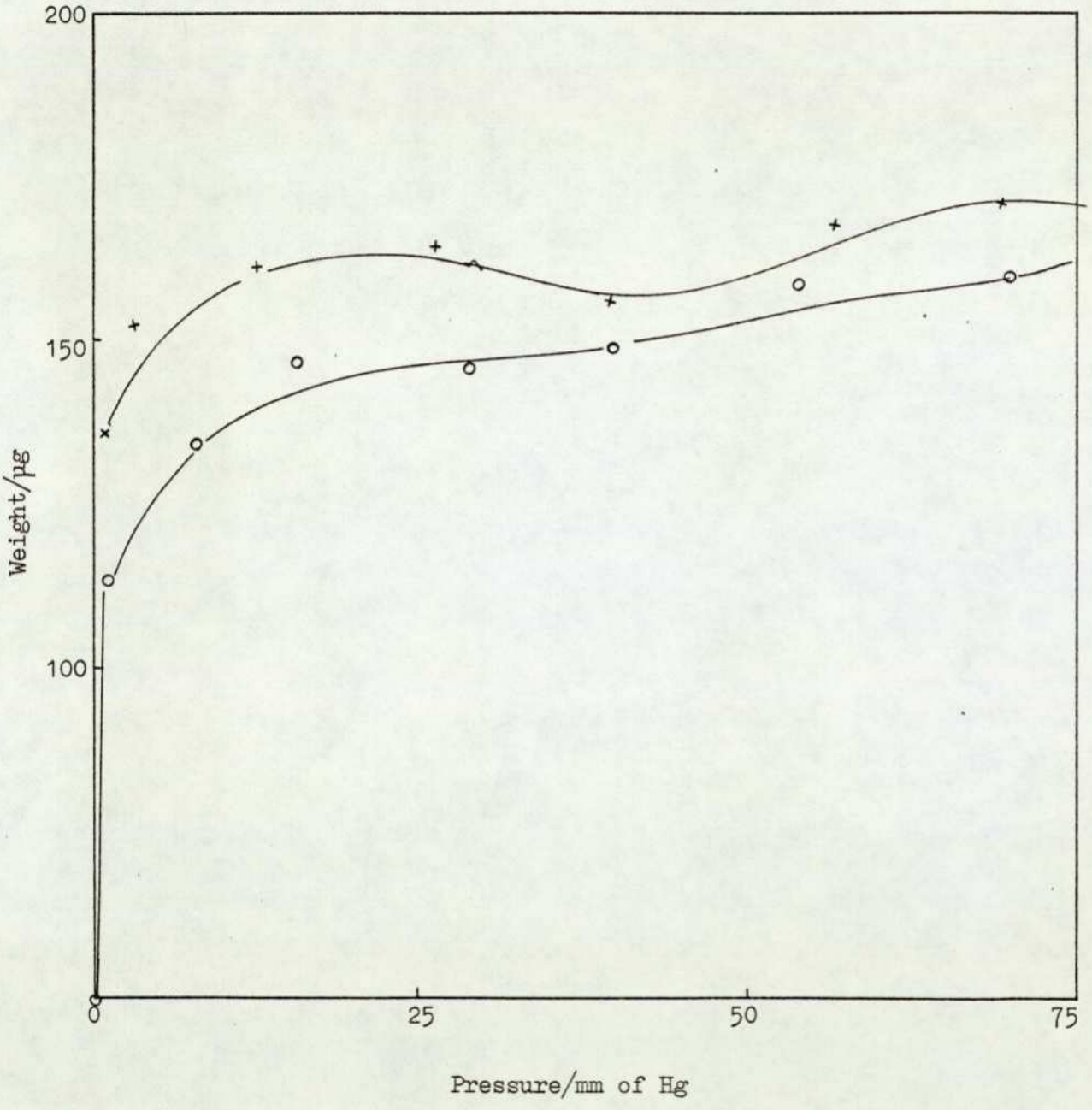

o : adsorption; x : desorption
Sample weight = 3.786 mg

CHAPTER 4

DISCUSSION

C H A P T E R 4

4.1 General Introduction: The Mode of Deactivation

The three general classes of deactivation processes are:-

(a) poisoning,

(b) fouling, and

(c) aging.

The preliminary results of this work showed that only small quantities of tetramethyl lead were required to reduce the activity of the catalyst severely. The small quantities of poison used show that fouling is not a significant process and life-tests in the absence of poison similarly rule out aging as being a significant contributory factor. Hence the present deactivation process is that of type (a), concerned with individual system, catalyst-reaction-poison. Such a selective poisoning may, however, be due to site selectivity in the absence of diffusion effects, or due to diffusion control, or a combination of both.

4.2 The Poisoning Process: General Evidence

The studies of the poisoning effect of tetramethyl lead on catalytic detectors described in this thesis have primarily centered on the microscopic scale and have involved a variety of techniques. The information obtained through this programme has enabled a partial evaluation of the nature of the interaction between the poison and the active catalyst sites. Coking may be ruled out as a significant factor, as the bead did not lose any sensitivity after prolonged operation in an atmosphere of n-heptane (Figures 17,18). Furthermore, neither of the scavengers (i.e. ethylene dibromide and ethylene dichloride) seemed to affect the sensitivity of the catalyst bead toward 1% methane. The initial results

showed however that only very small quantities of lead were required to reduce the activity of the catalyst bead drastically.

Comparisons of the topographies of the surface of poisoned and unpoisoned beads revealed no physical growth or particulate deposit of any kind that could be attributed to lead or compounds of lead; microscopically the physical characteristics of surface appeared virtually unchanged. In addition, elemental analysis using EDAX showed that lead was evenly dispersed on the surface. Cross-sectional examinations of beads by EDAX revealed in addition that hardly any lead had diffused into the central portions of beads. Thus the elemental and topographical studies showed together that the poisoning process is primarily an external surface effect. A drawback of this study of the surface has been that the same bead cannot be used for topographical and elemental examination both before and after poisoning, because the technique by its very nature is a destructive one. Hence only through examinations of series of poisoned and unpoisoned beads was it possible to draw the above conclusions. In effect, the poison was plugging the pores close to the external surface, thereby preventing reactant from reaching the active sites. This matter is discussed further in section 4.2.1.2.

Surface area measurements carried out on the poisoned and unpoisoned samples showed that there was a difference in the profile of the isotherms obtained, especially when zeolite coated beads were compared, (see Figures 56,57,61,62). This difference was especially noticeable when comparing isotherms of dealuminated hydrogen mordenite (DHM) that had been exposed to tetramethyl lead for different times, (see Figures 57,58 and 59). Although the technique used (gravimetric) is a very sensitive one, more samples are needed to carry out a really detailed study. The sorptiometric measurements provided no help in elucidating the mechanism

of the poisoning process (i.e. whether pore mouth or uniform poisoning was occurring (72)).

4.2.1 Physical Aspects

The rate-determining step in the catalytic detection of methane using the pellistor is the transfer of reactant through the gas phase to the catalyst surface (boundary layer diffusion control). Hence the rate will be strongly influenced by any changes in the inert or active porous structure surrounding the catalyst if these changes result in an outer porous layer around the catalyst in which transport processes or chemical reactions occur which are slower than diffusion in the gas phase. This matter is considered in the following section.

4.2.1.1 Boundary Layer Diffusion

Modified pellistors were surrounded by either a layer of inert alumina or a zeolite/kaolin mixture. The possibility therefore arises with these beads of the rate-controlling step no longer being diffusion through the boundary layer of gas close to the bead surface, but rather through this outer inert layer. The initial sensitivity of the alumina coated beads was around 50% of the original pellistors; this change was probably due to the rate-controlling step shifting from bulk diffusion in the gas phase to Knudsen diffusion through this outer layer (the small size of the samples precluded pore-size distribution measurements which would have been able to confirm this postulate).

The sensitivity of zeolite coated pellistors hardly changed from that observed with the originals. Diffusion in zeolites is an activated process (153) and an estimate may be obtained of the diffusion

coefficient for methane in mordenite at the operating temperature of the bead (viz. 873 K). From literature data (153) $D_{CH_4} = 3 \times 10^{-14}$ m^2 s^{-1} at 300 K and the energy of activation was found to be 8500 J mol^{-1} . Thus

$$D_{CH_4}(873) = 3 \times 10^{-14} \exp\left[-\frac{E}{R}\left(\frac{1}{873} - \frac{1}{373}\right)\right]$$

$$= 1.45 \times 10^{-13} \text{ m}^2 \text{ s}^{-1}$$

This value is much smaller than typical bulk diffusivities for molecules of molecular weight similar to methane at 873 K (typically, D_B 2×10^{-4} m^2 s^{-1}). Thus if the rate controlling step is diffusion through the zeolite pores a very marked drop in initial sensitivity would be expected. This is not observed, and it is therefore concluded that transpcrt of methane to the active sites below the zeolite layer in the zeolite-coated beads is not primarily through the microporous zeolite layer, but rather between the crystallites. This conclusion is further confirmed by the fact that pure kaolin coated beads also showed no drop in initial activity.

4.2.1.2 Pore Mouth Poisoning

It is convenient at this stage to summarise the theories of the effect of diffusion on the poisoning of heterogeneous catalysts in terms of two limiting theoretical models: pore mouth poisoning and uniform poisoning (72). The two limiting cases are a function of the strength and rate of adsorption of the impurities. The uniform poisoning model visualises the poison as adsorbing slowly, and to be highly mobile. Thus it will distribute itself uniformly throughout the bead. In other words, the activity of the catalyst will decrease uniformly at all points within the bead according to this model. At the other extreme, in the pore mouth poisoning model, the poison is considered to

be so strongly adsorbed that attachment to the surface occurs before the molecules have diffused any distance into the bead. The periphery (and hence the pore mouths) of the bead becomes completely poisoned while the interior maintains its initial activity. The poisoned region advances as more impurity diffuses to the active sites.

Considering the electron microscopic evidence (section 4.2), it is of interest that the poisoning curves obtained for all the specimens tested here have similar profiles to those proposed by Wheeler (72) for selective poisoning at pore mouths (see curves C & D in Figure 8 and compare with Figures 21,22,23). In the above comparisons it is implicitly assumed that the fraction poisoned $\propto$ is proportional to time h. The comparison of curve shapes in itself is not significant, but since the EDAX measurements indicate that the lead contaminant was only present to a significant degree on the peripheries of bead cross-sections, the curve similarities confirm that pore mouth poisoning was occurring.

4.2.1.3 Heat Transfer Effects

The foregoing assumes that the bead itself is isothermal. If this is not true, the situation becomes considerably more complex, with the effectiveness of the catalyst (see section 1.6.2) no longer restricted to values < 1, but able to reach values, greater than unity by orders of magnitude under certain conditions (154). The simple models of Wheeler for poisoning (section 1.6.3 and 4.2.1.2) are also modified.

Simple calculations are able to establish that in the case of the pellistor as used in the work described here, it is safe to assume isothermicity. Plate 7 (Chapter 3), shows that in a typical bead, the diameter of the coil is 0.8 mm and this is set within a bead of approximate diameter 1 mm, leaving a layer of catalyst around the

coil of 0.1 mm only. If the temperature of the coil is assumed to be 600°C, the following (admittedly simplified) calculations are possible.

Heat Transfer Estimates

Let thermal conductivity of Pt/Al_2O_3 $K_1 = 0.31\ J\ K^{-1}\ m^{-1}\ s^{-1}$

Let thermal conductivity of nitrogen $K_2 = 0.036\ J\ K^{-1}\ m^{-1}\ s^{-1}$ over temperature range of 0 - 600°C.

Models

For pellistor, from Plate 7 of thesis, it can be regarded as a cylinder. Heat conducted out from the wire, radius 0.4 mm to surface, radius 0.5 mm. Length of cylinder (L) 1 mm. $\Delta x = r_2 - r_1 = 0.1$ mm. For static air surrounding the bead, the thickness depends on the flow of air passed the system. A depletion layer of 0.1 mm has been quoted, but for heat loss a layer of 1 mm, or 3 mm which may be more realistic, will be assumed here. Also assuming a sphere of air radius 0.5 mm ($= R_1$) to a sphere of either radius 1.5 mm ($= R_2$, first case) or 3.5 mm ($= R_2$, second case. Δx therefore is either 1 or 3 mm.

Generally $$J = -K\ A \frac{dT}{dx} = K\ A \left| \frac{\Delta T}{\Delta x} \right|$$

As heat moves out the area of cross section is changing. So consider the change in heat flux with radius. Since the area is expanding as r increases, J is a function of cross-sectional area. To a first approximation.

$$dJ = K \frac{\Delta T}{\Delta x} dA$$

For pellistor $$dJ = K_1 \left(\frac{873 - T}{0.0001}\right) d(2\pi rL)$$

For air boundary $dJ = K_2 \left(\frac{T - 298}{\Delta x_{air}}\right) d(4\pi R^2)$

Under steady state, flux out of pellistor must be equal to flux out of air boundary.

i.e. $J = K_1 \left(\frac{873 - T}{0.0001}\right) \int_{r_1}^{r_2} d(2\pi rL) = K_2 \left(\frac{T - 298}{\Delta x}\right) \int_{r_1}^{r_2} d(4\pi R^2)$

Substituting K_1, K_2, r_1, r_2 and for case 1 where the boundary layer is 1 mm, $R_1 = 0.5$ mm, $R_2 = 0.6$ mm, $\Delta x = 1$ mm

$$T = 872.86 \quad K$$

For case 2 where the boundary layer is 3 mm, $R_1 = 0.5$ mm, $R_2 = 3$ mm, $\Delta x = 2.5$ mm, then

$$T = 872.77 \quad K$$

Hence, it is acceptable to assume isothermicity.

4.2.2 Chemical Aspects

The kinetics of gas phase oxidation of methane have been studied extensively. The reaction proceeds by a radical chain mechanism (155,156), in which formaldehyde is an intermediate. The reaction scheme is arranged as follows (157):-

$$CH_4 + O_2 \longrightarrow CH_3^* + HO_2^* \qquad (1)\ \text{Initiation}$$

$CH_3^* + O_2 \longrightarrow CH_2O + OH^*$	(2)	}	}	Propagation of main reaction
$OH^* + CH_4 \longrightarrow CH_3^* + H_2O$	(3)	}	}	
$O_2 + CH_2O \longrightarrow HCO^* + HO_2^*$	(4)			Branching reaction
$HCO^* + O_2 \longrightarrow CO + HO_2^*$	(5)	}	}	Propagation of formaldehyde oxidation
$HO_2^* + CH_2O \longrightarrow H_2O_2 + HCO^*$	(6)	}	}	
$HO_2^* + CH_4 \longrightarrow CH_3^* + H_2O_2$	(7)			Induced oxidation of methane
$OH^* + CH_2O \longrightarrow HCO^* + H_2O$	(8)			Induced oxidation of formaldehyde
$OH^* + \text{wall} \longrightarrow \text{end}$	(9)			Termination

This oxidation scheme is discussed in the following sections.

4.2.2.1 The Dual Nature of the Poisoning Process

Hoare and Walsh (158,159) have examined the effect of surfaces on the rate of methane oxidation at 500°C, and they have considered specifically the inhibition effect of lead oxide. They suggested that the reactions of HO_2^* and H_2O_2 at the surface are important. The inhibiting effect of lead monoxide on the oxidation of both methane (158) and ethers (160) led Walsh and co-workers to propose a detailed mechanism for the anti-knock action of tetraethyl lead (TEL) (160,161). According to this theory, the anti-knock action is a consequence of the destruction of free radicals such as HO_2^* and H_2O_2 when these molecules impinge on the surfaces of lead oxide particles formed from lead alkyl. When TEL is heated in the presence of oxygen to a temperature greater than $\sim 180°C$, it forms lead monoxide (160) which

is first produced as a colloidal fog of solid particles, and is then deposited as a lead monoxide film. The actual inhibiting effect is exerted by the lead monoxide surface rather than by gas phase molecules of lead monoxide (160,162).

In the presence of a catalyst, the mechanism of methane oxidation is somewhat similar, and has been outlined by Firth (42). The oxidation of methane to carbon dioxide and water vapour occurs through a series of reaction steps involving partially oxidised intermediates adsorbed on the catalysts. It is, therefore, probable that tetramethyl lead (TML) acts as an inhibitor in the present system by virtue of its formation of lead monoxide through a similar mechanism to that proposed by Walsh et al (159,160), and that the inhibition persists because of the deposition of involatile oxide on the surface of the catalyst. The gradual accumulation of lead monoxide on the surface gives rise to an even spread which eventually coats the pore mouths and cracks. It must be true therefore that deactivation of the beads involves two processes:-

(i) The availability of active sites (i.e. Pd, Pt atoms or crystallites) for the competitive adsorption of methane and oxygen molecules are reduced due to lead oxide deposition.

(ii) The lead monoxide itself not only blocks off catalytic sites, but also provides a surface for the active destruction of HO_2^* radicals by reaction with H_2O_2 molecules to form water and oxygen (158,159):

$$2HO_2^* + H_2O_2 \longrightarrow 2H_2O + 2O_2$$

(The postulates above assume, of course, that TML is readily oxidised to lead monoxide under the conditions used, which is realistic because the bead surface is maintained at $\sim 600°C$ to promote the oxidation of methane).

These two processes operating together readily poison the catalyst, and therefore only a very small quantity of TML present in the feed stream is enough to deactivate the detector bead.

In the case of combustion engines, 1,2-dichloroethane and 1,2-dibromoethane are also added to the leaded gasoline in order to scavenge the lead oxide out of the combustion chamber (after it has accomplished its purpose of suppressing "knock") as lead chloride and lead bromide. Consequently the lead that is present in the atmosphere, is most probably to be found in halogenated forms. However, these components are readily oxidised to lead monoxide again on the surface of the bead and thus the deactivation process which is brought about by halogenated airborne lead probably also follows the two schemes outlined above.

4.2.2.2 The Mechanism of Poison Resistance Using Mordenite

Results show that zeolite-coated beads substantially improve poison resistance. This is probably partly due to the fact that the zeolite coating has a large "surface area" ($\sim 500\ m^2\ g^{-1}$). Thus surrounding the catalyst bead with such a zeolite/clay coating in effect restricts the deposition of lead monoxide on the active catalyst centres by trapping it in the zeolite micropores whilst still allowing the methane and oxygen molecules to diffuse through to the active sites. However, this is only part of the explanation. Dealuminated hydrogen mordenite (DHM) is known to chemisorb molecules by reaction with hydroxyl "nests" within the structure (163). It is highly likely that the especially high effectiveness of this zeolite in improving poison resistance is partly due to such reactions as

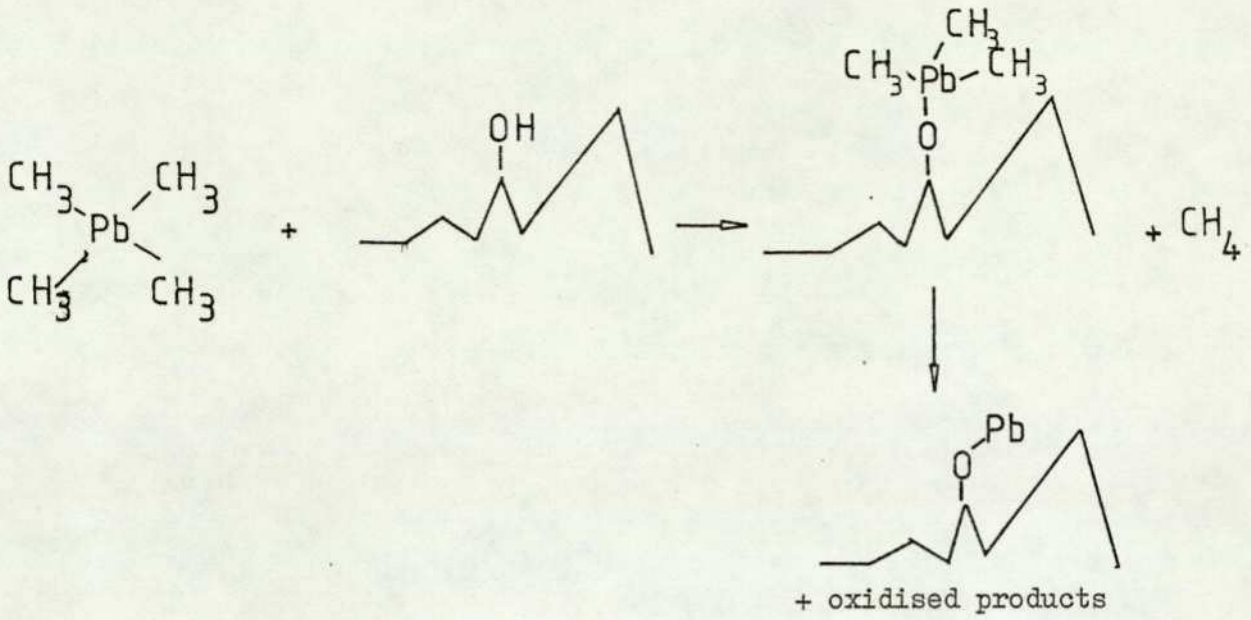

Thus the tetramethyl lead molecules are chemisorbed within the zeolite crystallites, and then further reactions take place to finally give non-labile compounds of lead. Small molecules such as methane, which would not be chemisorbed, and whose diffusivities are higher (153), pass through the molecular sieve crystallites without reaction and thus reach the catalyst surface.

4.3 Comparison Between Effectiveness of Alumina, Kaolin, and Zeolite Coatings

Beads coated with alumina did prove to be slightly more resistant to poisoning than the original pellistors, but these had their initial sensitivity to 1% methane (as evidenced by the mV readings) reduced to only about half that of the corresponding uncoated beads. This reduction in initial sensitivity was probably due to a transfer of diffusion control from the boundary layer of gas (section 4.2.1.1) to the porous alumina surrounding of the bead. The final coat of alumina was deposited by an impregnation method of "dip and heat" cycles. Thus

this alumina coat effectively obstructed access of both poison and reactant to the active sites simultaneously. Another series of beads were coated with a final homogeneous mixture of alumina and a small quantity of the catalyst, again by an impregnation method, but in this case the outer layer was alumina plus catalyst, and not just inert alumina.

In general, results indicate that both types of mordenite used (i.e. hydrogen mordenite prepared from ammonium mordenite, and dealuminated hydrogen mordenite (DHM) prepared by acid treatment of sodium mordenite) were very effective at improving poison resistance, and of these two forms, samples coated with DHM showed the best resistance to poisoning, in addition to the least zero drift. Among the different ratios of DHM: kaolin tested, the 6:4 ratio was the most effective. Comparing Figures 43, 44 & 38, 39, it is evident that the poison resistance originated from the zeolite rather than the kaolin clay binder. Accurate and rigorous comparisons of the results for different ratios are difficult as the amount of zeolite/binder mixture deposited on the bead was not easily reproducible. However the observed optimum ratio of 6:4 DHM: kaolin is a value which seems consistent with the need to maximise the zeolite content (and hence poison resistance) whilst also seeking to maximise the binder content (and hence obtain a catalyst bead with good mechanical properties).

The extent of coverage of the bead by the zeolite/kaolin mixture also affects the degree of poison resistance. The thicker the coating of zeolite/kaolin, the lower is the initial response and the greater is the poison resistance. Therefore, again, another compromise, this time one involving the coating thickness, is needed to give a pellistor with a maximal poison resistance. Sodium mordenite was

not as effective at improving poison resistance as the two hydrogen forms.

4.4 Comparisons with Other Work

Firth et al (51,52,64) carried out some early investigations involving zeolites in an attempt to produce poison resistant catalysts. They maintained that by enclosing the ions that are responsible for catalytic activity within the micropores of a zeolite, it should be possible to prevent access of large poison molecules to the catalytic ions while smaller reactant molecules still had easy access. However in this project, the sorptive rather than the molecular sieve properties of a zeolite are being used, by incorporating into the conventional support catalyst zeolite crystallites as selective sorbents. The reason behind using zeolites as a means to improving the poison resistance of gas detectors has already been discussed in section 1.7.

4.5 Suggestions for Further Work

The experimental difficulties associated in working with the very small bead sizes that were encountered in this work could be overcome by using the microcatalytic reactor as detailed by J.G. Bucknell (104), although modifications of his set-up would be necessary. Here the sample needs to be in a powdered form and packed into a bed. Furthermore, if the chromatographic technique (104,142) for measuring surface areas was adopted instead of the gravimetric method used here, the microreactor containing the catalyst bed could then be conveniently transferred from one instrument (for monitoring catalyst activity)

to another (for measuring surface area) without the catalyst bed itself being disturbed, or impurities being inadvertently introduced.

A further approach toward elucidating the mode of poisoning could be a kinetic study coupled with active surface area measurements using carbon monoxide as adsorbate (164). Such an analysis would give a quantitative relationship between the observed rate (i.e. the activity left) and the number of active sites remaining for different levels of poisoning. Since

$$F = \frac{1}{1 + \alpha h} \quad \text{(see section 1.6.3)}$$

where F = fraction of activity left,

α = fraction poisoned, and

h = Thiele modulus $\left(=L\sqrt{\frac{2k}{rD}}\right)$,

the relationship of F and α should (hopefully) further confirm the mode of poisoning as being in conformity with the pore mouth model rather than the homogeneous one (see sections 1.6.3 & 4.2.1.2).

As a final suggestion for further work, poison resistance could be further increased by improving the method of preparation of the detector beads, and then for a given method of preparation, finding the combination of conditions that maximise the improvement in resistance. For instance, the development of other methods for coating the beads with the zeolite/clay mixture, such as spray drying, or a hot-pressing technique, both of which should give rise to a more reproducible bead, could then be followed by a more detailed program examining many different zeolite:binder ratios, thus optimising resistance of the beads to both decay and poisons.

4.6 Conclusions

In summary, the deactivation of the catalyst bead is brought about by the deposition of lead oxide on the outer surfaces which renders the active sites further in the catalysts partially inaccessible to reactant molecules through pore mouth poisoning, and also severely inhibits methane oxidation reaction on the outer surfaces. On coating the bead with a zeolite, especially dealuminated hydrogen mordenite (DHM), the poisoning action is markedly delayed. The initial loss of activity seen in mordenite coated beads occurs through the inhibitive action of lead oxide, which is 'trapped' within the zeolite lattice, and as a result of greater diffusion limitation, slowing the transport of methane molecules to the active sites. After prolonged operation in a poisoned atmosphere a large amount of lead oxide accumulates in the zeolite lattice, and deactivation then occurs by a three-fold process:-

(i) the inhibitive action of lead oxide on methane oxidation;

(ii) a serious obstruction of reactant and product to and from the active sites; and

(iii) lead finally penetrating through the zeolite layer and reaching the active sites within the bead.

Improved poison resistance in the form of an external zeolite layer arises from a combination of both physical and chemical transport and adsorption phenomena.

APPENDICES

APPENDIX I

Relationship between Out of Balance Voltage and Concentration of Fuel

The fundamental equation for the Wheatstone bridge is

$$\frac{R_1}{R_3} = \frac{R_2}{R_4} \qquad (1)$$

at balance conditions. Also the difference in potential between the arm AB due to $R_1 + \Delta R$ and the arm AD due to R_2 is equal to ΔV, the out balance voltage i.e. ... (see Figure 4)

$$I_1 (R_1 + \Delta R) - I_2 R_2 = \Delta V \qquad (2)$$

but the potential drop across arm ABC must be the same as that across ADC, whence

$$I_1 (R_1 + \Delta R + R_3) = I_2 (R_2 + R_4) \qquad (3)$$

Rearranging equation (3)

$$I_1 = \frac{I_2 (R_2 + R_4)}{R_1 + \Delta R + R_3} \qquad (4)$$

and substituting equation (4) into equation (2) gives

$$\frac{I_2 (R_2 + R_4) (R_1 + \Delta R)}{R_1 + \Delta R + R_3} - I_2 R_2 = \Delta V \qquad (5)$$

Simplifying equation (5) further gives

$$I_2 (R_1 R_4 - R_2 R_3 + R_4 \Delta R) = (R_1 + R_3) \Delta V + \Delta R \Delta V \qquad (6)$$

But $R_1 R_4 = R_2 R_3$ from equation (1). Thus

$$I_2 R_4 \Delta R = (R_1 + R_3) \Delta V + \Delta R \Delta V \qquad (7)$$

and assuming $\Delta R \Delta V \rightarrow 0$

$$I_2 R_4 \Delta R = (R_1 + R_3) \Delta V \qquad (8)$$

or $$\frac{\Delta R}{\Delta V} = \frac{(R_1 + R_3)}{I_2 R_4} \qquad (9)$$

ΔV can be replaced by V since ΔV is the difference between the voltage at balance conditions (V = 0) and V; therefore equation (9) becomes

$$\frac{\Delta R}{V} = \frac{(R_1 + R_3)}{I_2 R_4} \qquad (10)$$

Now ΔR is brought about by a small rise in temperature ΔT in resistance R_1; ΔR as a function of temperature can be expressed by

$$R_1 = R_o (1 + DT + BT^2) \qquad (11)$$

where R_o is the resistance of the catalytic calorimeter at 0°C, T is the temperature of the catalyst (°C), D and B are constants in the platinum resistance thermometer equation and R_T is the resistance at T°C. Differentiating equation (11) with respect to T gives

$$\frac{dR}{dT} = R_o (D + 2BT) \qquad (12)$$

or, for a small finite change ΔR for ΔT

$$\Delta T = \frac{\Delta R}{R_o (D + 2BT)} \qquad (13)$$

Substituting ΔR from equation (10) into equation (13) gives

$$\Delta T = \frac{V (R_1 + R_3)}{I_2 R_4 R_o (D + 2BT)} \qquad (14)$$

Equation (14) describes the relationship between the voltage V produced across the bridge due to a temperature rise (ΔT). If the temperature rise ΔT is produced by a small increase $\Delta(\frac{dH}{dt})$ in the rate of supply of heat, then

$$\Delta\left(\frac{dH}{dt}\right) = \frac{\partial}{\partial T}\left(\frac{dH}{dt}\right)\Delta T = \frac{V (R_1 + R_3)}{I_2 R_4 R_o (D + 2BT)} \cdot \frac{d^2 H}{dT.dt} \qquad (15)$$

where $(\frac{dH}{dt})$ is the rate of supply of heat to the catalyst at T°C. If the increase $\Delta(\frac{dH}{dt})$ is brought about by oxidation of the fuel and the catalyst, then the rate of oxidation of the fuel $\frac{d(\text{Fuel})}{dt}$ is given by

$$\frac{d\,(\text{Fuel})}{dt} = \frac{V\,(R_1 + R_3)}{I_2 R_4 R_o\,(D + 2BT)\;\alpha\,\Delta H} \cdot \frac{d^2H}{dT\;dt} \qquad (16)$$

where ΔH is the enthalpy of oxidation of the fuel and α is the fraction of the heat of oxidation given to the catalytic element.

Equation (16) can be rewritten with V as the subject of the expression:-

$$V = \frac{I_2 R_4 R_o (D + 2BT)\;\alpha\,\Delta HA}{(R_1 + R_3)\;(d^2H/dTdt)}\,\gamma_F \qquad (17)$$

where γ_F is the rate of reaction of the fuel on unit area of catalyst, and A is the area of that catalyst.

When the reaction rate on the surface is fast compared with the rate of diffusion of the fuel to the catalyst surface, and oxygen is in excess, ensuring complete oxidation of the fuel, then the rate of reaction γ_F is controlled by the rate of diffusion of the fuel to the catalyst surface. In a binary gas mixture, the rate of diffusion of gas 1 into gas 2 is given by the molal flux N_1,

$$N_1 = D_{12}\,\frac{d(G)}{dx} \qquad (18)$$

D_{12} is the inter-diffusion coefficient of gas 1 into gas 2 and $\frac{d(G)}{dx}$ is the concentration gradient with respect to gas 1. For the system under consideration, this latter function becomes just the concentration gradient of the fuel F across a depletion layer surrounding the transducer.

Thus the out of balance bridge voltage V, is obtained by combining

equations (17) and (18) to give

$$V = \frac{I_2 R_4 R_o (D + 2BT) \propto \Delta H\, A}{(R_1 + R_3)\,(d^2H/dT.dt)}\, D_{12}\, \frac{d(F)}{dx} \qquad (19)$$

where $\frac{d(F)}{dx}$ is the concentration gradient of the fuel across the depletion layer surrounding the element. When the catalytic element is maintained at a constant temperature and the total pressure remaining constant then a number of parameters in equation (19) remain substantially constant irrespective of the nature of the fuel. Thus under these conditions, I_2 is fixed, $(\frac{d^2H}{dT.dt})$ is almost constant for the dilute fuel-air mixtures encountered up to the lower-explosion limit, $\propto$ is constant and the resistances are of fixed values. The surface area of the catalyst is fixed. In addition, $\frac{d(F)}{dx}$ will be proportional to (F) since the thickness of the depletion layer is then constant. Then under these conditions equation (19) reduces to

$$V = K\, \Delta H\, D_{12}(F) \qquad (20)$$

where K is a constant.

Equation (20) thus predicts that for a given fuel, the out of balance voltage is proportional to the concentration of the fuel, and for different fuels V is proportional to the function $\Delta H\, D_{12}(F)$.

In this appendix reference has been made to the following two papers - references (42) (67) :-

(1) ref. 42 : Firth, J.G., Trans. Faraday Soc., 62, 2566, (1966).

(2) ref. 67 : Firth, J.G., Jones, A. and Jones, T.A., Combustion Flame; June 1973, 20, 303.

APPENDIX II

Reaction Rates in Porous Catalyst: Derivation of Equations for a Spherical Catalyst Pellet

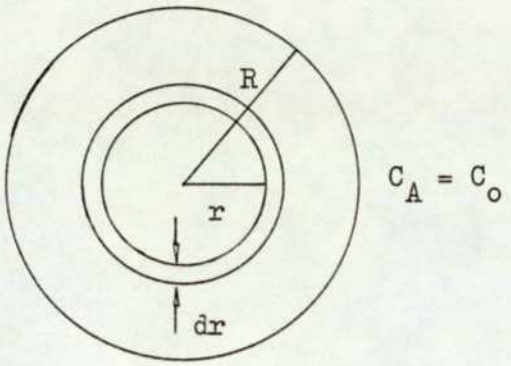

Diffusion of reactant across the differential spherical annular shell of radius r is given by Fick's first Law as

$$V_A = -4\pi r^2 D_e \frac{dC_A}{dr} \qquad (1)$$

where D_e is an effective diffusivity. The fundamental equation for reaction within a spherical shell of radius r and thickness dr must be equal to the difference between the flux entering the shell at (r + dr) and that leaving at r, viz:-

$$-dV_A = 4\pi r^2 dr\, S\, k\, C_A^n \qquad (2)$$

where S is a surface area per unit volume. dV_A is also obtained by differentiating equation (1) with respect to r as a product.

$$\frac{dV_A}{dr} = -\left[8\pi r D_e \frac{dC_A}{dr} + 4\pi r^2 D_e \frac{d^2 C_A}{dr^2}\right]$$

$$- dV_A = \left[8 \pi r D_e \frac{dC_A}{dr} + 4 \pi r^2 D_e \frac{d^2C_A}{dr^2} \right] dr \qquad (3)$$

Assuming a first order reaction (n = 1) in equation (2), and equating equations (3) and (2) gives

$$dr \left[8 \pi r D_e \frac{dC_A}{dr} + 4 \pi r^2 D_e \frac{d^2C_A}{dr^2} \right] = 4 \pi r^2 S k C_A \, dr$$

$$\text{or} \qquad \frac{2}{r} \frac{dC_A}{dr} + \frac{d^2C_A}{dr^2} = \frac{S k C_A}{D_e} \qquad (4)$$

If $h = R\sqrt{\frac{S k}{D_e}}$ where h represents a Thiele modulus, then

$$\frac{h^2}{R^2} = \frac{S k}{D_e} \qquad (5)$$

Substituting equation (5) in equation (4) and rearranging gives

$$\left[\frac{d^2C_A}{dr^2} + \frac{2}{r} \frac{dC_A}{dr} \right] = \frac{h^2}{R^2} C_A = b^2 C_A \qquad (6)$$

To simplify let $C_A = \frac{v}{r}$ (7)

where v may also be some function of r.

Differentiating equation (7) with respect to r gives

$$\frac{dC_A}{dr} = - \frac{v}{r^2} + \left[\frac{1}{r} \frac{dv}{dr} \right] \qquad (8)$$

Differentiating equation (8) again yields the second differential:-

$$\frac{d^2C_A}{dr^2} = \left[\frac{2v}{r^3} - \frac{1}{r^2} \frac{dv}{dr} + \frac{1}{r} \frac{d^2v}{dr^2} - \frac{1}{r^2} \frac{dv}{dr} \right] \qquad (9)$$

$$\text{or} \qquad \frac{d^2C_A}{dr^2} = \frac{2v}{r^3} - \frac{2}{r^2}\frac{dv}{dr} + \frac{1}{r}\frac{d^2v}{dr^2} \tag{10}$$

Multiplying equation (8) by $\frac{2}{r}$ to give $\frac{2}{r}\frac{dC_A}{dr}$ which forms part of equation (6) gives

$$\frac{2}{r}\frac{dC_A}{dr} = -\frac{2v}{r^3} + \frac{2}{r^2}\frac{dv}{dr} \tag{11}$$

Finally, summing equations (10) and (11) results in an alternate form of equation (8):-

$$\frac{d^2C_A}{dr^2} + \frac{2}{r}\frac{dC_A}{dr} = \frac{1}{r}\frac{d^2v}{dr^2} = b^2 C_A \tag{12}$$

Equation (12) may be written as

$$\frac{d^2v}{dr^2} = r\,b^2\,C_A \tag{13}$$

and since from equation (7), $C_A = \frac{v}{r}$,

$$\frac{d^2v}{dr^2} = r\,b^2\frac{v}{r} = b^2 v \tag{14}$$

$$\text{or} \qquad \frac{d^2v}{dr^2} - b^2 v = 0 \tag{15}$$

Thus equation (6), is transformed into a form of the auxiliary equation

$$m^2 - b^2 = 0 \qquad \text{where } m = \pm b$$

The solution to equation (15) is

$$v = C_1 e^{br} + C_2 e^{-br} \tag{16}$$

where C_1 and C_2 are constants of integration.

Substituting for $v = C_A r$ from equation (7) gives

$$C_A r = C_1 e^{br} + C_2 e^{-br} \tag{17}$$

Rearranging equation (17),

$$C_A = \frac{C_1}{r} e^{br} + \frac{C_2}{r} e^{-br} \tag{18}$$

then differentiating equation (18) as a product with respect to r results in

$$\frac{dC_A}{dr} = C_1\left[\frac{be^{br}}{r} - \frac{1}{r^2} e^{br}\right] + C_2\left[\frac{-be^{br}}{r} - \frac{1}{r^2} e^{-br}\right] \tag{19}$$

Multiplying equation (19) throughout by r^2

$$r^2 \frac{dC_A}{dr} = C_1\left[be^{br} r - e^{br}\right] + C_2\left[e^{-br}(-b)r - e^{-br}\right] \tag{20}$$

Solving equation (20) first of all with the boundary condition $\frac{dC_A}{dr} = 0$ at $r = o$ yields

$$o = -C_1 - C_2 \tag{21}$$

that is

$$C_1 = -C_2 \tag{22}$$

Then, expressing equation (18) in terms of C_A and C_1 only,

$$C_A = \frac{C_1}{r}\left[e^{br} - e^{-br}\right] \tag{23}$$

which is equivalent to

$$C_A = \frac{2C_1}{r}\left[\frac{e^{br} - e^{-br}}{2}\right] \tag{24}$$

But $\left[\frac{e^{br} - e^{-br}}{2}\right] = \sinh br$

thus equation (24) becomes

$$C_A = \frac{2C_1}{r} \sinh br \tag{25}$$

If the second boundary condition that $C_A = C_o$ at $r = R$ is now introduced, equation (25) yields

$$C_o = \frac{2C_1}{R} \sinh bR \tag{26}$$

Dividing equations (25) by (26) gives

$$\frac{C_A}{C_o} = \frac{R \sinh br}{r \sinh bR} \tag{27}$$

and since $b = h/R$ (equation 6),

$$\frac{C_A}{C_o} = \frac{R \sinh (hr/R)}{r \sinh h} \tag{28}$$

Rearranging equation (28) then yields

$$C_A = \frac{C_o R}{\sinh h}\left[\frac{1}{r} \sinh (hr/R)\right] \tag{29}$$

Next, differentiating (29) with respect to r as a product function yields

$$\frac{dC_A}{dr} = \frac{C_o R}{\sinh h}\left[\frac{h}{rR} \cosh (hr/R) - \frac{1}{r^2} \sinh (hr/R)\right] \tag{30}$$

or $$\frac{dC_A}{dr} = \frac{C_o R/r \; h/R \cosh (hr/R) - C_o R/r^2 \sinh (hr/R)}{\sinh h} \tag{31}$$

Taking $\frac{R}{r}$ common factor and transferring to the denominator gives

$$\frac{dC_A}{dr} = \frac{C_o\ h/R \cosh (hr/R) - C_o\ 1/r \sinh (hr/R)}{r/R \sinh h} \qquad (32)$$

$\frac{dC_A}{dr}$ at r = R describes the concentration gradient at the outer surface of the pellet, so that equation (32) becomes under these conditions

$$\left[\frac{dC_A}{dr}\right]_{r = R} = \frac{C_o\ h/R \cosh (hR/R) - C_o\ 1/R \sinh (hR/R)}{R/R \sinh h} \qquad (33)$$

Rearranging

$$\left[\frac{dC_A}{dr}\right]_{r = R} = \frac{C_o\ h/R \cosh h - C_o\ 1/R \sinh h}{\sinh h} \qquad (34)$$

Taking the common factor $\frac{C_o}{R}$ outside yields

$$\left[\frac{dC_A}{dr}\right]_{r = R} = \frac{C_o}{R}\left[\frac{h \cosh h - \sinh h}{\sinh h}\right] \qquad (35)$$

Equation (35) can be further simplified to

$$\left[\frac{dC_A}{dr}\right]_{r = R} = \frac{C_o}{R}\left[\frac{h}{\tanh h} - 1\right] \qquad (36)$$

$$\left[\frac{dC_A}{dr}\right]_{r = R} = \frac{C_o h}{R}\left[\frac{1}{\tanh h} - \frac{1}{h}\right] \qquad (37)$$

It is now desired to obtain the total reaction rate throughout the single catalyst pellet, corresponding to the concentration gradient of equation (37). The overall rate of reaction equals the rate of mass transfer into the pellet.

$$\text{Rate of mass transfer into the pellet} = 4\pi R^2 D_e \left[\frac{dC_A}{dr}\right] \qquad (38)$$

Substituting $\left[\frac{dC_A}{dr}\right]$ from equation (37) into (38) yields

$$\text{Rate} = 4\pi R^2 D_e \frac{C_o h}{R}\left[\frac{1}{\tanh h} - \frac{1}{h}\right] \qquad (39)$$

Equation (39) describes the rate of reaction throughout one spherical porous pellet. However, if the internal surface of the porous pellet were all exposed to reactant of concentration C_o, the rate would just be

$$\text{Rate} = \frac{4}{3}\pi R^3 k S C_o \qquad (40)$$

The effectiveness factor f (or fraction of surface available as it is sometimes called), is obtained by dividing equation (40) into (39) to yield

$$f = \frac{3 D_e h}{R^2 k S}\left[\frac{1}{\tanh h} - \frac{1}{h}\right] \qquad (41)$$

Substituting $\frac{D_e}{k S} = \frac{R^2}{h^2}$ from equation (5) into equation (41)

$$f = \frac{3}{h}\left[\frac{1}{\tanh h} - \frac{1}{h}\right] \qquad (42)$$

The fraction of surface available f is defined by equation (42) for a first order irreversible reaction in a sphere.

APPENDIX III

Theoretical Calculation for the Concentration of Lead in the Gas Stream

In this appendix, the procedure for estimating by theoretical calculation the concentrations of lead in a gas stream resulting from bubbling air through TML/n-heptane solutions is described.

Tests were originally carried out with TML in n-heptane in the presence of 'scavengers', and Associated Octel supplied the following specified solution: concentration of TML = 0.79 $cm^3\ dm^{-3}$. In later work, scavenger-free TML in n-heptane was used. The solutions supplied had to be further diluted with n-heptane to give the desired concentration of lead in the final gas stream. An example of the calculation of the dilution factor for a solution of 0.79 $cm^3\ dm^{-3}$ TML with scavengers in n-heptane is given below; similar calculations for other scavenger-free solutions were carried out.

DATA

Specification of TML (with scavengers) as Supplied by Associated Octel Co. Ltd.

Component	% w/w	Specific gravity	Volume/cm^3
TML	50.87	1.995	25.4736
Dibromoethane	17.86	2.179	8.1956
1, 2-dichloroethane	18.81	1.235	15.2295
Toluene	12.45	0.861	14.4599
Dye	0.06	-	-

$$\% \text{ v/v TML in TML with scavengers} = \frac{\text{Volume TML} \times 100}{\Sigma \text{ Volume}} = 40.205$$

Molecular weight of TML = 267.33 g mol^{-1} (i.e. TML is 77.5% lead)

Molecular weight of n-heptane = 100.2 g mol^{-1}

Specific gravity n-heptane = 0.687

Calculations

Let vapour pressure of TML at room temperature be ϕ mm Hg.

Let atmospheric pressure at room temperature be p mm Hg.

Let volume of TML with scavengers be V_T cm^3.

Let volume of n-heptane be V_L cm^3.

The volume of TML in V_T cm^3 of TML with scavengers is $(\frac{V_T \times 40.2}{100})$, and

$$\text{amount of TML present} = \left[\frac{40.2 \times 1.995}{100 \times 267.33}\right] V_T \text{ mol} = 3 \times 10^{-3} V_T \text{ mol} \quad (1)$$

Similarly, the moles of n-heptane in V_L cm^3 of heptane liquid is

$$\left[\frac{0.687}{100.2}\right] V_L = 6.856 \times 10^{-3} V_L \text{ mol} \quad (2)$$

From (1) and (2), the mole fraction of TML is

$$X_{TML} = \frac{3V_T}{3V_T + 6.856 V_L} \quad (3)$$

Assuming the TML in n-heptane liquid mixture behaves ideally, Raoult's Law is obeyed, i.e.

$$\text{Partial pressure of TML} = \phi X_{TML} \quad (4)$$

and the volume of TML (in m^3) per m^3 of gas at equilibrium will be

$$\frac{\phi X_{TML}}{p} \quad (5)$$

Changing units to a concentration of TML, expressed in terms of mg m^{-3} of gas,

$$\text{Concentration of TML in mg m}^{-3} = \frac{1000\ (\emptyset/p)\ X_{TML} \times 267.33 \times 10^6}{22400}$$

$$= 1.1934 \times 10^7\ (\emptyset/p)\ X_{TML}\ \text{mg m}^{-3} \qquad (6)$$

But the TML is only 77.5% lead by weight, thence the concentration of lead per cubic metre of gas $= 1.1934 \times 10^7 \times 0.775\ (\emptyset/p)\ X_{TML}$

Therefore mg of lead $m^{-3} = 9.249 \times 10^6\ (\emptyset/p)\ X_{TML}$ (7)

With equation (7), a solution dilution factor for the solution supplied by Associated Octel Co. Ltd. may be calculated. Since the leaded gas stream was diluted with 4 parts air to 1 part leaded gas stream, if the final lead concentration required is x, then the original supplied solution must be diluted such that a vapour concentration of 5x is in equilibrium with the liquid. For example, if 20 mg m^{-3} of lead is required in the final gas stream, then equation (7) must be equated to 100, as follows:

$$100 = 9.249 \times 10^6 (\emptyset/p)\ X_{TML}$$

Substituting for $\emptyset$, p, and X_{TML}

$$100 = 9.249 \times 10^6 (33.5/760) \left[\frac{3V_T}{3V_T + 6856.3} \right]$$

(assuming $V_L = 1000$)

So that $V_T = 0.5607\ cm^3$ (8)

Now the solution sent by Associated Octel Co. Ltd. contained 0.79 cm^3 TML with scavengers per cubic decimetre of n-heptane. For this volume of n-heptane, the above calculation showed that 0.56 cm^3 of TML were required. The supplied solution was therefore diluted from one cubic decimetre to 1.410 dm^3 with n-heptane to ensure the correct concentration of lead in the gas stream. Two assumptions are implicit in the above calculation. These are:-

(i) that the atmospheric pressure is 760 mm Hg, and

(ii) that the activities of n-heptane and TML approximate to their concentrations.

Assumption (i) can be allowed for easily, by applying a correction factor of $760/p$ to equation (8) where p is the actual atmospheric pressure on the day of experiment. Assumption (ii) is difficult to allow for, since the activity coefficients of TML are unknown.

The air/lead concentrations were checked by direct analysis of the gas stream using 0.2 mol dm^{-3} ICl solution to trap the lead, and atomic absorption spectrophotometry was used as the means of quantitatively determining the lead.

In the case of scavenger free TML/toluene, the composition of the solution was as follows:

Components	% w/w	Specific gravity	Volume/cm^3
TML	80	1.995	40.100
Toluene	20	0.861	23.228

and the % v/v TML $= \dfrac{\text{Volume TML} \times 100}{\sum \text{Volume}} = 63.3204$

Amount of TML $= 4.7254 \times 10^{-3}\ V_T$ mol

Amount of Heptane $= 6.856 \times 10^{-3}\ V_L$ mol

Mole fraction TML (X_{TML}) $= \dfrac{4.7254\ V_T}{4.7254\ V_T + 6.856\ V_L}$

Assuming ideal behaviour of TML in n-heptane, Raoult's Law is obeyed, so that partial pressure of TML = ϕX_{TML}

Therefore concentration of TML $= 1.1934 \times 10^7 (\frac{\phi}{p})\ X_{TML}$ mg m^{-3} and TML is 77.5% lead.

Therefore concentration of lead in the air/gas mixture =

$$1.1934 \times 10^7 \times 0.775 \times (\frac{\phi}{p})\ X_{TML} \text{ mg } m^{-3} \qquad (9)$$

Using a dilution ratio of 4:1 of air to leaded gas stream, and assuming the amount of lead required in the final gas stream is 20 mg m^{-3} then (9) must be equated to 100, as follows:

$$100 = 1.1934 \times 10^{7} \times 0.775 \left(\frac{\phi}{p}\right) X_{TML}$$

(Assuming $V_L = 1000\ cm^3$), so that

$$V_T = 0.356\ cm^3 \text{ at } 760mm.\ Hg \text{ pressure,}$$

correcting for atmospheric pressure of the day when the solution was prepared yields

$$V_T = 0.356 \times \frac{760}{747} = 0.36\ cm^3$$

The solution supplied by Associated Octel in this particular case contained a concentration of TML in heptane of 1.58 $cm^3\ dm^{-3}$.
To bring the concentration to 0.36 $cm^3\ dm^{-3}$, it was therefore necessary that the overall solution be diluted from 1 dm^3 to 4.39 dm^3 with n-heptane.

Appendix IV - Elemental Identification by Energy Dispersive Analysis of X-rays (EDAX) (p. 262) removed for copyright reasons

APPENDIX V

Determination of Nickel as an Impurity in the Unpoisoned Beads Using Polarographic Technique

Preparation of Stock Solutions

(1) "AnalaR" grade nickel chloride hexahydrate was dried in an oven at 80°C for 24 hours to give the anhydrous yellow form, molecular weight 129.616. 2.2077 g of anhydrous nickel chloride were dissolved in 1 dm^3 of deionized distilled water, giving solution A, containing 1 g dm^{-3} nickel.

(ii) 0.1 mol dm^{-3} potassium chloride solution was used as the background medium. 14.910 g of "AnalaR" grade potassium chloride were dissolved in 2 dm^3 of deionized water, (solution B).

(iii) 5 cm^3 of solution A were diluted to 250 cm^3 using the 0.1 mol dm^{-3} potassium chloride solution, to give solution C (containing 20 ppm nickel (20 $\mu g\ cm^{-3}$)).

(iv) 5 cm^3 of solution C were diluted to 250 cm^3, again using 0.1 mol dm^{-3} potassium chloride solution, to give solution D (containing 0.4 ppm nickel (400 ng cm^{-3} or 400 ppb)).

(v) Preparation of the sample solution: Twelve compensator beads with the end platinum wires cut off were weighed in a platinum crucible. The beads were then dissolved as follows. Two drops of concentrated sulphuric acid were added, followed by 10 cm^3 of hydrochloric acid. This mixture was evaporated very slowly on a hot plate. After six hours of slow evaporation, only 3 cm^3 of the resultant solution were left, and this was diluted with 15 cm^3 of 0.5 mol dm^{-3} HCl. The whole solution was again evaporated down very slowly with occasional additions of 0.1 mol dm^{-3}

potassium chloride solution B. After ~18 hours of slow evaporation, the solution left was diluted to 50 cm^3 with solution B.

Polarographic Analysis

The polarogram of 50 cm^3 of the original solution was recorded. The settings of the instrument were as follows:

Mode of Operation	:	Differential Pulse
Initial Potential	:	-0.9 V
Potential Range	:	1.5 V
Scan Rate	:	2 mV s^{-1}
Modulation Amplitude	:	50
Current Range	:	0.5 mA
Filter	:	0.3 mV s^{-1}
External Cell Switch	:	ON Position
Droptime	:	2 s
Sensitivity on X-axis	:	(40 x 1.5) mV cm^{-1}
Sensitivity on Y-axis	:	(40 x 4) mV cm^{-1}

The above settings were kept constant throughout the investigation. The height of the mercury reservoir was also kept fixed, to avoid changes in drop size with time.

The "doping technique" was used to calculate the amount of nickel in the original solution. For this, the original solution was doped with 1 cm^3 of nickel chloride (solution A). containing 1 g dm^{-3}; a marked increase in peak height was observed. From literature values (Rubber Handbook), the half-wave potential of nickel in 0.1 mol dm^{-3} potassium chloride occurs at -1.1 V. The polarograph of the original solution and the doped solution showed the half-wave potential of nickel to be at

-1.05 and -1.15 V respectively, which were in good agreement with the literature value. This was futher confirmed by recording the polarogram of the standard solution C containing 20 ppm (20 $\mu g\ cm^{-3}$) nickel, where the half-wave potential was -1.12 V. The peak of the original solution was a double one, due to the high concentration of aluminium, which has a half-wave potential of around -1.3 V. Since this effect was not observed in either the polarogram of solution C or the doped solution, it could only have been due to the aluminium present. This was further confirmed by other experiments.

The potassium chloride solution used was "AnalaR", and contained nickel as an impurity, listed under heavy metals. Ideally, the potassium chloride should have been recrystallised to remove the nickel, but instead a polarograph of 0.1 mol dm^{-3} potassium chloride blank solution was run using the same sensitivity settings, and no nickel was picked up. However, increasing the sensitivity on the Y-axis to (0.4 x 8) mV cm^{-1} gave a peak due to nickel. At this sensitivity the amount of nickel present was in the region of parts per billion (10^9).

Throughout this work, triply distilled mercury was used, and deionized water for making up solutions. All glassware was thoroughly cleaned with chromic acid. It was important that the system was thoroughly cleaned and that all variables were kept as constant as possible (i.e. drop-size, droptime, cell conditions, and electrical connections). All solutions had to be shaken vigorously before running the polarograph, also nitrogen gas was bubbled through each solution for about 3-4 minutes before recording the polarogram, to remove dissolved oxygen.

Results and Calculations

Two polarograms were recorded:-

(i) The original solution was doped with 20 μl (μdm^{-3}) of solution A,

and with sensitivity on Y-axis set to (40 x 1.0) mV cm^{-1} .

(ii) The original solution was doped with 1 cm^3 of solution A, and with sensitivity on Y-axis set to (40 x 4) mV cm^{-1} .

The amount of nickel was calculated from the expression

$$C_u = \frac{i_1 v C_s}{i_2 v + (i_2 - i_1) V}$$

where V = original sample volume,

v = volume of standard solution added,

i_1 = peak height of sample solution,

i_2 = peak height of doped solution,

C_u = concentration of original solution,

C_s = concentration of standard solution added.

Results were : (i) 1.8% (w/w) nickel per bead.

(ii) 1.7% (w/w) nickel per bead.

These data are in conformity with the level of nickel expected from the EDAX measurements.

REFERENCES

References

1. Charles N. Satterfield, 'Mass Transfer in Heterogeneous Catalysis', MIT Press, Cambridge, 1970.

2. Eugene E. Petersen, 'Chemical Reaction Analysis', Prentice Hall Inc., 1965.

3. J. M. Thomas, and W. J. Thomas, 'Introduction to the Principles of Heterogeneous Catalysis', Academic Press Inc., N. Y., 1967.

4. I. Langmuir, J. Am. Chem. Soc., 38, 221, 1916.

5. D. O. Hayward, and B. M. W. Trapnell, 'Chemisorption', 2nd. ed., Butterworths and Co., London, 1964.

6. D. M. Young, and A. D. Crowell, 'Physical Adsorption of Gases', Butterworths and Co., London, 1962.

7. C. N. Hinshelwood, 'The Kinetics of Chemical Change', Clarendon Press, Oxford, Chapter 8, 1940; G. M. Schwab, 'Catalysis', Macmillan, London 1940; E. K. Rideal, J. Soc. Chem. Ind., London 62, 335, 1943; D. D. Eley, Advances in Catalysis, 1, 157, 1948; Quart. Rev., 3, 209, 1949.

8. J. M. Smith, Chemical Engineering Kinetics,Chapter 9, 2nd. ed., McGraw-Hill Book Comapny, 1970.

9. F. G. Ciapetta, C. J. Plank, 'Catalysis', ed. P. H. Emmett, Reinhold Pub. Corp., N. Y., vol 1, Chapter 7, 1954.

10. S. Berkman, J. C. Morrell, G. Egloff, 'Catalysis', Reinhold Pub. Corp., N. Y., 1940.

11. P. Sabatier, 'Catalysis in Organic Chemistry', trans. by E. E. Reid in 'Catalysis , Then and Now', Franklin Pub. Co., Englewood, N. J., 1965.

12. H. S. Taylor, Proc. Roy. Soc., A108, 105, London, 1925.

13. A. A. Balandin, 'Advances in Catalysis', Academic Press Inc., N. Y., X, 96, 1958.

14. O. Beeck, Disc. Faraday Soc., 8, 118, 1950.

15. A. A. Balandin, 'Advances in Catalysis', Academic Press Inc., N. Y., X, 96, 1958.

16. M. Boudart, J. Am. Chem. Soc., 72, 1040, 1950.

17. D. A. Dowden, Research, 1, 239, 1948.

18. D. A. Dowden, P. W. Reynolds, Disc Faraday Soc., 8, 187, 1950.

19. F. C. Tompkins, Proc. 6th Int. Conf. Catalysis, I, 32, 1976.

20. V. B. Kazansky, ibid, I, 50.

21. M. Prettre, C. Eichner, M. Perrin, Trans. Faraday Soc., 42, 335, 1946.

22. J. K. Dixon, J. E. Longfield, 'Catalysis' ed. P. H. Emmett, Reinhold Pub. Corp., N. Y., 7, 183, 1960.

23. J. Matui, B. Jasuda, J. Soc. Chem. Ind. Japan, 43, 117, 1940.

24. H. Davy, Phil. Trans. Roy. Soc., 1817.

25. G. Philips, J. Am. Chem. Soc., 16, 164 & 255, 1894.

26. S. A. Fokin, Zhur. Russ. Fiz-Khim obshchestra, 40, 273, 1908.

27. S. S. Medvedev, Trudy, Khim, Inst. im Karpora, 3, 54, 1924.

28. J. R. Campbell, J. Soc. Chem. Ind., 48, 93T, 1929.

29. L. H. Royerson, L. E. Swearigen, J. Am. Chem. Soc., 50, 2872, 1928; J. Phys. Chem., 32, 192, 1928.

30. W. P. Yant, C. O. Hawk, J. Am. Chem. Soc., 49, 1454, 1927.

31. W. A. Bone, R. V. Wheeler, J. Chem. Soc., 83, 1074, 1903.

32. N. Hempel, Ber., 12, 1006, 1879.

33. H. Richard, Z. anorg. Chem., 38, 76, 1904.

34. E. H. Boomer, V. Thomas, C. A. Johnson, Canad. J. Res., B.15, 360, 1937.

35. E. H. Boomer, S. N. Naldrett, Canad. J. Res., B.25, 494, 1947.

36. B. Yoschikawa, Bull. Inst. Phys. Chem. Res. Tokyo, 10, 251, 1931.

37. K. Neumann, H. Wang, Z. angew. Chem., 46, 57, 1933.

38. A. Janes, J. Soc. Chem. Ind., 70, 636A, 1923.

39. R. B. Anderson, K. C. Stein, J. J. Feenan, L. J. E. Hofer, Ind. Eng. Chem., 53, 809, 1961.

40. T. V. Andrusch kevich, V. V. Poporskii, G. K. Boreskov, Kinet & Katal, 6, 860, 1965.

41. C. F. Cullis, T. G. Nevell, D. L. Trimm, J. Chem. Soc., Faraday Trans., 1, 68, (Pt 8), 1406, 1972.

42. J. G. Firth, Trans. Faraday Soc., 62, 2566, 1966.

43. Alan Jones, J. G. Firth, T. A. Jones, Sci. Instrum. (J, Phys., E.), 8, 37, 1975.

44. R. Mezaki, C. C. Watson, Ind. Eng. Chem. (Proc. Res. dev.), 5, 62, 1966.

45. O. P. Ahuja, G. P. Mathur, Can. J. Chem. Eng., 45, 367, 1967.

46. T. G. Nevell, PHD Thesis, London University, 1968.

47. J. G. Firth, H. B. Holland, Trans. Faraday Soc., 65, 1121, 1969.

48. C. F. Cullis, D. E. Keene, D. L. Trimm, J. Catal., 19, 378, 1970.

49. C. F. Cullis, D. E. Keene, D. L. Trimm, Trans. Faraday Soc., 67, 864, 1971.

50. J. G. Firth, S. J. Gentry, A. Jones, J. Catal., 34, 159, 1974.

51. J. G. Firth, H. B. Holland, Trans. Faraday Soc., 65, 1891, 1969.

52. J. G. Firth, H. B. Holland, Nature, 217, 1252, 1968.

53. R. Rudham, M. K. Sanders, J. Catal.,27, 287, 1972.

54. G. M. Schwab, A. M. Watson, J. Catal., 4, 570, 1965.

55. C. H. Royerson, L. E. Swearingen, J. Phys. Chem., 33, 192, 1929.

56. R. D. Gift, 'Evaluation of Methanometry in Coal Mines', Atlantic Research Corporation, Report H0110927, July 1972, prepared for U.S. Bureau of Mines, Pittsburgh Mining Research Center, 4800 Forbes Avenue, Pittsburgh, Pa. 15213.

57. P. Buissiere, B. E. Domanski, M. Prettre, 'On the Evaporation of Platinum during Combustion of Methane', C. R. Acad. Sci., Paris 243, 1870, 1956.

58. J. P. Strange, U.S. Patent 2,805,134., 1955.

59. A. R. Baker, 'A Resistance Methanometer employing low-temperature Catalytic Element', Safety in Mines Res., Rep. No. 162, March 1959.

60. A. R. Baker, British Patent 892,530., 1958.

61. J. Seiger, British Patent 864,239., 1958.

62. Young Ho Kim, U.S. patent 3,586,486., 1971.

63. J. G. Firth, H. B. Holland, J. Appl. Chem. & Biotechnol., 21, 139, May 1971.

64. J. G. Firth, H. B. Holland, Nature, 212, 1036, Dec 1966.

65. C. F. Cullis, T. G. Nevell, D. L Trimm, Sci. Instrum. (J. Phys., E.), 6(4), 384, 1973.

66. A. R. Baker. J. G. Firth, Mining Engineer, 128, 237, Jan. 1969.

67. J. G. Firth, A. Jones, T. A. Jones, Combustion Flame, 20, 303, June 1973.

68. E. B. Maxted, Adv. Catalysis, 3, 129, 1951.

69. A. Voorhies jr., Ind. Eng. Chem., 37, 318, 1945.

70. E. B. Maxted, A. Marsden, J. Chem. Soc., 766, 1945.

71 C. G. Bond, Discussions Faraday Soc., 41, 200, 1966.

72. A. Wheeler, Advances in Catalysis, 3, 249, 1951.

73. E. W. Thiele, Ind. Eng. Chem., 31, 916, 1939.

74. J. B. Zeldowitsch, Acta Physicochim. USSR, 10, 583, 1939.

75. A. Wheeler, 'Catalysis', Vol 2, ed. P. H. Emmett, Reinhold Pub. Corp., N. Y., Vol. 2, 1956.

76. P. B. Weisz, Chem. Eng. Progr. Symp. Ser., 55 (25), 29, 1959.

77. P. B. Weisz, Z. Physik Chem., Neue Folge, 11, 1, 1957, in English.

78. P. B. Weisz and C. D. Prater, Advances in Catalysis, VI, 143, 1954.

79. E. Wicke, Chem.-Ing.-Tech., 29, 305, 1957.

80. E. Wicke and R. Kallenbach, Kolloid.z., 97, 135, 1941.

81. C. L. Midgley, T. A. Boyd, Ind. Eng. Chem., 14, 894, 1922.

82. P. P. Buck, P. R. Ryerson, Preprints, Division of Petroleum Chemistry, ACS meeting Detroit, p D-5, p D-21, April 1965.

83. P. R. Boyd, Lancet, 1, 181, 1957.

84. J. M. Gill, J. H. Huguet, E. A. Pearson, J. Water Pollution Control Federation, 32, 858, 1960.

85. N. Castellino, G. Colicchio, B. Grieco, P. Piccoli, A. Rossi, Arch. Mal. Prof., 25, 203, 1964.

86. D. Caujolle, M. C. Voisin, Ann. Pharm. Franc., 24, 17, 1966.

87. J. E. Cremer, Brit. J. Ind. Med., 16, 191, 1959.

88. J. E. Cremer, Occ. Health Rev., 17, 14, 1965.

89. R. K. Davis, A. W. Horton, E. E. Larson, K. L. Stemmer, Arch. Environ. Health, 6, 473, 1963.

90. M. Gherardi, G. Salvi, Folia Med. (Naples), 45, 1254, 1962.

91. M. Magistretti, N. Zurlo, F. Scollo, D. Pacillo, Med. Lavoro, 54, 486, 1963.

92. K. Ohmori, Japan J. Hygiene, 20, 340, 1965.

93. V. Scarinci, Arch. Sci. Biol. (Bologna), 44, 153, 1960.

94. G. W. H. Schepers, Arch. Environ. Health, 8, 277, 1964.

95. F. Springman, E. Bingham, K. L. Stemmer, Arch. Environ. Health, 6, 469, 1963.

96. C. D. Stevens, C. J. Feldhake, R. A. Kehoe, J. Pharm. and Exper. Therap., 128, 90, 1960.

97. Working group on Lead Contamination, "Survey of Lead in the Atmosphere of Three Urban Communities", PHS, Div. Air Pollution, Cincinnati, Ohio, Jan. 1965.

98. R. S. Yolles, H. Wise, Critical Reviews in Environmental Control, 2 (1), 125, 1971.

99. J. F. Roth, Division of Petr. Chem., ACS, Los Angeles Meeting, Preprint, Vol. 16, 2, page E53, March 1971.

100. L. L. Hegedus, K. Baron, J. Catalysis, 37, 129, 1975.

101. J. L. Bomback, M. A. Wheeler, J. Tabock, J. Janowski, Environ. Sci. Techn., 9 (2), 139, 1975.

102. J. Mooi, J. P. Kuebrich, M. F. L. Johnson, F. J. Chloupek, Proc., Div., Refining, Am. Petrol. Inst., 53, 14, 1973.

103. E. C. Su, E. E. Weaver, SAE (Tech. Paper), Paper 730594, 1973.

104. J. G. Bucknell, Ph.D Thesis, The City University, London, 1977.

105. R. L. Klimish, C. Jerry, J. C. Schlatler, Adv. Chem. Ser., 143, 103, 1975.

106. D. McArthur, Adv. Chem. Ser. 143, 85, 1975.

107. R. M. Barrer, J. Soc. Chem. Ind., 64, 130, London, 1945.

108. R. M. Barrer, J. Chem. Soc., pp 127, 2158, 1948.

109. L. Reikert, Adv. in Cat., 21, 281, 1970.

110. H. F. Leach, Annu. Rept. Progr. Chem., A 68, 195, 1971.

111. D. W. Breck, 'Zeolite Molecular Sieves, Structure, Chemistry and Use', Pub. John Wiley & Sons, 1974.

112. J. A. Rabo, 'Zeolite Chemistry and Catalysis', ACS Monograph 171, Am. Chem. Soc. 1976.

113. W. M. Meier, Z. Krist., 115, 439, 1961.

114. R. M. Barrer, D. L. Peterson, Proc. Roy. Soc., (A) 280, 466, 1964.

115. R. Beecher, A. Voorhies jr., P. E. Eberly jr., Ind. Eng. Chem. Prod. Res. Develop., 7, 203, 1968.

116. L. B. Sand, in 'Molecular Sieves', Society of Chemical Industry, p 71, London 1968.

117. M. M. Dubinin, G. M. Federova, G. M. Plavnik, L. I. Piguzova, E. N. Prokofeva, Isz. Akad. Nauk. SSSR, Ser. Khim, 11, 2429, 1968.

118. D. M. Teague, Report to Chrysler Corp., No. E-8546-1, May 11, 1974.

119. K. Otto, C. N. Montreuil, Environ. Sci. Tech., 10 (2), 154, 1976.

120. D. M. Teague, L. B. Clougherty, A. N. Speca, Environ. Health Perspect., 10, 113, 1975.

121. C. W. Oatley, W. C. Nixon, R. F. W. Pease, Advances in Electronics and Electron Physics, 21, 181, 1965.

122. R. Castaing, Advances in Electronics and Electron Physics, XIII, 317, 1960.

123. D. G. Blears, R. T. Coventry, 'Development of Continuous Organic Lead-in-Air Monitors', Proc. of Symp. on Chemical Process Hazards; The Inst. of Chem. Engineers, April 1974.

124. L. W. Andrews, J. Am. Chem. Soc., 25, 756, 1903.

125. E. B. Sandell, 'Colorimetric Metal Analysis', 3rd. ed., Interscience Pub. Inc., N. Y., 1965.

126. N. L. Soulages, Anal. Chem., 38, 28, 1966.

127. N. L. Soulages, J. Gas Chromatog, 6, 356, 1968.

128. E. J. Bonelli, H. Hartman, Anal. Chem., 35, 1980, 1963.

129. H. L. Dawson, Jr., Anal. Chem., 35, 542, 1963.

130. R. J. Reynolds, K. Aldous, 'Atomic Absorption Spectroscopy', Pub. Griffin, London 1970.

131. H. Shapiro, F. W. Frey, 'The Organic Compounds of Lead', Interscience Pub., N. Y., 1968.

132. R. M. Barrer, J. Klinowski, J. Chem. Soc., Faraday Trans. I, Phys. Chem., Pt 1, 690, 1975.

133. K. E. Burke, C. M. Davis, Anal. Chem., 36, No.1, p172, 1964.

134. S. Brunauer, P. H. Emmett, and E. Teller, J. Am. Chem. Soc., 60, 309, 1938.

135. S.J.Gregg, K.S.W.Sing, 'Adsorption, Surface Area & Porosity' Acad.Press (1963)

136. E. P. Barrett, L. G. Joyner and P. P. Halenda, J. Am. Chem. Soc., 73, 373, 1951.

137. C. Pierce, J. Phys. Chem., 57, 149, 1953.

138. L. S. Ettre, 'Applications of the Continuous Flow Method and the model 212-D Sorptometer for Surface Studies', Perkin Elmer, Application No. SO-AP-002, 1966.

139. A. Wheeler, 'Catalysis' ed. P. H. Emmett, Vol.11, p 23, Reinhold Publishing Corporation, New York, 1955.

140. F. M. Nelson and F. T. Eggertsen, Anal. Chem., 30, 1837, 1958.

141. H. W. Daeschner, F. H. Stross, Anal. Chem., 34, 1150, 1962.

142. M. G. Farey B. G. Tucker, Anal. Chem., 43, 1307, 1971.

143. J. W. McBain, A. M. Bakr, J. Am. Chem. Soc., 48, 690, 1926.

144. Vacuum Microbalance Techniques, Vol.1 and Vol.2, Plenum Press, New York, 1961 and 1962.

145. Techniques with Cahn Electrobalance, no. 3, Cahn Instrument Company, Paramount, California.

146. A. L. Houde, Discussion at Third Symposium on Vacuum Microbalance Techniques, Los Angeles, 1962.

147. P. H. Emmett, "Measurement of the Surface Area of Solid Catalysts". Catalysis 1 31-74, Reinhold Publ. Corp., N. Y. (1954).

148. W. D. Harkins, G. Jura. J. Am. Chem. Soc., 66, 1356, 1944; ibid, 66, 1362, 1944; ibid, 66, 1366, 1944.

149. G. Jura, W. D. Harkins, J. Am. Chem. Soc., 68, 1941, 1946.

150. H. K. Livingston, J. Am. Chem. Soc., 66, 569, 1944.

151. J. A. Poulis, J. M. Thomas, J. Sci. Instrum., 40, 1963.

152. M. M. Dubinin, Quart Rev. of Chem. Soc., 9, 101, 1959; Chem. Rev., 60, 235, 1960.

153. D. W. Breck, 'Zeolite Molecular Sieves, Structure, Chemistry and Use', Pub. John Wiley & Sons, p 683, 688, 1974.

154. P. B. Weisz, J. S. Hicks, Chem. Eng. Sci., 17, 265, 1962.

155. W. A. Bone, J. B. Gardner, Proc. R. Soc. A, 154, 297, 1936.

156. R. G. W. Norrish, S. G. Foord, Proc. R. Soc. A, 157, 503, 1936.

157. P. G. Ashmore, 'Catalysis and Inhibition of Chemical Reactions', Butterworths, London, 1963.

158. D.E.Hoare,A. D. Walsh, Fifth (International) Symposium on Combustion; Reinhold, 467, N. Y., 1955.

159. D. E. Hoare, A. D. Walsh, Proc. R. Soc. A, 215, 454, 1952.

160. G. H. N. Chamberlain, A. D. Walsh, Proc. R. Soc. A, 215, 175,1952.

161. G. H. N. Chamberlain, D. E. Hoare, A. D. Walsh, Disc. Faraday Soc., 14, 89, 1953.

162. D. Downs, A. D. Walsh, R. W. Wheeler, Trans. Roy. Soc., 243, 463, London, 1951.

163. R. M. Barrer, R. G. Jenkins, G. Peters, Proc. 4th Int. Conf. Mol. Sieves, Chicago, ACS Symp. Ser., 258, 1977.

164. J. J. F. Scholten, A. Van Montfoort, J. Catal., 1, 85, 1962.